Spin Transport and Exchange Coupling in Ballistic Magnetic Multilayers

Thesis

The Open University
Department of Mathematics and Statistics

Spin Transport and Exchange Coupling in Ballistic Magnetic Multilayers

Valentin Fadeev

Submitted in part fulfilment of the requirements for the degree of
Doctor of Philosophy in Mathematics of The Open University, May 2020

Abstract

In this work we study a set of related problems in the theory of ballistic spin transport. We draw special attention to the phenomenon of exchange coupling, which is interesting both from the theoretical point of view, and the possible applications in spintronics. For the calculations we employ the Landauer transfer matrix formalism, testing its assumptions, extending it to new models and establishing links with other branches of physics.

Acknowledgements

I would like to express my immense gratitude to my supervisor Dr Andrey Umerski for supporting and guiding me throughout the highly non-linear flow that this work turned out to be. I cannot thank my wife enough for her understanding and patience while I had to carve out significant portions of family time to complete the thesis, as well as my mother who, on more than one occasion, encouraged me not to give up. I would like to thank Dr Rachel Traylor for the fruitful discussions that greatly helped me keep the momentum during the process of writing up.

Dedication

To the memory of Charles Kittel and Philip Warren Anderson.

Contents

List of Tables

List of Figures

List of Acronyms

CIP *current-in-plane*. xiii, 12–14

CPP *current-perpendicular-to-plane*. xiii–xv, 12–14, 34, 42, 102, 103

DRAM *dynamic random access memory*. 9

GMR *giant magnetoresistance*. 11, 12

IEC *interlayer exchange coupling*. 6, 7, 89–91, 98, 104, 105

MBE *molecular beam epitaxy*. 15

MJ *Müller-Jones*. 83

MJ *Spin Müller-Jones*. 83

MRAM *magnetoresistive random access memory*. xiii, 11, 12, 14, 16

MTJ *magnetic tunnel junction*. xiii, 11–14

RKKY *Ruderman–Kittel–Kasuya–Yosida*. 69

SHE *spin hall effect*. xiii, 14, 15

SMF *spinmotive force*. 16, 17

SOI *spin-orbit interaction*. 14, 16

SOT *spin-orbit torque*. xiii, 15

SPINFET *spin-field effect transistor*. 10

SSL *single spin logic*. 10

STT *spin-transfer torque*. xiii, 12, 14, 17

SV *spin valve*. xiii, 11–13

TAS *thermally-assisted switching*. 14

TMR *tunnelling magnetoresistance*. 11, 12

Chapter 1

Introduction

1.1 Motivation and Objectives

The present study deals with a class of problems in an area of electronic transport known as *spintronics*. This is a relatively recent field of research and an engineering discipline that was brought about towards the end of the 20th century through the advances in material science and measurement techniques. Its subsequent development was accelerated by the rapid adoption of the early discoveries by electronic device manufacturers, predominantly in the sector of information storage and retrieval. Tremendous progress in nano-fabrication technology allowed researchers to study certain phenomena which would have previously been impossible to observe experimentally because they would be disturbed or destroyed by the effects of impurities in the sample. Novel phenomena, such as *spin current* and spin torque, became of central importance, as the physical processes underlying a new generation of electronic circuits. Furthermore, as the observations shifted towards the mesoscopic and nanoscale ranges, some of the well known concepts, such as electrical conductance and resistance, had to be redefined because their macroscopic interpretations no longer made sense for structures comprised of a small number of atomic layers. Mathematical model of spin current, which will be the main focus of this research, is an interesting concept in itself too. Much of the intuition about the generation, conservation and symmetries of the more familiar charge current does not necessarily apply to

spin-polarised transport. Some of the known facts and prior results obtained for charge transfer often inform the problems formulated for its spin counterpart throughout this work, only to lead to the realisation of how different the behaviour may be in the latter case.

A common scheme of reasoning applied to problems in solid state theory is the following one. Firstly, idealised model calculations are performed to extract certain qualitative features, for example the existence and number of oscillation periods observed under variation of the parameters. This is often followed by reformulating the problem for a more realistic model (e.g. tight-binding or *ab initio*) and repeating the calculations to determine if the features predicted in the previous step still manifest themselves. Finally, the conclusions may be validated against the available experimental data. Our study is mathematically oriented, therefore we focus on the study of a model system which is, in some circumstances, exactly solvable. In practice, however, the exact solution may not be particularly illuminating with respect to reasoning about the system behaviour. Hence, we discuss and extend a formalism that encapsulates most of the complexity and retains the physical intuition throughout the manipulation. Furthermore, the results obtained within this formalism can be often almost directly translated into the language of the more realistic models. These results will be of the strictly qualitative nature. Nevertheless, our choice of computational framework, and the way we apply it, opens the possibility – in the future research – to validate these results by transcribing them into a form suitable for realistic numerical simulations.

In Chapter 2, following an overview of the background material about the history of spintronics and the physics of spin, we describe a non-relativistic spin-resolved Hamiltonian. We gradually enhance it to cover the presence of exchange splitting and in-plane rotation of the magnetisation. We then depart from this particular form of the Hamiltonian for a while, and introduce the Landauer method for calculating conductance in terms of the transmission probability. We discuss the various extensions of the formalism to the case of the spin degree of freedom, multiple scatterers and, ultimately, many terminals (Landauer-Büttiker method). Two ideas must be emphasised here. Firstly, when discussing transmission in multilayer structures we recognise the role of successive reflections that electrons undergo between the interfaces. It will become clear in the subsequent chapters that only if we account for all possible reflections can

certain types of symmetries exhibited by the spin current components be rigorously proved and physically explained. Since it is usually rather tedious to calculate analytically the transmission across more than two interfaces, while summing over all reflections, this is often omitted in the literature, and approximations in one reflection are considered instead. Secondly, we make a clear separation between the general formalism of the transmission and reflection matrices, and its particular application to the problem described earlier. In this case the coefficients can be exactly calculated based on the continuity equations for the wave functions at the interfaces. However, we note that the values could in fact be set based on phenomenological considerations or fitted from experimental data instead. The chapter culminates with the introduction of spin current. We define it in terms of the transmission formalism, and treat the charge and spin components as constituents of a general mathematical object of a quaternionic structure (although we do not make use of any further algebraic properties of quaternions in what follows). We comment on the distinction between the exchange and transport parts of the current, which sets up the exposition of their various properties in the following two chapters.

Chapter 3 contains an extensive investigation of the mechanism through which spin current arises in ballistic multilayers, and the various symmetries it exhibits. The aim is to provide a clear demonstration of how the qualitatively new features arise, as we include successive reflections between the interfaces. Particular attention is paid to the properties of the out-of-plane component of spin current which plays an important role in the transfer of torque, and may therefore be crucial for applications. It is shown that under certain assumptions about the device symmetry current components may vanish identically. This is an important observation because such assumptions are often made in model calculations in order to simplify the analytical derivations. Here we see that certain qualitative information may be lost in the process, leading to potentially incorrect conclusions about the behaviour of spin current. The contents of Section 2.5.2 and the entire Chapter 3 comprise an extended version of the discussion presented in the paper [1] co-written by the author. Section 3.6 is fully contributed by the author.

An investigation of the asymptotic properties of current oscillations is provided at the end of the chapter. It is motivated by the earlier work of other authors [2] on an similar problem

for charge conductance. It also serves to demonstrate the convenience of working with the transfer matrix formalism, and the physical clarity of the results obtained via the low-reflection approximation.

In Chapter 4 we point out the deep analogies that exist between the multilayer problems in linear optics and electron transport, which often look very similar from the transfer matrix method point of view [3]. Beyond the immediate similarities, we note that there are some established methods of calculating the polarisation properties of the optical multilayers which admit a straightforward interpretation in the context of spin current, however, they do not seem to have been widely adopted within the spintronics community. The particular techniques that we discuss are the Iwasawa decomposition and the Müller-Jones calculus. While a deeper investigation of both of these methods is tangential to the main theme of our study and is therefore deferred to future research, we outline the main points of interest and indicate the possible further areas of study.

In Chapter 5 we apply the Landauer formalism to the study of *interlayer exchange coupling* (IEC), a form of electromagnetic interaction between ferromagnets by means of itinerant conduction electrons. This effect is of great interest because it provides one possible path towards generating large spin currents with very low charge transfer. For applications this means greater energy efficiency and further miniaturisation of the devices. The theoretical study here, however, starts with the observation that IEC is closely related to one of the spin current components, and that it can exist in a system completely isolated from the environment. This represents a novel use case of the Landauer formalism, which traditionally contains the assumption that a conducting material is coupled to phase-randomising macroscopic reservoirs. We construct a model where the device is gradually isolated from the outside world and interpret the resulting solution, both physically and mathematically. Studying such systems, which we refer to as *closed*, is particularly interesting because it clearly demonstrates the stark differences in the behaviour of the charge current and the components of the spin current. While the charge current vanishes in an isolated system, following the classical intuition, the same is not true for the out-of-plane component of the spin current. To support the argument, we complement the proof with an equivalent derivation based on the spectral density formalism. We largely

follow the quantum-well theory of IEC, as set out in [4] and [5], which again demonstrates the fundamental role of reflections in generating the total phase shift of the electrons in the spacer. That phase shift gives rise to the transfer of torque to a ferromagnetic layer.

Finally, Chapter 6 deals with the problem of spin transport in geometries with more than two terminals. Besides the motivation from device engineering, this provides an example of generalising the Landauer transfer matrix method to a model that, to the authors' knowledge, has not been considered before. Spin-resolved transmission across multi-terminal junctions has been studied for the case of a diffusive central region [6] and for some very specific geometries [7], [8]. Reduction to the ballistic regime is discussed in [6], however, it is done with some drastic simplifications, without accounting for successive reflections between the segments adjacent to the junction. The discussion in [8] also incorporates spin-orbit interaction which complicates the results but does not necessarily add much insight into the flow of amplitude across the central region of the structure. In keeping with the overall approach of this study, we take the existing results for charge transport, based on the work of Büttiker [9], [10], as the starting point, and generalise them to the spin degree of freedom. We go beyond the assumption of a single thin scatterer given in the example in [10] and introduce the structure which is similar to that studied in [6], however, in this case the transport is ballistic, and all reflections are accounted for.

1.2 On the Use of Notation

In this work we find ourselves having to deal with a wide range of mathematical objects. While we strive to adhere to the established conventions, certain trade-offs are deemed necessary in order to maintain the overall consistency and clarity. Thus we use over-bar notation, for example $\bar{k}_{\|}$, $\bar{M}$, to denote 2- and 3-dimensional vector quantities. 4-dimensional vectors make the occasional appearance and will be denoted by double over-bar, for example $\bar{\bar{s}}$, to make the distinction clearer. Small boldface Latin letters stand for 2×2 matrices, such as $\mathbf{r}$ and $\mathbf{t}$, whereas Greek letters denote spinors, for instance $\boldsymbol{\psi}$, $\boldsymbol{\alpha}$, unless otherwise indicated. One

exception is made for the Pauli matrices, which follow the standard convention $\boldsymbol{\sigma}_\nu$. Vector and matrix notation may be composed, whereby $\bar{\boldsymbol{\sigma}}$, $\bar{\bar{\mathbf{j}}}$ denote 3- and 4-component vectors of matrices, respectively. Capital boldface letters are used for 4×4 matrices, such as $\mathbf{T}$, $\mathbf{S}$. A 6×6 matrix makes a single entry in Chapter 5 and is distinguished using the check mark $\check{\mathbf{S}}$. Quantum-mechanical operators, without reference to a representation, are customarily decorated with hats, for example, $\hat{\mathcal{H}}$, $\hat{\mathbf{s}}$. Certain higher-dimensional objects, whose scope is limited to the second half of Chapter 4, are denoted by Fraktur script $\mathfrak{J}$, $\mathfrak{M}$, in order to emphasize certain similarities between the formalisms under discussion there. Greek indices, such as ν, run over the set of spatial indices $\{x, y, z\}$, and the "timelike" 0 component (where applicable), while Latin indices, such as i are usually reserved for indexing in multilayers. We use $\mathbf{0}$ and $\mathbf{1}$ to denote the zero and identity matrices, respectively. For brevity we do not specify their dimensions explicitly, which can always be inferred from the context. Finally, in order to prevent it being conflated with the running index, an augmented notation i is employed for the imaginary unit.

Chapter 2

Background Theory

2.1 Overview of Spintronics

Traditional electronics is based largely on the methods of controlling the flow and accumulation of charge carried by electrons in conductive media. Storage and retrieval of digital information in volatile memory, such as *dynamic random access memory* (DRAM), is widely implemented by means of detecting the presence or absence of accumulated charge in capacitors. Logic circuit designs rely on the properties of certain semi-conducting materials that allow switching current on and off along parts of the contour. Although charge plays a crucial role in the processes underlying the electronic devices, it is not the only property of the carriers that can be useful for applications. Electrons also possesses an intrinsic angular momentum, called *spin*, that is observed by the way it interacts with external magnetic fields, orbital momenta and other spins. Under certain conditions it is possible to generate the flow of spin through material. This flow is called *spin current* and it will be central to our studies. Unlike charge current, which is a scalar quantity, spin current has three spatial components, and those can exhibit very different behaviour from each other under variation of the material parameters. Furthermore, spin is an essentially quantum-mechanical property of a particle. It has no classical analogue, therefore, certain effects related to it cannot be observed at macroscopic scales. This is why the models we study describe nanoscale structures, measuring a small number of atomic layers across.

The idea to use the flow of spin, in a controlled way, in electronic devices gave rise to *spintronics*, as a branch of research and an engineering discipline. It dates back to the work by Leo Esaki and his group at IBM in 1960s on the magnetoresistance of antiferromagnetic EuSe placed between metal electrodes [11]. The crucial observation is that spin polarisation of conducting electrons affects their transmission and scattering rates in certain materials. Consequently, it is possible to engineer structures that exhibit noticeable differences in conductance, depending on the polarisation of current passing through them. This in turn, paves the way to novel methods of reading and storing information.

Before discussing specific examples in detail we shall give a broad classification of the spintronics-based devices (according to [12]). From the point of view of the physical mechanism used to encode and read information spintronics-based technologies can be roughly split into *monolithic* and *hybrid*. In the former case the spin state is used directly for storing information. A monolithic spin device can be realised, for example, as an array of quantum dots each trapping a single electron in bistable spin polarisation. The initial orientations of spins therefore correspond to the input bits. An extreme example of this approach was introduced in 1994 and is referred to as *single spin logic* (SSL). In hybrid spintronics, on the other hand, spin degree of freedom is only used as a proxy for processing information. One such proxy is the connection between the polarisation state of the device and its electrical resistance. Depending on whether or not the flow of carriers is actively modulated by an externally applied field devices may be described as *active* or *passive*, respectively. Active devices are characterised by the capability to amplify an input signal. Historically, the first example of an active device utilising the spin degree of freedom to control the carrier flow to be proposed is the Datta-Das *spin-field effect transistor* (SPINFET) [13]. Examples of passive devices include sensors, read heads and magnetic memory cells. In order to avoid conflating the topic with the field of quantum computing, we note that the distinction between *quantum* and *classical* spintronics is made solely on the basis of the type of information processed using a given device. However, it is more common for the quantum computations using spin to be discussed in the context of monolithic spintronics, specifically SSL. Our discussion here will be focused on the models of hybrid passive classical devices. We shall now give a brief overview of some types of these devices and the physical

phenomena enabling their operation.

In 1988 the discovery of the *giant magnetoresistance* (GMR) in Fe/Cr structures not only stimulated further research, but, within the space of less than 10 years led to the first spintronics-based devices becoming commercially available, specifically in the form of magnetic read heads [14]. In 1994 a magnetic read sensor became the first commercial GMR-based product [15]. Shortly after that, in 1997, IBM released the first GMR read head for magnetic hard disks [16]. In the same year Honeywell presented the first MRAM module utilising GMR [12]. MRAM is a type of non-volatile memory that is expected to achieve new levels of endurance, power efficiency and miniaturisation. GMR read heads have found widespread use in personal computers and media storage devices, such as Apple iPods.

While GMR is realised in metallic structures, *tunnelling magnetoresistance* (TMR) [17], [18], another phenomenon important in applications, arises in multilayer structures with insulators, for example CoFeB-MgO interfaces. GMR is the principal mechanism underlying the design of the SV type of magnetic components that find use in read sensors. TMR motivates the design of MTJ which have been the basis of read heads in all hard drives past 2008, and also form the building blocks of the next generation of spintronics-based devices. A common trait to both GMR and TMR is the influence that the relative orientation of magnetic moments in the layers has on the overall electrical resistance of the device. Depending on whether the magnetisation of the layers is aligned in the parallel (ferromagnetic, FM) or anti-parallel (anti-ferromagnetic, AF) direction, the overall channel resistance will vary between $R_{\uparrow\uparrow}$ and $R_{\uparrow\downarrow}$. This has to do with the fact that ferromagnets exhibit an imbalance of the up- (majority) and down-spin (minority) populations characterised by the respective densities of states $N_{\uparrow}$ and $N_{\downarrow}$, as depicted in Figure 2.1. Roughly speaking, in the AF configuration the majority electrons do not have as many available states to propagate into on the right-hand side. The magnetoresistive effect δ can then be expressed as follows

$$\delta = \frac{R_{\uparrow\downarrow} - R_{\uparrow\uparrow}}{R_{\uparrow\uparrow}} \tag{2.1}$$

For GMR δ can achieve values in the range $0.4 - 1.1$ at room temperature, whereas for TMR it can be as high as 10. This effect is the principal mechanism for implementing the processes

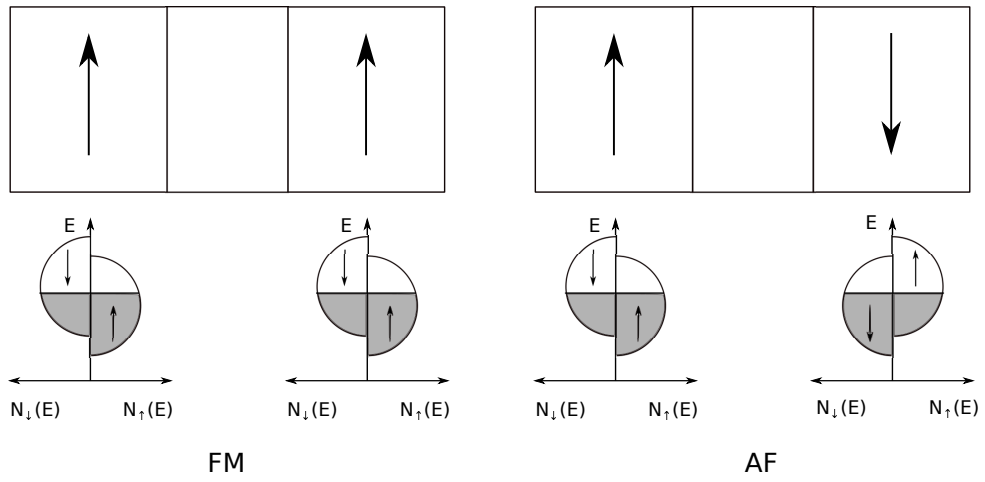

Figure 2.1: Illustration of the origin of spin-dependent conductance in the ferromagnetic (FM) and antiferromagnetic (AF) configurations.

of reading data from memory cells. Instead of the presence or absence of electric charge, the 1 and 0 bit states correspond to the high and low resistance measured across the device.

A typical structure of the so-called nanopillar used in the magnetisation switching experiments is shown in Figure 2.2. It is usually given an elliptic or a rectangular form measuring approximately 200 nm×100 nm. It consists of a relatively thick magnetic reference layer (RL), an intermediate layer (IL) and a free layer (FL). The RL acts as a polariser for the injected charge current I_{C}, since its magnetisation $\bar{M}_1$ is fixed via interaction with a large antiferromagnet, such as PtMn (not shown). The polarised current emerging from RL interacts with the spins in the FL and exerts a torque, known as STT, which, if strong enough, is capable of reversing the magnetisation $\bar{M}_2$. The intermediate layer (IL) can be a normal metal (Cu, Cr) or an insulator (AlO, MgO), depending on which the nanopillar belongs to the SV (GMR) or MTJ (TMR) type. We note that the real fabrications usually consist of many more layers (for chemical stability, heat absorption etc) than the simplified schematic shown here.

Depending on the direction of the current passing through the structure two principal geometries of multilayers are distinguished, namely the CIP and CPP, as shown in Figure 2.3. The "plane" here is that of the interface between the layers. Most of the early applications of GMR, such as read heads and MRAM sense lines, were based on the CIP geometry. However, CPP elements based on MTJ, such as spin-transfer torque STT-MRAM (Figure 2.4), have displaced GMR in applications. These structures can exhibit high room-temperature TMR, greater thermal

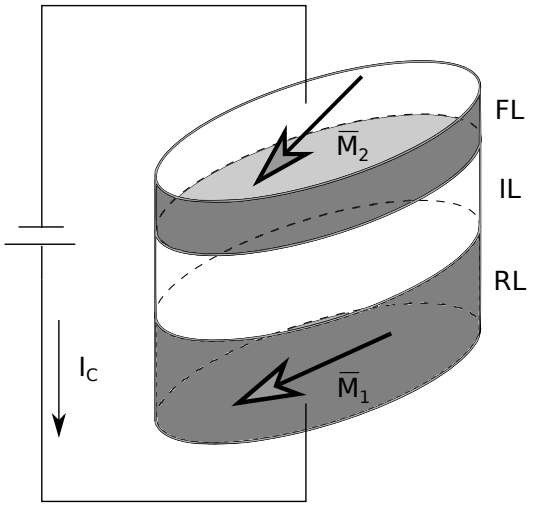

Figure 2.2: Schematic structure of a magnetic nanopillar consisting of the magnetic reference (RL) and free (switching) (FL) layers and the interlayer (IL). The latter could be a conductor or an insulator turning the device into a SV or a MTJ, respectively. Magnetisation of the RL $\bar{M}_1$ is fixed along the long axis of the ellipse. When charge current I_C passes across the structure the magnetisation of the FL $\bar{M}_2$ can be excited into precession or reversed.

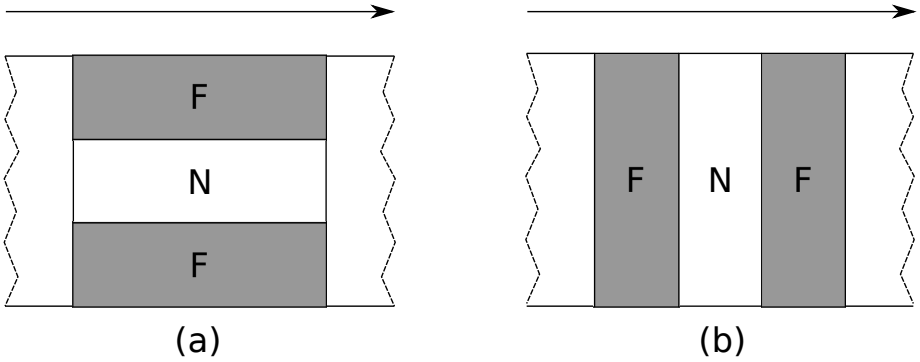

Figure 2.3: Typical device geometries in spintronics models: (a) current in plane (CIP), (b) current perpendicular to plane (CPP). Arrow shows the direction of current flow.

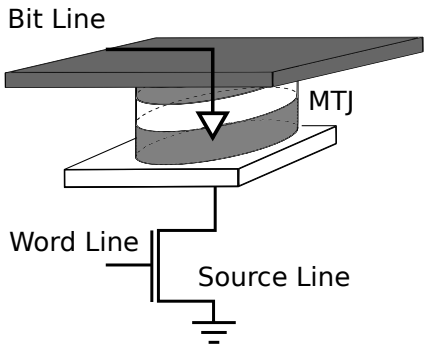

Figure 2.4: Simplified view of a STT-MRAM cell with an access transistor. The source line is connected to the source of the transistor. The word line is connected to the gate and is used to activate the cell for memory operations. Current going through the bit line is used to read and write bits by switching the free layer of the MTJ.

stability and allow for energy-efficient magnetisation switching [19]. Another advantage of the CPP STT-based switching over the older MRAM designs, where switching was driven by magnetic fields, is greater accuracy and less write disturbing of adjacent memory cells. However, although the CPP spintronic effects are superior to those of CIP, in order to observe them the junctions must be of much higher quality, with fewer impurities and near-perfect interfaces. We note that the injection of spin-polarised current is not the only switching mechanism available. Optically induced spin current [20], spin pumping [21], [22] and *thermally-assisted switching* (TAS) [23], [24] are seen as viable alternatives being actively researched.

Switching and detection of the magnetisation typically require currents of different magnitude. Therefore, it makes sense, from the point of view of device durability and efficiency, to separate the read and write contours. This results in the design of *three-terminal* memory devices. Such structures help overcome correlations between read and write voltages and reduce energy consumption. One of the schemes used for the writing paths is based on effect of *spin-orbit interaction* (SOI). Fundamentally, SOI is a relativistic effect arising as a higher-order term in the expansion of the Dirac equation at low energies [12]. However, it can be greatly amplified in solid crystals, for example in heavy metals (Au, Pt) or III-IV semiconductor heterostructures in the presence of structural and bulk inversion asymmetry, as well as external electric fields. SOI underlies a family of phenomena known as SHE. In particular, the SHE gives rise to the pure spin current I_{S} from charge current I_{C}, flowing in the transverse direction, as depicted in Figure 2.5.

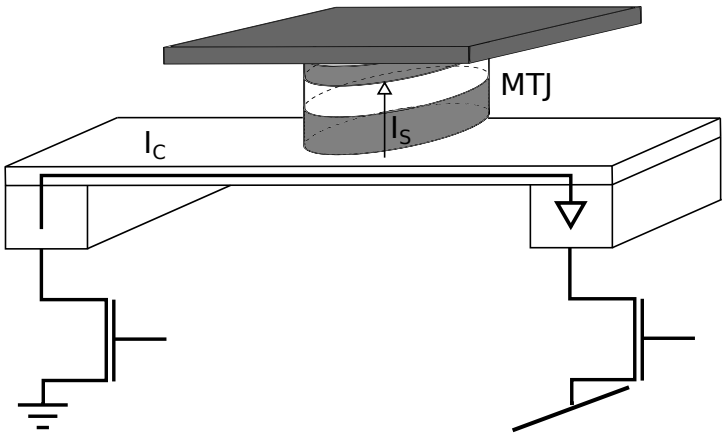

Figure 2.5: Schematic of a 3-terminal SOT RAM device. Due to spin-orbit interaction charge current I_C gives rise to transverse spin current I_S by means of the SHE.

Since this study is focussed on ballistic transport, we shall now put it in the context of the other possible regimes and the corresponding ranges of scales. We shall also explain how certain features of the modern fabrication techniques are related to the assumptions made in our models. Many practical difficulties associated with observing and manipulating the useful spin-related processes have at their core the requirement for the conservation of spin states. Inelastic scattering by lattice vibrations and magnetic impurities in samples lead to rapid relaxation. Overcoming this problem requires, on the one hand, materials to be extremely pure and, on the other hand, the samples to be relatively small in size ($\leq 1\mu$m). For example [25], at room temperature the characteristic inelastic scattering time satisfies $\tau_{\text{in}} \approx \hbar/k_{\text{B}}T \approx 10^{-13}$ s. At Fermi velocity $v_{\text{F}} \approx 10^8$ cm/s $= 10^{16}$ Å/s the inelastic scattering mean free path $l_{\text{in}} = v_{\text{F}}\tau_{\text{in}} \approx 10^3$ Å. The typical elastic mean free path at which the phase information is conserved is only of the order of 10^2 Å. However, the progress made in nano-fabrication of extremely pure nanomaterials in the recent decades has made it possible to study spin currents experimentally. Techniques such as sputtering, *molecular beam epitaxy* (MBE) and optical and electron-beam lithography allow fabricating superlattices that are nanosize in one direction, referred to as multilayers. At temperatures $T < 1$ K, coherent lengths of the waves will be larger than the characteristic sample size. To put into perspective the class of models studied here, we mention the main transport regimes typically distinguished [25]. Consider a number of characteristic lengths, such as the elastic mean free path l, the length L and width W of the sample and localization length ξ. The case where $W, L < l < \xi$ is referred to as *ballistic* regime, where

impurity scattering is ignored, and all scattering happens at the interfaces. The second case, where $W < l < L < \xi$, and impurity and interfacial scattering are equally important, is called the *quasi-ballistic* regime. The third possibility is the *diffusive* regime where $l < W, L < \xi$ and a significant amount of impurities or structural disorder is present. Finally the *strongly localised* case occurs when $L > \xi$. We will be working within the ballistic regime, studying scattering at the interfaces in multilayer nanoscale devices. In doing so, we will assume the interfaces "perfect" in the sense that there are no defects affecting the scattering process. A valid question to ask here is how adequate this assumption is with respect to the experimental scenarios. The answer is that due to the nature of the fabrication process, when individual layers of atoms are deposited atop of one another, and crystals are grown epitaxially the interfaces are indeed close to being perfect. A common type of defect that may occur is a step-like change in thickness, which can be neglected, assuming a sufficiently small cross-section of the sample under consideration.

Spintronics is a large and rapidly developing field. We finish this introduction by highlighting some of its currently active and emerging strands of research. SOI continues to attract a lot of attention. It is closely related to the family of spin Hall effects (anomalous, inverse, injection, quantum) which play an important role in the design of three-terminal switching devices, as we saw earlier. The study of SHE is further linked to the concept of *topological insulators* [26], [27], [28]. These are the materials that exhibit different electrical properties in bulk (insulating) and on the surface (conducting), where the surface states are topologically protected, i.e. are stable under minor variations of the material parameters. Combining thermal effects with spin transport gives rise to the field of *spin caloritronics* [29], [30], [31]. It deals, in particular, with the thermoelectric properties of magnetic multilayers and thermal spin transfer torque, which find applications in TAS-MRAM devices. Spin-rotation coupling, which has its roots in the gyromagnetic effects first discovered in 1915 (Barnett effect, Einstein-de Haas effect), can be used for mechanical generation of spin current and manipulating electron spins in paramagnetic states. The new experiments demonstrating spin current generated by the motion of rigid and elastic bodies and fluids opened up a new area of research known as *spin mechatronics* [32]. *spinmotive force* (SMF) [33], [34] is another emerging concept that can be utilised to generate

spin current in magnetic conductors. It is similar, in the underlying physics, to STT. However, while STT characterises angular momentum transfer from electron spins to the magnet, SMF is responsible for energy transfer. SMF enables efficient energy conversion between magnetic and electric systems and paves the way to the designs of active devices with zero stand-by power ("normally off"). Finally, a topic that has created a lot of interest recently is that concerning the dynamics of magnetic vortices and magnetic solitons, or *skyrmions* [35], [36]. These are the curled in-plane spin configurations that arise at particular ranges of scales in cylindrical and other regularly-shaped magnetic elements. Characterised by their "topological charges" – chirality and polarity – these arrangements open new possibilities for encoding bits of information and building high-density magnetic storage media.

It is not our intention, within the scope of this work, to provide an overview of the topics comprising the modern spintronics that would be anywhere near a complete one. Nevertheless, the above survey, hopefully, provides enough motivation for the interest in the subject. We now move on to the mathematical study of a number of problems about ballistic spin-resolved transport in magnetic multilayers.

2.2 Physics and Formalism of Spin

In this section we shall summarise some of the standard results of the quantum mechanics of spin that will be required for further discussion [12]. Since spin is discovered through its contribution to the total angular momentum of the electron, its mathematical representation is modelled on that of the orbital angular momentum $\hat{\mathbf{l}}$. Components of $\hat{\mathbf{l}}$ satisfy the following commutation relations

$$\left[\hat{\mathbf{l}}_\lambda, \hat{\mathbf{l}}_\mu\right] = \mathrm{i}\hbar\varepsilon_{\lambda\mu\nu}\hat{\mathbf{l}}_\nu,$$

where $\varepsilon_{\lambda\mu\nu}$ is the Levi-Civita symbol. Consequently, following Pauli, similar relations are postulated for the spin operator $\hat{\mathbf{s}}$

$$[\hat{\mathbf{s}}_\lambda, \hat{\mathbf{s}}_\mu] = \mathrm{i}\hbar\varepsilon_{\lambda\mu\nu}\hat{\mathbf{s}}_\nu$$

Since the early experiments (Stern-Gerlach [37]) it has been observed that spin projection takes one of two values, regardless of the chosen spatial axis of reference. These values must be the eigenvalues of the projections of $\hat{\mathbf{s}}_\nu$ and are shown to be $\pm\hbar/2$. It follows that $\hat{\mathbf{s}}_\nu$ must be represented by 2×2 traceless Hermitian matrices $\boldsymbol{\sigma}_\nu$

$$\hat{\mathbf{s}}_\nu = \frac{\hbar}{2}\boldsymbol{\sigma}_\nu.$$

Although multiple choices are possible, historically the following canonical Pauli matrices are used to represent spin operator components

$$\boldsymbol{\sigma}_x = \begin{bmatrix} 0 & 1 \\ 1 & 0 \end{bmatrix}, \qquad \boldsymbol{\sigma}_y = \begin{bmatrix} 0 & -\mathrm{i} \\ \mathrm{i} & 0 \end{bmatrix}, \qquad \boldsymbol{\sigma}_z = \begin{bmatrix} 1 & 0 \\ 0 & -1 \end{bmatrix},$$

collectively denoted by the Pauli vector $\bar{\boldsymbol{\sigma}} = (\boldsymbol{\sigma}_x, \boldsymbol{\sigma}_y, \boldsymbol{\sigma}_z)$ leading to the compact notation

$$\hat{\mathbf{s}} = \frac{\hbar}{2}\bar{\boldsymbol{\sigma}}.$$

Consider the eigenvalues of the operator $\hat{\mathbf{s}} \cdot \bar{b}$, where $\bar{a}$, $\bar{b}$ are arbitrary vectors and $\bar{n}$ is a unit vector in $\mathbb{R}^3$. Applying the standard formula

$$(\bar{a} \cdot \bar{\boldsymbol{\sigma}})\left(\bar{b} \cdot \bar{\boldsymbol{\sigma}}\right) = \left(\bar{a} \cdot \bar{b}\right)\mathbf{1} + \mathrm{i}\left(\bar{a} \times \bar{b}\right) \cdot \bar{\boldsymbol{\sigma}},$$

where $\mathbf{1}$ is the unit 2×2 matrix, we obtain

$$(\bar{\boldsymbol{\sigma}} \cdot \bar{n})^2 = \mathbf{1}.$$

This means that $\bar{\boldsymbol{\sigma}} \cdot \bar{n}$ has eigenvalues ± 1, therefore $\hat{\mathbf{s}} \cdot \bar{n}$ has eigenvalues $\pm\hbar/2$. This is consistent with the fact that measurement of spin projection along any axis always yields $\pm\hbar/2$.

2.3 Pauli Equation

In order to perform calculations over the spin-resolved states Schrödinger equation must be extended to take spin degree of freedom into account. In the general case we would be led to considering the relativistic Dirac equation. However, if the relativistic effects are not important, an appropriate approximation is given by the so-called Pauli equation [12]

$$\left(\hat{\mathcal{H}} + \frac{\hbar}{\mathrm{i}}\frac{\partial}{\partial t}\mathbf{1}\right)\boldsymbol{\psi} = \mathbf{0}, \tag{2.2}$$

where $\hat{\mathcal{H}}$ is represented by a 2×2 matrix, $\mathbf{1}$ and $\mathbf{0}$ are the unit and zero matrix, respectively, and

$$\boldsymbol{\psi} = \begin{bmatrix} \psi^{\uparrow} \\ \psi^{\downarrow} \end{bmatrix}$$

is a spin-$\frac{1}{2}$ wave function. For the rest of the discussion we will work with the time-independent version of (2.2). The Hamiltonian $\hat{\mathcal{H}}$ will typically consist of the following terms

$$\hat{\mathcal{H}} = \hat{\mathcal{H}}_0 + \hat{\mathcal{H}}_{\mathrm{Z}} + \hat{\mathcal{H}}_{\mathrm{SO}}, \tag{2.3}$$

where $\hat{\mathcal{H}}_0$ is the spin-independent part which is typically the free-particle Hamiltonian $-\frac{\hbar^2}{2m}\nabla^2$ multiplied by the unit 2×2 matrix. $\hat{\mathcal{H}}_{\mathrm{Z}}$ is the Zeeman interaction term that takes into account the interaction of the carrier spin with external magnetic fields. $\hat{\mathcal{H}}_{\mathrm{SO}}$ is the spin-orbit interaction term describing the coupling of spin to kinetic momentum. Although $\hat{\mathcal{H}}_{\mathrm{SO}}$ is important in many applications when doing calculations in crystalline structures with high atomic numbers, for the purposes of our investigation it will be disregarded. The energy of interaction of the electron's magnetic moment $\bar{\mu}_e$ with an external field of flux density $\bar{B}$ is

$$E_B = -\bar{\mu}_e \cdot \bar{B},$$

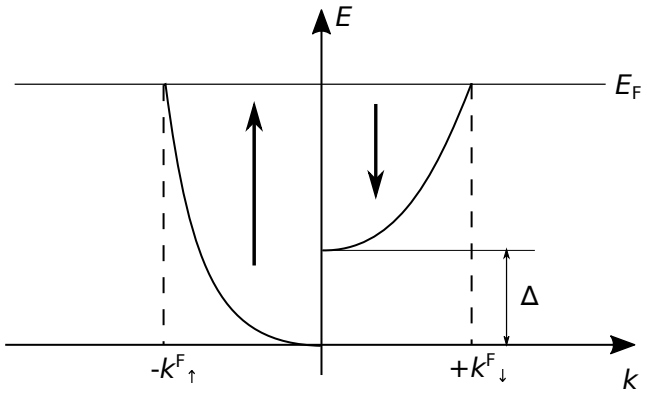

Figure 2.6: Dispersion relation in the Stoner-Wohlfarth model of a ferromagnet.

where $\bar{\mu}_e$ is related to spin angular momentum via the gyromagnetic Landé factor $g \approx 2$. Therefore, $\hat{\mathcal{H}}_{\mathrm{Z}}$ is found to have the following form

$$\hat{\mathcal{H}}_{\mathrm{Z}} = -\frac{g\mu_B}{2}\bar{B}\cdot\bar{\boldsymbol{\sigma}}, \tag{2.4}$$

where μ_{B} is the Bohr magneton. If we assume the magnetic field to be directed along the z-axis, then (2.4) takes the form

$$\hat{\mathcal{H}}_{\mathrm{Z}} = \begin{bmatrix} \frac{\Delta_{\mathrm{Z}}}{2} & 0 \\ 0 & -\frac{\Delta_{\mathrm{Z}}}{2} \end{bmatrix},$$

where $\Delta_{\mathrm{Z}} = -g\mu_B B_z$ is the Zeeman splitting term. The key point here is that electrons experience different electrostatic potential depending on their spin polarisation. Later, when we consider current passing through ferromagnetic materials we shall adopt a similar model based on the concept of exchange splitting energy Δ separating the majority and minority spin bands. This corresponds to the Stoner-Wohlfarth model of the band structure in a ferromagnet where two parabolic bands, for the majority and minority spin population, respectively, are displaced by the exchange splitting energy, as illustrated in Figure 2.6. Separating the transport according to the majority and minority carrier populations is the main idea behind the so-called two-current model proposed by Mott [38]. The assumption is that at temperatures sufficiently below Curie temperature most scattering mechanisms will not cause spin flip or spin relaxation. As the result, we can think about the spin-polarised current as two independent current flows. The resulting Schrödinger equation, assuming the effective magnetic field is aligned with the z

axis, then has the following form

$$-\frac{\hbar^2}{2m}\nabla^2\boldsymbol{\psi} + \mathbf{v}(0)\boldsymbol{\psi} = E\boldsymbol{\psi}, \tag{2.5}$$

where

$$\mathbf{v}(0) = \left(v_0\mathbf{1} + \frac{\Delta}{2}\boldsymbol{\sigma}_z\right), \tag{2.6}$$

and v_0 is the spin-independent potential. However, in the present work we will consider situations where magnetisation of a ferromagnetic layer is rotated in the xz plane by an arbitrary angle θ with respect to the spin polarisation axis of the incoming electrons. In this case the potential acquires dependency on the polarisation angle

$$-\frac{\hbar^2}{2m}\nabla^2\boldsymbol{\psi} + \mathbf{v}(\theta)\boldsymbol{\psi} = E\boldsymbol{\psi}, \tag{2.7}$$

where

$$\mathbf{v}(\theta) = \mathbf{s}(-\theta)\mathbf{v}(0)\mathbf{s}(\theta), \tag{2.8}$$

and $\mathbf{s}(\theta)$ is the spin rotation matrix

$$\mathbf{s}(\theta) = \exp\left(-\mathrm{i}\theta\boldsymbol{\sigma}_y/2\right) = \begin{bmatrix} \cos\left(\frac{\theta}{2}\right) & \sin\left(\frac{\theta}{2}\right) \\ -\sin\left(\frac{\theta}{2}\right) & \cos\left(\frac{\theta}{2}\right) \end{bmatrix}. \tag{2.9}$$

This is where the model departs from the simple two-current picture because of the combined effect of the precession of the majority and minority spins interacting with the field of the ferromagnet has on the total spin transfer. The following discussion will be based on the model in which electrons are free to move in the xz-plane, referred to as *in-plane directions*, but experience confining potential in the y direction, known as the *out-of-plane* one. In particular, components of the momentum $k_\perp = k_y$ and $\bar{k}_\parallel = (k_x, k_z)$ will play distinct roles in the subsequent calculations, as illustrated in Figure 2.7, which also indicates that we will generally assume rotational in-plane symmetry. With this structure in mind we can look solutions of (2.7) of the form

$$\boldsymbol{\psi} = \frac{1}{\sqrt{A}}e^{\mathrm{i}\bar{k}_\parallel\cdot\bar{r}}\boldsymbol{\chi}(y), \tag{2.10}$$

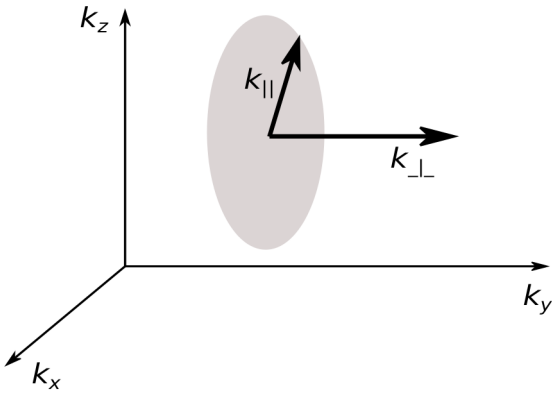

Figure 2.7: In-plane $\bar{k}_{\parallel} = (k_x, k_z)$ and out-of-plane $k_{\perp}$ components of the wave vector.

where $\bar{r} = (x, z)$ is the in-plane radius-vector and A is the cross-section area. Substituting (2.10) into (2.7) leads to the following equation for $\boldsymbol{\chi}$

$$-\frac{\hbar^2}{2m}\frac{\mathrm{d}^2}{\mathrm{d}y^2}\boldsymbol{\chi} + \mathbf{v}(\theta)\boldsymbol{\chi} = E\boldsymbol{\chi}. \tag{2.11}$$

Finally, we make the change $\boldsymbol{\chi} = \mathbf{s}(-\theta)\boldsymbol{\phi}$ which leads to the following solution for the case of a constant potential

$$\boldsymbol{\phi} = \begin{bmatrix} \alpha^{\uparrow} e^{\mathrm{i}k_{\perp}^{\uparrow} y} \\ \alpha^{\downarrow} e^{\mathrm{i}k_{\perp}^{\downarrow} y} \end{bmatrix} + \begin{bmatrix} \beta^{\uparrow} e^{-\mathrm{i}k_{\perp}^{\uparrow} y} \\ \beta^{\downarrow} e^{-\mathrm{i}k_{\perp}^{\downarrow} y} \end{bmatrix}, \tag{2.12}$$

where

$$k_{\perp}^{\uparrow,\downarrow} = \sqrt{\frac{2m}{\hbar^2}\left(E - v_0 \mp \frac{\Delta}{2}\right) - \left\|\bar{k}_{\parallel}\right\|^2}. \tag{2.13}$$

The negative and positive signs in (2.13) correspond to the up ($\uparrow$) and down-polarised ($\downarrow$) case, respectively. In a non-magnetic medium, where $\Delta = 0$ and $k_{\perp}^{\uparrow,\downarrow} = k_{\perp}$ the solution reduces to

$$\boldsymbol{\phi} = \boldsymbol{\alpha} e^{\mathrm{i}k_{\perp} y} + \boldsymbol{\beta} e^{-\mathrm{i}k_{\perp} y}, \tag{2.14}$$

where $\boldsymbol{\alpha} = [\alpha^{\uparrow} \quad \alpha^{\downarrow}]^T$, $\boldsymbol{\beta} = [\beta^{\uparrow} \quad \beta^{\downarrow}]^T$. From now on we will drop the $\perp$ subscript, understanding $k > 0$ to mean the out-of-plane component, unless otherwise specified.

2.4 Larmor Precession

Understanding how moving spins interact with the magnetisation of a medium is crucial to reasoning about the origin and properties of spin current. Here we derive a standard result that will be used further to interpret the calculations of spin current based on the solutions of (2.11). This result is known as the Larmor's theorem. It is used to characterise the motion of spins in an external magnetic field. Using the Heisenberg equation for the spin operator and Hamiltonian $\hat{\mathcal{H}} = \hat{\mathcal{H}}_0 + \hat{\mathcal{H}}_{\rm Z}$, as defined in (2.3), we obtain

$$\frac{d\hat{\mathbf{s}}}{dt} = \frac{\mathrm{i}}{\hbar}\left[\hat{\mathcal{H}}, \hat{\mathbf{s}}\right] = \frac{\mathrm{i}}{\hbar}\left[\hat{\mathcal{H}}_{\rm Z}, \hat{\mathbf{s}}\right], \tag{2.15}$$

since $\hat{\mathcal{H}}_0$ is spin-independent and therefore commutes with $\hat{\mathbf{s}}$. Writing (2.15) in components we obtain

$$\frac{d\hat{\mathbf{s}}_\lambda}{dt} = -\frac{\mathrm{i}g\mu_{\rm B}}{2}\left(B_\mu\left(\boldsymbol{\sigma}_\mu\boldsymbol{\sigma}_\lambda - \boldsymbol{\sigma}_\lambda\boldsymbol{\sigma}_\mu\right) + B_\nu\left(\boldsymbol{\sigma}_\nu\boldsymbol{\sigma}_\lambda - \boldsymbol{\sigma}_\lambda\boldsymbol{\sigma}_\nu\right)\right), \tag{2.16}$$

where (λ, μ, ν) run over permutations of (x, y, z). Using the commutation relations for Pauli matrices we deduce

$$\frac{d\hat{\mathbf{s}}_\lambda}{dt} = -\frac{g\mu_{\rm B}}{2}\left(B_\mu\boldsymbol{\sigma}_\nu - B_\nu\boldsymbol{\sigma}_\mu\right),$$

$$\frac{d\hat{\mathbf{s}}_\lambda}{dt} = -\frac{g\mu_{\rm B}}{\hbar}\left(\bar{B}\times\hat{\mathbf{s}}\right)_\lambda.$$

Therefore,

$$\frac{d\hat{\mathbf{s}}}{dt} = \bar{\Omega}\times\hat{\mathbf{s}}, \tag{2.17}$$

where $\bar{\Omega} = -\frac{g\mu_{\rm B}}{\hbar}\bar{B}$. Equation (2.17) describes the precession of spin around the magnetisation axis, as illustrated schematically in Figure 2.8. In reality damping terms will be added to the right-hand side of (2.17) which will cause the spin to relax eventually and align (or anti-align) itself with the precession axis. However, we need not be concerned with relaxation at present. Instead we will demonstrate later in Chapter 3 how precession terms, with additional phase shifts acquired after multiple scatterings, contribute to spin current.

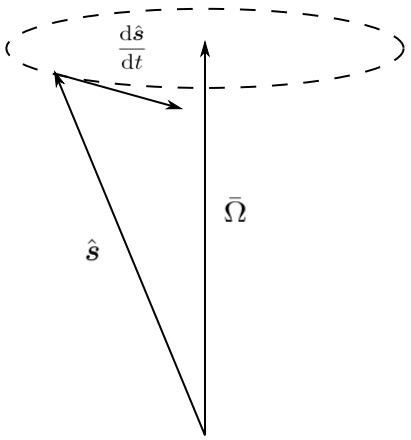

Figure 2.8: Schematic depiction of the spin axis kinematics as given by the Larmor theorem.

2.5 Landauer Formalism

2.5.1 Introduction

In this section we introduce the Landauer model of conductance in nano-scale structures. We briefly summarise the development of the Landauer formula (not necessarily in the exact chronological order), starting from a single-moded perfect conductor and building up to multi-moded transport with scattering and, ultimately, to multi-terminal devices. A fully rigorous discussion using the methods of linear response theory can be found in the article by S.D. Douglas and A. Szafer [39] and is beyond the scope of the current study. Instead we present some important intermediate steps motivating the final result and linking it to the material of the following sections.

Before the 1980's origins of electrical resistance were mainly studied in the context of irreversibility and dissipation phenomena, resulting from various forms of interactions (electron-electron, electron-phonon, electron-impurity). The role of contacts in experimental settings was viewed as a minor perturbation. However, with new experiments conducted at mesoscopic scales [40], [41] the effect of coupling a sample to the contacts was appreciated, and a different model of conductance was introduced by Landauer [42]. That model identified conductance with the probability that electrons are transmitted across the sample. The Landauer picture introduces a conceptual separation where all dissipation and phase randomising arises in large reservoirs

to which the sample is attached via reflectionless contacts. The sample itself is free from interactions and can be treated from the point of view of the ballistic transport. Electrons arrive into the sample from the reservoirs at all allowed energies up to the Fermi level, all possible distributions of momenta components and all spin orientations.

We will be using the Landauer formalism to calculate spin current. Combined with the transfer matrix method discussed later in this section, it provides a computational framework that transparently maps onto the underlying physics. With certain simplifications, it will also be possible to obtain closed-form expressions in some cases. Such results often retain the essential phenomenology and allow us to draw broadly valid qualitative conclusions. For the sake of clarity, we will temporarily revert to the spin-degenerate case and discuss the basic formulae, as they apply to charge transport. We will then bring spin back into the picture, as an extension of the original method. Ultimately, we will consider the case of multiple scattering interfaces.

The Landauer approach evolves from the idea of identifying conductance with transmission, in other words, treating it within the setting of a scattering problem. When we study the flow of current through solids at mesoscopic scales the classical Ohmic conductance

$$G = \frac{\rho S}{L},$$

where ρ is the density, S the cross-section area and L the length of the sample, would appear to grow indefinitely, as L gets smaller. However, there are experimental results clearly demonstrating that at nano-scale levels conductance approaches a certain limiting value [41] and varies in discrete steps proportionate to that value. It can be shown that this value is $\frac{e^2}{\hbar}$, per spin channel, and is known as the *quantum of conductance* [43]. This leads to the conclusion, which at first seems counter-intuitive, that a perfect single-moded conductor must have non-zero resistance of about 12.9 kΩ. In order to explain this fact it is necessary to consider the effects of coupling to the sources and sinks of current. The model assumes that the sample is connected, via perfectly conducting leads, to macroscopic reservoirs characterised by well-defined electrochemical potentials. Electrons can escape into reservoirs via the leads without undergoing any reflections. However, when going in the other direction, there occurs

a redistribution of carriers between a large number of available states in the reservoirs and only a few of them in the conductor which gives rise to non-zero resistance. Under the above assumptions and, bearing in mind the quasi-one-dimensional structure of the model described at the end of Section 2.3, we can derive the Landauer formula by considering electrons moving from one reservoir across the system. Firstly, note that the in-plane confinement will give rise to quantised modes (2.10) with energies

$$E = E_n + \frac{\hbar k_\perp^2}{2m},$$

where E_n is the cut-off energy below which a mode cannot propagate. Now consider a single conducting mode at zero temperature and recall that the one-dimensional density of states $D(E)$ is given by

$$D(E) = \frac{4L}{hv(E)}, \tag{2.18}$$

where $E > E_n$ and v is the group velocity, L is the length of the sample, and the factor of 4 accounts for carriers moving in both directions and both spin bands. If μ_1, μ_2 are the chemical potentials in the reservoirs then under the applied bias $\mu_1 - \mu_2 = -eV$ the left-to-right electron density will be half the total (2.18), and the current is calculated as follows [44] (Ch.18)

$$I = \frac{D(E)eV}{2L} ev = \frac{2}{hv} ve^2 V = \frac{2e^2}{h} V.$$

Hence, $G = I/V = 2e^2/h$ which is precisely the quantum of conductance, with the factor of 2 for spin degeneracy. Accounting for the number of transverse modes M is done by summation, as follows [10]

$$M(E) = \sum_n \vartheta(E - E_n),$$

where $\vartheta(t) = 1$ if $t > 0$ and $\vartheta(t) = 0$ otherwise. If M is constant for energies between μ_1 and μ_2 then it acts as a multiplier for conductance

$$G = \frac{2e^2}{h} M. \tag{2.19}$$

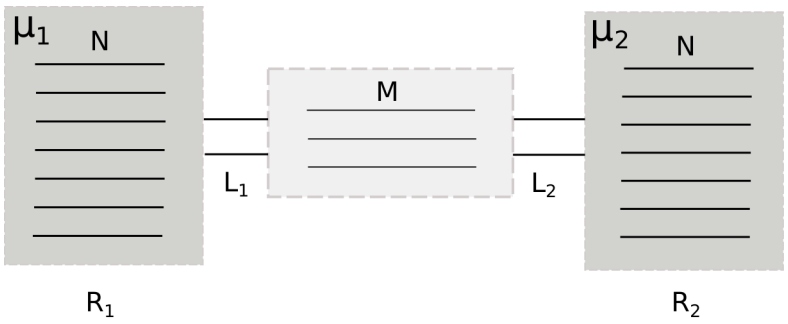

Figure 2.9: Ballistic conductor with M transverse conducting modes attached, via reflectionless leads, to large contacts with N modes each and with chemical potentials set at μ_1 and μ_2, respectively.

If the conductor is not perfect transmission of an electron emerging from one of the leads will only occur with some average probability T with the remaining probability $R = 1 - T$ of being reflected back. Therefore, (2.19) gets an extra factor of T

$$G = \frac{2e^2}{h} MT. \tag{2.20}$$

Formula (2.20) may be viewed as the mesoscopic analogue to Einstein's relation for conductivity in diffusive transport

$$\sigma = e^2 N_s D, \tag{2.21}$$

where σ is the conductivity, N_s is the density of states and D is the diffusion constant. There is an important conceptual difference between (2.20) and (2.21). Namely, *conductivity* is a local quantity that relates current density to an external electric field. *Conductance*, on the other hand, is a global quantity that connects current to voltage.

The assumption about the reservoirs having infinite number of modes is essential for the rest of the discussion. Consider the system shown in Figure 2.9 where a conductor with M modes is connected to reservoirs R_1 and R_2, each containing N modes, via reflectionless leads L_1 and L_2, respectively. As demonstrated in [42], when the numbers of modes M and N are comparable we get the following expression for conductance

$$G = \frac{2e^2}{\pi h} M \frac{N}{N - (2/\pi) M v_{\mathrm{F}}^{-1}}, \tag{2.22}$$

where v_{F} is the carrier velocity at the Fermi level. Evidently, as $N \to \infty$ in (2.22), (2.20) is

recovered. We can also rewrite (2.20) as follows

$$\begin{aligned} G^{-1} &= \frac{h}{2e^2M}\frac{1}{T} = \frac{h}{2e^2M} + \frac{h}{2e^2M}\frac{1-T}{T} \\ &= \frac{h}{2e^2M} + \frac{h}{2e^2M}\frac{R}{T} \\ &= G_{\mathrm{C}}^{-1} + G_{\mathrm{A}}^{-1}. \end{aligned}$$

where G_{C} is the contact resistance and G_{A} is the "actual" resistance of the ballistic conductor. The latter becomes 0 for a perfect conductor, where no resistance occurs. The former is precisely the quantised resistance due to coupling to the contacts. Although (2.20) is important from the conceptual point of view, this is not exactly how accounting for multiple current-carrying channels is done in practical calculations. This is because (2.20) does not describe interference between the modes. Instead, transmission between M the incoming and the outgoing modes is described by an $M \times M$ matrix $\mathbf{t}$, where each component t_{ij} is the transmission probability amplitude between modes i and j, and the following result for conductance is derived rigorously using linear response theory [45], [39]

$$G = \frac{e^2}{h}\mathrm{tr}\{\mathbf{t}\mathbf{t}^\dagger\}. \tag{2.23}$$

Being able to express the conductance across a series of layers in a multilayer structure in terms of transmission (and reflection) matrices will be the goal of the final section of this chapter. We will not be considering multiple transverse modes arising from confinement. In our model the multi-moded transport will be represented by the up- and down-spin channels, in the spirit of the Mott two-current theory, but with additional effects arising from non-collinear polarisation.

For more realistic calculations of transmission yet another generalisation is required that does not only take into account multiple conducting modes, but also multiple terminals. In a typical experimental schematic, besides current-carrying leads, there will also be two or more voltage probes attached to the sample, see Figure 2.10. At mesoscopic and nano-scales, these probes typically cannot be assumed non-invasive, in the sense that they can significantly affect the flow of carriers. Following Büttiker [46], all terminals are treated in a uniform way, that is, without any inherent distinction between the "leads" and the "probes", leading to a symmetric

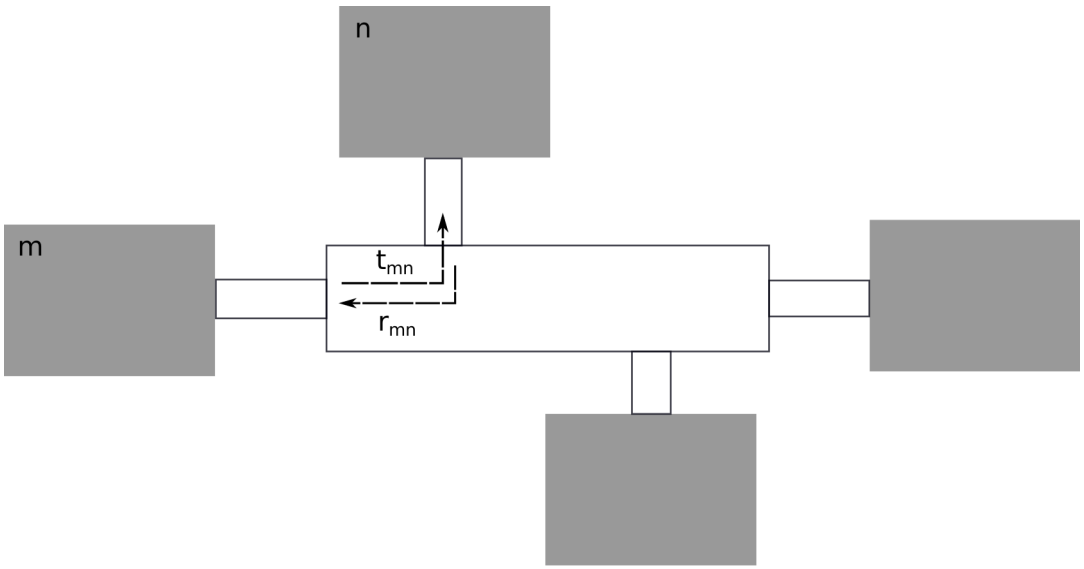

Figure 2.10: Multi-terminal structure with transmission and reflection between the contacts.

formula for electric current I_m in a given lead (probe) m

$$I_m = \sum_{n=1}^{N_{\mathrm{L}}} G_{mn} V_n \qquad \begin{cases} G_{mn} &= \dfrac{e^2}{h} \mathrm{tr}\{\mathbf{t}_{mn}^{\dagger} \mathbf{t}_{mn}\}, \quad m \neq n, \\ \\ G_{nn} &= \dfrac{e^2}{h} \mathrm{tr}\{\mathbf{r}_{nn}^{\dagger} \mathbf{r}_{nn} - \mathbf{1}\}. \end{cases} \tag{2.24}$$

where m and n are indices of various leads whose total number is N_{L}, V_n are electrostatic potentials in the leads, I_m is the charge current in lead m and $\mathbf{t}_{mn}$, $\mathbf{r}_{mn}$ are transmission and reflection matrices, respectively, between leads m and n. We will now proceed to describe an extension of the Landauer method to systems with multiple scattering interfaces. We will also derive specific expressions for the transmission and reflection matrices, as those feature in (2.23) and (2.24), and build up a framework for calculations over multilayer structures.

2.5.2 Systems with Multiple Scatterers

In this section we present a detailed discussion of the ballistic scattering model and introduce the important transfer matrix formalism. Used in conjunction with the Landauer theory discussed in Section 2.5.1 it will allow us to study conductance and, subsequently, spin current in multilayer structures.

When studying transport phenomena it is neither very useful nor interesting to consider just one electromagnetically uniform piece of conducting material. We mostly deal with heterostructures consisting of layers having different electrochemical and magnetic properties. We are looking for a method of reasoning about transmission of electrons from the macroscopic reservoirs into an arbitrary layer of such structures. Building blocks for most of our subsequent calculations will be provided by reflection and transmission coefficients that we referred to in the discussion of the Landauer formula in Section 2.5.1. These coefficients can be determined analytically from the Schrödinger's equation, by matching wave functions at the interface, under the usual requirement of continuity of the wave-function itself and its velocity flow. In this case they will be functions of the wave vector and will depend on the electrostatic potential profiles in the neighbouring layers. On the other hand, they can also be fitted from *ab initio* calculations or experimental data.

We now introduce some notational conventions by considering a single scattering event at the interface of two layers. Firstly, we consider the case of a single spin channel. If a wave of unit amplitude hits an interface (Figure 2.12) it will be partially reflected with amplitude r and transmitted with amplitude t. We will need to distinguish the waves arriving from the left ($-\infty$) and the right ($+\infty$) direction, and will therefore denote the transmitted and reflected amplitudes of the right-moving states t' and r', respectively. Subscripts will be used to signify the layers between which transmission and reflection happen, for example t'_{mn}, denoting transmission from layer m to n where $m < n$. When we consider transmission across multiple interfaces, left-to-right for the sake of argument, the transmitted amplitude t' will serve as the "incoming" wave for the next interface.

When both spin channels are taken into account the transmission and reflection amplitudes become 2×2 complex matrices $\mathbf{r}$, $\mathbf{t}$, $\mathbf{r}'$ and $\mathbf{t}'$, respectively. These matrices are taken to be diagonal, because we disregard spin-dependent scattering, for example

$$\mathbf{t} = \begin{bmatrix} t^{\uparrow} & 0 \\ 0 & t^{\downarrow} \end{bmatrix}, \qquad \mathbf{r} = \begin{bmatrix} r^{\uparrow} & 0 \\ 0 & r^{\downarrow} \end{bmatrix} \qquad .$$

In a typical calculation we will want to know the transmitted and reflected amplitudes within a given layer of the heterostructure, under certain boundary conditions. This can be done directly by solving Schrödinger's equation in each layer and matching wave functions at the interfaces. However, that method has some drawbacks. It requires solving systems of linear equations where algebraic complexity increases rapidly with the number of steps, to the point when it becomes difficult to reason about the results qualitatively. It is also not particularly amenable to generalisation to arbitrary potential profiles and effects such as spin-dependent scattering. It turns out, that there exists a composition law that allows us to express amplitudes in a layer recursively in terms of the those in the preceding layers. This law can be obtained in a very general manner without any dependence on a particular analytic (or numeric) form of the coefficients. We find these useful properties in the so-called *transfer matrix* or **T**-matrix. The 4×4 **T**-matrix connects amplitudes on the left of the interface to those on the right. If $\boldsymbol{\alpha}_j$, $\boldsymbol{\beta}_j$ are the amplitudes of the right- and left-moving waves to the left of the scatterer, respectively, and $\boldsymbol{\alpha}_{j+1}$, $\boldsymbol{\beta}_{j+1}$ are the amplitudes to the right (see Figure 2.11), the transfer matrix establishes the following relation

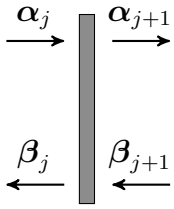

Figure 2.11: Incoming and outgoing waves near a scattering interface.

$$\begin{bmatrix} \boldsymbol{\alpha}_j \\ \boldsymbol{\beta}_j \end{bmatrix} = \mathbf{T}_{j\,j+1} \begin{bmatrix} \boldsymbol{\alpha}_{j+1} \\ \boldsymbol{\beta}_{j+1} \end{bmatrix}. \tag{2.25}$$

The form of **T** in terms of transmission and reflection amplitudes can be established by considering boundary conditions at the left and right lead, corresponding to waves of unit amplitude arriving from infinity, as illustrated in Figure 2.12. Writing **T** in the block form where $\mathbf{h}_{ij}$ are complex 2×2 submatrices we obtain the following equations

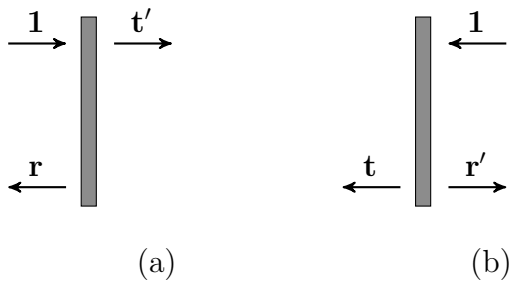

Figure 2.12: Incident and reflected waves near a scattering interface: (a) left-incident unit wave, (b) right-incident unit wave.

$$\begin{aligned}\begin{bmatrix}\mathbf{1}\\ \mathbf{r}\end{bmatrix} &= \begin{bmatrix}\mathbf{h}_{11} & \mathbf{h}_{12}\\ \mathbf{h}_{21} & \mathbf{h}_{22}\end{bmatrix}\begin{bmatrix}\mathbf{t}'\\ \mathbf{0}\end{bmatrix},\\ \begin{bmatrix}\mathbf{0}\\ \mathbf{t}\end{bmatrix} &= \begin{bmatrix}\mathbf{h}_{11} & \mathbf{h}_{12}\\ \mathbf{h}_{21} & \mathbf{h}_{22}\end{bmatrix}\begin{bmatrix}\mathbf{r}'\\ \mathbf{1}\end{bmatrix}.\end{aligned} \tag{2.26}$$

Solving the four equations of (2.26) for $\mathbf{h}_{ij}$ we obtain

$$\mathbf{T}_{j\,j+1} = \begin{bmatrix}\mathbf{t}'^{-1} & -\mathbf{t}'^{-1}\mathbf{r}'\\ \mathbf{r}\mathbf{t}'^{-1} & \mathbf{t}-\mathbf{r}\mathbf{t}'^{-1}\mathbf{r}'\end{bmatrix}. \tag{2.27}$$

Applying (2.25) recursively we can obtain a general relation for the amplitudes in two layers indexed m and n

$$\begin{bmatrix}\boldsymbol{\alpha}_m\\ \boldsymbol{\beta}_m\end{bmatrix} = \mathbf{T}_{mn}\begin{bmatrix}\boldsymbol{\alpha}_n\\ \boldsymbol{\beta}_n\end{bmatrix}. \tag{2.28}$$

where

$$\mathbf{T}_{mn} = \mathbf{T}_{m\,m+1}\mathbf{T}_{m+1\,m+2}\ldots\mathbf{T}_{n-1\,n} \tag{2.29}$$

The composition rule (2.29) means that the form of $\mathbf{T}$ in terms of transmission and reflection matrices is preserved and gives a method of calculating amplitudes across several interfaces. Suppose we are given $\mathbf{T}_{mn}$ and $\mathbf{T}_{np}$, where $m < n < p$. Then using (2.27) and (2.29) we can

calculate the transmission from n to p as follows

$$\begin{bmatrix} \mathbf{t'}_{mp}^{-1} & -\mathbf{t'}_{mp}^{-1}\mathbf{r'}_{mp} \\ \mathbf{r}_{mp}\mathbf{t'}_{mp}^{-1} & \mathbf{t}_{mp} - \mathbf{r}_{mp}\mathbf{t'}_{mp}^{-1}\mathbf{r'}_{mp} \end{bmatrix} = \begin{bmatrix} \mathbf{t'}_{mn}^{-1} & -\mathbf{t'}_{mn}^{-1}\mathbf{r'}_{mn} \\ \mathbf{r}_{mn}\mathbf{t'}_{mn}^{-1} & \mathbf{t}_{mn} - \mathbf{r}_{mn}\mathbf{t'}_{mn}^{-1}\mathbf{r'}_{mn} \end{bmatrix} \begin{bmatrix} \mathbf{t'}_{np}^{-1} & -\mathbf{t'}_{np}^{-1}\mathbf{r'}_{np} \\ \mathbf{r}_{np}\mathbf{t'}_{np}^{-1} & \mathbf{t}_{np} - \mathbf{r}_{np}\mathbf{t'}_{np}^{-1}\mathbf{r'}_{np} \end{bmatrix}. \tag{2.30}$$

Performing multiplication on the right-hand side and comparing both sides block-wise we obtain

$$\mathbf{t'}_{mp} = \mathbf{t'}_{np}(\mathbf{1} - \mathbf{r'}_{mn}\mathbf{r}_{np})^{-1}\mathbf{t'}_{mn}, \tag{2.31a}$$

$$\mathbf{r'}_{mp} = \mathbf{r'}_{np} + \mathbf{t'}_{np}(\mathbf{1} - \mathbf{r'}_{mn}\mathbf{r}_{np})^{-1}\mathbf{r'}_{mn}\mathbf{t}_{np}, \tag{2.31b}$$

$$\mathbf{t}_{mp} = \mathbf{t}_{mn}(\mathbf{1} - \mathbf{r}_{np}\mathbf{r'}_{mn})^{-1}\mathbf{t}_{np}, \tag{2.31c}$$

$$\mathbf{r}_{mp} = \mathbf{r}_{mn} + \mathbf{t}_{mn}\mathbf{r}_{np}(\mathbf{1} - \mathbf{r'}_{mn}\mathbf{r}_{np})^{-1}\mathbf{t'}_{mn}. \tag{2.31d}$$

The following factors appearing throughout (2.31) deserve special notation

$$\overrightarrow{\mathbf{r}}_n \equiv (\mathbf{1} - \mathbf{r'}_{mn}\mathbf{r}_{np})^{-1}, \qquad \overleftarrow{\mathbf{r}}_n \equiv (\mathbf{1} - \mathbf{r}_{np}\mathbf{r'}_{mn})^{-1}, \tag{2.32}$$

where $\overrightarrow{\mathbf{r}}_n$, $\overleftarrow{\mathbf{r}}_n$, as will now be shown, stand for the sums of consecutive reflections within layer n contributed by electrons moving in the left-to-right and right-to-left directions, respectively. Defining the *strength of confinement* in layer n through expression $\|\mathbf{r'}_{mn}\mathbf{r}_{np}\|_{\mathrm{F}}$ (where $\|.\|_{\mathrm{F}}$ is the Frobenius norm, defined for matrix $\mathbf{A}$ as $\|\mathbf{A}\|_{\mathrm{F}} = \sqrt{\mathrm{tr}\,(\mathbf{A}\mathbf{A}^{\dagger})}$, we can expand (2.32) for $\|\mathbf{r'}_{mn}\mathbf{r}_{np}\|_{\mathrm{F}} < 1$ as follows [47]:

$$\begin{aligned} \overrightarrow{\mathbf{r}}_n &= \mathbf{1} + \mathbf{r'}_{mn}\mathbf{r}_{np} + \mathbf{r'}_{mn}\mathbf{r}_{np}\mathbf{r'}_{mn}\mathbf{r}_{np} + \ldots, \\ \overleftarrow{\mathbf{r}}_n &= \mathbf{1} + \mathbf{r}_{np}\mathbf{r'}_{mn} + \mathbf{r}_{np}\mathbf{r'}_{mn}\mathbf{r}_{np}\mathbf{r'}_{mn} + \ldots. \end{aligned} \tag{2.33}$$

The physical meaning of (2.33) is the summation over consecutive reflections undergone by electrons between layers m and p. This process can be interpreted as summing over the Feynman paths [10], as shown schematically in Figure 2.13. In the following chapters we will be dealing with multilayer structures with layers numbered from 1 through to N. The layers may be of non-magnetic (NM) or ferromagnetic (FM) nature, and will typically appear in the interleaving

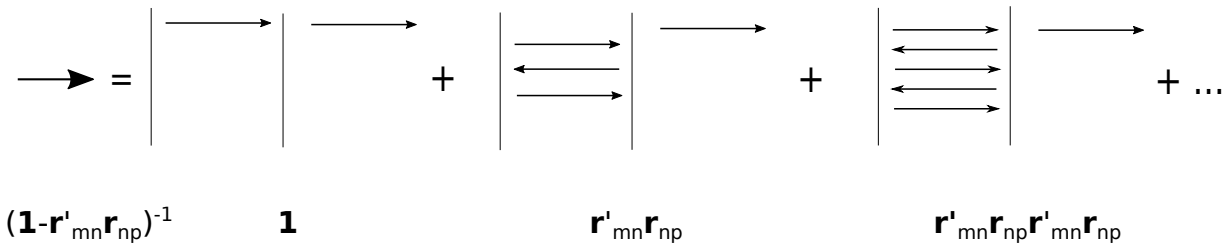

Figure 2.13: Summing over consecutive reflections within a layer.

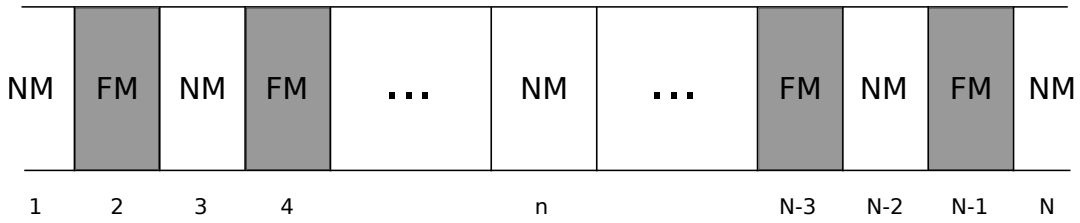

Figure 2.14: Schematic of a general multilayer CPP structure with alternating non-magnetic (NM) ferromagnetic (FM) layers. Layers labelled 1 and N represent the left and right semi-infinite non-magnetic leads, respectively.

order, as shown in Figure 2.14. Layers 1 and N correspond to the left and right semi-infinite NM leads, respectively. We will be interested in what happens in some NM layer indexed n, $1 < n < N$. When counting reflection in layer n we will need to account for electrons escaping into both of the neighbouring layers, undergoing multiple reflections there and coming back. The recursive property of the transfer matrix method suggests that in this case we must replace reflection matrices between adjacent layers with those calculated across all layers up until the leads. Thus, the summation goes as follows

$$\overrightarrow{\mathbf{r}}_n = \mathbf{1} + \mathbf{r'}_{1n}\mathbf{r}_{nN} + \mathbf{r'}_{1n}\mathbf{r}_{nN}\mathbf{r'}_{1n}\mathbf{r}_{nN} + \cdots = \left(\mathbf{1} - \mathbf{r'}_{1n}\mathbf{r}_{nN}\right)^{-1}, \tag{2.34a}$$

$$\overleftarrow{\mathbf{r}}_n = \mathbf{1} + \mathbf{r}_{nN}\mathbf{r'}_{1n} + \mathbf{r}_{nN}\mathbf{r'}_{1n}\mathbf{r}_{nN}\mathbf{r'}_{1n} + \cdots = \left(\mathbf{1} - \mathbf{r}_{nN}\mathbf{r'}_{1n}\right)^{-1}. \tag{2.34b}$$

We can derive (2.34) in a more systematic way, using the transfer matrix composition law. Indeed, consider $\mathbf{T}_{1N}$ containing the information about transmission across the entire structure. By (2.29) we can write

$$\mathbf{T}_{1N} = \mathbf{T}_{1n}\mathbf{T}_{nN}. \tag{2.35}$$

From (2.31a) we find the left-to-right transmission across the entire system

$$\mathbf{t'}_{1N} = \mathbf{t'}_{nN} \left(\mathbf{1} - \mathbf{r'}_{1n}\mathbf{r}_{nN}\right)^{-1} \mathbf{t'}_{1n}. \tag{2.36}$$

Now $\mathbf{t'}_{nN}$ describes the transmission from layer n through to N, whereas $\left(\mathbf{1} - \mathbf{r'}_{1n}\mathbf{r}_{nN}\right)^{-1} \mathbf{t'}_{1n}$ accounts for the total transmitted amplitude of right-moving electrons into layer n. We denote this part of transmission, due to the *left-incident* electrons, $\overrightarrow{\mathbf{a}}_n$. According to (2.14), wave function in the layer consists of the right-moving and the left-moving parts. Having accounted for the right-moving amplitude through $\overrightarrow{\mathbf{a}}_n$ we find the left-moving part denoted $\overrightarrow{\mathbf{b}}_n$ simply factoring in one more reflection $\mathbf{r}_{nN}$ off the part of the structure to the right of layer n. Finally, we obtain

$$\overrightarrow{\mathbf{a}}_n = \left(\mathbf{1} - \mathbf{r'}_{1n}\mathbf{r}_{nN}\right)^{-1} \mathbf{t'}_{1n}, \qquad \overrightarrow{\mathbf{b}}_n = \mathbf{r}_{nN}\overrightarrow{\mathbf{a}}_n. \tag{2.37}$$

Thus if an electron incident from the left has amplitude $\overrightarrow{\boldsymbol{\alpha}}_0$ then after scattering the total right- and left-propagating states in the non-magnetic layer n are related to $\overrightarrow{\boldsymbol{\alpha}}_0$ as follows

$$\overrightarrow{\boldsymbol{\alpha}_n} = \overrightarrow{\mathbf{a}}_n \overrightarrow{\boldsymbol{\alpha}}_0 \qquad \overrightarrow{\boldsymbol{\beta}_n} = \overrightarrow{\mathbf{b}}_n \overrightarrow{\boldsymbol{\alpha}}_0 \tag{2.38}$$

A similar argument, using (2.34b), leads us to defining $\overleftarrow{\mathbf{a}}_n$ and $\overleftarrow{\mathbf{b}}_n$, representing the total left- and right-moving waves contributed by the *right-incident* electrons.

$$\overleftarrow{\mathbf{b}}_n = \left(\mathbf{1} - \mathbf{r}_{nN}\mathbf{r'}_{1n}\right)^{-1} \mathbf{t}_{nN}, \qquad \overleftarrow{\mathbf{a}}_n = \mathbf{r'}_{1n}\overleftarrow{\mathbf{b}}_n. \tag{2.39}$$

This concludes the discussion of the general transfer matrix formalism. We have already found, based on the example of counting reflections in a multilayer, that it provides a convenient framework for computations while keeping the apparent connection to the underlying physics. In the following section we will finally introduce spin current, before proceeding to apply the transfer matrix to study its properties within the setting of a particular device geometry.

2.6 Spin Current

In this section we define spin current that will take the central role in later chapters. We describe some of its important mathematical properties and connect the definition with the transfer matrix method introduced the previous section.

Spin current characterises the flow of spin in a medium. Since electrons carry spin in the same sense as they carry charge, a flow of electrons necessarily creates a flow of spin. Motivation for the definition of spin current comes from generalisation of the more familiar charge current, which is especially clear in the context of charge and spin conservation, respectively. Classically, the flow of charge is described by the following equation

$$\int_V \frac{\partial \rho}{\partial t} \mathrm{d}\bar{r} = -\int_{\partial V} \bar{j}_0 \cdot \mathrm{d}\bar{s}, \tag{2.40}$$

Where ρ is the charge density, $\bar{j}_0$ is the charge current density (in 3D), for some charge contained in a closed region of space V with surface ∂V. Applying the divergence theorem to (2.40) we obtain

$$\frac{\partial \rho}{\partial t} + \nabla \bar{j}_0 = 0. \tag{2.41}$$

Spin current density $\bar{j}_\nu$ where $\nu = \{x, y, z\}$ can be introduced via an equation analogous to (2.41). For clarity, since we are temporarily considering the 3-dimensional case, we will conduct the argument in components in the spin projection index ν. Recall that the spin density operator in the single-particle case is defined as follows

$$\hat{\rho}_\nu^{(s)} = \frac{\hbar}{2} \boldsymbol{\psi}^\dagger \boldsymbol{\sigma}_\nu \boldsymbol{\psi} \tag{2.42}$$

Differentiating $\hat{\rho}_\nu^{(s)}$ with respect to time and using the Pauli equation (2.2) with $\hat{\mathcal{H}} = \hat{\mathcal{H}}_0 + \hat{\mathcal{H}}_\mathrm{Z}$, as defined in (2.3), (2.4) we obtain

$$\begin{aligned} \frac{\partial}{\partial t} \hat{\rho}_\nu^{(s)} &= -\frac{\hbar^2}{4m\mathrm{i}} \left(\boldsymbol{\psi}^\dagger \boldsymbol{\sigma}_\nu \nabla^2 \boldsymbol{\psi} - \nabla^2 \boldsymbol{\psi}^\dagger \boldsymbol{\sigma}_\nu \boldsymbol{\psi} \right) + \frac{1}{2\mathrm{i}} \boldsymbol{\psi}^\dagger \left[\boldsymbol{\sigma}_\nu, \mathbf{v} \right] \boldsymbol{\psi} \\ &= -\frac{\hbar^2}{4m\mathrm{i}} \nabla \left(\boldsymbol{\psi}^\dagger \boldsymbol{\sigma}_\nu \nabla \boldsymbol{\psi} - \nabla \boldsymbol{\psi}^\dagger \boldsymbol{\sigma}_\nu \boldsymbol{\psi} \right) + \frac{1}{2\mathrm{i}} \boldsymbol{\psi}^\dagger \left[\boldsymbol{\sigma}_\nu, \mathbf{v} \right] \boldsymbol{\psi} \end{aligned} \tag{2.43}$$

In a non-magnetic medium in the absence of exchange splitting potential $\mathbf{v}$, as defined in (2.6), has the form $\mathrm{diag}[V, V]$, and the second term on the right in (2.43) vanishes. We thus obtain a continuity equation

$$\frac{\partial}{\partial t}\hat{\rho}_{\nu}^{(s)} + \nabla \bar{j}_{\nu} = 0 \tag{2.44}$$

where

$$\bar{j}_{\nu} = \frac{\hbar^2}{4m\mathrm{i}} \left(\boldsymbol{\psi}^{\dagger} \boldsymbol{\sigma}_{\nu} \nabla \boldsymbol{\psi} - \nabla \boldsymbol{\psi}^{\dagger} \boldsymbol{\sigma}_{\nu} \boldsymbol{\psi} \right) \tag{2.45}$$

is the sought expression for spin current density. Equations (2.44) and (2.45) represent the only point in the scope of this work where we use vector notation for spin current density to mean the dependence on 3 dimensions in the real space. From this point on, following the discussion in Section 2.3, we only work with the part of the wave function dependent on one spatial dimension. Therefore $\bar{j}$ shall always mean a vector whose components correspond to the 3 spatial projections of spin. By (2.14) wave function has the form $\boldsymbol{\psi} = \boldsymbol{\alpha} e^{iky} + \boldsymbol{\beta} e^{-iky}$. Assuming $k \in \mathbb{R}_+$ (conducting medium), equation (2.45) can then be written in terms of amplitudes

$$\bar{j} = k \left(\boldsymbol{\alpha}^{\dagger} \bar{\boldsymbol{\sigma}} \boldsymbol{\alpha} - \boldsymbol{\beta}^{\dagger} \bar{\boldsymbol{\sigma}} \boldsymbol{\beta} \right). \tag{2.46}$$

In order to apply the transfer matrix to spin current we would like to switch from amplitudes to the language of transmission matrices developed in Section 2.5.1. In order to do that we shall distinguish, in addition to the left- and right-propagating waves, contributions from the up- and down-polarised electrons. Let $|\uparrow\rangle = [1 \quad 0]^T$ be the up-spin polarised state incident from the left. Then from (2.38) and (2.45) we deduce that

$$|\boldsymbol{\alpha}\rangle = \overrightarrow{\mathbf{a}} \, |\uparrow\rangle \qquad |\boldsymbol{\beta}\rangle = \overrightarrow{\mathbf{b}} \, |\uparrow\rangle .$$

Therefore the contribution to current density from this state $\overrightarrow{\bar{j}}^{\uparrow}$ is expressed as follows

$$\overrightarrow{\bar{j}}^{\uparrow} = \left\langle \uparrow \middle| \, \bar{\mathbf{j}} \, \middle| \uparrow \right\rangle = k \left(\langle \uparrow | \, \overrightarrow{\mathbf{a}}^{\dagger} \bar{\boldsymbol{\sigma}} \, \overrightarrow{\mathbf{a}} \, | \uparrow \rangle - \langle \uparrow | \, \overrightarrow{\mathbf{b}}^{\dagger} \bar{\boldsymbol{\sigma}} \, \overrightarrow{\mathbf{b}} \, | \uparrow \rangle \right). \tag{2.47}$$

Starting from the down-spin polarised state $|\downarrow\rangle = [0 \quad 1]^T$ we can obtain a similar expression for the corresponding contribution $\overrightarrow{\bar{j}}^{\uparrow} = \left\langle \uparrow \middle| \, \bar{\mathbf{j}} \, \middle| \uparrow \right\rangle$. Now adding both contributions, denoting

$\overrightarrow{\bar{j}} = \overrightarrow{\bar{j}}^{\uparrow} + \overrightarrow{\bar{j}}^{\downarrow}$, we find

$$\overrightarrow{\bar{j}} = k\left(\langle\uparrow|\,\overrightarrow{\mathbf{a}}^{\dagger}\bar{\boldsymbol{\sigma}}\,\overrightarrow{\mathbf{a}}\,|\uparrow\rangle + \langle\downarrow|\,\overrightarrow{\mathbf{a}}^{\dagger}\bar{\boldsymbol{\sigma}}\,\overrightarrow{\mathbf{a}}\,|\downarrow\rangle\right) - k\left(\langle\uparrow|\,\overrightarrow{\mathbf{b}}^{\dagger}\bar{\boldsymbol{\sigma}}\,\overrightarrow{\mathbf{b}}\,|\uparrow\rangle + \langle\downarrow|\,\overrightarrow{\mathbf{b}}^{\dagger}\bar{\boldsymbol{\sigma}}\,\overrightarrow{\mathbf{b}}\,|\downarrow\rangle\right) \tag{2.48}$$

Using the fact that $\langle\uparrow|\,\mathbf{z}\,|\uparrow\rangle + \langle\downarrow|\,\mathbf{z}\,|\downarrow\rangle = \mathrm{tr}\,\{\mathbf{z}\}$ for an arbitrary 2×2 matrix $\mathbf{z}$, summing over the up- and down-polarised states can be expressed as taking the trace

$$\overrightarrow{\bar{j}} = k\,\mathrm{tr}\left\{\overrightarrow{\mathbf{a}}^{\dagger}\bar{\boldsymbol{\sigma}}\,\overrightarrow{\mathbf{a}} - \overrightarrow{\mathbf{b}}^{\dagger}\bar{\boldsymbol{\sigma}}\,\overrightarrow{\mathbf{b}}\right\}, \tag{2.49}$$

where the difference under the trace is between the terms representing the right- and left-moving current, respectively. Using the circular property of the trace we can write (2.49) as follows

$$\overrightarrow{\bar{j}} = k\,\mathrm{tr}\left\{\left(\overrightarrow{\mathbf{a}}\,\overrightarrow{\mathbf{a}}^{\dagger} - \overrightarrow{\mathbf{b}}\,\overrightarrow{\mathbf{b}}^{\dagger}\right)\bar{\boldsymbol{\sigma}}\right\}. \tag{2.50}$$

Denoting

$$\overrightarrow{\mathbf{m}} = \overrightarrow{\mathbf{a}}\,\overrightarrow{\mathbf{a}}^{\dagger} - \overrightarrow{\mathbf{b}}\,\overrightarrow{\mathbf{b}}^{\dagger} \tag{2.51}$$

we can write (2.50) in a more compact form

$$\overrightarrow{\bar{j}} = k\,\mathrm{tr}\left\{\overrightarrow{\mathbf{m}}\bar{\boldsymbol{\sigma}}\right\} \tag{2.52}$$

Finally, adding contribution from the right-incident electrons $\overleftarrow{\bar{j}}$ obtained in a similar way, denoting $\bar{j} = \overrightarrow{\bar{j}} + \overleftarrow{\bar{j}}$ and introducing the *total transmission* $\mathbf{m} = \overrightarrow{\mathbf{m}} + \overleftarrow{\mathbf{m}}$ we can write

$$\bar{j} = k\,\mathrm{tr}\,\{\mathbf{m}\bar{\boldsymbol{\sigma}}\}. \tag{2.53}$$

We have derived the expression for spin current density up to (2.44) exploiting the analogy with charge current. Furthermore, if we define $\boldsymbol{\sigma}_0 = \frac{2e}{\hbar}\mathbf{1}$ and write $\bar{\bar{\boldsymbol{\sigma}}} = (\boldsymbol{\sigma}_0, \bar{\boldsymbol{\sigma}})$ for a 4-tuple of $\boldsymbol{\sigma}_0$ and the components of $\bar{\boldsymbol{\sigma}}$ we can have charge current included as a special case and write the 4-component current density $\bar{\bar{j}}$ as follows

$$\bar{\bar{j}} = k\,\mathrm{tr}\,\{\mathbf{m}'\bar{\bar{\boldsymbol{\sigma}}}\}, \tag{2.54}$$

where the prime signifies that we include the transmission matrix of the charge current component. Some general conclusions can be immediately drawn from (2.53). Based on the fact that any complex 2×2 matrix admits a unique expansion in terms of the identity matrix and the Pauli matrices [48] we can write

$$\mathbf{m}' = \sum_{\nu \in \{0,x,y,z\}} u_\nu \boldsymbol{\sigma}_\nu, \tag{2.55}$$

where the expansion coefficients are found from the relation

$$u_\nu = \frac{1}{2} \operatorname{tr} \{\mathbf{m}' \boldsymbol{\sigma}_\nu\} \tag{2.56}$$

Therefore, current density components up to a factor of $\frac{1}{2k}$, are the expansion coefficients of the transmission matrix in (2.55). Of particular interest here is the out-of-plane component $\nu = y$. Since only $\boldsymbol{\sigma}_y$ is pure imaginary, we deduce that $\mathbf{m}$ cannot be purely real for the out-of-plane component to exist (expansion coefficients (2.56) are in general complex, but current components are real). Another observation we can make is that current density does not depend on the direction of polarisation of incident electrons. Indeed, if we replace $|\sigma\rangle$, where $\sigma = \uparrow, \downarrow$ with $\mathbf{s}(\theta)\,|\sigma\rangle$ where $\mathbf{s}(\theta)$ is the spin rotation matrix (2.9), then following (2.49) and, noting that $\langle\sigma|$ is replaced with $\langle\sigma|\,\mathbf{s}(-\theta)$, we see that the rotation gets cancelled by virtue of the circular property of the trace.

Our discussion so far has been centred on current density. We shall now introduce the physically significant concept of *current*. In order to understand how current is obtained from density, note that in the calculations leading up to (2.46) and (2.53) we implicitly assumed that the wave functions are evaluated at a particular point in momentum space. More specifically, in order to evaluate the current density we must pick the values of the in-plane momentum $\bar{k}_\parallel = (k_x, k_z)$. Now recall that in the Landauer model we assume that electrons arrive from macroscopic reservoirs at all possible in-plane momenta and energies up to the Fermi level E_F. Electron distribution in the reservoirs, given the electrostatic potential μ and temperature T,

are characterised by the Fermi function

$$f(E,\mu,T)=\frac{1}{e^{(E-\mu)/k_{\mathrm{B}}T}+1}. \tag{2.57}$$

where k_{B} is the Boltzmann's constant. Let μ_L and μ_R be the chemical potentials in the left and right reservoirs, respectively, and denote $f_L \equiv f(E-\mu_L)$ and $f_R \equiv f(E-\mu_R)$. We further assume that μ_L and μ_R are displaced by an infinitesimal bias $\mu_L - \mu_R = eV_b$. This assumption has to do with the fact that we will be dealing with conducting systems. It is practically challenging to maintain a finite bias across a nano-scale conductor. Since the bias is infinitesimal, it will also be ignored when calculating one-electron states from the Schrödinger equation. Finally, the incident electrons arrive at either of the possible spin projection with respect to the chosen spin quantisation axis. Note that, as demonstrated in the previous paragraph, the result does not depend on the choice of the axis. It follows that the value of current is found by adding the contributions from all (equally) possible electron states arriving into the system, that is integrating over in-plane momentum and energy, and summing over spin projections

$$J_\nu=\int_{\mathrm{BZ}_1}\mathrm{d}\bar{k}_\parallel\int_{-\infty}^{+\infty}\mathrm{d}E\,D(E)\left(f_L\overrightarrow{j}_\nu+f_R\overleftarrow{j}_\nu\right), \tag{2.58}$$

where $D(E)$ is the density of states, the integration is, in general, carried out over the first Brillouin zone BZ_1. In the parabolic band this will mean integrating over $0\le|\bar{k}_\parallel|\le k_{\mathrm{F}}$ where $k_{\mathrm{F}}=\sqrt{2mE_{\mathrm{F}}}/\hbar$ is the Fermi wave vector. In the analytic calculations we will additionally assume in-plane rotational symmetry, so that the integral can be done in polar coordinates. From (2.58), after symmetrising over the Fermi functions, we can extract two important constituents of spin current. These are the the "static" or *exchange* current J_ν^{ex} and the bias-driven *transport* current J_ν^{tr} defined as follows

$$\begin{aligned}
J_\nu &= J_\nu^{\mathrm{ex}}+J_\nu^{\mathrm{tr}}\\
J_\nu^{\mathrm{ex}} &= \frac{1}{2}\int_{\mathrm{BZ}_1}\mathrm{d}\bar{k}_\parallel\int_{-\infty}^{-\infty}\mathrm{d}E\,D(E)\left[\left(f_L+f_R\right)\left(\overrightarrow{j}_\nu+\overleftarrow{j}_\nu\right)\right]\\
J_\nu^{\mathrm{tr}} &= \frac{1}{2}\int_{\mathrm{BZ}_1}\mathrm{d}\bar{k}_\parallel\int_{-\infty}^{-\infty}\mathrm{d}E\,D(E)\left[\left(f_L-f_R\right)\left(\overrightarrow{j}_\nu-\overleftarrow{j}_\nu\right)\right].
\end{aligned} \tag{2.59}$$

An important feature of J_ν^{ex} is that it can exist in the absence of any bias. It contributes to interlayer exchange coupling discussed in Chapter 5. In fact, we will be able show using the Landauer method that $\overrightarrow{j}_\nu = -\overleftarrow{j}_\nu$ for $\nu = 0, x, z$, so J_ν^{ex} is comprised only of the out-of-plane component. On the other hand, J_ν^{tr}, in the case of an infinitesimal bias $f_L - f_R \sim -eV_b\delta(E-\mu)$, is proportional to V_b. It represents the net flow as the difference between the left- and right-propagating currents. Lastly, we remark that in this study we do not consider the temperature dependence explicitly, hence all the calculations are performed assuming $T = 0$.

This chapter concludes the introductory material required for the main discussion of this work. Equipped with the Landauer formalism and, having introduced spin current, we will now proceed to examine the properties of the latter in the setting of a particular device geometry.

Chapter 3

Symmetries and Oscillations of Spin Current

3.1 Spin Current in a Magnetic Multilayer

3.1.1 Introduction

In Chapter 2 we developed a general framework of the transfer matrix method without relying on a particular expression for the wave function. Here we will provide an implementation based on the solutions of (2.11) for a specific device model. Namely, we introduce the CPP-type (recall Figure 2.3) layered structure of the so-called *switching* geometry. It consists of a conducting non-magnetic slab, referred to as the spacer (S) placed between two ferromagnetic layers, as shown in Figure 3.1. The magnets to the left and right of the spacer are labelled as the polarising (PM) and the switching (SM) one, respectively. The system is connected to semi-infinite non-magnetic leads. The coordinate system is introduced in such a way that the y axis runs perpendicularly to the layer interfaces (out-of-plane direction), while the xz plane is parallel to the interfaces (in-plane). Magnetic moment of the PM is tilted in-plane at an angle to the z axis, and magnetisation of the SM is aligned with the z axis. Finally, we take the in-plane dimensions of the system to be much smaller than the out-of-plane ones. In other

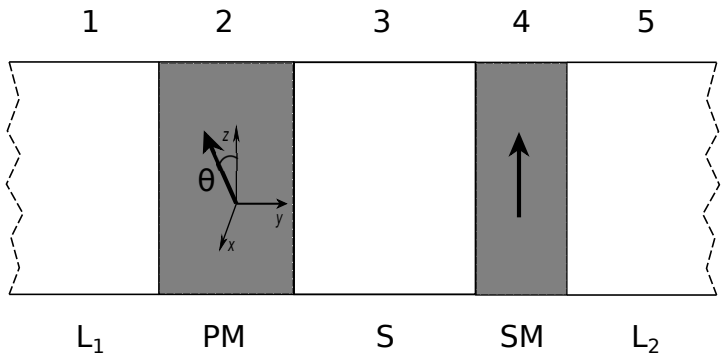

Figure 3.1: Schematic of the multilayer structure consisting of a non-magnetic spacer (S), sandwiched between polarising (PM) and switching (SM) magnets and connected to semi-infinite non-magnetic leads (L_1, L_2).

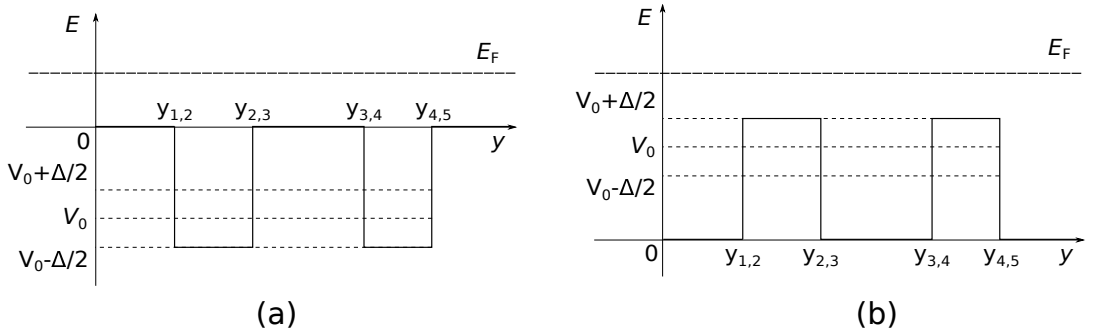

Figure 3.2: Potential profile of a multilayer in the presence of exchange splitting Δ: (a) double well and (b) double barrier. E_{F} shows the relative position of the Fermi level.

words, the structure is treated as a quasi-one-dimensional one. The motivation to study models such as this one stems from the discovery of current-induced excitation and even reversal (or *switching*) of magnetisation of magnetic layers separated by the spacer. This phenomenon was first predicted by Berger and Slonczewski [49], [50], and subsequently received experimental confirmation [51], [52]. When unpolarised electrons are injected into the left lead and pass through the PM their spins begin to precess around its magnetisation axis (recall the Larmor's theorem (2.17)). As will be seen later, this precession will give rise to spin polarisation and, consequently, spin current in the spacer. Absorption of the transverse component of this spin current by the SM is equivalent to the torque applied to its magnetic moment, and is what ultimately causes the switching. We will now derive the transfer matrix (2.27) explicitly by solving the Schrödinger's equation (2.11). For simplicity we assume that electrostatic potentials in the leads and the spacer are equal and set to 0, and denote the out-of-plane components of the wave vectors in those layers $k_1 = k_3 = k$. Further, without significant loss of generality,

we may assume that potentials and exchange splitting in both magnets are equal too, hence $k_2^{\uparrow,\downarrow} = k_4^{\uparrow,\downarrow} = k^{\uparrow,\downarrow}$. Let $y_{n,n+1}$ be the longitudinal coordinates of the interfaces between layers n and $n+1$ and set the origin at the first interface, so that $y_{1,2} = 0$. Note that the thicknesses of the PM, S and SM are generally taken to be different from each other. Figure 3.2 shows two typical examples of the potential profile we will be using in our model. We denote the the angle that the magnetic moment in layer n makes with z axis when rotated in xz plane θ. For non-magnetic layers we set $\theta_n = 0$ by convention. Matching the wave functions and their derivatives at the interfaces we obtain the following equations

$$\boldsymbol{\chi}_n(y_{n,n+1}) = \boldsymbol{\chi}_{n+1}(y_{n,n+1}), \qquad \frac{\mathrm{d}}{\mathrm{d}y}\boldsymbol{\chi}_n(y_{n,n+1}) = \frac{\mathrm{d}}{\mathrm{d}y}\boldsymbol{\chi}_{n+1}(y_{n,n+1}). \tag{3.1}$$

Writing (3.1) explicitly in terms of (2.12) we find

$$\begin{aligned}
&\mathbf{s}^{-1}(\theta_n)\begin{bmatrix}\alpha_n^{\uparrow}e^{\mathrm{i}k_n^{\uparrow}y_{n,n+1}}\\ \alpha_n^{\downarrow}e^{\mathrm{i}k_n^{\downarrow}y_{n,n+1}}\end{bmatrix} + \mathbf{s}^{-1}(\theta_n)\begin{bmatrix}\beta_n^{\uparrow}e^{-\mathrm{i}k_n^{\uparrow}y_{n,n+1}}\\ \beta_n^{\downarrow}e^{-\mathrm{i}k_n^{\downarrow}y_{n,n+1}}\end{bmatrix} \qquad (3.2a)\\
&= \mathbf{s}^{-1}(\theta_{n+1})\begin{bmatrix}\alpha_{n+1}^{\uparrow}e^{\mathrm{i}k_{n+1}^{\uparrow}y_{n,n+1}}\\ \alpha_{n+1}^{\downarrow}e^{\mathrm{i}k_{n+1}^{\downarrow}y_{n,n+1}}\end{bmatrix} + \mathbf{s}^{-1}(\theta_{n+1})\begin{bmatrix}\beta_{n+1}^{\uparrow}e^{-\mathrm{i}k_{n+1}^{\uparrow}y_{n,n+1}}\\ \beta_{n+1}^{\downarrow}e^{-\mathrm{i}k_{n+1}^{\downarrow}y_{n,n+1}}\end{bmatrix}\\
&\mathbf{s}^{-1}(\theta_n)\begin{bmatrix}\mathrm{i}k_n^{\uparrow}\alpha_n^{\uparrow}e^{\mathrm{i}k_n^{\uparrow}y_{n,n+1}}\\ \mathrm{i}k_n^{\downarrow}\alpha_n^{\downarrow}e^{\mathrm{i}k_n^{\downarrow}y_{n,n+1}}\end{bmatrix} + \mathbf{s}^{-1}(\theta_n)\begin{bmatrix}-\mathrm{i}k_n^{\uparrow}\beta_n^{\uparrow}e^{-\mathrm{i}k_n^{\uparrow}y_{n,n+1}}\\ -\mathrm{i}k_n^{\downarrow}\beta_n^{\downarrow}e^{-\mathrm{i}k_n^{\downarrow}y_{n,n+1}}\end{bmatrix}\\
&= \mathbf{s}^{-1}(\theta_{n+1})\begin{bmatrix}\mathrm{i}k_{n+1}^{\uparrow}\alpha_{n+1}^{\uparrow}e^{\mathrm{i}k_{n+1}^{\uparrow}y_{n,n+1}}\\ \mathrm{i}k_{n+1}^{\downarrow}\alpha_{n+1}^{\downarrow}e^{\mathrm{i}k_{n+1}^{\downarrow}y_{n,n+1}}\end{bmatrix} + \mathbf{s}^{-1}(\theta_{n+1})\begin{bmatrix}-\mathrm{i}k_{n+1}^{\uparrow}\beta_{n+1}^{\uparrow}e^{-\mathrm{i}k_{n+1}^{\uparrow}y_{n,n+1}}\\ -\mathrm{i}k_{n+1}^{\downarrow}\beta_{n+1}^{\downarrow}e^{-\mathrm{i}k_{n+1}^{\downarrow}y_{n,n+1}}\end{bmatrix}. \qquad (3.2b)
\end{aligned}$$

The structure of (3.2) will become clearer if we factor out the coefficients

$$\mathbf{s}^{-1}(\theta_n)\left\{\begin{bmatrix} e^{\mathrm{i}k_n^{\uparrow}y_{n,n+1}} & 0 \\ 0 & e^{\mathrm{i}k_n^{\downarrow}y_{n,n+1}} \end{bmatrix}\begin{bmatrix}\alpha_n^{\uparrow}\\ \alpha_n^{\downarrow}\end{bmatrix} + \begin{bmatrix} e^{-\mathrm{i}k_n^{\uparrow}y_{n,n+1}} & 0 \\ 0 & e^{-\mathrm{i}k_n^{\downarrow}y_{n,n+1}} \end{bmatrix}\begin{bmatrix}\beta_n^{\uparrow}\\ \beta_n^{\downarrow}\end{bmatrix}\right\} \tag{3.3a}$$
$$= \mathbf{s}^{-1}(\theta_{n+1})\left\{\begin{bmatrix} e^{\mathrm{i}k_{n+1}^{\uparrow}y_{n,n+1}} & 0 \\ 0 & e^{\mathrm{i}k_{n+1}^{\downarrow}y_{n,n+1}} \end{bmatrix}\begin{bmatrix}\alpha_{n+1}^{\uparrow}\\ \alpha_{n+1}^{\downarrow}\end{bmatrix} + \begin{bmatrix} e^{-\mathrm{i}k_{n+1}^{\uparrow}y_{n,n+1}} & 0 \\ 0 & e^{-\mathrm{i}k_{n+1}^{\downarrow}y_{n,n+1}} \end{bmatrix}\begin{bmatrix}\beta_{n+1}^{\uparrow}\\ \beta_{n+1}^{\downarrow}\end{bmatrix}\right\}$$

$$\mathbf{s}^{-1}(\theta_n)\left\{\begin{bmatrix} \mathrm{i}k_n^{\uparrow}e^{\mathrm{i}k_n^{\uparrow}y_{n,n+1}} & 0 \\ 0 & \mathrm{i}k_n^{\downarrow}e^{\mathrm{i}k_n^{\downarrow}y_{n,n+1}} \end{bmatrix}\begin{bmatrix}\alpha_n^{\uparrow}\\ \alpha_n^{\downarrow}\end{bmatrix}\right. \tag{3.3b}$$
$$\left. + \begin{bmatrix} -\mathrm{i}k_n^{\uparrow}e^{-\mathrm{i}k_n^{\uparrow}y_{n,n+1}} & 0 \\ 0 & -\mathrm{i}k_n^{\downarrow}e^{-\mathrm{i}k_n^{\downarrow}y_{n,n+1}} \end{bmatrix}\begin{bmatrix}\beta_n^{\uparrow}\\ \beta_n^{\downarrow}\end{bmatrix}\right\}$$
$$= \mathbf{s}^{-1}(\theta_{n+1})\left\{\begin{bmatrix} \mathrm{i}k_{n+1}^{\uparrow}e^{\mathrm{i}k_{n+1}^{\uparrow}y_{n,n+1}} & 0 \\ 0 & \mathrm{i}k_{n+1}^{\downarrow}e^{\mathrm{i}k_{n+1}^{\downarrow}y_{n,n+1}} \end{bmatrix}\begin{bmatrix}\alpha_{n+1}^{\uparrow}\\ \alpha_{n+1}^{\downarrow}\end{bmatrix}\right.$$
$$\left. + \begin{bmatrix} -\mathrm{i}k_{n+1}^{\uparrow}e^{-\mathrm{i}k_{n+1}^{\uparrow}y_{n,n+1}} & 0 \\ 0 & -\mathrm{i}k_{n+1}^{\downarrow}e^{-\mathrm{i}k_{n+1}^{\downarrow}y_{n,n+1}} \end{bmatrix}\begin{bmatrix}\beta_{n+1}^{\uparrow}\\ \beta_{n+1}^{\downarrow}\end{bmatrix}\right\}.$$

Now introducing the following notation

$$\mathbf{\Psi} = [\alpha_n^{\uparrow}, \alpha_n^{\downarrow}, \beta_n^{\uparrow}, \beta_n^{\downarrow}]^T, \quad \mathbf{S}(\theta) = \begin{bmatrix} \mathbf{s}(\theta) & 0 \\ 0 & \mathbf{s}(\theta) \end{bmatrix}, \tag{3.4}$$

we can write (3.3) in a compact form

$$\mathbf{S}(-\theta_n)\mathbf{X}(k_n^{\uparrow,\downarrow}, y_{n,n+1})\mathbf{\Psi}_n = \mathbf{S}(-\theta_{n+1})\mathbf{X}(k_{n+1}^{\uparrow,\downarrow}, y_{n,n+1})\mathbf{\Psi}_{n+1}, \tag{3.5}$$

where

$$\mathbf{X}(k^{\uparrow,\downarrow}, y) = \begin{bmatrix} e^{\mathrm{i}k^{\uparrow}y} & 0 & e^{-\mathrm{i}k^{\uparrow}y} & 0 \\ 0 & e^{\mathrm{i}k^{\downarrow}y} & 0 & e^{-\mathrm{i}k^{\downarrow}y} \\ \mathrm{i}k^{\uparrow}e^{\mathrm{i}k^{\uparrow}y} & 0 & -\mathrm{i}k^{\uparrow}e^{-\mathrm{i}k^{\uparrow}y} & 0 \\ 0 & \mathrm{i}k^{\downarrow}e^{\mathrm{i}k^{\downarrow}y} & 0 & -\mathrm{i}k^{\downarrow}e^{-\mathrm{i}k^{\downarrow}y} \end{bmatrix}. \tag{3.6}$$

Note that (3.6) can be factorised as follows

$$\mathbf{X} = \begin{bmatrix} \mathbf{e} & \mathbf{e}^{-1} \\ \mathrm{i}\mathbf{k}\mathbf{e} & -\mathrm{i}\mathbf{k}\mathbf{e}^{-1} \end{bmatrix} = \begin{bmatrix} \mathbf{1} & \mathbf{1} \\ \mathrm{i}\mathbf{k} & -\mathrm{i}\mathbf{k} \end{bmatrix} \begin{bmatrix} \mathbf{e} & \mathbf{0} \\ \mathbf{0} & \mathbf{e}^{-1} \end{bmatrix}, \tag{3.7}$$

where

$$\mathbf{e}\left(k^{\uparrow,\downarrow}, y\right) = \begin{bmatrix} e^{\mathrm{i}k^{\uparrow}y} & 0 \\ 0 & e^{\mathrm{i}k^{\downarrow}y} \end{bmatrix} \qquad \mathbf{k}\left(k^{\uparrow,\downarrow}\right) = \begin{bmatrix} k^{\uparrow} & 0 \\ 0 & k^{\downarrow} \end{bmatrix},$$

which is similar to the notation used by P. Bruno in [5], for the spinless case. Multiplying (3.5) on the right by $\mathbf{X}^{-1}(k_n^{\uparrow,\downarrow}, y_{n,n+1})\mathbf{S}(\theta_n)$ we obtain

$$\mathbf{\Psi}_n = \mathbf{X}^{-1}(k_n^{\uparrow,\downarrow}, y_{n,n+1})\mathbf{S}(\theta_n - \theta_{n+1})\mathbf{X}(k_{n+1}^{\uparrow,\downarrow}, y_{n,n+1})\mathbf{\Psi}_{n+1}. \tag{3.8}$$

We now define the *transfer matrix* $\mathbf{T}_{n,n+1}$ between two neighbouring layers as follows

$$\mathbf{T}_{n,n+1} = \mathbf{X}^{-1}(k_n^{\uparrow,\downarrow}, y_{n,n+1})\mathbf{S}(\theta_n - \theta_{n+1})\mathbf{X}(k_{n+1}^{\uparrow,\downarrow}, y_{n,n+1}), \tag{3.9}$$

so that the amplitude vectors in the neighbouring layers are related by a concise equation

$$\mathbf{\Psi}_n = \mathbf{T}_{n,n+1}\mathbf{\Psi}_{n+1}, \tag{3.10}$$

or, more generally and in accordance with (2.28), (2.29)

$$\mathbf{\Psi}_m = \mathbf{T}_{m,n}\mathbf{\Psi}_n, \tag{3.11}$$

for arbitrary layers $1 \leq m < n \leq N$, where N is the total number of layers ($N = 5$ in our case). We will now derive the expressions for transmission and reflection matrices (2.27) from (3.9). Inverting (3.7) we obtain

$$\mathbf{X}^{-1}(k^{\uparrow,\downarrow}, y) = \frac{1}{2}\begin{bmatrix} \mathbf{e}^{-1} & -\mathrm{i}\mathbf{e}^{-1}\mathbf{k}^{-1} \\ \mathbf{e} & \mathrm{i}\mathbf{e}\mathbf{k}^{-1} \end{bmatrix}. \tag{3.12}$$

In the following calculation we set $\theta_n = \theta_{n+1}$ for clarity, and discuss the dependence on polarisation later. We also suppress the explicit dependence on $y_{n,n+1}$. With the above considerations in mind we obtain

$$\begin{aligned}\mathbf{T}_{n,n+1} = \mathbf{X}^{-1}(k_n^{\uparrow,\downarrow})\mathbf{X}(k_{n+1}^{\uparrow,\downarrow}) &= \begin{bmatrix} \frac{1}{2}\mathbf{e}^{-1}(k_n^{\uparrow,\downarrow}) & -\frac{\mathrm{i}}{2}\mathbf{e}^{-1}(k_n^{\uparrow,\downarrow})\mathbf{k}^{-1}(k_n^{\uparrow,\downarrow}) \\ \frac{1}{2}\mathbf{e}(k_n^{\uparrow,\downarrow}) & -\frac{\mathrm{i}}{2}\mathbf{e}(k_n^{\uparrow,\downarrow})\mathbf{k}(k_n^{\uparrow,\downarrow})^{-1} \end{bmatrix} \\ &\times \begin{bmatrix} \mathbf{e}(k_{n+1}^{\uparrow,\downarrow}) & \mathbf{e}^{-1}(k_{n+1}^{\uparrow,\downarrow}) \\ \mathrm{i}\mathbf{k}(k_{n+1}^{\uparrow,\downarrow})\mathbf{e}(k_{n+1}^{\uparrow,\downarrow}) & -\mathrm{i}\mathbf{k}(k_{n+1}^{\uparrow,\downarrow})\mathbf{e}^{-1}(k_{n+1}^{\uparrow,\downarrow}) \end{bmatrix} \\ &= \begin{bmatrix} \frac{1}{2}\mathbf{k}\Big(\frac{k_{n+1}^{\uparrow,\downarrow}+k_n^{\uparrow,\downarrow}}{k_n^{\uparrow,\downarrow}}\Big)\mathbf{e}(k_{n+1}^{\uparrow,\downarrow}-k_n^{\uparrow,\downarrow}) & \frac{1}{2}\mathbf{k}\Big(\frac{-k_{n+1}^{\uparrow,\downarrow}+k_n^{\uparrow,\downarrow}}{k_n^{\uparrow,\downarrow}}\Big)\mathbf{e}(-k_{n+1}^{\uparrow,\downarrow}-k_n^{\uparrow,\downarrow}) \\ \frac{1}{2}\mathbf{k}\Big(\frac{-k_{n+1}^{\uparrow,\downarrow}+k_n^{\uparrow,\downarrow}}{k_n^{\uparrow,\downarrow}}\Big)\mathbf{e}(k_{n+1}^{\uparrow,\downarrow}+k_n^{\uparrow,\downarrow}) & \frac{1}{2}\mathbf{k}\Big(\frac{k_{n+1}^{\uparrow,\downarrow}+k_n^{\uparrow,\downarrow}}{k_n^{\uparrow,\downarrow}}\Big)\mathbf{e}(-k_{n+1}^{\uparrow,\downarrow}+k_n^{\uparrow,\downarrow}) \end{bmatrix}. \end{aligned} \tag{3.13}$$

Comparing (3.13) with (2.27) we can get the following expressions

$$\mathbf{t'}_{n,n+1} = 2\mathbf{k}\left(\frac{k_n^{\uparrow,\downarrow}}{k_{n+1}^{\uparrow,\downarrow}+k_n^{\uparrow,\downarrow}}\right)\mathbf{e}^{-1}(k_{n+1}^{\uparrow,\downarrow}-k_n^{\uparrow,\downarrow}), \tag{3.14a}$$

$$\mathbf{t}_{n,n+1} = 2\mathbf{k}\left(\frac{k_n^{\uparrow,\downarrow}}{k_{n+1}^{\uparrow,\downarrow}+k_n^{\uparrow,\downarrow}}\right)\mathbf{e}^{-1}(k_{n+1}^{\uparrow,\downarrow}-k_n^{\uparrow,\downarrow}), \tag{3.14b}$$

$$\mathbf{r'}_{n,n+1} = -\mathbf{k}\left(\frac{k_n^{\uparrow,\downarrow}-k_{n+1}^{\uparrow,\downarrow}}{k_n^{\uparrow,\downarrow}+k_{n+1}^{\uparrow,\downarrow}}\right)\mathbf{e}^{-1}(2k_{n+1}^{\uparrow,\downarrow}), \tag{3.14c}$$

$$\mathbf{r}_{n,n+1} = \mathbf{k}\left(\frac{k_n^{\uparrow,\downarrow}-k_{n+1}^{\uparrow,\downarrow}}{k_n^{\uparrow,\downarrow}+k_{n+1}^{\uparrow,\downarrow}}\right)\mathbf{e}(2k_n^{\uparrow,\downarrow}). \tag{3.14d}$$

We will now show how the angular dependence is taken into account when magnetic and non-magnetic layers are interleaved. The crucial observation here is that for non-magnetic layers all matrices in (3.14) are proportional to identity, and therefore commute with the rotation matrix. In particular, consider transmission from the left lead to the spacer (layer 1 to 3). From (2.29) we obtain

$$\mathbf{T}_{13} = \mathbf{T}_{12}\mathbf{T}_{23}. \tag{3.15}$$

Let $\theta_2 = \theta$. Bearing in mind that the lead and the spacer are non-magnetic ($\theta_1 = \theta_3 = 0$), and using (3.9) we find

$$\begin{aligned}\mathbf{T}_{12} &= \mathbf{X}^{-1}(k, y_{12})\mathbf{S}(0-\theta)\mathbf{X}(k_2^{\uparrow,\downarrow}, y_{12}) = \mathbf{S}(-\theta)\mathbf{X}^{-1}(k, y_{12})\mathbf{X}(k_2^{\uparrow,\downarrow}, y_{12}),\\ \mathbf{T}_{23} &= \mathbf{X}^{-1}(k_2^{\uparrow,\downarrow}, y_{23})\mathbf{S}(\theta-0)\mathbf{X}(k, y_{23}) = \mathbf{X}^{-1}(k_2^{\uparrow,\downarrow}, y_{23})\mathbf{X}(k, y_{23})\mathbf{S}(\theta).\end{aligned} \tag{3.16}$$

Therefore, the angular dependence of $\mathbf{T}_{13}$ is expressed as follows

$$\mathbf{T}_{13}(\theta) = \mathbf{S}(-\theta)\mathbf{T}_{13}(0)\mathbf{S}(\theta). \tag{3.17}$$

By means of block multiplication, it can be shown that similar relations hold for transmission and reflection submatrices, in particular

$$\mathbf{t'}_{13}(\theta) = \mathbf{s}(-\theta)\mathbf{t'}_{13}(0)\mathbf{s}(\theta). \tag{3.18}$$

We finish this section by establishing some important algebraic relations between the transmission and reflection matrices following from conservation of the charge current. This time we consider the general case, and do not make any assumptions about whether the layers spanned are magnetic or not, nor about the polarisation angles. Hence, in general none of $\mathbf{t'}$, $\mathbf{t}$, $\mathbf{r'}$, $\mathbf{r}$ commute. The requirement that the charge current between two conducting layers m and n is conserved can be stated in terms of amplitudes as follows

$$\sum_{\nu=\uparrow,\downarrow} k_m^\nu(|\boldsymbol{\alpha}_m^\nu|^2 - |\boldsymbol{\beta}_m^\nu|^2) = \sum_{\nu=\uparrow,\downarrow} k_n^\nu(|\boldsymbol{\alpha}_n^\nu|^2 - |\boldsymbol{\beta}_n^\nu|^2). \tag{3.19}$$

Defining $\mathbf{K} = \mathrm{diag}\,[k^\uparrow, k^\downarrow, -k^\uparrow, -k^\downarrow]$ and recalling the notation of (3.4) we can write (3.19) in a compact form

$$\boldsymbol{\Psi}_m^\dagger \mathbf{K}_m \boldsymbol{\Psi}_m = \boldsymbol{\Psi}_n^\dagger \mathbf{K}_n \boldsymbol{\Psi}_n. \tag{3.20}$$

Now using (3.11) we obtain

$$\boldsymbol{\Psi}_n^\dagger \mathbf{T}_{mn}^\dagger \mathbf{K}_m \mathbf{T}_{mn} \boldsymbol{\Psi}_n = \boldsymbol{\Psi}_n^\dagger \mathbf{K}_n \boldsymbol{\Psi}_n. \tag{3.21}$$

Since $\mathbf{\Psi}_n$ is chosen arbitrarily, we deduce

$$\mathbf{T}^{\dagger}_{mn}\mathbf{K}_m\mathbf{T}_{mn} = \mathbf{K}_n. \tag{3.22}$$

Taking the Hermitian conjugate of (2.27) we obtain

$$\mathbf{T}^{\dagger} = \begin{bmatrix} \mathbf{t'}^{\dagger\,-1}_{mn} & \mathbf{t'}^{\dagger\,-1}_{mn}\mathbf{r}^{\dagger}_{mn} \\ -\mathbf{r'}^{\dagger}_{mn}\mathbf{t'}^{\dagger\,-1}_{mn} & \mathbf{t}^{\dagger}_{mn} - \mathbf{r'}^{\dagger}_{mn}\mathbf{t'}^{\dagger\,-1}_{mn}\mathbf{r}^{\dagger}_{mn} \end{bmatrix}. \tag{3.23}$$

Substituting (3.23) into (3.22) we find

$$\begin{bmatrix} \mathbf{t'}^{\dagger\,-1}_{mn} & \mathbf{t'}^{\dagger\,-1}_{mn}\mathbf{r}^{\dagger}_{mn} \\ -\mathbf{r'}^{\dagger}_{mn}\mathbf{t'}^{\dagger\,-1}_{mn} & \mathbf{t}^{\dagger}_{mn} - \mathbf{r'}^{\dagger}_{mn}\mathbf{t'}^{\dagger\,-1}_{mn}\mathbf{r}^{\dagger}_{mn} \end{bmatrix} \begin{bmatrix} \mathbf{k}_n & \mathbf{0} \\ \mathbf{0} & -\mathbf{k}_n \end{bmatrix} \begin{bmatrix} \mathbf{t'}^{-1}_{mn} & -\mathbf{t'}^{-1}_{mn}\mathbf{r'}_{mn} \\ \mathbf{r}_{mn}\mathbf{t'}^{-1}_{mn} & \mathbf{t}_{mn} - \mathbf{r}_{mn}\mathbf{t'}^{-1}_{mn}\mathbf{r'}_{mn} \end{bmatrix} = \begin{bmatrix} \mathbf{k}_m & \mathbf{0} \\ \mathbf{0} & -\mathbf{k}_m \end{bmatrix}. \tag{3.24}$$

Multiplying through on the left and comparing both sides block-wise leads to the the following equations

$$\mathbf{t'}^{\dagger}_{mn}\mathbf{k}_n\mathbf{t'}_{mn} + \mathbf{r}^{\dagger}_{mn}\mathbf{k}_m\mathbf{r}_{mn} = \mathbf{k}_m, \tag{3.25a}$$

$$\mathbf{t}^{\dagger}_{mn}\mathbf{k}_m\mathbf{t}_{mn} + \mathbf{r'}^{\dagger}_{mn}\mathbf{k}_n\mathbf{r'}_{mn} = \mathbf{k}_n, \tag{3.25b}$$

$$\mathbf{t}_{mn}\mathbf{k}_n^{-1}\mathbf{t}^{\dagger}_{mn} + \mathbf{r}_{mn}\mathbf{k}_m^{-1}\mathbf{r}^{\dagger}_{mn} = \mathbf{k}_m^{-1}, \tag{3.25c}$$

$$\mathbf{t'}_{mn}\mathbf{k}_m^{-1}\mathbf{t'}^{\dagger}_{mn} + \mathbf{r'}_{mn}\mathbf{k}_n^{-1}\mathbf{r'}^{-1}_{mn} = \mathbf{k}_n^{-1}. \tag{3.25d}$$

Without any further assumptions there are no simplifications to be attained in (3.25), however, as will be shown later, certain symmetries of the matrices can be exploited when both m and n are non-magnetic. For the sake of completeness we mention that another common way to express the transfer matrix is that in terms of currents, as opposed to wave function amplitudes (see for example, the exposition in Appendix H of [53]). The passage to the current picture is done by rescaling $\tilde{\mathbf{\Psi}} = \mathbf{\Xi}\mathbf{\Psi}$ where $\mathbf{\Xi} = \mathrm{diag}\left[\sqrt{k^{\uparrow}}, \sqrt{k^{\downarrow}}, \sqrt{k^{\uparrow}}, \sqrt{k^{\downarrow}}\right]$. Our transfer matrix is related to the new one by $\tilde{\mathbf{T}}_{mn} = \mathbf{\Xi}_m\mathbf{T}_{mn}\mathbf{\Xi}_n^{-1}$. Assuming for a moment that all matrices

involved are diagonal we find that this is equivalent to the following rescaling:

$$\tilde{\mathbf{r}}_{mn} = \mathbf{r}_{mn}, \quad \tilde{\mathbf{t}}_{mn} = \sqrt{\frac{k_n}{k_m}}\mathbf{t}_{mn}, \quad \tilde{\mathbf{r}'}_{mn} = \mathbf{r'}_{mn}, \quad \tilde{\mathbf{t}'}_{mn} = \sqrt{\frac{k_n}{k_m}}\mathbf{t'}_{mn}. \tag{3.26}$$

Substituting (3.26) into (3.25) we can derive the more familiar-looking conservation equations

$$\tilde{\mathbf{r}}^{\dagger}_{mn}\tilde{\mathbf{r}}_{mn} + \tilde{\mathbf{t}}^{\dagger}_{mn}\tilde{\mathbf{t}}_{mn} = \mathbf{1}, \quad \tilde{\mathbf{r}'}^{\dagger}_{mn}\tilde{\mathbf{r}'}_{mn} + \tilde{\mathbf{t}'}^{\dagger}_{mn}\tilde{\mathbf{t}'}_{mn} = \mathbf{1}, \quad \tilde{\mathbf{r}}^{\dagger}_{mn}\tilde{\mathbf{r}}_{mn} = \tilde{\mathbf{r}'}^{\dagger}_{mn}\tilde{\mathbf{r}'}_{mn}, \quad \tilde{\mathbf{t}}^{\dagger}_{mn}\tilde{\mathbf{t}}_{mn} = \tilde{\mathbf{t}'}^{\dagger}_{mn}\tilde{\mathbf{t}'}_{mn}. \tag{3.27}$$

We will, however, continue performing our calculations in the amplitude picture. This will make the algebra more straightforward when we have to deal both with conductors, and insulators (k is real or imaginary, respectively). We now have everything we need to begin calculating spin current components in the spacer. Investigating the various properties of these components with the aid if the transmission formalism will occupy the remainder of this chapter.

3.1.2 Approximation without Reflections in the Spacer

In this section we calculate the in-plane and out-of-plane components of spin current in the spacer, investigate their origin, and demonstrate the role of successive reflection in the layers as contributing factors to the out-of plane spin current.

We begin by making an approximation where we ignore any reflections that happen to the right of the PM|S interface (see Figure 3.3). This amounts to disregarding any effect the SM has on transmission, which we will be including back later. The amplitudes of an electron injected in the left lead $\overrightarrow{\boldsymbol{\alpha}}_1$ and transmitted into the spacer $\overrightarrow{\boldsymbol{\alpha}}_3$ are related as follows

$$\overrightarrow{\boldsymbol{\alpha}}_3 = \mathbf{t'}_{13}\overrightarrow{\boldsymbol{\alpha}}_1. \tag{3.28}$$

Since the magnetisation direction in the PM is rotated in-plane by angle θ, $\mathbf{t}'_{13}$ actually depends

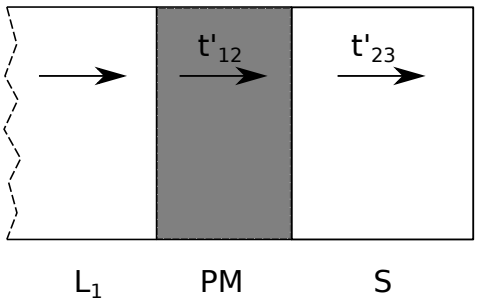

Figure 3.3: Transmission from the left lead into the spacer without accounting for reflections.

on θ, as shown in (3.18). Denote the entries of $\mathbf{t}'_{13}$ at $\theta = 0$ as follows

$$\mathbf{t}'_{13}(0) = \begin{bmatrix} t^{\uparrow} & 0 \\ 0 & t^{\downarrow} \end{bmatrix}. \tag{3.29}$$

Then, for an arbitrary θ we have

$$\mathbf{t}'_{13}(\theta) = \begin{bmatrix} t^{\uparrow}\cos^2\left(\frac{1}{2}\theta\right) + t^{\downarrow}\sin^2\left(\frac{1}{2}\theta\right) & (t^{\uparrow} - t^{\downarrow})\sin\left(\frac{1}{2}\theta\right)\cos\left(\frac{1}{2}\theta\right) \\ (t^{\uparrow} - t^{\downarrow})\sin\left(\frac{1}{2}\theta\right)\cos\left(\frac{1}{2}\theta\right) & t^{\uparrow}\sin^2\left(\frac{1}{2}\theta\right) + t^{\downarrow}\cos^2\left(\frac{1}{2}\theta\right) \end{bmatrix} \tag{3.30}$$

In order to simplify the algebra further, we also neglect the repeated reflections within the polarising magnet. This corresponds to the lowest order in the geometric expansion of (2.31a)

$$\mathbf{t}'_{13} = \mathbf{t}'_{23}(\mathbf{1} - \mathbf{r}'_{12}\mathbf{r}_{23})^{-1}\mathbf{t}'_{12} \approx \mathbf{t}'_{23}\mathbf{t}'_{12}. \tag{3.31}$$

We now need to impose boundary conditions by way of choosing a particular value for $\overrightarrow{\boldsymbol{\alpha}}_1$, that is, fixing the amplitude and polarisation of an incident electron. We do this by considering separately the up- and down-polarised electrons with respect to z axis. From the discussion in Section 2.6 we know that the current density does not depend on the overall rotation angle when summed over spin projections. Taking the up-spin case first, we set

$$\overrightarrow{\boldsymbol{\alpha}}_1 = \begin{bmatrix} 1 \\ 0 \end{bmatrix}. \tag{3.32}$$

Inserting (3.32) in (2.46) we obtain the up-spin components of the current density in the spacer

$$\overrightarrow{j}^{\uparrow}_{x} = k\overrightarrow{\boldsymbol{\alpha}}^{\dagger}_{3}\boldsymbol{\sigma}_{x}\overrightarrow{\boldsymbol{\alpha}}_{3} = 2k\Re\{[\mathbf{t'}_{13}(\theta)]^{*}_{11}[\mathbf{t'}_{13}(\theta)]_{12}\}, \tag{3.33}$$

$$\overrightarrow{j}^{\uparrow}_{y} = k\overrightarrow{\boldsymbol{\alpha}}^{\dagger}_{3}\boldsymbol{\sigma}_{y}\overrightarrow{\boldsymbol{\alpha}}_{3} = 2k\Im\{[\mathbf{t'}_{13}(\theta)]^{*}_{11}[\mathbf{t'}_{13}(\theta)]_{12}\}. \tag{3.34}$$

After some straightforward algebra we obtain

$$\begin{aligned}[\mathbf{t'}_{13}(\theta)]^{*}_{11}[\mathbf{t'}_{13}(\theta)]_{12} = \frac{1}{2}\sin\theta\Big(\big(|t^{\uparrow}|^{2}\cos^{2}\left(\tfrac{1}{2}\theta\right) - |t^{\downarrow}|^{2}\sin^{2}\left(\tfrac{1}{2}\theta\right)\big) \\ - \big(t^{\uparrow *}t^{\downarrow} - 2\Re\{t^{\uparrow *}t^{\downarrow}\}\sin^{2}\left(\tfrac{1}{2}\theta\right)\big)\Big),\end{aligned} \tag{3.35}$$

Where $|t^{\sigma}|^{2} = t^{\sigma *}t^{\sigma}$, $\sigma = \uparrow, \downarrow$. Inserting (3.35) in (3.34) we can write

$$\overrightarrow{j}^{\uparrow}_{x} = k\left(\sin\theta\left(|t^{\uparrow}|^{2}\cos^{2}\left(\tfrac{1}{2}\theta\right) - |t^{\downarrow}|^{2}\sin^{2}\left(\tfrac{1}{2}\theta\right)\right) - \frac{1}{2}\sin\left(2\theta\right)\Re\{t^{\uparrow *}t^{\downarrow}\}\right), \tag{3.36a}$$

$$\overrightarrow{j}^{\uparrow}_{y} = k\sin\theta\Im\{t^{\downarrow *}t^{\uparrow}\}, \tag{3.36b}$$

or, written out explicitly

$$\begin{aligned}\overrightarrow{j}^{\uparrow}_{x} = 16\sin\theta k^{3}\left(\frac{{k^{\uparrow}}^{2}}{(k+k^{\uparrow})^{4}}\cos^{2}\left(\tfrac{1}{2}\theta\right) - \frac{{k^{\downarrow}}^{2}}{(k+k^{\downarrow})^{4}}\sin^{2}\left(\tfrac{1}{2}\theta\right)\right) \\ - \frac{8k^{3}k^{\uparrow}k^{\downarrow}\sin\left(2\theta\right)\cos\left((k^{\uparrow}-k^{\downarrow})L_{\mathrm{PM}}\right)}{(k+k^{\uparrow})^{2}(k+k^{\downarrow})^{2}},\end{aligned} \tag{3.37a}$$

$$\overrightarrow{j}^{\uparrow}_{y} = \frac{8k^{3}k^{\uparrow}k^{\downarrow}\sin\theta\sin\left((k^{\uparrow}-k^{\downarrow})L_{\mathrm{PM}}\right)}{(k+k^{\uparrow})^{2}(k+k^{\downarrow})^{2}}, \tag{3.37b}$$

where $L_{\mathrm{PM}} = y_{2,3} - y_{1,2}$ is the thickness of the PM. For incident down-spin electrons we set

$$\overrightarrow{\boldsymbol{\alpha}}_{1} = \begin{bmatrix}0\\1\end{bmatrix}. \tag{3.38}$$

The current density components are, therefore, found as follows

$$\overrightarrow{j}^{\downarrow}_{x} = k\overrightarrow{\boldsymbol{\alpha}}^{\dagger}_{3}\boldsymbol{\sigma}_{x}\overrightarrow{\boldsymbol{\alpha}}_{3} = 2k\Re\{[\mathbf{t}'_{13}(\theta)]^{*}_{22}[\mathbf{t}'_{13}(\theta)]_{12}\}, \tag{3.39}$$

$$\overrightarrow{j}^{\downarrow}_{y} = k\overrightarrow{\boldsymbol{\alpha}}^{\dagger}_{3}\boldsymbol{\sigma}_{y}\overrightarrow{\boldsymbol{\alpha}}_{3} = 2k\Im\{[\mathbf{t}'_{13}(\theta)]^{*}_{22}[\mathbf{t}'_{13}(\theta)]_{12}\}. \tag{3.40}$$

Similarly to (3.35) and (3.36) we obtain

$$\begin{aligned}[\mathbf{t}'_{13}(\theta)]^{*}_{22}[\mathbf{t}'_{13}(\theta)]_{12} = \frac{1}{2}\sin\theta\,\Big(\big(|t^{\uparrow}|^{2}\sin^{2}\left(\tfrac{1}{2}\theta\right) - |t^{\downarrow}|^{2}\cos^{2}\left(\tfrac{1}{2}\theta\right)\big) \\ + \big(t^{\downarrow *}t^{\uparrow} - 2\Re\{t^{\downarrow *}t^{\uparrow}\}\sin^{2}\left(\tfrac{1}{2}\theta\right)\big)\Big),\end{aligned} \tag{3.41}$$

and

$$\overrightarrow{j}^{\downarrow}_{x} = k\left(\sin\theta\left(|t^{\uparrow}|^{2}\cos^{2}\left(\tfrac{1}{2}\theta\right) - |t^{\downarrow}|^{2}\sin^{2}\left(\tfrac{1}{2}\theta\right)\right) + \frac{1}{2}\sin\left(2\theta\right)\Re\{t^{\uparrow *}t^{\downarrow}\}\right), \tag{3.42a}$$

$$\overrightarrow{j}^{\downarrow}_{y} = -k\sin\theta\Im\{t^{\downarrow *}t^{\uparrow}\}. \tag{3.42b}$$

Again, written explicitly

$$\begin{aligned}\overrightarrow{j}^{\downarrow}_{x} = 16\sin\theta k^{3}\left(\frac{{k^{\uparrow}}^{2}}{(k+k^{\uparrow})^{4}}\sin^{2}\left(\tfrac{1}{2}\theta\right) - \frac{{k^{\downarrow}}^{2}}{(k+k^{\downarrow})^{4}}\cos^{2}\left(\tfrac{1}{2}\theta\right)\right) \\ + \frac{8k^{3}k^{\uparrow}k^{\downarrow}\sin\left(2\theta\right)\cos\left((k^{\uparrow}-k^{\downarrow})L_{\mathrm{PM}}\right)}{(k+k^{\uparrow})^{2}(k+k^{\downarrow})^{2}},\end{aligned} \tag{3.43a}$$

$$\overrightarrow{j}^{\downarrow}_{y} = -\overrightarrow{j}^{\uparrow}_{y}. \tag{3.43b}$$

Thus we have calculated the in-plane and out-of-plane spin current density components in the spacer, disregarding any reflections in the spacer and the polarising magnet. Note that we do not examine the second in-plane component j_z here. The reason for that is that we assume the system to possess in-plane axisymmetry. Therefore, j_z behaves exactly the same way as j_x, up to an in-plane rotation. A few important observations follow from this calculation. Firstly, consider the in-plane component $\overrightarrow{j}^{\sigma}_{x}$. From (3.37a) and (3.43a) it is clear that it consists of two terms, one of which is independent of L_{PM} and another one which oscillates in L_{PM}. The first

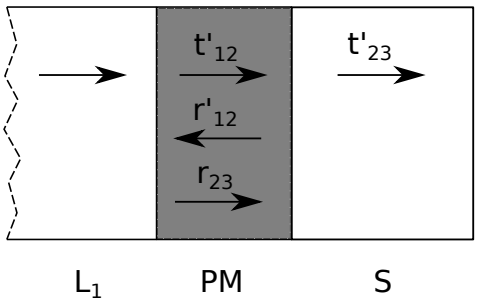

Figure 3.4: Transmission from the left lead into the spacer, including a pair of reflections in the polarising magnet.

term is due to wave function matching at the interface. It vanishes when $\theta = 0$, that is when the magnetisation of the PM is parallel or anti-parallel to the spin orientation of the incident electrons. The second term is due to Larmor precession (2.17), as electrons pass through the PM. It vanishes when $\theta = 0, \pi$ corresponding to the absence of precession, and when $\theta = \pi/2$ corresponding to pure out-of-plane precession. $\overrightarrow{j}^{\sigma}_{y}$, in turn, consists only of a precessional term which vanishes when $\theta = 0$ or $\theta = \pi$, that is, when there is no precession. Adding the respective equations in (3.37) and (3.43) we find the total current density $\overrightarrow{j}_{\nu}$

$$\overrightarrow{j}_{x} = \overrightarrow{j}^{\uparrow}_{x} + \overrightarrow{j}^{\downarrow}_{x} = k \sin\theta \left(|t'^{\uparrow}_{13}(0)|^2 - |t'^{\downarrow}_{13}(0)|^2 \right) = k \sin\theta \, \mathrm{tr} \left\{ \mathbf{t'}_{13}(0) \mathbf{t'}^{\dagger}_{13}(0) \boldsymbol{\sigma}_z \right\}, \tag{3.44a}$$

$$\overrightarrow{j}_{y} = \overrightarrow{j}^{\uparrow}_{y} + \overrightarrow{j}^{\downarrow}_{y} = 0. \tag{3.44b}$$

We can interpret (3.44) by saying that the effect of the PM is to rotate in-plane the incident electrons polarised with respect to z axis by angle θ and give them different weights of $|t'^{\sigma}_{13}(0)|^2$ depending on the wave function matching in the respective spin bands. It also causes spin precession, however, that effect turns out to be exactly equal and opposite for the up- and down-polarised electron. Therefore, the out-of-plane component, which is purely due to precession (disregarding the effect of the SM), vanishes identically. Adding reflections within the PM does not change the qualitative picture in this case. For example, if we retain one pair of reflections in expansion (3.31), as illustrated by Figure 3.4, we obtain

$$\mathbf{t}'_{13} = \mathbf{t'}_{23}(\mathbf{1} - \mathbf{r'}_{12}\mathbf{r}_{23})^{-1}\mathbf{t'}_{12} \approx \mathbf{t'}_{23}\mathbf{t'}_{12} + \mathbf{t'}_{23}\mathbf{r'}_{12}\mathbf{r}_{23}\mathbf{t'}_{12}, \tag{3.45}$$

In order to calculate the current density from (3.45) we can use equations (3.36) and (3.42), except that the components t^σ of $\mathbf{t'}_{13}(0)$ in (3.29) are given as follows

$$t^\sigma = \frac{4kk^\sigma}{k+k^\sigma} e^{\mathrm{i}(k-k^\sigma)L_{\mathrm{PM}}} \left(1 + \left(\frac{k-k^\sigma}{k+k^\sigma}\right)^2 e^{2\mathrm{i}k^\sigma L_{\mathrm{PM}}}\right). \tag{3.46}$$

From (3.46) we find

$$|t^\sigma|^2 = \frac{16kk^{\sigma 2}}{(k+k^\sigma)^4} \left(1 + \left(\frac{k-k^\sigma}{k+k^\sigma}\right)^4 + 2\cos\left(2k^\sigma L_{\mathrm{PM}}\right) \left(\frac{k-k^\sigma}{k+k^\sigma}\right)^2\right), \tag{3.47}$$

$$\begin{aligned} t^{\uparrow *} t^\downarrow = \frac{16k^2 k^\uparrow k^\downarrow}{(k+k^\uparrow)^2(k+k^\downarrow)^2} \Bigg(& e^{\mathrm{i}(k^\uparrow - k^\downarrow)} + \left(\frac{(k-k^\uparrow)(k-k^\downarrow)}{(k+k^\uparrow)(k+k^\downarrow)}\right)^2 e^{-\mathrm{i}(k^\uparrow - k^\downarrow)L_{\mathrm{PM}}} \\ & + \left(\frac{k-k^\uparrow}{k+k^\uparrow}\right)^2 e^{-\mathrm{i}(k+k^\uparrow)L_{\mathrm{PM}}} + \left(\frac{k-k^\downarrow}{k+k^\downarrow}\right)^2 e^{\mathrm{i}(k+k^\downarrow)L_{\mathrm{PM}}} \Bigg). \end{aligned} \tag{3.48}$$

From (3.47), (3.48) and (3.36), (3.42) it is clear that the interpretation given above still holds, in the sense that $\overrightarrow{j}_x$ consists of a wave function term and a precessional term, while $\overrightarrow{j}_y$ is purely precessional and vanishes when summed over the spin projections. Including more reflections within the PM simply adds the terms with angular frequencies $2L_{\mathrm{PM}}k^\uparrow$, $2L_{\mathrm{PM}}k^\downarrow$, $2L_{\mathrm{PM}}(k^\uparrow - k^\downarrow)$, $2L_{\mathrm{PM}}(k^\uparrow - k^\downarrow)$ and higher harmonics to the precessional term.

3.1.3 Reflections in the Spacer

We shall now improve on the approximation made in Section 3.1.2 by including reflections in the spacer, and examine the effect of that on spin current density components. We begin by adding a single reflection inside the spacer resulting from the transmitted wave with amplitude $\overrightarrow{\boldsymbol{\alpha}}_3$, as defined in (3.28), being reflected back into the spacer from the interface with the switching magnet, as depicted in Figure 3.5. We are looking for the contribution to the current density by the left-moving states in the spacer, generated by the electrons injected in the left lead. We denote this part of current density by $\overrightarrow{j}^{\mathrm{R1}}_\nu$, emphasising the fact that we only account for one reflection in the spacer. To calculate the relevant amplitude we take the right-moving wave

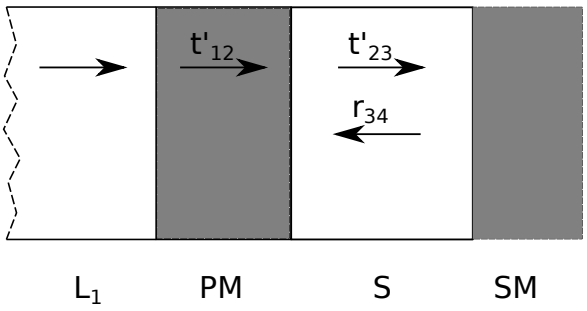

Figure 3.5: Transmission from the left lead into the spacer, including one reflection in the spacer.

(3.28) and reflect it from the S|SM interface through multiplying on the left by $\mathbf{r}_{34}$

$$\overrightarrow{\boldsymbol{\beta}}_3 = \mathbf{r}_{34}\overrightarrow{\boldsymbol{\alpha}}_3 = \mathbf{r}_{34}\mathbf{t'}_{13}\overrightarrow{\boldsymbol{\alpha}}_1. \tag{3.49}$$

It is this last term that we shall now examine because the transmitted right-moving part $\overrightarrow{\boldsymbol{\alpha}}_3$ has already been discussed in the previous section. In the notation of (2.38) we have $\overrightarrow{\mathbf{a}}_3 = \mathbf{t'}^{\dagger}_{13}$, $\overrightarrow{\mathbf{b}}_3 = \mathbf{r}_{34}\mathbf{t'}^{\dagger}_{13}$. Current density from the left-moving electrons can therefore be found using (2.51), (2.52), where we set

$$\overrightarrow{\mathbf{m}}^{\mathrm{R1}} = \overrightarrow{\mathbf{b}}^{\dagger}_3\overrightarrow{\mathbf{b}}_3 = \mathbf{r}_{34}\mathbf{t'}_{13}(\theta)\mathbf{t'}^{\dagger}_{13}(\theta)\mathbf{r}^{\dagger}_{34} = \mathbf{r}_{34}\mathbf{s}(-\theta)\mathbf{t'}_{13}(0)\mathbf{t'}^{\dagger}_{13}(0)\mathbf{s}(\theta)\mathbf{r}^{\dagger}_{34}, \tag{3.50}$$

and

$$\overrightarrow{j}^{\mathrm{R1}}_{\nu} = k\,\mathrm{tr}\left\{\overrightarrow{\mathbf{m}}^{\mathrm{R1}}\boldsymbol{\sigma}_{\nu}\right\}.$$

Now from (3.14d) we have

$$\mathbf{r}_{34} = \mathbf{k}\left(\frac{k - k_4^{\uparrow,\downarrow}}{k + k_4^{\uparrow,\downarrow}}\right)\mathbf{e}\left(2k, y_3\right).$$

From (2.55) we recall that for $\overrightarrow{j}_y$ not to vanish identically $\overrightarrow{\mathbf{m}}^{\mathrm{R1}}$ must not be real. Since $\mathbf{e}\left(2k, y_3\right)$ is diagonal, it commutes with the other factors comprising $\overrightarrow{\mathbf{m}}^{\mathrm{R1}}$ and cancels out with its Hermitian conjugate. Therefore, the only possibility that remains is that at least one of $k_4^{\uparrow}$ or $k_4^{\downarrow}$ be pure imaginary. Physically, this means that the SM must be either a half-metallic ferromagnet (which acts as an insulator for one of the spin bands) or a magnetic insulator.

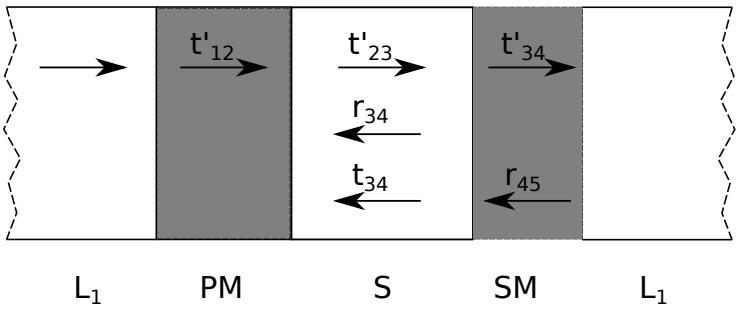

Figure 3.6: Transmission from the left lead into the spacer, including one reflection in the spacer and one reflection within the switching magnet.

Evaluating (3.50) in components we obtain

$$\begin{aligned}\overrightarrow{\mathbf{m}}^{\mathrm{R1}} &= \mathbf{r}_{34}\mathbf{s}(-\theta)\mathbf{t}'_{13}(0)\mathbf{t}'^{\dagger}_{13}(0)\mathbf{s}(\theta)\mathbf{r}^{\dagger}_{34} \\ &= \begin{bmatrix} f^{\uparrow}f^{*\uparrow}\left(|t'^{\uparrow}|^2\cos^2\left(\frac{1}{2}\theta\right)+|t'^{\downarrow}|^2\sin^2\left(\frac{1}{2}\theta\right)\right) & f^{\uparrow}f^{*\downarrow}\left(|t'^{\downarrow}|^2-|t'^{\uparrow}|^2\right)\sin\left(\frac{1}{2}\theta\right)\cos\left(\frac{1}{2}\theta\right) \\ f^{\downarrow}f^{*\uparrow}\left(|t'^{\downarrow}|^2-|t'^{\uparrow}|^2\right)\sin\left(\frac{1}{2}\theta\right)\cos\left(\frac{1}{2}\theta\right) & f^{\downarrow}f^{*\downarrow}\left(|t'^{\downarrow}|^2\cos^2\left(\frac{1}{2}\theta\right)+|t'^{\uparrow}|^2\sin^2\left(\frac{1}{2}\theta\right)\right), \end{bmatrix}\end{aligned}$$

where $f^{\uparrow,\downarrow}=\frac{k-k_4^{\uparrow,\downarrow}}{k+k_4^{\uparrow,\downarrow}}$. This gives the following expressions for the current density

$$\overrightarrow{j}{}_x^{R1} = k\,\mathrm{tr}(\overrightarrow{\mathbf{m}}^{\mathrm{R1}}\boldsymbol{\sigma}_x) = k\sin\theta\left(|t'^{\uparrow}|^2-|t'^{\downarrow}|^2\right)\Re\{f^{\uparrow}f^{*\downarrow}\}, \tag{3.51}$$

$$\overrightarrow{j}{}_y^{R1} = k\,\mathrm{tr}(\overrightarrow{\mathbf{m}}^{\mathrm{R1}}\boldsymbol{\sigma}_y) = k\sin\theta\left(|t'^{\uparrow}|^2-|t'^{\downarrow}|^2\right)\Im\{f^{\uparrow}f^{*\downarrow}\}. \tag{3.52}$$

When the SM is a metallic ferromagnet $\overrightarrow{j}{}_y^{R1}=0$, and we need to consider contribution from the second-order reflection $\overrightarrow{j}{}_y^{R2}$. This is given by electrons that escape into the SM, reflect off the interface with the right lead and transmit back into the spacer, as shown in Figure 3.6. Expanding (2.31d) we obtain

$$\mathbf{r}_{35} = \mathbf{r}_{34}+\mathbf{t}_{34}\mathbf{r}_{45}(\mathbf{1}-\mathbf{r}'_{34}\mathbf{r}_{45})^{-1}\mathbf{t}'_{34} \approx \mathbf{r}_{34}+\mathbf{t}_{34}\mathbf{r}_{45}\mathbf{t}'_{34}. \tag{3.53}$$

We focus here on the second term in (3.53) (denote it $\mathbf{r}_{35}^{\mathrm{R2}}$) which is given in components as follows

$$r_{35}^{\mathrm{R2}\sigma} = \frac{4kk_4^{\sigma}}{(k_4^{\sigma}+k)^3}e^{2\mathrm{i}k(L_{\mathrm{PM}}+L_{\mathrm{S}})+2\mathrm{i}k_4^{\sigma}L_{\mathrm{SM}}}, \tag{3.54}$$

where $L_{\mathrm{S}} = y_{3,4} - y_{2,3}$ $L_{\mathrm{SM}} = y_{4,5} - y_{3,4}$ are the thicknesses of the spacer and the switching magnet, respectively. From (3.54) it is clear that $r_{35}^{\mathrm{R2}\sigma}$ cannot be real due to the presence of a complex exponential factor. Transmission matrix $\overrightarrow{\mathbf{m}}^{\mathrm{R2}}$ in this case has the form

$$\overrightarrow{\mathbf{m}}^{\mathrm{R2}} = \mathbf{r}_{35}\mathbf{s}(-\theta)\mathbf{t'}_{13}(0)\mathbf{t'}^{\dagger}_{13}(0)\mathbf{s}(\theta)\mathbf{r}^{\dagger}_{35}, \tag{3.55}$$

Calculations similar to those preformed in (3.51) and (3.52) yield

$$\overrightarrow{j}_{y}^{\mathrm{R2}} = k\sin\theta\left(|t'^{\uparrow}|^2 - |t'^{\downarrow}|^2\right)c^{\uparrow}c^{\downarrow}\sin\left(L_{\mathrm{SM}}(k_4^{\uparrow} - k_4^{\downarrow})\right), \tag{3.56}$$

where $c^{\sigma} = -4kk_4^{\sigma}(k - k_4^{\sigma})/(k + k_4^{\sigma})^3$. From the above analysis we conclude that the spin current generated by the left-incident electrons, as they pass through the PM into the spacer only has an in-plane component. The out-of-plane component arises if we take into account the precession these electrons undergo in the SM, as they are reflected back into the spacer.

3.2 Symmetry Under Exact Matching

In calculations of spin-related effects some authors have found it convenient to assume that electrons in one of the spin bands experience equal potentials across all layers of the system (see for example [4], [49] or [54]). This is known as *exact matching* and is done for demonstration purposes, because the resulting expressions become much simpler. However, as will be shown in this section, this assumption turns out to correspond to a rather special case because the out-of-plane spin current vanishes under such assumption.

Suppose that we have exact matching in the up-spin band, so that $k_1 = k_2^{\uparrow} = k_3 = k_4^{\uparrow} = k_5 = k$. Then from (3.14c), (3.14d) we see that at $\theta = 0$

$$\mathbf{r'}_{n,n+1} = \begin{bmatrix} 0 & 0 \\ 0 & r'^{\downarrow}_{n,n+1} \end{bmatrix}, \qquad \mathbf{r}_{n,n+1} = \begin{bmatrix} 0 & 0 \\ 0 & r^{\downarrow}_{n,n+1} \end{bmatrix}, \tag{3.57}$$

where $r'^{\downarrow}_{n,n+1} = -\frac{k^{\downarrow}_n - k^{\downarrow}_{n+1}}{k^{\downarrow}_n + k^{\downarrow}_{n+1}} e^{-2ik_{n+1}y_{n,n+1}}$, $r^{\downarrow}_{n,n+1} = \frac{k^{\downarrow}_n - k^{\downarrow}_{n+1}}{k^{\downarrow}_n + k^{\downarrow}_{n+1}} e^{2ik_n y_{n,n+1}}$ and $n = 1, 3$. Expressions (3.57) can be written more compactly as $\mathbf{r'}_{n,n+1} = r'^{\downarrow}_{n,n+1}\mathbf{p}^{\downarrow}$, $\mathbf{r}_{n,n+1} = r^{\downarrow}_{n,n+1}\mathbf{p}^{\downarrow}$ where $\mathbf{p}^{\downarrow} = \left[\begin{smallmatrix} 0 & 0 \\ 0 & 1 \end{smallmatrix}\right]$ is the down-spin projection operator. Furthermore, since

$$\mathbf{r}'_{n,n+2} = \mathbf{r}'_{n+1,n+2} + \mathbf{t}'_{n+1,n+2}\left(\mathbf{1} - \mathbf{r}'_{n,n+1}\mathbf{r}_{n+1,n+2}\right)^{-1}\mathbf{r}'_{n,n+1}\mathbf{t}_{n+1,n+2},$$
$$\mathbf{r}_{n,n+2} = \mathbf{r}_{n,n+1} + \mathbf{t}_{n,n+1}\mathbf{r}_{n+1,n+2}(\mathbf{1} - \mathbf{r'}_{n,n+1}\mathbf{r}_{n+1,n+2})^{-1}\mathbf{t'}_{n,n+1}.$$

we also have $\mathbf{r'}_{n,n+2}, \mathbf{r}_{n,n+2} \propto \mathbf{p}^{\downarrow}$ at $\theta = 0$. These conclusions are intuitively clear because the up-spin electrons do not experience any reflections under exact matching. Another simplification we can exploit that is not specific to exact matching, but rather follows from the interleaving of magnetic and non-magnetic layers in our model, is the commutativity of some of the transmission and reflection matrices. Generally, in the presence of exchange splitting and in-plane polarisation, none of them commute. However, in the particular case where the leads and the spacer are non-magnetic, we obtain factorisations of the form $\mathbf{r}'_{n,n+2}(\theta) = \mathbf{s}(-\theta)\,\mathbf{r}'_{n,n+2}(0)\,\mathbf{s}(\theta)$, $\mathbf{t}'_{n,n+2}(\theta) = \mathbf{s}(-\theta)\,\mathbf{t}'_{n,n+2}(0)\,\mathbf{s}(\theta)$, and similarly for $\mathbf{r}_{n,n+2}$ and $\mathbf{t}_{n,n+2}$ $(n = 1, 3)$, as was shown in (3.18). Therefore, since $\mathbf{t}'(0)$, $\mathbf{t}(0)$, $\mathbf{r}'(0)$ and $\mathbf{r}(0)$ are diagonal, all transmission and reflection matrices across layers 1-3 and 3-5 commute, and so do their Hermitian conjugates. Hence from (3.25), since $k_1 = k_3$, we deduce that

$$\begin{aligned} \mathbf{r}^{\dagger}_{n,n+2}\mathbf{r}_{n,n+2} + \mathbf{t}^{\dagger}_{n,n+2}\mathbf{t}_{n,n+2} = \mathbf{1}, \qquad & \mathbf{r'}^{\dagger}_{n,n+2}\mathbf{r'}_{n,n+2} + \mathbf{t'}^{\dagger}_{n,n+2}\mathbf{t'}_{n,n+2} = \mathbf{1}, \\ \mathbf{r}^{\dagger}_{n,n+2}\mathbf{r}_{n,n+2} = \mathbf{r'}^{\dagger}_{n,n+2}\mathbf{r'}_{n,n+2}, \qquad & \mathbf{t}^{\dagger}_{n,n+2}\mathbf{t}_{n,n+2} = \mathbf{t'}^{\dagger}_{n,n+2}\mathbf{t'}_{n,n+2}, \end{aligned} \tag{3.58}$$

where $n = 1, 3$. Now, from (2.49) we find that the right-moving current density contributed by the electrons incident from the left lead is proportional to

$$\mathrm{tr}\left\{\overrightarrow{\mathbf{a}}^{\dagger}_3\boldsymbol{\sigma}_\nu\overrightarrow{\mathbf{a}}_3\right\} = \mathrm{tr}\left\{(\mathbf{1} - \mathbf{r}^{\dagger}_{35}\mathbf{r'}^{\dagger}_{13})^{-1}\boldsymbol{\sigma}_\nu(\mathbf{1} - \mathbf{r}'_{13}\mathbf{r}_{35})^{-1}\mathbf{t}'_{13}\mathbf{t'}^{\dagger}_{13}\right\}. \tag{3.59}$$

Using commutativity of $\mathbf{t}_{13}$ and $\mathbf{t'}^{\dagger}_{13}$, and the identity $\mathbf{t'}^{\dagger}_{13}\mathbf{t}^{\dagger}_{13} = \mathbf{1} - \mathbf{r'}^{\dagger}_{13}\mathbf{r}^{\dagger}_{13}$ from (3.58) we deduce

$$\begin{aligned} \mathrm{tr}\left\{\overrightarrow{\mathbf{a}}^{\dagger}_3\boldsymbol{\sigma}_\nu\overrightarrow{\mathbf{a}}_3\right\} = \mathrm{tr}\left\{(\mathbf{1} - \mathbf{r}^{\dagger}_{35}\mathbf{r'}^{\dagger}_{13})^{-1}\boldsymbol{\sigma}_\nu(\mathbf{1} - \mathbf{r}'_{13}\mathbf{r}_{35})^{-1}\right\} \\ - \mathrm{tr}\left\{(\mathbf{1} - \mathbf{r'}^{\dagger}_{13}\mathbf{r}^{\dagger}_{35})^{-1}(\mathbf{r'}^{\dagger}_{13}\boldsymbol{\sigma}_\nu\mathbf{r'}_{13})(\mathbf{1} - \mathbf{r}_{35}\mathbf{r}'_{13})^{-1}\right\}. \end{aligned}$$

For the out-of-plane component, we notice that the second term vanishes because $\mathbf{r'}^{\dagger}_{13}\boldsymbol{\sigma}_y\mathbf{r'}_{13} = \mathbf{s}(-\theta)\mathbf{r'}^{\dagger}_{13}(0)\,\mathbf{s}(\theta)\,\boldsymbol{\sigma}_y\,\mathbf{s}(-\theta)\mathbf{r'}_{13}(0)\,\mathbf{s}(\theta) \propto \mathbf{s}(-\theta)\mathbf{p}^{\downarrow}\,\boldsymbol{\sigma}_y\,\mathbf{p}^{\downarrow}\,\mathbf{s}(\theta) = \mathbf{0}$. Hence

$$\mathrm{tr}\left\{\overrightarrow{\mathbf{a}}^{\dagger}_3\boldsymbol{\sigma}_y\overrightarrow{\mathbf{a}}_3\right\} = \mathrm{tr}\left\{(\mathbf{1}-\mathbf{r}^{\dagger}_{35}\mathbf{r'}^{\dagger}_{13})^{-1}\boldsymbol{\sigma}_y(\mathbf{1}-\mathbf{r'}_{13}\mathbf{r}_{35})^{-1}\right\}. \tag{3.60}$$

Likewise, for the left-moving current

$$\mathrm{tr}\left\{\overrightarrow{\mathbf{b}}^{\dagger}_3\boldsymbol{\sigma}_y\overrightarrow{\mathbf{b}}_3\right\} = \mathrm{tr}\left\{\overrightarrow{\mathbf{a}}^{\dagger}_3\mathbf{r}^{\dagger}_{35}\boldsymbol{\sigma}_y\mathbf{r}_{35}\overrightarrow{\mathbf{a}}_3\right\} = 0. \tag{3.61}$$

A similar argument, when applied to the right-incident current, gives the results

$$\mathrm{tr}\left\{\overleftarrow{\mathbf{a}}^{\dagger}_3\boldsymbol{\sigma}_y\overleftarrow{\mathbf{a}}_3\right\} = 0, \tag{3.62}$$

$$\mathrm{tr}\left\{\overleftarrow{\mathbf{b}}^{\dagger}_3\boldsymbol{\sigma}_y\overleftarrow{\mathbf{b}}_3\right\} = \mathrm{tr}\left\{(\mathbf{1}-\mathbf{r'}^{\dagger}_{13}\mathbf{r}^{\dagger}_{35})^{-1}\boldsymbol{\sigma}_y(\mathbf{1}-\mathbf{r}_{35}\mathbf{r'}_{13})^{-1}\right\}. \tag{3.63}$$

But $\mathbf{s}^T = \mathbf{s}^{-1}$, so that $\mathbf{r}_{35}(\theta)$ and $\mathbf{r'}_{13}(\theta)$ are symmetric, whereas $\boldsymbol{\sigma}_y$ is antisymmetric. Hence

$$\left[(\mathbf{1}-\mathbf{r'}^{\dagger}_{13}\mathbf{r}^{\dagger}_{35})^{-1}\boldsymbol{\sigma}_y(\mathbf{1}-\mathbf{r}_{35}\mathbf{r'}_{13})^{-1}\right]^T = -\left[(\mathbf{1}-\mathbf{r'}_{13}\mathbf{r}_{35})^{-1}\boldsymbol{\sigma}_y(\mathbf{1}-\mathbf{r}^{\dagger}_{35}\mathbf{r'}^{\dagger}_{13})^{-1}\right], \tag{3.64}$$

so that taking the trace of both sides of (3.64) and comparing with (3.60) we deduce that

$$\mathrm{tr}\left\{\overleftarrow{\mathbf{b}}^{\dagger}_3\boldsymbol{\sigma}_y\overleftarrow{\mathbf{b}}_3\right\} = -\,\mathrm{tr}\left\{\overrightarrow{\mathbf{a}}^{\dagger}_3\boldsymbol{\sigma}_y\overrightarrow{\mathbf{a}}_3\right\}.$$

Hence the total out-of-plane transport spin current in the spacer vanishes

$$j^{\mathrm{tr}}_y = \overrightarrow{j}_y - \overleftarrow{j}_y = 0. \tag{3.65}$$

We shall now try to understand from the physics point of view how the assumption of the exact matching leads to (3.65). First of all, because $\mathbf{r}_{35}(0) \sim \mathbf{r'}_{35}(0) \propto \mathbf{p}^{\downarrow}$ and $\mathbf{r}_{13}(\theta) \sim \mathbf{r'}_{13}(\theta) \propto \mathbf{s}^{-1}(\theta)\mathbf{p}^{\downarrow}\mathbf{s}^{-1}(\theta)$, then any state reflected off the SM or PM is projected onto the down state along the same quantisation axis as the magnetisation. So it is not surprising that all states in the spacer, reflected off the PM or SM, have zero out-of-plane spin component:

$\langle \mathbf{r}_{35}(0)\boldsymbol{\alpha}'_3| \boldsymbol{\sigma}_y |\mathbf{r}_{35}(0)\boldsymbol{\alpha}_3\rangle = \langle \mathbf{r}_{13}(\theta)\boldsymbol{\beta}'_3| \boldsymbol{\sigma}_y |\mathbf{r}_{13}(\theta)\boldsymbol{\beta}_3\rangle = 0$. This explains (3.61) and (3.62), and in the spacer we only have to consider right moving states originating from the left lead ($\overrightarrow{\mathbf{a}}_3$) and left moving states originating from the right lead ($\overleftarrow{\mathbf{b}}_3$). Comparing (3.60) and (3.59) we note that, as far as the out-of-plane spin current is concerned, electrons emitted from the left lead pass through the polarising magnet, as if it had unit transmission matrix. The same holds for electrons from the right lead passing through the switching magnet, by virtue of (3.63). Since the contribution to the out-of-plane spin current from left and right only involves reflections off the polarising and switching magnet interfaces, we might reasonably expect $\overrightarrow{j}_y = \pm \overleftarrow{j}_y$. Now exact matching should not lead to vanishing of the exchange coupling, since, as is discussed at length in Chapter 5, the latter is determined by the magnetic configuration of the system and does not require any external supply of electrons. Therefore, we must have $\overrightarrow{j}_y = \overleftarrow{j}_y$.

3.3 Symmetry Under Reversal of Polarisation

We now come back to the case of a general potential profile, without the assumption about exact matching. In Section 2.6 we saw that the overall in-plane rotation of the system leaves the spin current invariant. We now examine the symmetry of the spin current with respect to reversal of the magnetisation angle θ in the PM. We note the following identity

$$\mathbf{s}(-\theta) = \boldsymbol{\sigma}_z \mathbf{s}(\theta)\, \boldsymbol{\sigma}_z,$$

so that $\mathbf{r}_{13}(-\theta) = \mathbf{s}(\theta)\mathbf{r}_{13}(0)\,\mathbf{s}(-\theta) = \boldsymbol{\sigma}_z\, \mathbf{r}_{13}(\theta)\boldsymbol{\sigma}_z$, and similarly for the other $(1,3)$ reflection and transmission matrices. Hence from (2.37), for a system with PM magnetisation $\theta_2 = -\theta$

$$\begin{aligned}
\overrightarrow{\mathbf{a}}_3(-\theta) &= \Big(\mathbf{1} - \mathbf{r}'_{13}(-\theta)\mathbf{r}_{35}(0)\Big)^{-1} \mathbf{t}'_{13}(-\theta) \\
&= \Big(\mathbf{1} - \boldsymbol{\sigma}_z\mathbf{r}'_{13}(\theta)\boldsymbol{\sigma}_z\mathbf{r}_{35}(0)\Big)^{-1} \boldsymbol{\sigma}_z\mathbf{t}'_{13}(\theta)\boldsymbol{\sigma}_z \\
&= \boldsymbol{\sigma}_z \Big(\mathbf{1} - \mathbf{r}'_{13}(\theta)\boldsymbol{\sigma}_z\mathbf{r}_{35}(0)\boldsymbol{\sigma}_z\Big)^{-1} \mathbf{t}'_{13}(\theta)\boldsymbol{\sigma}_z \\
&= \boldsymbol{\sigma}_z \Big(\mathbf{1} - \mathbf{r}'_{13}(\theta)\mathbf{r}_{35}(0)\Big)^{-1} \mathbf{t}'_{13}(\theta)\boldsymbol{\sigma}_z \\
&= \boldsymbol{\sigma}_z\, \overrightarrow{\mathbf{a}}_3(\theta)\boldsymbol{\sigma}_z.
\end{aligned} \tag{3.66}$$

and similarly for $\overleftarrow{\mathbf{a}}_3$, $\overrightarrow{\mathbf{b}}_3$ and $\overleftarrow{\mathbf{b}}_3$. Hence

$$\begin{aligned}\mathrm{tr}\{\overleftrightarrow{\mathbf{a}}_3^\dagger(-\theta)\boldsymbol{\sigma}_\nu\overleftrightarrow{\mathbf{a}}_3(-\theta)\} &= \mathrm{tr}\{\overleftrightarrow{\mathbf{a}}_3^\dagger(\theta)\boldsymbol{\sigma}_z\boldsymbol{\sigma}_\nu\boldsymbol{\sigma}_z\overleftrightarrow{\mathbf{a}}_3(\theta)\},\\ \mathrm{tr}\{\overleftrightarrow{\mathbf{b}}_3^\dagger(-\theta)\boldsymbol{\sigma}_\nu\overleftrightarrow{\mathbf{b}}_3(-\theta)\} &= \mathrm{tr}\{\overleftrightarrow{\mathbf{b}}_3^\dagger(\theta)\boldsymbol{\sigma}_z\boldsymbol{\sigma}_\nu\boldsymbol{\sigma}_z\overleftrightarrow{\mathbf{b}}_3(\theta)\}.\end{aligned} \tag{3.67}$$

However,

$$\boldsymbol{\sigma}_z\boldsymbol{\sigma}_\nu\boldsymbol{\sigma}_z = \eta_\nu\boldsymbol{\sigma}_\nu, \quad \text{where } \eta_x = \eta_y = -1 \text{ and } \eta_z = 1.$$

Hence we deduce that

$$j_x(-\theta) = -j_x(\theta), \qquad j_y(-\theta) = -j_y(\theta), \qquad j_z(-\theta) = j_z(\theta). \tag{3.68}$$

in the spacer. Now for spin current in the leads the argument is very similar. For example, in the right lead $\overrightarrow{\boldsymbol{\alpha}}_5 = \overrightarrow{\mathbf{a}}_5\overrightarrow{\boldsymbol{\alpha}}_1$, however $\overrightarrow{\mathbf{a}}_5(\theta) = \mathbf{t}'_{35}(0)\overrightarrow{\mathbf{a}}_3(\theta)$. Analogously to (3.67) we obtain

$$\mathrm{tr}\{\overrightarrow{\mathbf{a}}_5^\dagger(-\theta)\boldsymbol{\sigma}_\nu\overrightarrow{\mathbf{a}}_5(-\theta)\} = \mathrm{tr}\{\overrightarrow{\mathbf{a}}_3^\dagger(\theta)\boldsymbol{\sigma}_z\mathbf{t}'^\dagger_{35}\boldsymbol{\sigma}_\nu\mathbf{t}'_{35}\boldsymbol{\sigma}_z\overrightarrow{\mathbf{a}}_3(\theta)\}. \tag{3.69}$$

Since $\mathbf{t}'_{35}$ is diagonal, it is easily checked that $\boldsymbol{\sigma}_z\mathbf{t}'^\dagger_{35}\boldsymbol{\sigma}_\nu\mathbf{t}'_{35}\boldsymbol{\sigma}_z = \eta_\nu\mathbf{t}'^\dagger_{35}\boldsymbol{\sigma}_\nu\mathbf{t}'_{35}$, and the relations (3.68) hold for the right lead too. Finally, in the left lead $\overleftarrow{\boldsymbol{\beta}}_1 = \overleftarrow{\mathbf{b}}_1\overleftarrow{\boldsymbol{\beta}}_5$ and $\overleftarrow{\mathbf{b}}_1(\theta) = \mathbf{t}_{13}(\theta)\overleftarrow{\mathbf{b}}_3(0)$, hence

$$\overleftarrow{\mathbf{b}}_1(-\theta) = \boldsymbol{\sigma}_z\mathbf{t}_{13}(\theta)\boldsymbol{\sigma}_z\overleftarrow{\mathbf{b}}_3(0),$$

and, similarly to (3.69) we obtain

$$\begin{aligned}\mathrm{tr}\{\overleftarrow{\mathbf{b}}_1^\dagger(-\theta)\boldsymbol{\sigma}_\nu\overleftarrow{\mathbf{b}}_1(-\theta)\} &= \mathrm{tr}\{\overleftarrow{\mathbf{b}}_3^\dagger(0)\boldsymbol{\sigma}_z\mathbf{t}_{13}^\dagger(\theta)\boldsymbol{\sigma}_z\boldsymbol{\sigma}_\nu\boldsymbol{\sigma}_z\mathbf{t}_{13}(\theta)\boldsymbol{\sigma}_z\overleftarrow{\mathbf{b}}_3(0)\}\\ &= \mathrm{tr}\{\boldsymbol{\sigma}_z\overleftarrow{\mathbf{b}}_3(0)\overleftarrow{\mathbf{b}}_3^\dagger(0)\boldsymbol{\sigma}_z\mathbf{t}_{13}^\dagger(\theta)\boldsymbol{\sigma}_z\boldsymbol{\sigma}_\nu\boldsymbol{\sigma}_z\mathbf{t}_{13}(\theta)\}\\ &= \eta_\nu\,\mathrm{tr}\{\overleftarrow{\mathbf{b}}_3(0)\overleftarrow{\mathbf{b}}_3^\dagger(0)\mathbf{t}_{13}^\dagger(\theta)\boldsymbol{\sigma}_\nu\mathbf{t}_{13}(\theta)\}\\ &= \eta_\nu\,\mathrm{tr}\{\overleftarrow{\mathbf{b}}_3^\dagger(0)\mathbf{t}_{13}^\dagger(\theta)\boldsymbol{\sigma}_\nu\mathbf{t}_{13}(\theta)\overleftarrow{\mathbf{b}}_3(0)\}.\end{aligned} \tag{3.70}$$

Therefore, the symmetry (3.68) holds in the leads too.

3.4 Reflection Symmetry

Now let us consider a system in which potentials in the leads are the same $k_1 = k_5$, and those in the PM and SM are the same $k_2^{\uparrow,\downarrow} = k_4^{\uparrow,\downarrow}$, and also the thicknesses of the PM and SM are the same. We say that such a system possesses *reflection symmetry* in the sense that the transmission and reflection coefficient for the left- and right-moving electrons are the same, up to a phase. Indeed, when $\theta_2 = \theta_4 = 0$ we obtain from (3.14a)-(3.14d):

$$\mathbf{t}'_{13} = e^{\mathrm{i}(k_1-k_3)\phi}\mathbf{t}_{35}, \tag{3.71a}$$

$$\mathbf{t}_{13} = e^{\mathrm{i}(k_1-k_3)\phi}\mathbf{t}'_{35}, \tag{3.71b}$$

$$\mathbf{r}'_{13} = e^{-2\mathrm{i}k_3\phi}\mathbf{r}_{35}, \tag{3.71c}$$

$$\mathbf{r}_{13} = e^{2\mathrm{i}k_1\phi}\mathbf{r}'_{35}, \tag{3.71d}$$

where $\phi = y_{23} + y_{34}$. However, as $\mathbf{r}(\theta) = \mathbf{s}(-\theta)\mathbf{r}(0)\,\mathbf{s}(\theta)$ etc, then they also hold for any $\theta_2 = \theta_4$. We might also expect that electrons incident from the left on the SM, shall be equivalent to electrons incident from the right on the PM i.e. $\overrightarrow{\boldsymbol{\alpha}}_3 \sim \overleftarrow{\boldsymbol{\beta}}_3$. This is proved as follows. From (2.37) and (3.71a)–(3.71d)

$$\begin{aligned}
\overleftarrow{\mathbf{b}}_3(\theta) &= \Big(\mathbf{1} - \mathbf{r}_{35}(0)\mathbf{r}'_{13}(\theta)\Big)^{-1}\mathbf{t}_{35}(0) \\
&= \Big(\mathbf{1} - \mathbf{r}'_{13}(0)\mathbf{s}(-\theta)\mathbf{r}_{35}(0)\mathbf{s}(\theta)\Big)^{-1}\mathbf{t}_{35}(0) \\
&= e^{-\mathrm{i}(k_1-k_3)\phi}\mathbf{s}(-\theta)\Big(\mathbf{1} - \mathbf{s}(\theta)\mathbf{r}'_{13}(0)\mathbf{s}(-\theta)\mathbf{r}_{35}(0)\Big)^{-1}\mathbf{s}(\theta)\mathbf{t}'_{13}(0) \\
&= e^{-\mathrm{i}(k_1-k_3)\phi}\mathbf{s}(-\theta)\Big(\mathbf{1} - \mathbf{r}'_{13}(-\theta)\mathbf{r}_{35}(0)\Big)^{-1}\mathbf{t}'_{13}(-\theta)\mathbf{s}(\theta) \\
&= e^{-\mathrm{i}(k_1-k_3)\phi}\mathbf{s}(-\theta)\overrightarrow{\mathbf{a}}_3(-\theta)\mathbf{s}(\theta),
\end{aligned} \tag{3.72}$$

where $\overrightarrow{\mathbf{a}}_3(-\theta)$ corresponds to a system with $\theta_2 = -\theta$. Further from (3.66)

$$\overleftarrow{\mathbf{b}}_3(\theta) = e^{-\mathrm{i}(k_1-k_3)\phi}\mathbf{s}(-\theta)\boldsymbol{\sigma}_z\overrightarrow{\mathbf{a}}_3(\theta)\boldsymbol{\sigma}_z\mathbf{s}(\theta). \tag{3.73}$$

Likewise from (2.37)

$$\begin{aligned}\overleftarrow{\mathbf{a}}_3(\theta) &= \mathbf{r}'_{13}(\theta)\overleftarrow{\mathbf{b}}_3(\theta)\\ &= e^{-\mathrm{i}(k_1-k_3)\phi}\mathbf{s}(-\theta)\mathbf{r}'_{13}(0)\boldsymbol{\sigma}_z\overrightarrow{\mathbf{a}}_3(\theta)\boldsymbol{\sigma}_z\mathbf{s}(\theta)\\ &= e^{-\mathrm{i}(k_1+k_3)\phi}\mathbf{s}(-\theta)\boldsymbol{\sigma}_z\mathbf{r}_{35}(0)\overrightarrow{\mathbf{a}}_3(\theta)\boldsymbol{\sigma}_z\mathbf{s}(\theta)\\ &= e^{-\mathrm{i}(k_1+k_3)\phi}\mathbf{s}(-\theta)\boldsymbol{\sigma}_z\overrightarrow{\mathbf{b}}_3(\theta)\boldsymbol{\sigma}_z\mathbf{s}(\theta).\end{aligned} \tag{3.74}$$

From (2.49) we deduce

$$\begin{aligned}\mathrm{tr}\{\overleftarrow{\mathbf{b}}_3^\dagger(\theta)\boldsymbol{\sigma}_\nu\overleftarrow{\mathbf{b}}_3(\theta)\} &= \mathrm{tr}\{\overrightarrow{\mathbf{a}}_3^\dagger(\theta)\boldsymbol{\sigma}_z\,\mathbf{s}(\theta)\,\boldsymbol{\sigma}_\nu\,\mathbf{s}(-\theta)\boldsymbol{\sigma}_z\overrightarrow{\mathbf{a}}_3(\theta)\},\\ \mathrm{tr}\{\overleftarrow{\mathbf{a}}_3^\dagger(\theta)\boldsymbol{\sigma}_\nu\overleftarrow{\mathbf{a}}_3(\theta)\} &= \mathrm{tr}\{\overrightarrow{\mathbf{b}}_3^\dagger(\theta)\boldsymbol{\sigma}_z\,\mathbf{s}(\theta)\,\boldsymbol{\sigma}_\nu\,\mathbf{s}(-\theta)\boldsymbol{\sigma}_z\overrightarrow{\mathbf{b}}_3(\theta)\},\end{aligned}$$

which for $\boldsymbol{\sigma}_i = \boldsymbol{\sigma}_y$ reduces to

$$\begin{aligned}\mathrm{tr}\{\overleftarrow{\mathbf{b}}_3^\dagger(\theta)\boldsymbol{\sigma}_y\overleftarrow{\mathbf{b}}_3(\theta)\} &= -\,\mathrm{tr}\{\overrightarrow{\mathbf{a}}_3^\dagger(\theta)\boldsymbol{\sigma}_y\overrightarrow{\mathbf{a}}_3(\theta)\},\\ \mathrm{tr}\{\overleftarrow{\mathbf{a}}_3^\dagger(\theta)\boldsymbol{\sigma}_y\overleftarrow{\mathbf{a}}_3(\theta)\} &= -\,\mathrm{tr}\{\overrightarrow{\mathbf{b}}_3^\dagger(\theta)\boldsymbol{\sigma}_y\overrightarrow{\mathbf{b}}_3(\theta)\}.\end{aligned}$$

Hence the total out-of-plane transport spin current in the spacer vanishes for a symmetric system

$$j_y^{\mathrm{tr}} = \overrightarrow{j}_y - \overleftarrow{j}_y = 0.$$

The physical reason behind the vanishing of the out-of-plane spin current for a symmetric system can be inferred from the preceding equations. Firstly, from (3.72) (and its equivalent for $\overleftarrow{\mathbf{a}}_3$) we deduce that sending electrons from the left, polarised in the z-direction through the PM with magnetisation in the $-\theta$ direction, is equivalent to sending electrons from the right, polarised in the θ-direction through the SM. In particular $\overrightarrow{\boldsymbol{\alpha}}_3(-\theta) \sim \overleftarrow{\boldsymbol{\beta}}_3(\theta)$ and $\overrightarrow{\boldsymbol{\beta}}_3(-\theta) \sim \overleftarrow{\boldsymbol{\alpha}}_3(\theta)$ up to a phase and an in-plane rotation of the entire system by θ. However, because the out-of-plane component of spin current $\overleftrightarrow{j}_y(\theta)$ is invariant under in-plane rotations of the entire system, and is an odd function of θ, then $\overleftarrow{j}_y(\theta)$ and $\overrightarrow{j}_y(\theta)$ cancel in the transport spin current. In fact we recall that we are free to choose the quantisation axis of electrons emitted from the left and the right lead independently. Hence choosing the left lead to be aligned with the PM and the right to be aligned with the SM, it is clear that in the spacer $\overrightarrow{j}_\nu = \pm\overleftarrow{j}_\nu$. We do

not expect the exchange coupling to vanish for a symmetric system because it arises from the relative alignment of the magnetisations in PM and SM, which is not changed by the symmetry. Therefore, we must have $\overrightarrow{j}_y = \overleftarrow{j}_y$. Furthermore, in the next section we show that if $\nu = 0, x, z$ then $\overrightarrow{j}_\nu = -\overleftarrow{j}_\nu$, in any non-magnetic layer of any multilayer system. The symmetric system considered here may seem somewhat artificial. However, it is the vanishing of the out-of-plane transport spin current for this special case, which has been verified previously by numerical calculations on realistic systems [55], [56], that led the authors of [57] to conclude that the out-of-plane transport-spin current was a quadratic function of the applied bias. Instead, the vanishing of the linear bias dependence of the transport current was an artefact of the reflection symmetry in the ferromagnetic configuration of the system, that is when the moments of the two magnets separated (in case of [57]) by an insulating spacer were aligned in the same direction.

3.5 Flow Reversal Symmetry

In this section we examine the symmetry of the spin current density with respect to the reversal of the flow direction, in other words, exchanging the contributions from the left- and right-incident electrons. Consider a general multilayer, composed of N non-magnetic (NM) and ferromagnetic (FM) layers, sandwiched consecutively so that each FM layer has NM layers either side of it, as shown in Figure 2.14. The exchange field in each FM layer is at an arbitrary angle θ to the z-axis in the xz-plane, and the potentials in each layer are arbitrary except that the potentials in the two NM leads (NM_1 and NM_N) are assumed to be equal. Here we employ the notation $j_\nu^{(n)}$ to indicate that we are dealing with current components in layer n. Under these assumptions we are going to prove that all current density components, except the out-of-plane one, change sign under flow reversal, but have equal absolute values. This demonstrates that only the out-of-plane component contributes to the exchange current(see (2.59)).

In the left lead (layer 1), we have for the current density due to the left-incident electrons

$$\overrightarrow{j}_\nu^{(1)} = \mathrm{tr}\{\boldsymbol{\sigma}_\nu - \mathbf{r}_{1N}^\dagger \boldsymbol{\sigma}_\nu \mathbf{r}_{1N}\} = \mathrm{tr}\{\boldsymbol{\sigma}_\nu(\mathbf{1} - \mathbf{r}_{1N}\mathbf{r}_{1N}^\dagger)\} = \mathrm{tr}\{\boldsymbol{\sigma}_\nu \mathbf{t}_{1N}\mathbf{t}_{1N}^\dagger\},$$

where we have used (3.58), $\mathbf{t}_{1N}\mathbf{t}_{1N}^{\dagger} + \mathbf{r}_{1N}\mathbf{r}_{1N}^{\dagger} = \mathbf{1}$. Clearly then

$$\overleftarrow{j}_{\nu}^{(1)} = -\overrightarrow{j}_{\nu}^{(1)} = -\operatorname{tr}(\mathbf{t}_{1N}^{\dagger}\boldsymbol{\sigma}_{\nu}\mathbf{t}_{1N}).$$

In exactly the same way, we see that

$$\overleftarrow{j}_{\nu}^{(N)} = \operatorname{tr}(\mathbf{r'}_{1N}^{\dagger}\boldsymbol{\sigma}_{\nu}\mathbf{r'}_{1N} - \boldsymbol{\sigma}_{\nu}) = -\operatorname{tr}(\boldsymbol{\sigma}_{\nu}\mathbf{t'}_{1N}\mathbf{t'}_{1N}^{\dagger}) = -\overrightarrow{j}_{\nu}^{(N)}.$$

We deduce that there are no components of the exchange current in the leads

$$\overrightarrow{j}_{\nu}^{(1)} + \overleftarrow{j}_{\nu}^{(1)} = \overrightarrow{j}_{\nu}^{(N)} + \overleftarrow{j}_{\nu}^{(N)} = 0.$$

To deduce the relationship between $\overrightarrow{j}$ and $\overleftarrow{j}$ in a general non-magnetic layer we need to set the boundary conditions first. We impose those by defining the states in the right lead that arise due to the left- and right-incident electrons, respectively. Thus, for the electrons incident from the left lead their resulting contribution will be characterised only by the right-moving amplitude due to the transmission across the entire system with the transmission coefficient $\mathbf{t'}_{1N}$. In the 4-component notation of (3.4) we can write

$$\overrightarrow{\boldsymbol{\Psi}}_{N}^{\sigma} = \begin{bmatrix} \mathbf{t'}_{1N}\boldsymbol{\alpha}_{1}^{\sigma} \\ \mathbf{0} \end{bmatrix}, \quad \text{where } \boldsymbol{\alpha}_{1}^{\uparrow} = \begin{bmatrix} 1 \\ 0 \end{bmatrix}, \ \boldsymbol{\alpha}_{1}^{\downarrow} = \begin{bmatrix} 0 \\ 1 \end{bmatrix}. \tag{3.75}$$

Similarly, for electrons incident from the right lead the state in the right lead will consist of an unit wave coming in from infinity and the reflected wave with the reflection matrix

$$\overleftarrow{\boldsymbol{\Psi}}_{N}^{\sigma} = \begin{bmatrix} \mathbf{r'}_{1N}\boldsymbol{\alpha}_{N}^{\sigma} \\ \boldsymbol{\alpha}_{N}^{\sigma} \end{bmatrix}, \quad \text{where } \boldsymbol{\alpha}_{N}^{\uparrow} = \begin{bmatrix} 1 \\ 0 \end{bmatrix}, \ \boldsymbol{\alpha}_{N}^{\downarrow} = \begin{bmatrix} 0 \\ 1 \end{bmatrix}. \tag{3.76}$$

In any conducting non-magnetic layer n, where $k_n^{\uparrow} = k_n^{\downarrow} = k_n$, the spin current from electrons of spin orientation $\sigma = \uparrow, \downarrow$ incident on the left lead is given by (2.46) and (3.11)

$$\overrightarrow{j}_{\nu}^{(n)\sigma} = k_n \overrightarrow{\boldsymbol{\Psi}}_{n}^{\sigma\dagger}\boldsymbol{\Sigma}_{\nu}\overrightarrow{\boldsymbol{\Psi}}_{n}^{\sigma} = k_n \overrightarrow{\boldsymbol{\Psi}}_{N}^{\sigma\dagger}\mathbf{T}_{nN}^{\dagger}\boldsymbol{\Sigma}_{\nu}\mathbf{T}_{nN}\overrightarrow{\boldsymbol{\Psi}}_{N}^{\sigma},$$

where

$$\boldsymbol{\Sigma}_\nu = \boldsymbol{\sigma}_z \otimes \boldsymbol{\sigma}_\nu = \begin{bmatrix} \boldsymbol{\sigma}_\nu & \mathbf{0} \\ \mathbf{0} & -\boldsymbol{\sigma}_\nu \end{bmatrix}.$$

The total spin current $\overrightarrow{j}_\nu^{(n)} = \overrightarrow{j}_\nu^{(n)\uparrow} + \overrightarrow{j}_\nu^{(n)\downarrow}$ incident from the left is given by

$$\overrightarrow{j}_\nu^{(n)} = k_n \,\mathrm{tr}\left\{ \begin{bmatrix} \mathbf{t'}_{1N}^{\dagger} & \mathbf{0} \end{bmatrix} \mathbf{T}_{nN}^{\dagger} \boldsymbol{\Sigma}_\nu \mathbf{T}_{nN} \begin{bmatrix} \mathbf{t'}_{1N} \\ \mathbf{0} \end{bmatrix} \right\}. \tag{3.77}$$

Likewise, for electrons of spin $\sigma = \uparrow, \downarrow$ incident from the right, the spin current in layer n is

$$\overleftarrow{j}_\nu^{(n)\sigma} = k_n \overleftarrow{\boldsymbol{\Psi}}_n^{\sigma\dagger} \boldsymbol{\Sigma}_\nu \overleftarrow{\boldsymbol{\Psi}}_n^{\sigma} = k_n \overleftarrow{\boldsymbol{\Psi}}_N^{\sigma\dagger} \mathbf{T}_{nN}^{\dagger} \boldsymbol{\Sigma}_\nu \mathbf{T}_{nN} \overleftarrow{\boldsymbol{\Psi}}_N^{\sigma}.$$

Now, the total spin current $\overleftarrow{j}_\nu^{(n)} = \overleftarrow{j}_\nu^{(n)\uparrow} + \overleftarrow{j}_\nu^{(n)\downarrow}$ incident from the right is

$$\overleftarrow{j}_\nu^{(n)} = k_n \,\mathrm{tr}\left\{ \begin{bmatrix} \mathbf{r'}_{1N}^{\dagger} & \mathbf{1} \end{bmatrix} \mathbf{T}_{nN}^{\dagger} \boldsymbol{\Sigma}_\nu \mathbf{T}_{nN} \begin{bmatrix} \mathbf{r'}_{1N} \\ \mathbf{1} \end{bmatrix} \right\}. \tag{3.78}$$

Using the relation $\mathbf{t'}_{1,N}\mathbf{t'}_{1,N}^{\dagger} + \mathbf{r'}_{1,N}\mathbf{r'}_{1,N}^{\dagger} = \mathbf{1}$ from (3.58), (3.78) can be transformed as follows

$$\begin{aligned}
\overleftarrow{j}_\nu^{(n)} &= k_n \,\mathrm{tr}\left\{ \begin{bmatrix} \mathbf{r'}_{1N} \\ \mathbf{1} \end{bmatrix} \begin{bmatrix} \mathbf{r'}_{1N}^{\dagger} & \mathbf{1} \end{bmatrix} \mathbf{T}_{nN}^{\dagger} \boldsymbol{\Sigma}_\nu \mathbf{T}_{nN} \right\} \\
&= k_n \,\mathrm{tr}\left\{ \begin{bmatrix} \mathbf{r'}_{1N}\mathbf{r'}_{1N}^{\dagger} & \mathbf{r'}_{1N} \\ \mathbf{r'}_{1N}^{\dagger} & \mathbf{1} \end{bmatrix} \mathbf{T}_{nN}^{\dagger} \boldsymbol{\Sigma}_\nu \mathbf{T}_{nN} \right\} \\
&= k_n \,\mathrm{tr}\left\{ -\begin{bmatrix} \mathbf{t'}_{1N}^{\dagger}\mathbf{t'}_{1N} & \mathbf{0} \\ \mathbf{0} & \mathbf{0} \end{bmatrix} + \begin{bmatrix} \mathbf{1} & \mathbf{r'}_{1N} \\ \mathbf{r'}_{1N}^{\dagger} & \mathbf{1} \end{bmatrix} \mathbf{T}_{nN}^{\dagger} \boldsymbol{\Sigma}_\nu \mathbf{T}_{nN} \right\} \\
&= k_n \,\mathrm{tr}\left\{ -\begin{bmatrix} \mathbf{t'}_{1N}^{\dagger} & \mathbf{0} \end{bmatrix} \begin{bmatrix} \mathbf{t'}_{1N} \\ \mathbf{0} \end{bmatrix} + \begin{bmatrix} \mathbf{1} & \mathbf{r'}_{1N} \\ \mathbf{r'}_{1N}^{\dagger} & \mathbf{1} \end{bmatrix} \mathbf{T}_{nN}^{\dagger} \boldsymbol{\Sigma}_\nu \mathbf{T}_{nN} \right\}.
\end{aligned} \tag{3.79}$$

Comparing (3.79) with (3.77) we obtain

$$\overleftarrow{j}_\nu^{(n)} = -\overrightarrow{j}_\nu^{(n)} + k_n \,\mathrm{tr}\{\mathbf{W}\mathbf{L}_i\}$$

where

$$\mathbf{W} = \begin{bmatrix} \mathbf{1} & \mathbf{r'}_{1N} \\ \mathbf{r'}^{\dagger}_{1N} & \mathbf{1} \end{bmatrix}, \qquad \mathbf{L}_\nu = \mathbf{T}^{\dagger}_{nN} \mathbf{\Sigma}_\nu \mathbf{T}_{nN}.$$

In the case of charge current, $\nu = 0$ and so by (3.22), $\mathbf{L}_0 = k_N k_n^{-1} \mathbf{\Sigma}_0$. It follows that

$$\mathrm{tr}\{\mathbf{W}\mathbf{L}_0\} = \mathrm{tr}\left\{ \begin{bmatrix} \mathbf{1} & \mathbf{r'}_{1N} \\ \mathbf{r'}^{\dagger}_{1N} & \mathbf{1} \end{bmatrix} \begin{bmatrix} \boldsymbol{\sigma}_0 & \mathbf{0} \\ \mathbf{0} & -\boldsymbol{\sigma}_0 \end{bmatrix} \right\} = \mathrm{tr}\left\{ \begin{bmatrix} \mathbf{1} & \mathbf{r'}_{1N} \\ \mathbf{r'}^{\dagger}_{1N} & -\mathbf{1} \end{bmatrix} \right\} = 0,$$

hence for charge current $\overleftarrow{j}^{(n)}_0 = -\overrightarrow{j}^{(n)}_0$. For spin current, we proceed as follows. Clearly, both $\mathbf{L}_\nu$ and $\mathbf{W}$ are Hermitian. Further, from Equation (A.4), if $\nu = x$ or z then

$$\mathbf{L}^*_\nu = -\mathbf{I}\mathbf{L}_\nu\mathbf{I}, \quad \text{where } \mathbf{I} = \begin{bmatrix} \mathbf{0} & \mathbf{1} \\ \mathbf{1} & \mathbf{0} \end{bmatrix}.$$

Further, because $\mathbf{r'}$ is symmetric (A.2), then $\mathbf{W}^* = \mathbf{I}\mathbf{W}\mathbf{I}$. So on the one hand, taking the complex conjugate, we get

$$(\mathrm{tr}\{\mathbf{W}\mathbf{L}_\nu\})^* = \mathrm{tr}\{(\mathbf{W}\mathbf{L}_\nu)^\dagger\} = \mathrm{tr}\{\mathbf{L}^\dagger_\nu \mathbf{W}^\dagger\} = \mathrm{tr}\{\mathbf{W}\mathbf{L}_\nu\},$$

whilst on the other hand we get

$$(\mathrm{tr}\{\mathbf{W}\mathbf{L}_\nu\})^* = \mathrm{tr}\{\mathbf{W}^*\mathbf{L}^*_\nu\} = -\mathrm{tr}\{\mathbf{I}\mathbf{W}\mathbf{I}\mathbf{I}\mathbf{L}_\nu\mathbf{I}\} = -\mathrm{tr}\{\mathbf{W}\mathbf{L}_\nu\}.$$

So for $\nu = x$ or z we conclude that $\mathrm{tr}\{\mathbf{W}\mathbf{L}_\nu\} = 0$, and therefore

$$\overleftarrow{j}^{(n)}_\nu = -\overrightarrow{j}^{(n)}_\nu, \quad \nu \in \{0, x, z\}. \tag{3.80}$$

Hence the out-of-plane component is the only contributor to exchange coupling.

3.6 Asymptotic Behaviour

In the previous sections we were dealing exclusively with spin current density which, as noted in Section 2.6, is evaluated at some value of in-plane momentum $\bar{k}_{\parallel} = (k_x, k_z)$. Recall that in the Landauer model electrons arrive in the system at all possible momenta with equal probability. In this section we examine some properties pertaining to spin current, which is obtained by adding contributions of all those electron states, or more precisely, by integrating over in-plane momentum (see equation (2.58)). Of specific interest to us will be the oscillatory behaviour of the exchange spin current, as the thickness of the spacer L is increased. Motivation to study these oscillations stems from the fact that absorption of the out-of-plane component of spin current by the switching magnet exerts torque capable of changing the direction of the magnetisation. In order to achieve better switching efficiency it is desirable to fabricate the device so that a maximum of spin current is positioned near the S|SM interface. The relation between spin current and torque will be discussed in more detail in Chapter 5.

A similar calculation was previously performed for the electrical conductance G in a parabolic band [2]. It was shown that when all contributions to transmission are included, by integrating over the in-plane momenta, the resulting expression oscillates as a function of spacer thickness L with the amplitude decreasing as $1/\sqrt{L}$. Furthermore, when the potential profile is a rectangular well, with the Fermi energy level near the top, two distinct oscillation periods are observed. The first period is RKKY-like (from the *Ruderman–Kittel–Kasuya–Yosida* (RKKY), or indirect exchange interaction mediated by conduction electrons [25]) and arises from near those $\bar{k}_{\parallel}$-points where the spacer Fermi surface has extrema in the growth direction ($\bar{k}_{\parallel} = \bar{0}$). The second period arises from the boundary effects, near the top of the well, where transmission vanishes non-analytically. Here we perform a similar analysis for all components of the spin current, considering the cases where potential profile of the multilayer is a double barrier or a double well, that is, where potentials in the magnets are greater or less than those in the leads and the spacer, respectively. In each case we find only the RKKY type periods. This is because (after switching to polar coordinates) the integrand of the conductance has leading order $G \sim O(k^{-1/2})$ while the integrand of spin current components is $j_\nu \sim O(k^{1/2})$, where k

is the the out-of-plane wave vector. So the spin current density tends to zero in a smooth way near the zone boundary and the total spin current does not exhibit the non-RKKY-like period. Following the discussion in Section 2.6, spin current components in the spacer are obtained by integrating spin current density over the permissible values of $\bar{k}_\parallel$. For the parabolic model we assume the system having rotational symmetry in momentum space. We can therefore, switch to polar coordinates in xz-plane whereby the total current is given by the following formula

$$J_\nu(L) = 2\pi \int_0^{k_\mathrm{F}} j_\nu(k_\parallel, L) k_\parallel \mathrm{d}k_\parallel, \tag{3.81}$$

where $k_\mathrm{F} = \sqrt{2m(E_F - V)}/\hbar$, $V = V_1 = V_3 = V_5$ is the potential in the spacer and the leads, and $k_\parallel = |\bar{k}_\parallel|$. The double barrier or well profile is therefore characterised by the conditions $V_i - \Delta/2 > V$ and $V_i + \Delta/2 < V$, respectively, where $i = 2, 4$ (recall Figure 3.2). Assuming that reflections off the magnets are not too strong ($||\mathbf{r}'_{13}\mathbf{r}_{35}||_\mathrm{F} \ll 1$) we retain only the first-order reflections in the series expansion of the amplitude. Here we denote $k \equiv k_3$ for the out-of-plane wave-vector in the spacer, and also suppress the layer index j_ν because we are only interested in the spacer current (layer 3)at the current density in this section. For the current density generated by electrons incident from the left using (2.49) we obtain

$$\overrightarrow{j}_\nu = k \ \mathrm{tr}\left\{\left(\overrightarrow{\mathbf{a}}\,\overrightarrow{\mathbf{a}}^\dagger - \overrightarrow{\mathbf{b}}\,\overrightarrow{\mathbf{b}}^\dagger\right)\boldsymbol{\sigma}_\nu\right\},$$

where

$$\overrightarrow{\mathbf{a}} = \left(\mathbf{1} - \mathbf{r}'_{13}\mathbf{r}_{35}\right)^{-1}\mathbf{t}'_{13}, \qquad \overrightarrow{\mathbf{b}} = \mathbf{r}_{35}\overrightarrow{\mathbf{a}}. \tag{3.82}$$

Now expanding $\overrightarrow{\mathbf{a}}$ in a geometric series and retaining one reflection term we find

$$\overrightarrow{\mathbf{a}} \approx \mathbf{t}'_{13} + \mathbf{r}'_{13}\mathbf{r}_{35}\mathbf{t}'_{13}.$$

We are interested in the terms that are periodic in the spacer thickness L. Using (2.31) and (3.14) it is not hard to calculate the components of $\mathbf{t}'_{13}$, $\mathbf{r}'_{13}$ and $\mathbf{r}_{35}$ (at $\theta = 0$ for clarity)

explicitly

$$\mathbf{t'}_{13}(0) = \begin{bmatrix} t'^{\uparrow}_{13} & 0 \\ 0 & t'^{\downarrow}_{13} \end{bmatrix}, \qquad \mathbf{r'}_{13}(0) = \begin{bmatrix} r'^{\uparrow}_{13} & 0 \\ 0 & r'^{\downarrow}_{13} \end{bmatrix}, \qquad \mathbf{r}_{35}(0) = \begin{bmatrix} r^{\uparrow}_{35} & 0 \\ 0 & r^{\downarrow}_{35} \end{bmatrix}, \tag{3.83}$$

where

$$t'^{\sigma}_{13} = \frac{2kk_2^{\sigma}}{2kk_2^{\sigma}\cos(k_2^{\sigma}L_{\mathrm{PM}}) - \mathrm{i}(k^2+k_2^{\sigma 2})\sin(k_2^{\sigma}L_{\mathrm{PM}})} e^{-\mathrm{i}kL_{\mathrm{PM}}}, \tag{3.84a}$$

$$r'^{\sigma}_{13} = -\frac{\mathrm{i}(k^2-k_2^{\sigma 2})\sin(k_2^{\sigma}L_{\mathrm{PM}})}{2kk_2^{\sigma}\cos(k_2^{\sigma}L_{\mathrm{PM}}) - \mathrm{i}(k^2+k_2^{\sigma 2})\sin(k_2^{\sigma}L_{\mathrm{PM}})} e^{-2\mathrm{i}kL_{\mathrm{PM}}}, \tag{3.84b}$$

$$r^{\sigma}_{35} = -\frac{\mathrm{i}(k^2-k_4^{\sigma 2})\sin(k_4^{\sigma}L_{\mathrm{SM}})}{2kk_4^{\sigma}\cos(k_4^{\sigma}L_{\mathrm{SM}}) - \mathrm{i}(k^2+k_4^{\sigma 2})\sin(k_4^{\sigma}L_{\mathrm{SM}})} e^{2\mathrm{i}k(L_{\mathrm{PM}}+L)}, \tag{3.84c}$$

$\sigma = \uparrow, \downarrow$ and L_{PM}, L_{SM} are the thicknesses of the PM and the SM, respectively. From (3.84) it is clear that the periodicity in L is contained only in $\mathbf{r}_{35}$ via the factor of $e^{2\mathrm{i}kL}$. Expanding the current density we group the terms as follows

$$\begin{aligned}
\overrightarrow{j}_{\nu}/k &= \mathrm{tr}\left\{\overrightarrow{\mathbf{a}}^{\dagger}\boldsymbol{\sigma}_{\nu}\overrightarrow{\mathbf{a}}\right\} \approx \mathrm{tr}\left\{(\mathbf{t'}_{13} + \mathbf{r'}_{13}\mathbf{r}_{35}\mathbf{t'}_{13})^{\dagger}\boldsymbol{\sigma}_{\nu}[\mathbf{t'}_{13} + \mathbf{r'}_{13}\mathbf{r}_{35}\mathbf{t'}_{13}]\right\} \\
&= \mathrm{tr}\left\{\mathbf{t'}^{\dagger}_{13}\boldsymbol{\sigma}_{\nu}\mathbf{t'}_{13}\right\} + \mathrm{tr}\left\{\mathbf{t'}^{\dagger}_{13}\mathbf{r}^{\dagger}_{35}\mathbf{r'}^{\dagger}_{13}\boldsymbol{\sigma}_{\nu}\mathbf{r'}_{13}\mathbf{r}_{35}\mathbf{t'}_{13}\right\} \\
&+ \mathrm{tr}\left\{\mathbf{t'}^{\dagger}_{13}\mathbf{r}^{\dagger}_{35}\mathbf{r'}^{\dagger}_{13}\boldsymbol{\sigma}_{\nu}\mathbf{t'}_{13}\right\} + \mathrm{tr}\left\{\mathbf{t'}^{\dagger}_{13}\boldsymbol{\sigma}_{\nu}\mathbf{r'}_{13}\mathbf{r}_{35}\mathbf{t'}_{13}\right\} \\
&= \mathrm{tr}\left\{\left(\mathbf{t'}_{13}\mathbf{t'}^{\dagger}_{13} + \mathbf{r'}_{13}\mathbf{r}_{35}\mathbf{t'}_{13}\mathbf{t'}^{\dagger}_{13}\mathbf{r}^{\dagger}_{35}\mathbf{r'}^{\dagger}_{13}\right)\boldsymbol{\sigma}_{\nu}\right\} \\
&+ \mathrm{tr}\left\{\left(\mathbf{t'}_{13}\mathbf{t'}^{\dagger}_{13}\mathbf{r}^{\dagger}_{35}\mathbf{r'}^{\dagger}_{13} + \mathbf{r'}_{13}\mathbf{r}_{35}\mathbf{t'}_{13}\mathbf{t'}^{\dagger}_{13}\right)\boldsymbol{\sigma}_{\nu}\right\}.
\end{aligned} \tag{3.85}$$

The first term under trace in the last equality in (3.85) represents the constant (with respect to L) background because every factor is multiplied by its Hermitian conjugate, wherefore the factors of $e^{2\mathrm{i}kL}$ cancel out. The last term constitutes the oscillatory part. From (3.82) it follows that the expansion of the left-moving current is obtained by conjugating (3.85) with $\mathbf{r}_{35}$. Therefore, introducing the following notation

$$\overrightarrow{\mathbf{q}}^{\sim} = \mathbf{r'}_{13}\mathbf{r}_{35}\mathbf{t'}_{13}\mathbf{t'}^{\dagger}_{13}, \qquad \overrightarrow{\mathbf{p}}^{\sim} = \overrightarrow{\mathbf{q}}^{\sim} - \mathbf{r}_{35}\overrightarrow{\mathbf{q}}^{\sim}\mathbf{r}^{\dagger}_{35}, \tag{3.86}$$

we can write the oscillatory part of current density due to left-incident electrons $\overrightarrow{j}^{\sim}_{\nu}$ in a concise manner

$$\overrightarrow{j}^{\sim}_{\nu} = k\ \mathrm{tr}\left\{\left(\overrightarrow{\mathbf{p}}^{\sim} + \overrightarrow{\mathbf{p}}^{\sim\dagger}\right)\boldsymbol{\sigma}_{\nu}\right\} = 2k\Re\mathrm{tr}\left\{\overrightarrow{\mathbf{p}}^{\sim}\boldsymbol{\sigma}_{\nu}\right\}. \tag{3.87}$$

Note that since we are specifically interested in the oscillatory term in the low reflection approximation, we do not have to disregard higher order terms of the constant background part of the current. In fact for the purposes of plotting the approximation against the result of the exact calculation it may be desirable to retain more terms to achieve the correct shift of the plot along the energy axis. Therefore, we can preform the following re-summation of (3.82). Denoting

$$\mathbf{u} = \mathbf{t'}_{13}\mathbf{t'}^{\dagger}_{13}, \quad \mathbf{c} = \mathbf{r'}_{13}\mathbf{r}_{35}, \tag{3.88}$$

we find that, since all terms in the constant part must involve equal number of factors of $\mathbf{c}$ and their conjugates, the total background contribution from the right-moving electrons $\overrightarrow{\mathbf{q}}^{-}$ has the following form

$$\overrightarrow{\mathbf{q}}^{-} = \mathbf{u} + \mathbf{cuc}^{\dagger} + \mathbf{ccuc}^{\dagger}\mathbf{c}^{\dagger} + \ldots, \tag{3.89}$$

while including the right-moving electrons is done similarly to (3.86)

$$\overrightarrow{\mathbf{p}}^{-} = \overrightarrow{\mathbf{q}}^{-} - \mathbf{r}_{35}\overrightarrow{\mathbf{q}}^{-}\mathbf{r}^{\dagger}_{35},$$

giving the total constant background current density due to the left-incident electrons $\overrightarrow{j}^{-}_{i}$

$$\overrightarrow{j}^{-}_{\nu} = 2k\Re\,\mathrm{tr}\left\{\overrightarrow{\mathbf{p}}^{-}\boldsymbol{\sigma}_{\nu}\right\}.$$

In summary, we have separated current density in the spacer into the oscillatory and constant parts

$$\overrightarrow{j}_{\nu} = \overrightarrow{j}^{\sim}_{\nu} + \overrightarrow{j}^{-}_{\nu}, \tag{3.90}$$

where in the oscillatory part $\overrightarrow{j}^{\sim}_{\nu}$ we have retained one reflection term in the spacer. For electrons incident from the right lead the analysis is performed in a similar way starting from

the expression for the current density

$$\overleftarrow{j}_i = k \text{ tr} \left\{ \left(\mathbf{r}'_{13} \overleftarrow{\mathbf{b}} \ \overleftarrow{\mathbf{b}}^\dagger \mathbf{r}'^\dagger_{13} - \overleftarrow{\mathbf{b}} \overleftarrow{\mathbf{b}}^\dagger \right) \boldsymbol{\sigma}_i \right\},$$

and expanding $\overleftarrow{\mathbf{b}}$

$$\overleftarrow{\mathbf{b}} \approx \mathbf{t}_{35} + \mathbf{r}_{35} \mathbf{r}'_{13} \mathbf{t}_{35}.$$

Now, looking at (3.84) and (3.86) we see that the oscillatory factor is exactly e^{2ikL}. We can, therefore, write

$$\overleftrightarrow{\mathbf{p}}^{\sim} = \overleftrightarrow{\boldsymbol{\varrho}} e^{2ikL},$$

where matrix $\overleftrightarrow{\boldsymbol{\varrho}}$ does not depend on L, and define the amplitude factors

$$\overleftrightarrow{A}_\nu = k \text{ tr} \left\{ \overleftrightarrow{\boldsymbol{\varrho}} \boldsymbol{\sigma}_\nu \right\}. \tag{3.91}$$

Since we are interested in the behaviour of the static (exchange) current, we define the total amplitude A_ν by adding the contributions from the left- and right incident electrons.

$$A_\nu = \overrightarrow{A}_\nu + \overleftarrow{A}_\nu. \tag{3.92}$$

Now we can write down the expression for spin current density in the form suitable for further analysis

$$j^{\sim}_\nu(k_\parallel, L) = \Re \left\{ A_\nu(k_\parallel) e^{2ik(k_\parallel)L} \right\}. \tag{3.93}$$

We are ready at this point to use (3.81) to calculate the total current and investigate its asymptotic properties for large values of L. Since the current density in our case vanishes at the edge of the band $k_\parallel = k_\mathrm{F}$, we can extend the upper limit of integration to ∞.

$$J^{\sim}_\nu(L) = 2\pi \Re \int_0^\infty A(k_\parallel) e^{2ik(k_\parallel)L} k_\parallel dk_\parallel. \tag{3.94}$$

Integral (3.94) can be treated using the stationary phase approximation. In the parabolic model $k(k_\parallel)$ has a stationary point at $k_\parallel = 0$ (known as Γ-point in the band structure theory), as seen

from (2.13). Expanding k near 0 and adding an infinitesimal imaginary part $\mathrm{i}\delta$, $\delta > 0$ to the exponent to ensure convergence we obtain

$$J_\nu^\sim(L) = 2\pi A(0)\Re e^{2\mathrm{i}k(0)L_\mathrm{S}} \int_0^\infty e^{\mathrm{i}(k''(0)+\mathrm{i}\delta)L_\mathrm{S}k_\parallel^2} k_\parallel dk_\parallel + O\left(\frac{1}{L_\mathrm{S}^2}\right), \tag{3.95}$$

where we have replaced $A(k_\parallel)$ with its value at the stationary point, because that is the only one that will contribute to the value of the integral as $L \to \infty$. The integral in (3.95) is readily evaluated, whereby upon letting $\delta \to 0$ we find

$$J_\nu^\sim(L) = -\Re\frac{\pi A(0)}{\mathrm{i}k''(0)L_\mathrm{S}} e^{2\mathrm{i}k(0)L_\mathrm{S}} + O\left(\frac{1}{L_\mathrm{S}^2}\right) = \Re\frac{\pi A(0)k(0)}{\mathrm{i}L_\mathrm{S}} e^{2\mathrm{i}k(0)L_\mathrm{S}} + O\left(\frac{1}{L_\mathrm{S}^2}\right), \tag{3.96}$$

where we have used the fact that $k''(0) = -1/k(0)$. Finally, taking the real part, obtain the asymptotic formula for the oscillatory current in the spacer

$$J_\nu^\sim(L) = \frac{\pi A_\nu(0)k(0)}{L}\sin\left(2k(0)L\right) + O\left(\frac{1}{L^2}\right). \tag{3.97}$$

For a numerical demonstration we consider a model with relatively shallow potentials, so that confinement is not too strong, and the single-reflection approximation holds well. Here the

	V	Δ	θ	$y_{n+1} - y_n$
L_1	0.0	0.0	0.0	-
PM	$\pm$0.5	0.05	0.6	7.0
S	0.0	0.0	0.0	20.0
SM	$\pm$0.5	0.05	0.0	3.0
L_2	0.0	0.0	0.0	-

Table 3.1: Device parameters used to obtain figures 3.7-3.10.

positive and negative potentials in the magnets correspond to the double barrier and double well profile, respectively. We also set the Fermi level at $E_\mathrm{F} = 0.4$. In Figures 3.7, 3.8 we demonstrate the characteristic behaviour of the current density in momentum space as a function of $k_\parallel$. All components exhibit slow variation near the Γ-point ($k_\parallel = 0$) and a number of peaks (resonances) near the edge of the band. The number of peaks increases with the thickness of the spacer. When integrated over momentum, the peaks largely cancel each other, which is an illustration of why the stationary phase method works in this case. We also observe current density approach

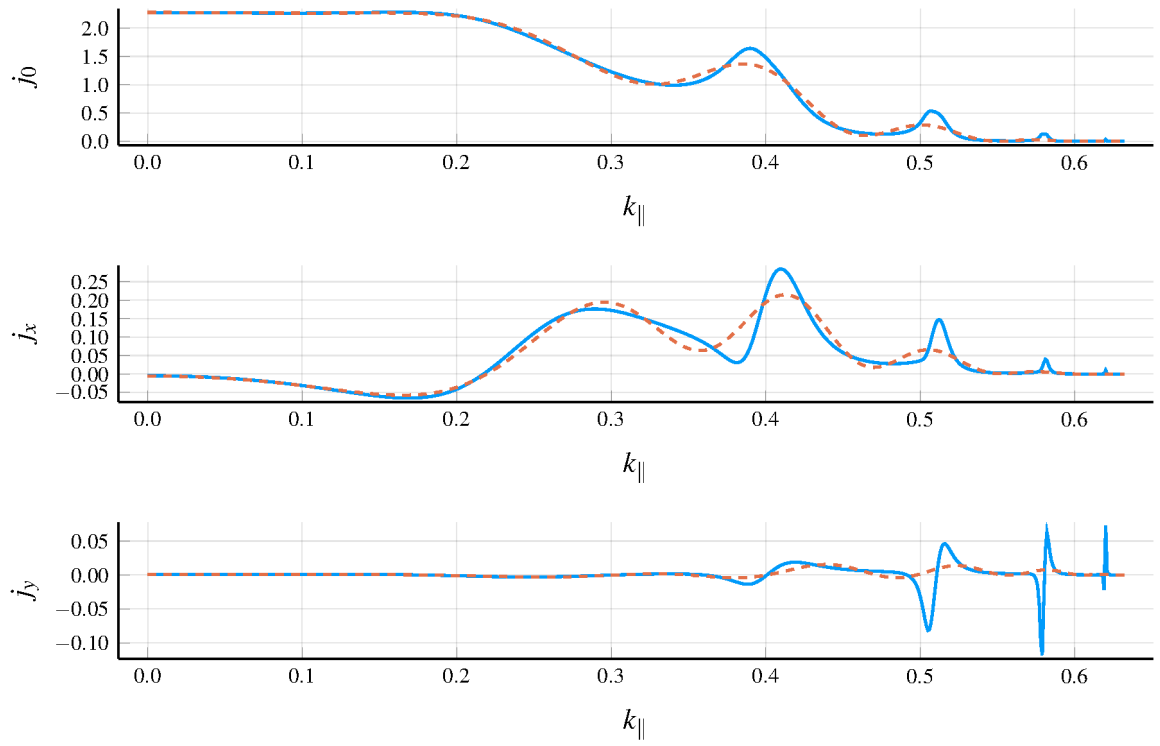

Figure 3.7: Current density components in momentum space, calculated adding all reflections (solid line) and one reflection (dashed line) for a double barrier potential.

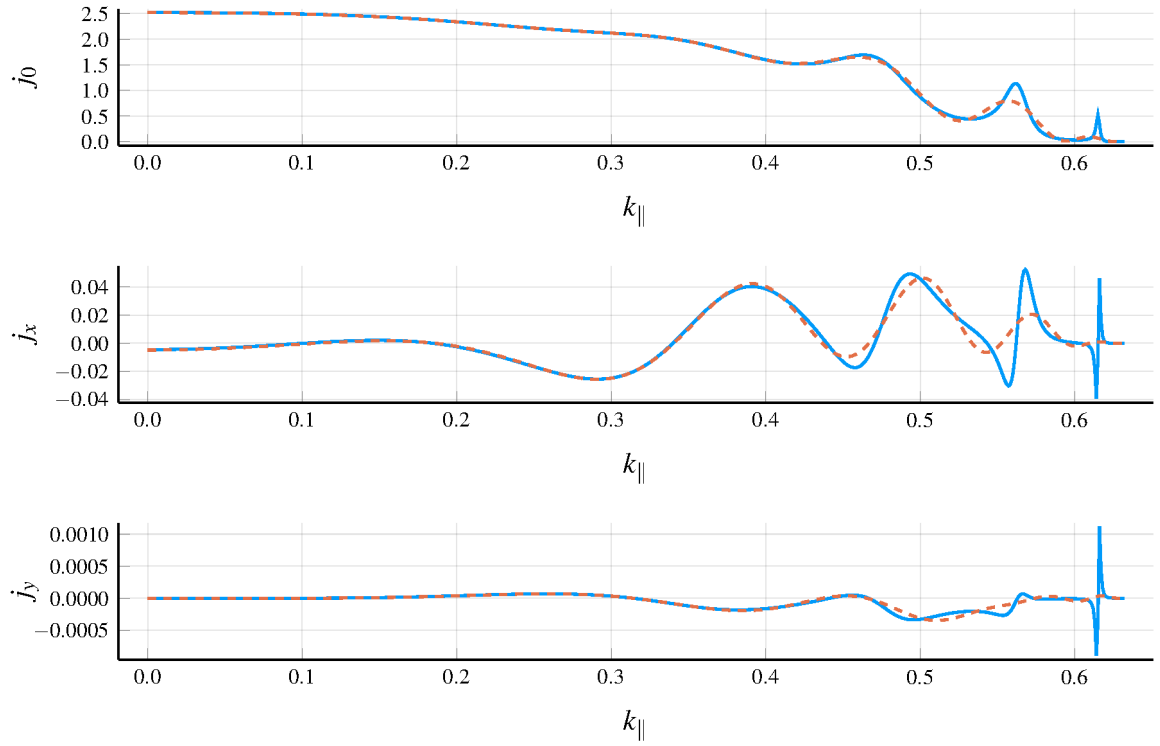

Figure 3.8: Current density components in momentum space, calculated adding all reflections (solid line) and one reflection (dashed line) for a double well potential.

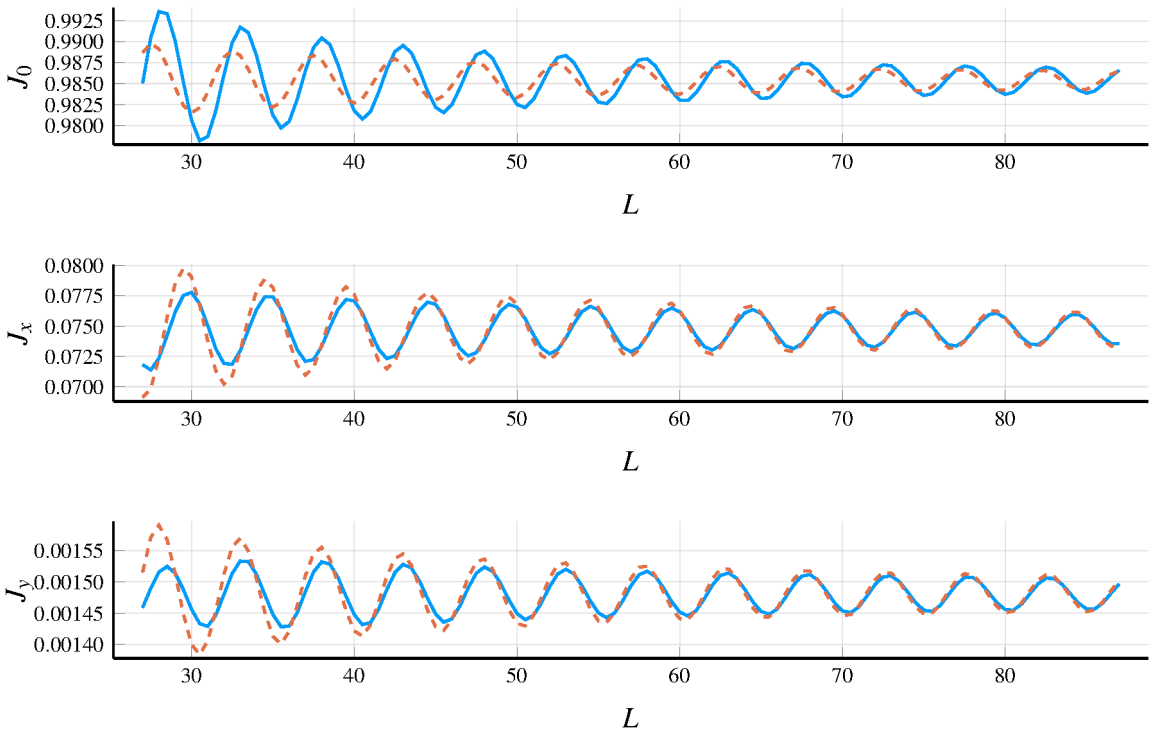

Figure 3.9: Oscillations of the total (integrated) current as a function of spacer thickness (solid line) and the asymptotic approximation (dashed line) for double barrier potential.

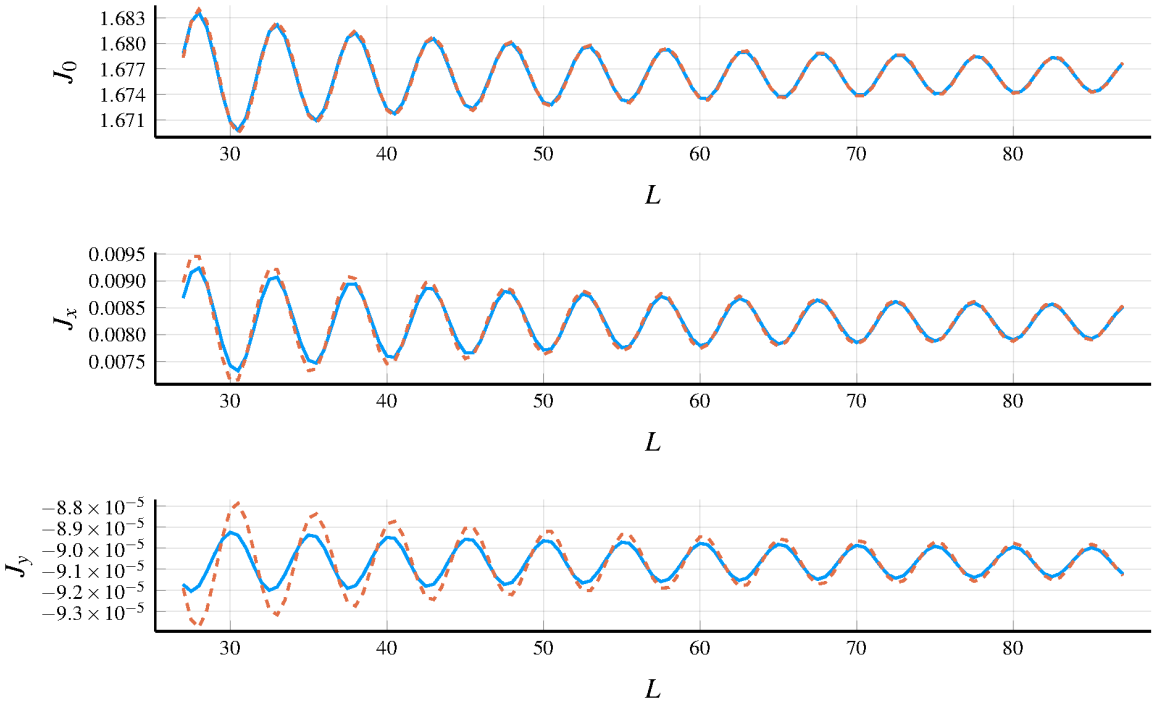

Figure 3.10: Oscillations of the total (integrated) current as a function of spacer thickness (solid line) and the asymptotic approximation (dashed line) for double well potential.

zero smoothly in each case. In Figures 3.9, 3.10 we plot the integrated current (3.81) as a function of the spacer thickness and compare it with the asymptotic approximation derived in (3.97). As remarked in the beginning of the section, we only observe one oscillation period determined by the value of the wave vector at the Γ-point, that is $k(0)$, as follows from (3.97).

We have thus provided an example of applying the transmission formalism developed in this chapter to extracting approximations and asymptotic behaviour of spin current in a multilayer. This is a generalisation of the approach previously employed to study charge current and transmission, specifically in [2], where the potential profile was a single barrier (well). Transmission and reflection matrices allow us to perform calculations for arbitrary multilayers in a straightforward and concise manner.

Chapter 4

Optical Analogies

This chapter constitutes a brief digression from the main narrative of this work, in order to put the transfer matrix in a wider mathematical context. Here we describe some results from linear optics and show how they may be borrowed and generalised by spintronics. We also indicate a number of possible future extensions of this research.

4.1 Iwasawa Decomposition

In the previous sections we concerned ourselves with various symmetries of the spin current and the corresponding transfer matrix. Here we give an outline of another type of symmetry that enables the application of a powerful and intuitive formalism leading to deeper understanding of the action of the transfer matrix. This approach can take advantage of a rich set of results and techniques primarily applied in the field of geometric optics, but hardly explored in the context of spintronics. We will confine ourselves to the proof of applicability of the method and some numeric illustrations, deferring a more detailed analytic treatment to future research.

The problem of classification of multilayers by their overall action on the properties of the incoming waves has been considered in linear optics [58], [59], as well as from the general viewpoint of the transfer matrix method [3]. Deep connections to hyperbolic geometry and

relativistic formalism space-time have been investigated. The idea of the geometric and, more generally, group-theoretic approach to the theory of reflection is to reduce the complicated processes inside the multilayer to a small number of parameters which are easily interpreted. In particular, illustrating the action of the transfer matrix by means of tracing out trajectories on the unit disk under the corresponding Möbius transforms [3] can be useful for understanding the structure of the transformation. In fact, Möbius transforms can describe transmission so conveniently that they have even been successfully extended to the matrix-valued [60] case and applied in the tight-binding setting. In order to extract the parameters providing the geometrical intuition for the transfer matrix, one particular factorisation has proved useful, namely, the *Iwasawa decomposition* [61]. It arises in the theory of Lie groups and reflects the statement that an element of a non-compact semi-simple Lie group factorises into an ordered product of the elements of a maximal compact subgroup, a maximal Abelian subgroup, and a maximal nilpotent subgroup (one of each). Further in this chapter we will give a detailed characterisation of these group elements. We will introduce the decomposition first in the spinless case, as it is used in geometric optics. There a lossless (where depolarisation does not occur) multilayer transfer matrix $\boldsymbol{\tau}$ has the form

$$\boldsymbol{\tau} = \begin{bmatrix} \frac{1}{t} & \frac{r^*}{t^*} \\ \frac{r}{t} & \frac{1}{t^*} \end{bmatrix} = \begin{bmatrix} \alpha & \beta \\ \beta^* & \alpha^* \end{bmatrix}.$$

Assuming we work in the current, rather than amplitude, picture the conservation equation $|r|^2 + |t|^2 = 1$ is satisfied, which implies $\det|\boldsymbol{\tau}| = +1$. This means that $\boldsymbol{\tau}$ belongs to $\mathrm{SU}(1,1)$. It is then established that the following factorisation holds [62], [63]

$$\boldsymbol{\tau} = \mathbf{k}(\phi)\mathbf{a}(\xi)\mathbf{n}(\nu), \tag{4.1}$$

where

$$\mathbf{k}(\phi) = \begin{bmatrix} \exp(\mathrm{i}\phi/2) & 0 \\ 0 & \exp(-\mathrm{i}\phi/2) \end{bmatrix},$$

$$\mathbf{a}(\xi) = \begin{bmatrix} \cosh(\xi/2) & \mathrm{i}\sinh(\xi/2) \\ -\mathrm{i}\sinh(\xi/2) & \cosh(\xi/2) \end{bmatrix},$$

$$\mathbf{n}(\nu) = \begin{bmatrix} 1 - \mathrm{i}\nu/2 & \nu/2 \\ \nu/2 & 1 + \mathrm{i}\nu/2 \end{bmatrix}.$$

The parameters $-2\pi \leq \phi \leq 2\pi$, and ξ, $\nu \in \mathbb{R}$ can be expressed in terms of the transfer matrix components as follows

$$\phi/2 = \arg(\alpha + \mathrm{i}\beta), \quad \xi/2 = \ln(1/|\alpha + \mathrm{i}\beta|), \quad \nu/2 = \Re(\alpha\beta^*)/|\alpha + \mathrm{i}\beta|^2.$$

In some cases it is convenient to conjugate $\boldsymbol{\tau}$ with the unitary matrix $\mathbf{u} = \frac{1}{\sqrt{2}}\left[\begin{smallmatrix} 1 & \mathrm{i} \\ \mathrm{i} & 1 \end{smallmatrix}\right]$,

$$\boldsymbol{\tau} \to \mathbf{u}\boldsymbol{\tau}\mathbf{u}^\dagger,$$

which sends $\boldsymbol{\tau}$ to an element in $\mathrm{SL}(2,\mathbb{R})$. The Iwasawa decomposition then takes the following form

$$\mathbf{k}(\phi) = \begin{bmatrix} \cos(\phi/2) & -\sin(\phi/2) \\ -\sin(\phi/2) & \cos(\phi/2) \end{bmatrix},$$

$$\mathbf{a}(\xi) = \begin{bmatrix} \exp(\xi/2) & 0 \\ 0 & \exp(-\xi/2) \end{bmatrix},$$

$$\mathbf{n}(\nu) = \begin{bmatrix} 1 & 0 \\ \nu & 1 \end{bmatrix}.$$

In this representation the factors have intuitive physical interpretations in geometric optics.

$\mathbf{k}(\phi)$ represents a rotation in the phase space, $\mathbf{a}(\xi)$ is the magnifier that scales up by the factor of $\exp(\xi/2)$ in real space and down by the same factor in momentum space, and $\mathbf{n}(\nu)$ acts as the ray transfer matrix of a lens of power ν (or focal length $1/\nu$). Thus the geometry of the Iwasawa decomposition for transfer matrices in $\mathrm{SL}(2,\mathbb{R})$ is well understood, and is used to explain certain phenomena, for example, the origin of the Thomas rotation [59].

We shall now establish the conditions under which the Landauer transfer matrix (2.27) acting on spin-resolved wave functions, which we have been studying here, can be factorised in a similar way. To this end, we will invoke a generalisation of the Iwasawa decomposition to the group of $2n \times 2n$ complex symplectic matrices $\mathrm{Sp}_n(\mathbb{C})$ and an explicit calculation algorithm [64], [65]. Precisely, following the exposition in [64], we consider the complex symplectic group

$$\mathrm{Sp}_n(\mathbb{C}) = \left\{ \mathbf{G} \in \mathrm{SL}_{2n}(\mathbb{C}) : \mathbf{G}^T \mathbf{\Omega}_{2n} \mathbf{G} = \mathbf{\Omega}_{2n} \right\},$$

where $\mathbf{\Omega}_{2n} = \left[\begin{smallmatrix} \mathbf{0} & \mathbf{1} \\ -\mathbf{1} & \mathbf{0} \end{smallmatrix}\right]$. Then the subgroups K, A and N corresponding to the Iwasawa factors are characterised as follows. K consists of $2n \times 2n$ unitary matrices that also belong to $\mathrm{Sp}_n(\mathbb{C})$ and can be shown to have the form

$$K = \left\{ \mathbf{C} = \begin{bmatrix} \mathbf{a} & -\mathbf{b}^* \\ \mathbf{b} & \mathbf{a}^* \end{bmatrix} : \mathbf{C} \in \mathrm{U}(2n) \right\} = \mathrm{U}(2n) \cap \mathrm{Sp}_n(\mathbb{C}).$$

A consists of positive diagonal matrices of the following form

$$A = \left\{ \mathrm{diag}\left[a_1, \ldots, a_n, a_1^{-1}, \ldots, a_n^{-1} \right] : a_1, \ldots, a_n > 0 \right\}.$$

Finally, N consists of unit upper-block-triangular matrices

$$N = \left\{ \begin{bmatrix} \mathbf{a} & \mathbf{b} \\ \mathbf{0} & (\mathbf{a}^{-1})^T \end{bmatrix} : \mathbf{a} \text{ unit upper triangular}, \mathbf{a}\mathbf{b}^T = \mathbf{b}\mathbf{a}^T \right\}.$$

Now consider $\mathbf{T}_{mn}$, as given by (2.27) where layers m and n are non-magnetic. Taking the transpose and making use of the symmetry of the submatrices under transposition, as shown

in (A.2), (A.3), we obtain

$$\mathbf{T}^T_{mn} = \frac{k_m}{k_n} \begin{bmatrix} \mathbf{t}^{-1}_{mn} & \mathbf{t}^{-1}_{mn}\mathbf{r}_{mn} \\ -\mathbf{r'}_{mn}\mathbf{t}^{-1}_{mn} & \mathbf{t'}_{mn} - \mathbf{r'}_{mn}\mathbf{t}^{-1}_{mn}\mathbf{r}_{mn} \end{bmatrix}. \tag{4.2}$$

Now assuming that the potentials in layers m and n are the same, that is $k_m = k_n$, we find, after some straightforward block multiplication, that indeed

$$\mathbf{T}^T \mathbf{\Omega}_4 \mathbf{T} = \mathbf{\Omega}_4. \tag{4.3}$$

Another way of proving (4.3) is to use the general block-wise form of $\mathbf{T}$ derived in Appendix A.2. Therefore, the transfer matrix is symplectic if it corresponds to the transmission between two non-magnetic layers with equal electrostatic potentials. We have thus established the conditions for applicability of the Iwasawa formalism to the spin-resolved transfer matrix. Its utility for the classification of *magnetic* multilayers, in the presence of in-plane and out-of-plane polarisation is an interesting problem to address, even if the increased dimensionality may not allow for a straightforward geometrical interpretation. With this we conclude the overview of the generalised Iwasawa decomposition within the context of this study.

4.2 Spin Müller-Jones Formalism

4.2.1 Müller-Jones Calculus

The transfer matrix method that we have been using so far does not originate in spintronics. Its variants are widely used in optics to study propagation of electromagnetic waves through layered media. In particular, certain analogies between the problems of optics and topics in electronic transport were outlined by Datta [10], however, in that discussion spin is explicitly omitted. An extensive study of reflection of electromagnetic and particle waves is contained in [66] that again is mostly concerned with non-magnetic media. We would like to highlight another matrix formalism that can be borrowed from optics, where it is a very commonly used technique, and

give an interpretation of that in the context of spin transfer, namely the *Müller-Jones* (MJ) calculus. In order to distinguish it from the standard MJ method, as it is known in optics, we will refer to the adaptation as the *Spin Müller-Jones* (MJ) formalism. To our knowledge, the apparatus of the MJ calculus has not been, to this day, systematically applied in spintronics. Some studies of spin current-induced torques [67] consider certain novel decompositions of the transfer matrix which may be connected to the MJ constructions. Derivation of the conductivity tensors in [68] involves formulae that have the form of those, which will appear below in the expressions of the Müller matrix components. However, the point of view of the MJ method is not directly adopted in either of those studies. The material of this chapter is largely exploratory, and is presented with a view of being further investigated and refined in the future research.

The *Jones calculus* was introduced by R.C. Jones in 1941 in a series of papers beginning with [69], and is used to study propagation of fully polarised light across linear optical elements. Important results from the group-theoretic point of view were obtained by R. Cloude [70]. The literature covering the formalism is extensive, and the list of references in [71] can be consulted for an overview. It is still an active area of research, and the recent developments, for example [72], [73] continue to define new representations and decompositions for advanced polarimetry studies. Here we present a short summary and a selection of definitions and results that present immediate interest from the perspective of spin transport.

Polarisation of light is described by the *Jones vector*, and the elements of the optical multilayer are described by their *Jones matrices*. The resulting mathematical framework is very similar to that of the transfer matrix method, in that the propagation across successive layers is described by the action of the product of their Jones matrices on the incident Jones vector. Electric field in a monochromatic plane wave is described by two complex numbers E_1 and E_2 representing the transverse components [74], [75]. These numbers can be combined into a spinor

$$\boldsymbol{\xi} = \begin{bmatrix} E_1 \\ E_2 \end{bmatrix} \qquad \boldsymbol{\xi}^\dagger = \begin{bmatrix} E_1^* & E_2^* \end{bmatrix}, \tag{4.4}$$

The product $\mathbf{c} = \boldsymbol{\xi}\boldsymbol{\xi}^\dagger$ is called the *coherency matrix*. Since $\mathbf{c}$ is Hermitian, it can be expanded in the basis of Pauli matrices

$$\mathbf{c} = \frac{1}{2}\sum_\nu s_\nu \boldsymbol{\sigma}_\nu, \tag{4.5}$$

where the expansion coefficients $s_\nu = \mathrm{tr}(\mathbf{c}\boldsymbol{\sigma}_\nu)$ are called the *Stokes parameters*. Suppose that in a different layer of an optical multilayer the transverse wave is described by spinor $\boldsymbol{\xi}'$. The 2×2 matrix $\mathbf{a}$ taking $\boldsymbol{\xi}$ to $\boldsymbol{\xi}'$ by means of

$$\boldsymbol{\xi}' = \mathbf{a}\boldsymbol{\xi} \tag{4.6}$$

is the Jones matrix. We can find the transformation law of the Stokes coefficients

$$s'_\nu = \mathrm{tr}\{\mathbf{c}'\boldsymbol{\sigma}_\nu\} = \mathrm{tr}\{\mathbf{a}\mathbf{c}\mathbf{a}^\dagger\boldsymbol{\sigma}_\nu\} = \frac{1}{2}\sum_\mu \mathrm{tr}\{\mathbf{a}\boldsymbol{\sigma}_\mu\mathbf{a}^\dagger\boldsymbol{\sigma}_\nu\}s_\mu = \sum_\mu M_{\mu\nu}s_\mu, \tag{4.7}$$

where $\mathbf{M} = [M_{\mu\nu}]$ is the *Müller-Jones matrix*. The Müller-Jones matrix satisfies the following identity [75]

$$\mathbf{M}^*\mathbf{L}\mathbf{M} = (\det \mathbf{M})^{\frac{1}{2}}\,\mathbf{L},$$

where $\mathbf{L} = \mathrm{diag}\,[1, -1, -1, -1]$ is the Lorentz metric. Combining the Stokes parameters into a 4-vector denoted $\bar{\bar{s}}$ (4.7) can be written as follows

$$\bar{\bar{s}}' = \mathbf{M}\bar{\bar{s}} \tag{4.8}$$

In other words, the Müller-Jones matrix describes the propagation of the Stokes vector through the system. Geometrically, (4.8) can be interpreted as the rotation of the Stokes vector on the Poincaré (Bloch) sphere [75], [12]. It is important to note that components of $\mathbf{M}$ in (4.8) may be obtained from experimental data, including the situations where the optical medium in question is a depolarizing one. In such cases $\mathbf{M}$ is referred to as the *Müller matrix* which in general cannot be expressed in terms of a Jones matrix. Furthermore, not every 4×4 matrix can even be a physically realisable Müller matrix. The necessary conditions for that and the relation between the Müller and Müller-Jones matrices are discussed at length in [76] and [77].

We will not go any further in to those at present, but just remark that any Müller matrix can be expressed as a convex sum of at most 4 Müller-Jones matrices.

4.2.2 Interpretation for Spin Transport

By direct analogy with of polarised light, we can substitute spinor wave-functions for the electric fields in the previous section and calculate the spin equivalents of the Jones and Müller-Jones matrices. Recall that, by virtue of (2.38), the spin-resolved wave function amplitude in layer n is related to that in layer 0 by

$$\boldsymbol{\alpha}_n = \mathbf{a}_n \boldsymbol{\alpha}_0.$$

Therefore, the transmission coefficient $\mathbf{a}_n$ assumes the role of the Jones matrix, and $\boldsymbol{\alpha}_n \boldsymbol{\alpha}_n^\dagger$ corresponds to the coherency matrix. Furthermore, as was suggested by the form of (2.56) spin current components are indeed the Stokes coefficients in the expansion in Pauli matrices (with identity, for charge current). Note that in optics the expansion basis is often taken in a different order, corresponding to $\{\boldsymbol{\sigma}_0, \boldsymbol{\sigma}_z, \boldsymbol{\sigma}_y, \boldsymbol{\sigma}_x\}$. However, we shall follow the "natural" order adopted in quantum mechanics, which also follows the exposition of the formalism in [75]. Taking into account the factor of k in the definition of spin current, relation (4.7) can then be rewritten as follows as follows

$$j'_\nu = \frac{1}{2}\frac{k'}{k} \sum_\mu \left(\mathrm{tr}\{\boldsymbol{\sigma}_\mu \mathbf{a} \boldsymbol{\sigma}_\nu \mathbf{a}^\dagger\} - \mathrm{tr}\{\boldsymbol{\sigma}_\mu \mathbf{b} \boldsymbol{\sigma}_\nu \mathbf{b}^\dagger\} \right) j_\mu \tag{4.9}$$

Defining matrix components

$$(\mathbf{M}_a)_{\mu\nu} = \frac{1}{2}\,\mathrm{tr}\{\boldsymbol{\sigma}_\mu \mathbf{a} \boldsymbol{\sigma}_\nu \mathbf{a}^\dagger\}, \qquad (\mathbf{M}_b)_{\mu\nu} = \frac{1}{2}\,\mathrm{tr}\{\boldsymbol{\sigma}_\mu \mathbf{b} \boldsymbol{\sigma}_\nu \mathbf{b}^\dagger\},$$

we can write (4.9) as follows

$$\bar{\bar{\mathbf{j}}}' = \frac{k'}{k} \left(\mathbf{M}_a - \mathbf{M}_b \right) \bar{\bar{\mathbf{j}}}, \tag{4.10}$$

where $\bar{\bar{\mathbf{j}}}$ stands for the 4-component current vector. Using (4.9) we can directly relate the current components between two non-magnetic layers of the system. Since we are primarily interested in calculating current in conducting layers, we have so far limited the discussion to

the form of the expression (2.46). However, if the layer in question is an insulator with $k_n = \mathrm{i}\varkappa_n$ where $\varkappa_n > 0$, we obtain instead a generalised notion of current for the case of an insulating spacer

$$\bar{\bar{\mathbf{j}}} = \mathrm{i}\varkappa \, \mathrm{tr}\left\{\boldsymbol{\alpha}\bar{\bar{\boldsymbol{\sigma}}}\boldsymbol{\beta}^{\dagger} - \boldsymbol{\beta}\bar{\bar{\boldsymbol{\sigma}}}\boldsymbol{\alpha}^{\dagger}\right\}. \tag{4.11}$$

Now note that the net current in the conducting case can be written in the following form (suppressing the wave vector multiplier)

$$\bar{\bar{\mathbf{j}}} = \mathrm{tr}\left\{\begin{bmatrix}\mathbf{a}^{\dagger} & \mathbf{b}^{\dagger}\end{bmatrix}(\boldsymbol{\sigma}_z \otimes \boldsymbol{\sigma}_{\nu})\begin{bmatrix}\mathbf{a} \\ \mathbf{b}\end{bmatrix}\right\},$$

extends the notation employed in (3.77). Furthermore, the insulating case can be expressed similarly

$$\bar{\bar{\mathbf{j}}} = \mathrm{tr}\left\{\begin{bmatrix}\mathbf{a}^{\dagger} & \mathbf{b}^{\dagger}\end{bmatrix}(\boldsymbol{\sigma}_y \otimes \boldsymbol{\sigma}_{\nu})\begin{bmatrix}\mathbf{a} \\ \mathbf{b}\end{bmatrix}\right\}.$$

This leads one to consider the following generalisation. Denote $\mathfrak{a} = \left[\begin{smallmatrix}\mathbf{a} \\ \mathbf{b}\end{smallmatrix}\right]$. Then the matrix

$$\mathfrak{J}_{\mu\nu} = \mathrm{tr}\left\{\mathfrak{a}^{\dagger}\left(\boldsymbol{\sigma}_{\mu} \otimes \boldsymbol{\sigma}_{\nu}\right)\mathfrak{a}\right\} = \mathrm{tr}\left\{\mathfrak{a}\mathfrak{a}^{\dagger}\left(\boldsymbol{\sigma}_{\mu} \otimes \boldsymbol{\sigma}_{\nu}\right)\right\} \tag{4.12}$$

contains information both about the conducting ($\mathfrak{J}_{z\nu}$), and insulating ($\mathfrak{J}_{y\nu}$) case. Here $\mathfrak{a}$ generalises the concept of the Jones matrix to the net spin current case. Consequently, it makes sense to define the counterpart of the Müller-Jones matrix as follows

$$\mathfrak{M}_{\lambda\rho\mu\nu} = \frac{1}{2}\,\mathrm{tr}\left\{\mathfrak{a}\left(\boldsymbol{\sigma}_{\lambda} \otimes \boldsymbol{\sigma}_{\rho}\right)\mathfrak{a}^{\dagger}\left(\boldsymbol{\sigma}_{\mu} \otimes \boldsymbol{\sigma}_{\nu}\right)\right\} \tag{4.13}$$

Group-theoretic analysis of (4.12) and (4.13), and the symmetries they satisfy could be an interesting line of research providing more direct proofs of certain symmetries of spin current in multilayers. These matrices could also be employed for the task of classification of magnetic multilayers, and the conditions under which various spin current components arise or vanish. Another potential advantage of the Müller formalism for spin current has to do with the fact that a general Müller matrix can describe depolarising media in optics. This means that its

analogue in spin transport could be used in calculations in the presence of spin relaxation in the multilayer. These topics, however, lie outside of the scope of the present work, and we defer further investigation to the future studies. We now return to the main theme of this thesis, and consider further applications and development of the Landauer formalism.

Chapter 5

Interlayer Exchange Coupling

In this chapter we define open and closed systems for the purposes of electron transport in multilayers and extend the Landauer method to the closed case. We study the behaviour of spin current components, as a system transitions from the open to the closed regime, and obtain an exact expression for the strength of the interlayer exchange coupling in terms of the out-of-plane spin current component, calculated using the Landauer method.

5.1 Introduction

Since the introduction of the Landauer formalism in Section 2.5.1 and throughout the subsequent discussion we have emphasised the importance of the assumption that the multilayer system is connected to large phase-randomising reservoirs. Those act as sources of electrons arriving at all permitted momenta, energies and spin projections, and also as sinks where the electrons escape to and, having undergone phase relaxation, no longer influence scattering processes in the layers. In the calculations of spin current this assumption manifested itself in two ways. Firstly, it led us to impose boundary conditions of the form (3.32), (3.38) or (3.75), (3.76) representing the states arriving into the system. Secondly, when calculating the total current we had to integrate over the in-plane momentum, energy and sum over the spin projections, as it was done in (2.58), in order to account for contributions of all possible states emitted

from the reservoirs. For the purposes of this study we shall refer to systems coupled to the environment, in this case in the form of the macroscopic reservoirs, as *open*. In this chapter we shall extend the Landauer method to a different class of models that do not require a supply of carriers, and can be considered completely isolated from the environment. We shall label these latter systems *closed*.

The particular physical phenomenon that we will be dealing with here is called *interlayer exchange coupling* (IEC). This is a form of interaction between magnetic materials that tends to align their magnetic moments parallel or anti-parallel to each other. There are five known mechanisms of exchange interaction (direct exchange, double exchange, superexchange, RKKY interaction and exchange via itinerant electrons) that apply depending on the degree of localisation of magnetic moments and whether the materials in question are metals or non-metals [25]. We shall assume the itinerant electron model, which commonly applies to the case of transition metals (Fe, Co, Ni), whereby the exchange interaction is mediated by electrons in the metallic spacer.

At its most fundamental, exchange interaction arises from the indistinguishability of particles and the Pauli exclusion principle. For example, a system of two electrons can be in a state with total spin $S = 0$ if the spins are aligned anti-parallel to each other, or $S = 1$ if they are parallel. It can then be shown [78] (§62) that these states correspond, respectively, to wave functions ϕ given by symmetrised and anti-symmetrised products of the individual electron wave functions ϕ_1 and ϕ_2

$$\phi = \frac{1}{\sqrt{2}} \left[\phi_1(\bar{r}_1)\phi_2(\bar{r}_2) \pm \phi_1(\bar{r}_2)\phi_2(\bar{r}_1)\right].$$

In particular, when $\bar{r}_1 = \bar{r}_2$ the antisymmetric solution vanishes because two electrons with parallel spins cannot be found in the same position, in a manifestation of the Pauli principle. The expectation of the interaction energy $\hat{U}(\bar{r}_2 - \bar{r}_1)$ is given by $A \pm J$, where

$$A = \iint \hat{U} \left|\phi_1(\bar{r}_1)\right|^2 \left|\phi_2(\bar{r}_2)\right|^2 \mathrm{d}V_1 \mathrm{d}V_2,$$
$$J = \iint \hat{U} \phi_1(\bar{r}_1)\phi_1^*(\bar{r}_2)\phi_2(\bar{r}_2)\phi_2^*(\bar{r}_1) \mathrm{d}V_1 \mathrm{d}V_2,$$

where A is the background (direct) term, and J is the exchange integral. The electrostatic interaction energy is given by the Heisenberg Hamiltonian

$$\hat{U} = -2J\hat{\mathbf{s}}_1\hat{\mathbf{s}}_2.$$

Thus the total spin of the system determines the possible values of energy. In solid crystals this quantum-mechanical exchange is often represented by an effective exchange field, also referred to as the molecular, or Weiss, field [44], derived within the mean field approximation. In our model this is taken into account via the exchange splitting terms.

When it comes to calculating the strength of IEC, there are two common approaches available. Those are the *energy method* and the *torque method*. The energy-based calculation implements the most intuitive approach, that is obtaining the total thermodynamic energy of the system when the magnetic moments are aligned in parallel and anti-parallel directions, respectively, and subtracting one from the other. This can be performed realistically, either within the tight-binding models with parameters fitted from experimental data, or using *ab initio* methods. The main practical disadvantage of the energy method stems from the fact that the total energy is usually rather large, while the difference can be very small (of the order of 1meV), leading to poor convergence. The torque method, on the other hand, is based on the observation that the coupling energy per unit angle is characterised by the torque exerted by one magnet on the other. That torque is related to the out-of-plane component of the spin current absorbed by the magnet at the interface. This method was first applied in [79] by Slonczewski to the case of an insulating spacer, and in [80] by Erickson *et al.*, to the case of a metallic spacer. We will be using the results developed in Chapters 2 and 3 to obtain a closed-form expression for the out-of-plane spin current and use that in the torque calculation of the exchange coupling. We will check it against the equivalent energy-based calculation using the spectral density formalism. Since the IEC does not require external supply of electrons, we will provide an interpretation of the result in the light of the Landauer formalism extended to the closed systems.

Lastly, we remark that IEC is a promising phenomenon for applications. The tendency for magnets to align in the parallel and anti-parallel configuration might be used as a mecha-

nism of switching the magnetisation direction for writing data to non-volatile magnetoresistive memory cells [81]. Since the interaction itself exists without any external supply of carriers and can be modulated by controlling the out-of-plane spin current in the spacer (which itself can be achieved with or without sending charge current through), the resulting devices could, in principle, be operated with extremely low power consumption.

5.2 Torque Method

This approach to calculating the IEC is based on the fact that the torque exerted on the switching magnet is due to the out-of-plane spin current in the spacer. Before discussing it we will require a certain result that expresses the out-of-plane spin current density as an exact derivative with respect to the magnetisation direction.

5.2.1 Spin Current As an Exact Derivative

We shall now prove that the out-of-plane current density is an exact derivative with respect to the polarisation angle. Since we are interested in the exchange part of the current, as defined in (2.59), we must add the left- and right-moving parts of both the left- and right-incident current in the layer of interest. We derive the general result for an n-th (non-magnetic) segment of an N-layer system, of the type depicted in Figure 2.14. For simplicity we assume that only the magnetisation of the layer adjacent to the spacer on the left is set at an angle of $\theta_{n-1} = \theta$ in-plane, and $\theta_k = 0$, $k \neq n-1$. Calculating the out-of-plane spin current due to electrons emerging from the left reservoir we obtain

$$\begin{aligned} \frac{1}{k_n} \overrightarrow{j}_y &= \mathrm{tr}\left\{ \overrightarrow{\mathbf{a}}^\dagger \boldsymbol{\sigma}_y \overrightarrow{\mathbf{a}} - \overrightarrow{\mathbf{b}}^\dagger \boldsymbol{\sigma}_y \overrightarrow{\mathbf{b}} \right\} \\ &= \mathrm{tr}\left\{ \mathbf{t'}^\dagger_{1n} \overrightarrow{\mathbf{r}}^\dagger_n \boldsymbol{\sigma}_y \overrightarrow{\mathbf{r}}_n \mathbf{t'}_{1n} \right\} \\ &\quad - \mathrm{tr}\left\{ \mathbf{t'}^\dagger_{1n} \overrightarrow{\mathbf{r}}^\dagger_n \mathbf{r}^\dagger_{nN} \boldsymbol{\sigma}_y \mathbf{r}_{nN} \overrightarrow{\mathbf{r}}_n \mathbf{t'}_{1n} \right\}, \end{aligned} \tag{5.1}$$

where $\overrightarrow{\mathbf{r}}_n$, $\overleftarrow{\mathbf{r}}_n$ are defined as in (2.34). Using the cyclic property of trace and the relations

$$\begin{aligned}
\overrightarrow{\mathbf{r}}_n \mathbf{r'}_{1n} &= \left(\mathbf{1} - \mathbf{r'}_{1n}\mathbf{r}_{nN}\right)^{-1} \mathbf{r'}_{1n} = \mathbf{r'}_{1n}\left(\mathbf{1} - \mathbf{r}_{nN}\mathbf{r'}_{1n}\right)^{-1} = \mathbf{r'}_{1n}\overleftarrow{\mathbf{r}}_n, \\
\mathbf{r}_{nN}\overrightarrow{\mathbf{r}}_n &= \mathbf{r}_{nN}\left(\mathbf{1} - \mathbf{r'}_{1n}\mathbf{r}_{nN}\right)^{-1} = \left(\mathbf{1} - \mathbf{r}_{nN}\mathbf{r'}_{1n}\right)^{-1}\mathbf{r}_{nN} = \overleftarrow{\mathbf{r}}_n\mathbf{r}_{nN},
\end{aligned}$$

we can transform the right-hand side as follows

$$\frac{1}{k_n}\overrightarrow{j}_y = \mathrm{tr}\left\{\overrightarrow{\mathbf{r}}_n \mathbf{t'}_{1n}\mathbf{t'}^{\dagger}_{1n}\overrightarrow{\mathbf{r}}^{\dagger}_n\boldsymbol{\sigma}_y\right\} - \mathrm{tr}\left\{\overleftarrow{\mathbf{r}}_n\mathbf{r}_{nN}\mathbf{t'}_{1n}\mathbf{t'}^{\dagger}_{1n}\mathbf{r}^{\dagger}_{nN}\overleftarrow{\mathbf{r}}^{\dagger}_n\boldsymbol{\sigma}_y\right\}. \tag{5.3}$$

We can now use (3.25d) to eliminate transmission matrices from (5.3) and work only with reflection coefficients thereafter. Taking advantage of the fact that the spacer and the leads are non-magnetic we obtain

$$\mathbf{t'}_{1n}\mathbf{t'}^{\dagger}_{1n} = \mathbf{k}_1\mathbf{k}_n^{-1}\left(\mathbf{1} - \mathbf{r'}_{1n}\mathbf{r'}^{\dagger}_{1n}\right).$$

With that in mind, (5.3) is written as follows

$$\begin{aligned}
\frac{1}{k_1}\overrightarrow{j}_y = \mathrm{tr}\left\{\overrightarrow{\mathbf{r}}_n\overrightarrow{\mathbf{r}}^{\dagger}_n\boldsymbol{\sigma}_y\right\} &- \mathrm{tr}\left\{\overrightarrow{\mathbf{r}}_n\mathbf{r'}_{1n}\mathbf{r'}^{\dagger}_{1n}\overrightarrow{\mathbf{r}}^{\dagger}_n\boldsymbol{\sigma}_y\right\} \\
&- \mathrm{tr}\left\{\overleftarrow{\mathbf{r}}_n\mathbf{r}_{nN}\mathbf{r}^{\dagger}_{nN}\overleftarrow{\mathbf{r}}^{\dagger}_n\boldsymbol{\sigma}_y\right\} + \mathrm{tr}\left\{\overleftarrow{\mathbf{r}}_n\mathbf{r}_{nN}\mathbf{r'}_{1n}\mathbf{r'}^{\dagger}_{1n}\mathbf{r}^{\dagger}_{nN}\overleftarrow{\mathbf{r}}^{\dagger}_n\boldsymbol{\sigma}_y\right\}.
\end{aligned} \tag{5.4}$$

Following similar steps for the left-moving current and noting that

$$\mathbf{t}_{nN}\mathbf{t}^{\dagger}_{nN} = \mathbf{k}_N\mathbf{k}_n^{-1}\left(\mathbf{1} - \mathbf{r}_{nN}\mathbf{r}^{\dagger}_{nN}\right),$$

which follows from (3.25c) we obtain

$$\begin{aligned}
\frac{1}{k_N}\overleftarrow{j}_y = \mathrm{tr}\left\{\overrightarrow{\mathbf{r}}_n\mathbf{r'}_{1n}\mathbf{r'}^{\dagger}_{1n}\overrightarrow{\mathbf{r}}^{\dagger}_n\boldsymbol{\sigma}_y\right\} &- \mathrm{tr}\left\{\overrightarrow{\mathbf{r}}_n\mathbf{r'}_{1n}\mathbf{r}_{nN}\mathbf{r}^{\dagger}_{nN}\mathbf{r'}^{\dagger}_{1n}\overrightarrow{\mathbf{r}}^{\dagger}_n\boldsymbol{\sigma}_y\right\} \\
&- \mathrm{tr}\left\{\overleftarrow{\mathbf{r}}_n\overleftarrow{\mathbf{r}}^{\dagger}_n\boldsymbol{\sigma}_y\right\} + \mathrm{tr}\left\{\overleftarrow{\mathbf{r}}_n\mathbf{r}_{nN}\mathbf{r}^{\dagger}_{nN}\overleftarrow{\mathbf{r}}^{\dagger}_n\boldsymbol{\sigma}_y\right\}.
\end{aligned} \tag{5.5}$$

Since we assume $k_1 = k_N = k$ throughout, adding (5.4) and (5.5) we can calculate the total exchange current density

$$\begin{aligned}
\frac{1}{k} j_y &= \frac{1}{k}\left(\overrightarrow{j}_y + \overleftarrow{j}_y\right) \\
&= \mathrm{tr}\left\{\overrightarrow{\mathbf{r}}_n \left(\mathbf{1} - \mathbf{r'}_{1n}\mathbf{r}_{nN}\mathbf{r}^{\dagger}_{nN}\mathbf{r'}^{\dagger}_{1n}\right)\overrightarrow{\mathbf{r}}^{\dagger}_n \boldsymbol{\sigma}_y\right\} \\
&\quad - \mathrm{tr}\left\{\overleftarrow{\mathbf{r}}_n \left(\mathbf{1} - \mathbf{r}_{nN}\mathbf{r'}_{1n}\mathbf{r'}^{\dagger}_{1n}\mathbf{r}^{\dagger}_{nN}\right)\overleftarrow{\mathbf{r}}^{\dagger}_n \boldsymbol{\sigma}_y\right\} \\
&= \mathrm{tr}\left\{\left(\overrightarrow{\mathbf{r}}_n - \overleftarrow{\mathbf{r}}_n\right)\boldsymbol{\sigma}_y + \mathrm{h.c.}\right\} \\
&= \mathrm{tr}\left\{\left(\mathbf{1} - \mathbf{r}_{nN}\mathbf{r'}_{1n}\right)^{-1}\mathbf{r}_{nN}\left[\boldsymbol{\sigma}_y, \mathbf{r'}_{1n}\right] + \mathrm{h.c.}\right\} \\
&= -2\mathrm{i}\,\mathrm{tr}\left\{\left(\mathbf{1} - \mathbf{r}_{nN}\mathbf{r'}_{1n}\right)^{-1}\mathbf{r}_{nN}\left(\frac{\mathrm{i}}{2}\left[\boldsymbol{\sigma}_y, \mathbf{r'}_{1n}\right]\right) - \mathrm{h.c.}\right\},
\end{aligned} \tag{5.6}$$

where h.c. stands for the Hermitian conjugate of the preceding term and $[,]$ is the standard commutator. Only reflections from the left represented by the factor $\mathbf{r'}_{1n}$ accrue polarisation, and the angular dependence is given by the following formula

$$\mathbf{r'}_{1n}(\theta) = e^{-\frac{\mathrm{i}\boldsymbol{\sigma}_y\theta}{2}}\mathbf{r'}_{1n}(0)e^{\frac{\mathrm{i}\boldsymbol{\sigma}_y\theta}{2}}. \tag{5.7}$$

Differentiating (5.7) with respect to θ we can write

$$\frac{\mathrm{d}}{\mathrm{d}\theta}\mathbf{r'}_{1n}(\theta) = -\frac{\mathrm{i}}{2}\left[\boldsymbol{\sigma}_y, \mathbf{r'}_{1n}\right]. \tag{5.8}$$

Substituting (5.8) into (5.6) and using the chain rule we obtain

$$j_y = -2\mathrm{i}k\frac{\mathrm{d}}{\mathrm{d}\theta}\,\mathrm{tr}\left\{\ln\left(\mathbf{1} - \mathbf{r}_{nN}\mathbf{r'}_{1n}\right) - \mathrm{h.c.}\right\}. \tag{5.9}$$

Rewriting (5.9) in terms of taking the imaginary part we finally arrive at the desired result

$$j_y = 4k\Im\frac{\mathrm{d}}{\mathrm{d}\theta}\ln\det\left(\mathbf{1} - \mathbf{r}_{nN}\mathbf{r'}_{1n}\right), \tag{5.10}$$

in the form of an exact derivative with respect to the magnetisation direction.

5.2.2 Description of the Method

We can now proceed to describe and apply the torque method. If we consider the thermodynamic potential as a function of the polarization angle, $\Omega(\theta)$ the parallel (P) and anti-parallel (AP) configurations will correspond to the values $\Omega(0)$ and $\Omega(\pi)$, respectively. We can therefore express the exchange energy U as follows

$$U = \Omega(0) - \Omega(\pi) = -\int_0^\pi \frac{\mathrm{d}\Omega}{\mathrm{d}\theta}\mathrm{d}\theta. \tag{5.11}$$

Here the integrand is the torque exerted on one magnetic moment by the other. As argued in [82], the torque on the switching magnet is determined by the total rate of change of the out-of-plane angular momentum absorbed by it which, by continuity, equates to the net spin current absorbed by the magnet. It is, therefore, found as the difference between the total spin current in the spacer $J_\nu^{(\mathrm{S})}$ and the right lead $J_\nu^{(\mathrm{L}_2)}$. Contribution to the torque per spin component $\frac{\mathrm{d}\Omega_\nu}{\mathrm{d}\theta}$ is thus found as follows

$$\frac{\mathrm{d}\Omega_\nu}{\mathrm{d}\theta} = J_\nu^{(\mathrm{S})} - J_\nu^{(\mathrm{L}_2)}, \tag{5.12}$$

We will suppress the layer label (S) for the spacer spin current in what follows. Unlike transport current that is carried by electrons at E_F, exchange current is contributed to by carriers at all energies up to E_F, as well as all possible values of in-plane momenta. This leads to the following expression for the total exchange spin current

$$J_\nu = \int_{\mathrm{BZ}_1} \mathrm{d}\bar{k}_\parallel \int_{-\infty}^{+\infty} \mathrm{d}E\, D(E) \left(f_\mathrm{L} \overrightarrow{j}_\nu(\bar{k}_\parallel, E) + f_\mathrm{R} \overleftarrow{j}_\nu(\bar{k}_\parallel, E) \right),$$

where

$$D(E) = \frac{1}{\pi}\frac{\mathrm{d}k}{\mathrm{d}E} = \frac{1}{2\pi k}$$

is the density of states in the lead per unit length and spin channel. The Fermi functions $f_\mathrm{L} \equiv f(E - \mu_\mathrm{L})$ and $f_\mathrm{R} \equiv f(E - \mu_\mathrm{R})$ characterise electron distributions of the left and right reservoirs with chemical potentials μ_L and μ_R, respectively. In 3.5 it was shown that $\overleftarrow{j}_\nu = -\overrightarrow{j}_\nu$

for both in-plane components $\nu = x, z$. Hence, when the system is in equilibrium, $\mu_{\mathrm{L}} = \mu_{\mathrm{R}} = \mu$, only the out-of-plane component ($\nu = y$) survives. Furthermore, since there can be no out-of-plane spin current in the leads, we find that (5.12) reduces to the following

$$\frac{\mathrm{d}\Omega}{\mathrm{d}\theta} = \frac{\mathrm{d}\Omega_y}{\mathrm{d}\theta} = J_y = \int_{\mathrm{BZ}_1} \mathrm{d}\bar{k}_{\parallel} \int_{-\infty}^{+\infty} \mathrm{d}E\, D(E) f(E-\mu) \left(\overrightarrow{j}_y + \overleftarrow{j}_y \right). \tag{5.13}$$

In Section 5.2.1 we showed that the current density can be expressed in terms of reflection matrices, as an exact derivative with respect to the polarization angle

$$\overrightarrow{j}_y + \overleftarrow{j}_y = 4k\Im \frac{\mathrm{d}}{\mathrm{d}\theta} \ln\det\left(\mathbf{1} - \mathbf{r}_{nN}\mathbf{r'}_{1n}\right). \tag{5.14}$$

From (5.13) and (5.14), after inserting a factor of $\frac{1}{2}$, since we are considering the torque transferred to one of the magnets only, we then obtain the following form of the total out-of-plane spin current

$$J_y = \frac{1}{\pi}\Im \int_{\mathrm{BZ}_1} \mathrm{d}\bar{k}_{\parallel} \int_{-\infty}^{+\infty} \mathrm{d}E\, f\left(E-\mu\right) \frac{\mathrm{d}}{\mathrm{d}\theta} \ln\det\left(\mathbf{1} - \mathbf{r}_{nN}\mathbf{r'}_{1n}\right). \tag{5.15}$$

Using (5.11) and (5.12) we obtain the exchange energy U after integrating over θ

$$U = -\frac{1}{\pi}\Im \int_{\mathrm{BZ}_1} \mathrm{d}\bar{k}_{\parallel} \int_{-\infty}^{+\infty} \mathrm{d}E\, f(E-\mu) \operatorname{tr}\ln\left(\mathbf{1} - \mathbf{r}'_{1n}(\theta)\mathbf{r}_{nN}\right)\Big|_0^{\pi}. \tag{5.16}$$

5.3 Energy Method

In this section we calculate exchange coupling using the energy method, loosely adapting the argument given in [5] where it is done for the multi-orbital case. We do not need the full generality here. Instead we make the proof compatible with the transmission formalism in order to compare the result with that obtained using the torque method.

We begin by considering a system with two magnets separated by a non-magnetic conducting spacer. The essence of the energy method is in calculating the difference between the ther-

modynamic potentials in the magnets, expressed in terms of the local density of states. This allows one to resolve the total energy in the up- and down-spin population which is required to calculate the coupling. We thus define the difference in thermodynamic potentials of the system U when the magnetisations of the magnets are in the P and AP alignment, respectively

$$U = \Omega_{\mathrm{P}}^{\uparrow} + \Omega_{\mathrm{P}}^{\downarrow} - \Omega_{\mathrm{AP}}^{\uparrow} - \Omega_{\mathrm{AP}}^{\downarrow}. \tag{5.17}$$

Here $\Omega_{\mathrm{P/AP}}^{\sigma}$ is the thermodynamic potential for electrons of spin orientation σ in a system where the magnetization is the P or AP state, and at finite temperature is given by the following formula [5]:

$$\Omega_{\mathrm{P|AP}}^{\sigma} = \int_{-\infty}^{+\infty} \mathrm{d}E\, F(E) \rho_{\mathrm{P|AP}}^{\sigma}(E), \tag{5.18}$$

where

$$F(E) = -k_{\mathrm{B}} T \ln \left[1 + \exp\left(\tfrac{\mu - E}{k_{\mathrm{B}} T} \right) \right]$$

is the anti-derivative of the Fermi distribution function and $\rho^{\sigma}(E)$ is the spin-resolved local density of states in the spacer, given in terms of the one-particle Green's function:

$$\rho^{\sigma}(E, L) = -\frac{1}{\pi} \Im \operatorname{tr} g_{\mathrm{LR}}^{\sigma}(E + \mathrm{i}0^{+}), \tag{5.19}$$

where g_{LR}^{σ} is the part of the spacer Green's function accounting for the interaction of the magnets via conduction electrons in the spacer, and L is the spacer thickness. Precisely, this means the following. Let g_{S} be the Green's function in the spacer of the original multilayer. Let g_{L}, g_{R} be the Green's functions in the spacer calculated in the presence of only one of the magnets (to the left or to the right, respectively), as if the other one did not exist. Then g_{LR} is found from the following expansion

$$g_{\mathrm{S}} = g_0 + g_{\mathrm{L}} + g_{\mathrm{R}} + g_{\mathrm{LR}},$$

where g_0 is the free-particle Green's function. As a side note, we mention that Green's function in a multilayer can be easily expressed in terms of the reflection amplitudes given by the transfer

matrix method. In the single-band case it is given by the following formula

$$g_n(y,y';E)=\begin{cases}\dfrac{m}{i\hbar^2k_n}\dfrac{\left(e^{-ik_ny'}+r'_{1n}e^{ik_ny'}\right)\left(e^{ik_ny}+r_{nN}e^{-ik_ny}\right)}{1-r_{nN}r'_{1n}}, & y>y'\\ \dfrac{m}{i\hbar^2k_n}\dfrac{\left(e^{ik_ny'}+r_{nN}e^{-ik_ny'}\right)\left(e^{-ik_ny}+r'_{1n}e^{ik_ny}\right)}{1-r'_{1n}r_{nN}}, & y<y'\end{cases}, \tag{5.20}$$

which is a generalisation of some results obtained in [83], [84] for single square-step potentials. In Appendix B we give a proof of (5.20), as well as the explicit formula for ρ, as given in [4]. Returning to the main proof we find that the exchange energy is expressed as follows

$$U=\sum_{\sigma=\uparrow,\downarrow}\int_{-\infty}^{+\infty}\mathrm{d}E\,F(E)\left[\rho^{\sigma}_{\mathrm{P}}(E)-\rho^{\sigma}_{\mathrm{AP}}(E)\right], \tag{5.21}$$

where P and AP signify that the density of states is calculated separately for each alignment of the magnets in the system, respectively. Expressing the sum over the spin states as taking a trace

$$\rho(E,l)=\sum_{\sigma=\uparrow,\downarrow}\rho^{\sigma}(E,L)=-\frac{1}{\pi}\Im\,\mathrm{tr}\,\mathbf{g}_{\mathrm{LR}}(E+\mathrm{i}0^{+}),$$

we use the following result featured in [5] and [85]

$$\mathrm{tr}\,\mathbf{g}_{\mathrm{LR}}=\frac{\mathrm{d}}{\mathrm{d}E}\,\mathrm{tr}\ln\left(\mathbf{1}-\mathbf{g}_0\boldsymbol{\tau}_{\mathrm{L}}\mathbf{g}_0\boldsymbol{\tau}_{\mathrm{R}}\right), \tag{5.22}$$

where

$$\boldsymbol{\tau}_i=\mathbf{v}_i\left(\mathbf{1}-\mathbf{g}_0\mathbf{v}_i\right)^{-1},$$

known as the T-matrix (not the same as the $\mathbf{T}$ transfer matrix). Using the following relations [53]

$$\mathbf{r}=\langle y\,|\,\mathbf{g}_0\,|\,y\rangle\,\langle -k\,|\,\boldsymbol{\tau}\,|\,k\rangle\,, \tag{5.23a}$$

$$\langle -k\,|\,\boldsymbol{\tau}\,|\,k\rangle=\int e^{\mathrm{i}(x'+x'')}\,\langle x''\,|\,\boldsymbol{\tau}\,|\,x'\rangle\,dx'dx'', \tag{5.23b}$$

inserting the resolution of identity and integrating, we can express (5.22) in terms of the reflec-

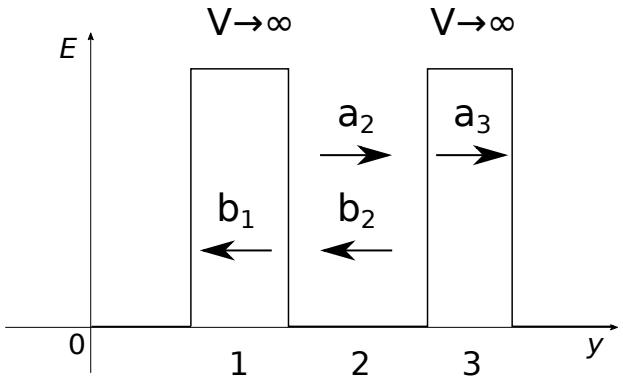

Figure 5.1: Model of a closed system consisting of a conducting layer placed between two insulators.

tion matrices

$$\operatorname{tr} \mathbf{g}_{\mathrm{LR}} = \frac{\mathrm{d}}{\mathrm{d}E} \operatorname{tr} \ln \left(\mathbf{1} - \mathbf{r'}_{1n} \mathbf{r}_{nN}\right), \tag{5.24}$$

which is equivalent to equation (5.16) in [5]. In this form it is clear that the P and AP alignments correspond to setting $\theta = 0$ and $\theta = \pi$ in $\mathbf{r'}_{1n}(\theta)$, respectively. Substituting (5.24) into (5.21) and integrating by parts we finally obtain

$$U = -\frac{1}{\pi} \Im \int_{\mathrm{BZ}_1} \mathrm{d}\bar{k}_{\parallel} \int_{-\infty}^{+\infty} \mathrm{d}E \, f(E-\mu) \operatorname{tr} \ln \left(\mathbf{1} - \mathbf{r'}_{1n}(\theta) \mathbf{r}_{nN}\right) \Big|_0^{\pi}, \tag{5.25}$$

which matches exactly the result (5.16) obtained earlier using the torque method.

5.4 Landauer Method for Closed Systems

We noted in the introduction to this chapter that IEC can exist in closed systems. The energy method of calculation in Section 5.3 is based on the spectral density formalism, and does not place any restrictions on what happens at the edges of the device. In other words, it works both in the open, and closed case. However, at the core of the torque calculation there are expressions for the spacer spin current that were earlier derived with the use of the Landauer method. More specifically, we have been applying boundary conditions of the form (3.32), (3.38) representing waves of unit amplitudes arriving from infinity. Now turning to the case of a closed system we note that while the transfer matrix formalism should still apply, new

boundary conditions must be specified to reflect the physical picture.

Consider a system consisting of a conducting spacer embedded in between the infinitely high insulating barriers, as shown in Figure 5.1. We will drop the overhead arrows indicating the spatial direction on the amplitudes, because there will be no ambiguity with respect to the direction of the flow in this example. There will be no electrons coming in from infinity on either side ($\mathbf{a}_1 = \mathbf{b}_3 = \mathbf{0}$). Instead there will be evanescent states present in the semi-infinite layers, and propagating states - in the conductor - whose amplitudes are related to each other as follows

$$\begin{aligned} \mathbf{a}_2 &= \mathbf{r}'_{12}\mathbf{b}_2, \qquad & \mathbf{a}_2 &= \mathbf{t}'^{-1}_{23}\mathbf{a}_3, \\ \mathbf{b}_2 &= \mathbf{t}^{-1}_{12}\mathbf{b}_1, \qquad & \mathbf{b}_2 &= \mathbf{r}_{23}\mathbf{a}_2, \end{aligned} \tag{5.26}$$

Eliminating $\mathbf{a}_2$ and $\mathbf{b}_2$ from (5.26) we obtain

$$\left(\mathbf{1} - \mathbf{r}'_{12}\mathbf{r}_{23}\right)\mathbf{t}'^{-1}_{23}\mathbf{a}_3 = \mathbf{0}.$$

The sufficient condition for non-trivial solutions in the spacer to exist is therefore given by the equation

$$\det\left(\mathbf{1} - \mathbf{r}'_{12}\mathbf{r}_{23}\right) = 0, \tag{5.27}$$

and the requirement that $\mathbf{t}'^{-1}_{23}\mathbf{a}_3$ belongs to the null-space of $\mathbf{1} - \mathbf{r}_{23}\mathbf{r}'_{12}$. Now (5.27) is a transcendental equation in energy. Its real solutions must correspond to the permitted energies of the states in the conducting spacer, that is the energy eigenvalues of the system. The result (5.27) readily generalises to the N-layer case if more layers are present between the spacer and the barriers, in which case we, as usual, label the spacer with index n. We will now show how the existence of these solutions is consistent with the calculation of the exchange energy in the spacer performed in earlier sections.

For the sake of clarity we will switch to the point of view of a single point in k-space and consider the exchange energy density denoted u given by the integral over energy in (5.25).

Integrating by parts we obtain

$$u = -\frac{1}{\pi}\Im \int_{-\infty}^{+\infty} \mathrm{d}E\, F(E) \frac{\mathrm{d}}{\mathrm{d}E} \ln\det\bigl(\mathbf{1} - \mathbf{r'}_{1n}(\theta)\mathbf{r}_{nN}\bigr)\Big|_{\theta=0}^{\theta=\pi}. \tag{5.28}$$

The boundary terms vanish at $E = +\infty$ suppressed by the factor of $F(E)$, and at $E = -\infty$ due to the cut off at the edge of the conducting band. Now defining

$$w(E,\theta) = \det\bigl(\mathbf{1} - \mathbf{r}_{nN}(E,\theta)\mathbf{r'}_{1n}(E)\bigr),$$

we note that (5.28) has the following form

$$u = -\frac{1}{\pi}\Im \int_{-\infty}^{+\infty} \mathrm{d}E\, F(E) \frac{\frac{\mathrm{d}}{\mathrm{d}E} w(E,\theta)}{w(E,\theta)}\Big|_{\theta=0}^{\theta=\pi}. \tag{5.29}$$

Integrals of the type (5.29) can be evaluated in terms of the logarithmic residues of w, as shown in [86] (Ch.5 §5.2). Going over to the complex plane and choosing the contour $\mathcal{C}$ as shown in Figure we find 5.2

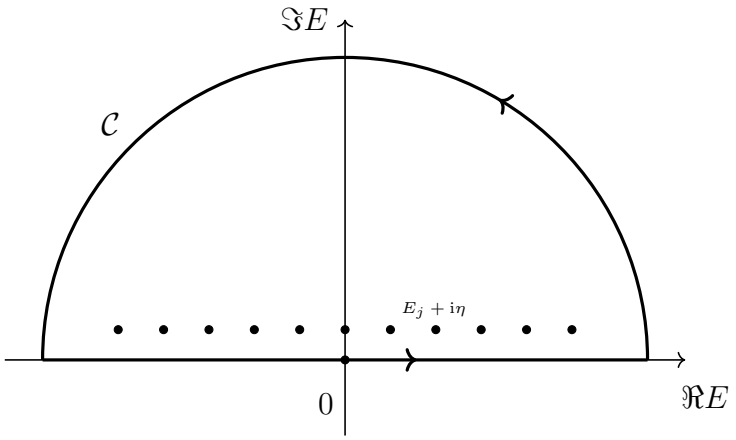

Figure 5.2: Integration contour going along a segment of the real axis and closed by a semi-circular arc in the upper half plane. The dots show the positions of the roots $E_j + \mathrm{i}\eta$ of $w(E)$, displaced by a positive infinitesimal imaginary part.

$$\int_{\mathcal{C}} F(z)\frac{w'(z)}{w(z)}\mathrm{d}z = 2\pi\mathrm{i}\sum_j n(\mathcal{C}, E_j)F(E_j), \tag{5.30}$$

where E_j are the roots of w (the discrete energy eigenvalues) and $n(\mathcal{C}, E_j)$ are the winding

numbers of w with respect to $\mathcal{C}$ at E_j. At zero temperature

$$\lim_{T\to 0_+} F(E) = \begin{cases} E - E_{\mathrm{F}}, & \text{for } E < E_{\mathrm{F}}, \\ 0, & \text{for } E \geq E_{\mathrm{F}}, \end{cases}$$

and, in the simplest case when all roots are non-degenerate, we obtain

$$u = 2\left(\sum_{E_j<E_{\mathrm{F}}} E_j(0) - \sum_{E_j<E_{\mathrm{F}}} E_j(\pi)\right), \tag{5.31}$$

In other words, exchange energy in a closed system expressed in terms of the sum over the roots of equation (5.27) is none other than the difference in energy between the parallel and anti-parallel configurations. This confirms the equivalence of the spin current (torque) and energy approaches. Note that for the contour integration to work we require $w(E)$ to decay sufficiently quickly as $|E|$ approaches the large semi-circle. While in principle a detailed analysis can be performed using the known general bounds on reflections coefficients [87], for the purposes of this discussion we content ourselves with a numerical verification. In Figure 5.3 we plot the values of $|E^2 w(E)|$ for a double potential barrier, along various rays of constant $\arg(E)$ in the upper half-plane. These demonstrate that $w(E)$ decays faster than $1/|E|^2$, which is sufficient to show that the integral over the semi-circle at infinity vanishes.

Let us summarise what we have done so far. We took the results derived within the Landauer formalism for open systems as the starting point to calculate the exchange energy in (5.16). We then imposed boundary conditions of the form (5.27) that represent a closed system and determine the energy values for the allowed states. What we found is that (5.16) expands into the sum over these permitted energies. The results are clear from the purely formal point of view. In the next section we will will elucidate the physics behind the behaviour of the spin current components, as system is gradually transformed form an open into a closed one.

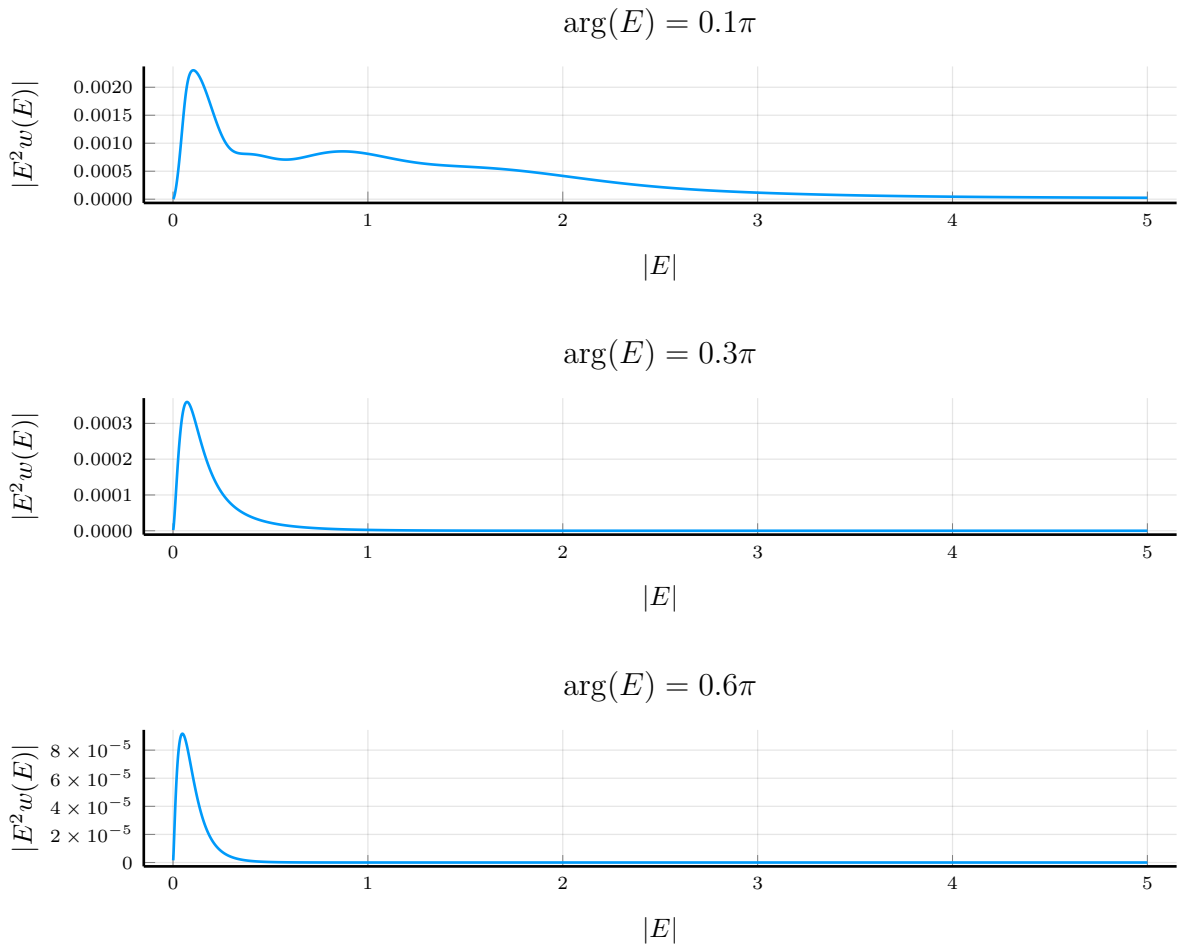

Figure 5.3: Numerical demonstration of the decay of $w(E)$ along various rays in the upper half-plane.

5.5 Transition Between the Open and Closed Regimes

We now explore numerically the transitioning process where a multilayer is gradually isolated from the leads. We start with the same 5-layer CPP structure considered in the previous chapter (see Figure 3.1). We then insert a pair of extra barriers between the leads and the magnets, as shown in Figure 5.4, with the parameters given in Table 5.1. We then increase the potentials in the barriers, as illustrated in Figure 5.5, gradually isolating the system. We show four stages of the transition process by varying the parameter

$$\alpha = \frac{V}{E_{\mathrm{F}}},$$

where V is the potential in the barriers and the energy scale is chosen so that $E_{\mathrm{F}} > 0$. In the first configuration $\alpha = 0$, that is the system is open, free from the influence of the extra

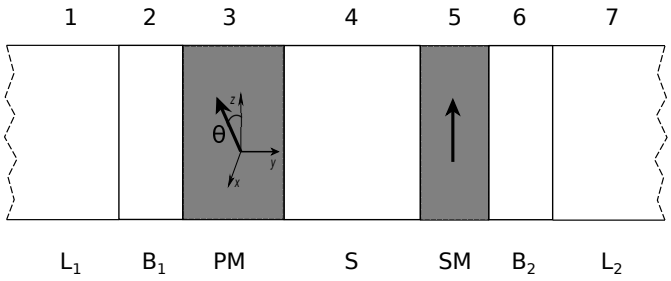

Figure 5.4: CPP multilayer with extra layers B_1 and B_2 separating the magnetic junction from the leads.

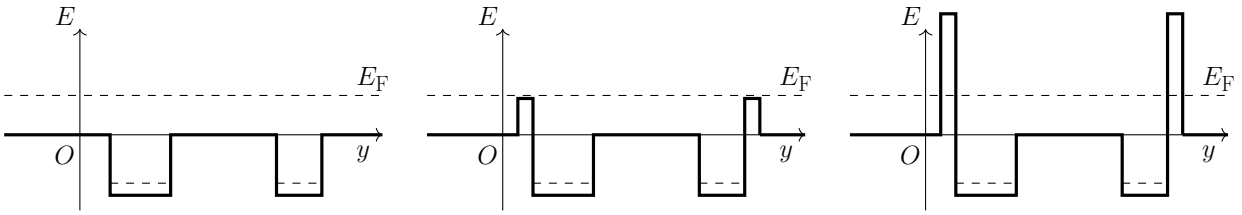

Figure 5.5: CPP multilayer with additional barriers gradually isolating it from the leads.

barriers. In the second one, $0 < \alpha < 1$, the height of the barriers is set between the level of the leads/spacer and the Fermi energy level, the system is partially confined. Further, the barrier height is set above the Fermi level, $\alpha > 1$, and the system is isolated. Lastly, in order to demonstrate the tendency in the current when the confinement is further increased, we produce the plot with $\alpha \gg 1$, where the system is strongly confined. In order to show the emergence of bound states in the spacer we plot the following function (note that with the addition of the barriers we now have a 7-layer system, that is $N = 7$, and the spacer index is $n = 4$)

$$\delta(\bar{k}_{\parallel}) = \left|\det\left(\mathbf{1} - \mathbf{r}_{47}\mathbf{r}'_{14}\right)\right|,$$

as shown in Figure 5.6. We take the absolute value merely for illustrative purposes, which does not alter the positions of the roots. We observe that as the barrier height is increased $\delta(\bar{k}_{\parallel})$ develops a sequence of roots at isolated values of $\bar{k}_{\parallel}$. These correspond to the positions of energy eigenvalues of the closed system at E_{F}.

We next look at the behaviour of the three spin current components in momentum space. In Figure 5.7 we see that the charge current density j_0 develops a series of sharp resonances that precisely correspond to the positions of the bound states of the system. The height of these

	V	Δ	θ	$y_{n+1} - y_n$
L_1	0.0	0.0	0.0	-
B_1	αE_{F}	0.0	0.0	1.0
PM	-0.1	0.05	0.6	7.0
S	0.0	0.0	0.0	20.0
SM	-0.1	0.05	0.0	3.0
B_2	αE_{F}	0.0	0.0	1.0
L_2	0.0	0.0	0.0	-

Table 5.1: Parameters of the model used to demonstrate the process of gradually turning an open system into a closed one. Extra potential barriers B_1 and B_2 are added between the leads and the magnets. The barrier height is then increased, which is controlled by parameter $\alpha = \frac{V}{E_{\mathrm{F}}}$,.

resonances gradually decreases at strong confinement. In agreement with that behaviour, the total current J_0 (integrated over the in-plane momentum) vanishes with the increasing barrier height, Figure 5.8. This fully expected because charge current cannot flow in an isolated system. Next, in Figure 5.9 we show the plot of the in-plane spin current density j_x. Similarly to the charge component, we observe resonances in $\bar{k}_{\|}$-space at the positions of the bound states that decay with the increase of the barrier height. The total in-plane spin current J_x also vanishes quickly after an initial increase, as shown in Figure 5.10. Lastly, in Figure 5.11 we display the behaviour of the out-of-plane component j_y. Here the situation is qualitatively different, as the resonances provide non-vanishing contributions under increasing confinement, and the total current therefore does not converge to zero, as seen in Figure 5.12. This is consistent with the fact that IEC survives in a closed system. In order to illustrate the point further, we plot the integrated values of all three components against the increasing barrier height, Figure 5.13. It is clearly seen that the total out-of-plane diverges, while the other two components disappear, as the system is isolated.

We now have an understanding of the behaviour of the spin current components as the multilayer system transitions from an open to a closed regime. As the states arriving from the reservoirs get cut off by insulating barriers, bound states emerge in the spacer. These latter ones cause the spin current components to develop resonances in momentum space. With increasing confinement these resonances gradually decay in j_0 and j_x. In the case of j_y, however, they become a set of δ-like terms of finite measure, leading to a non-vanishing out-of-plane current. This concludes our discussion of IEC and the extension of the Landauer formalism to

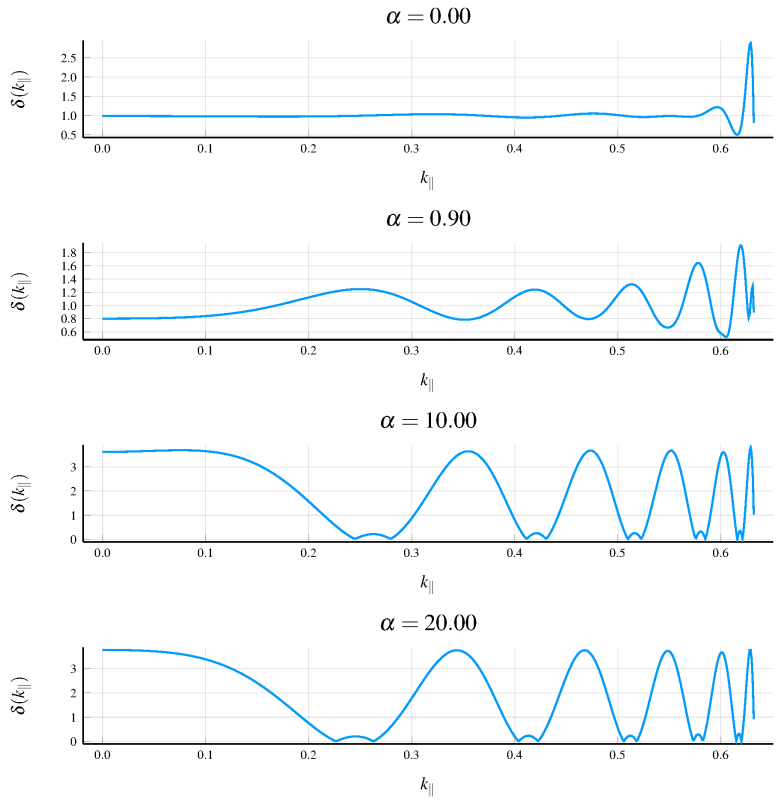

Figure 5.6: $\delta(\bar{k}_\parallel)$ plotted for different values of $\alpha = V/E_\mathrm{F}$. In the closed regime ($\alpha > 1$) distinct roots occur in momentum space.

closed systems. The subject, however, is far from being exhausted. Many more directions of future study can be developed, including the problems of efficient modulation of IEC for the purposes of switching, the effects of spin-orbit interaction, and IEC in multi-terminal geometries.

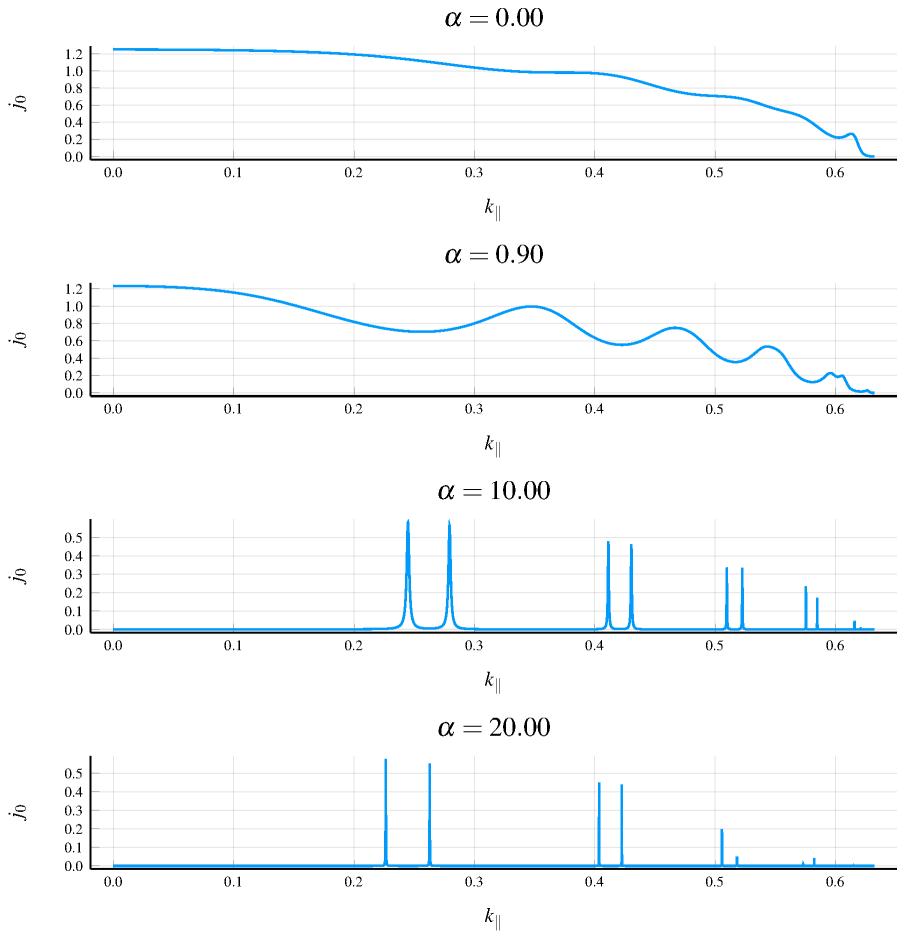

Figure 5.7: Charge current density in momentum space, plotted at different values of $\alpha = V/E_{\mathrm{F}}$, as the system is gradually turned to a closed one.

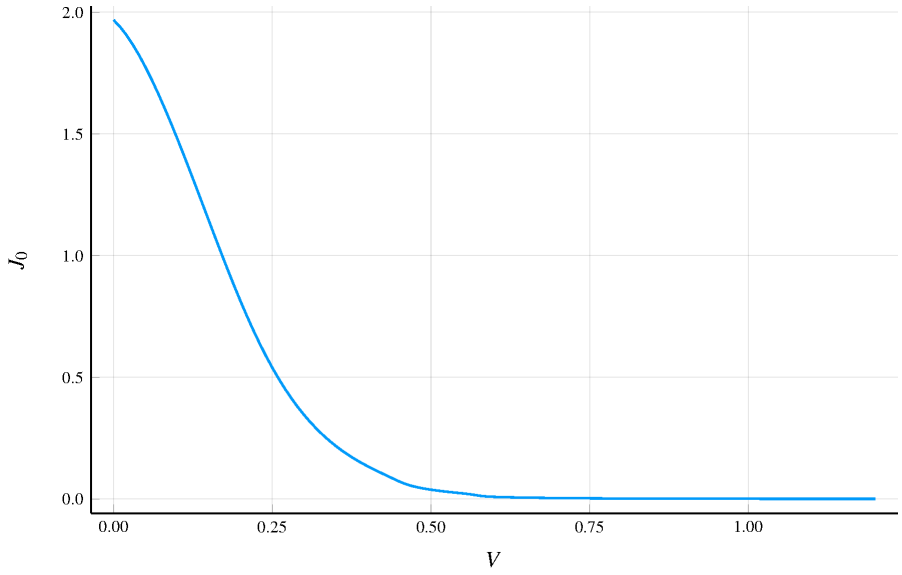

Figure 5.8: Charge current integrated over in-plane momentum, plotted as a function of the increasing insulating potential barrier height.

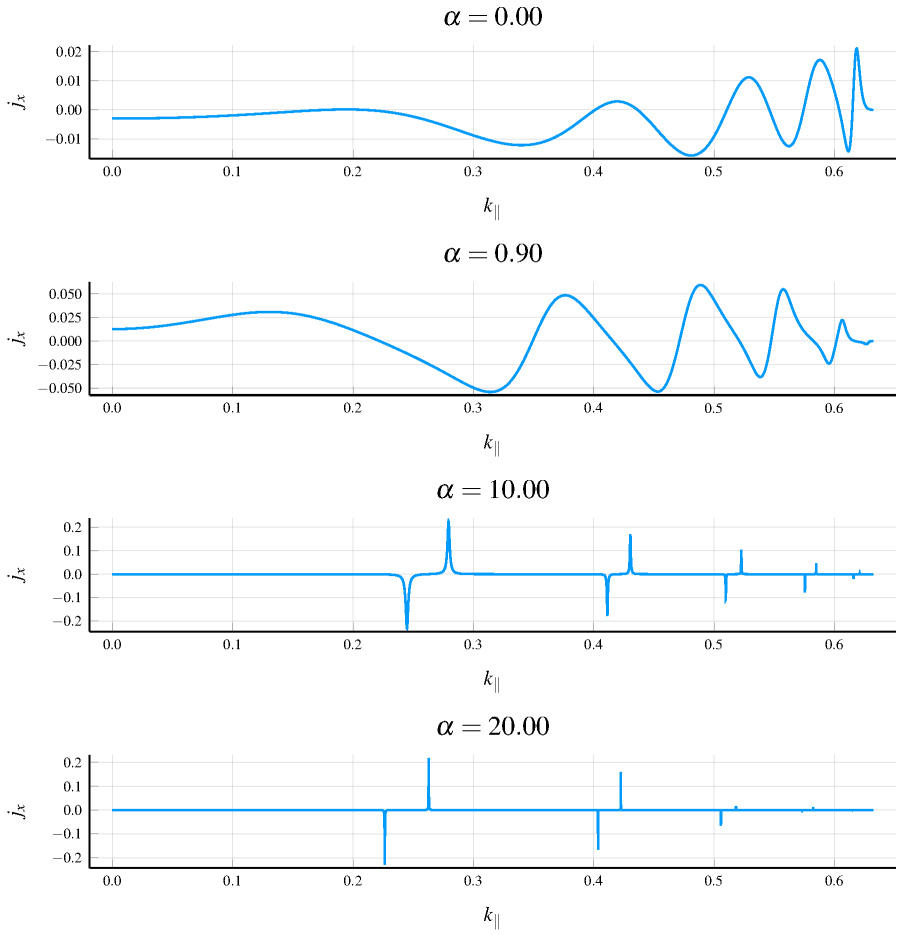

Figure 5.9: In-plane spin current density in momentum space, plotted at different values of $\alpha = V/E_F$, as the system is gradually turned to a closed one.

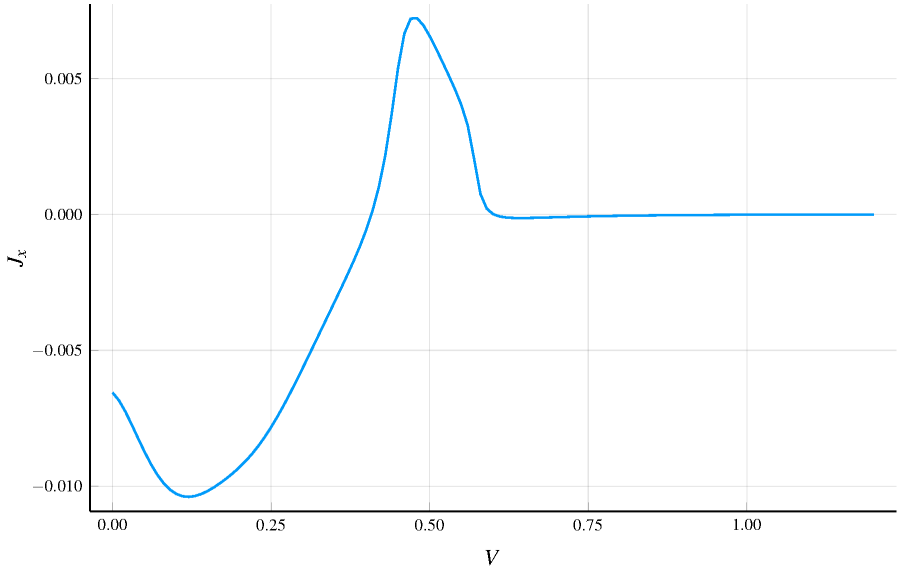

Figure 5.10: In-plane spin current integrated over in-plane momentum, plotted as a function of the increasing insulating potential barrier height.

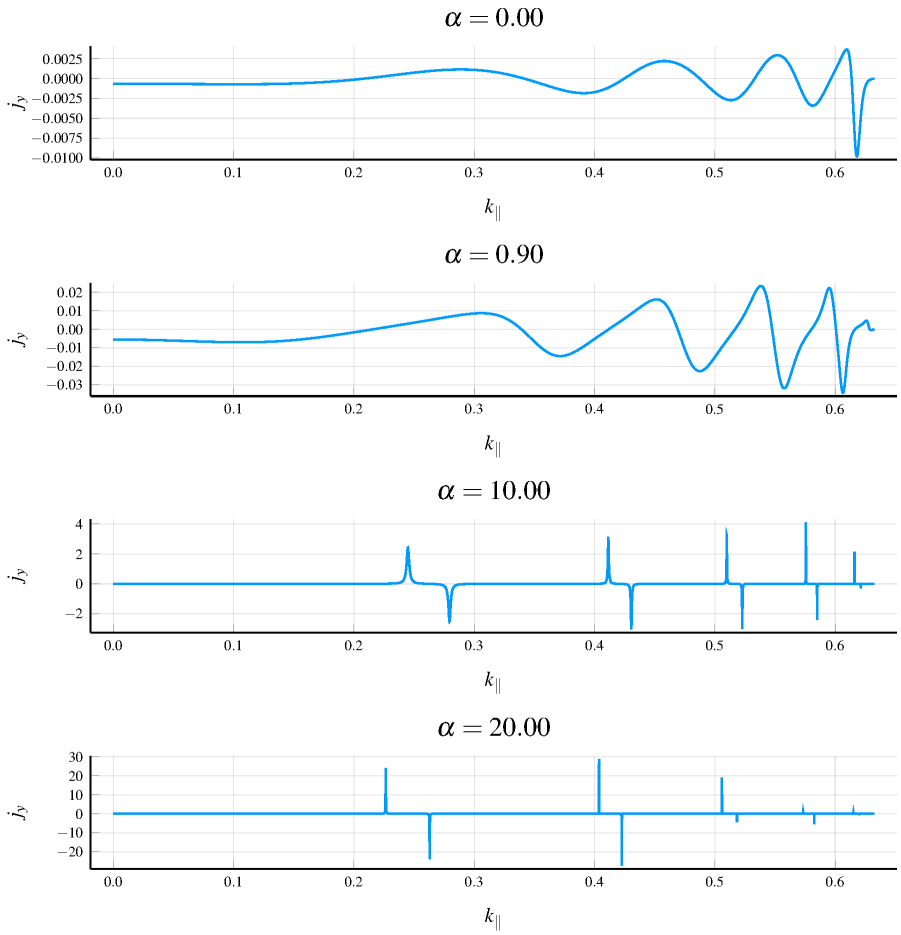

Figure 5.11: Out-of-plane spin current density in momentum space, plotted at different values of $\alpha = V/E_F$, as the system is gradually turned to a closed one.

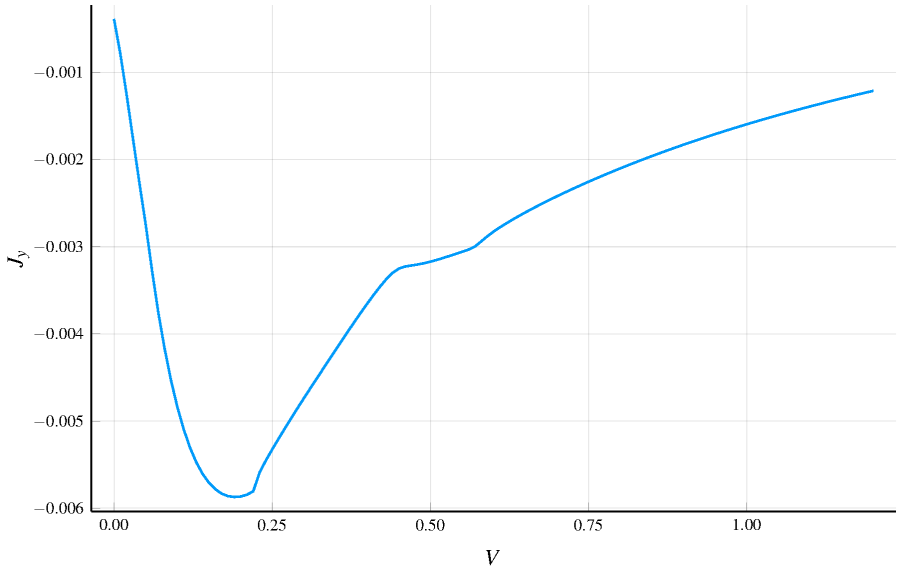

Figure 5.12: Out-of-plane spin current integrated over in-plane momentum, plotted as a function of the increasing insulating potential barrier height.

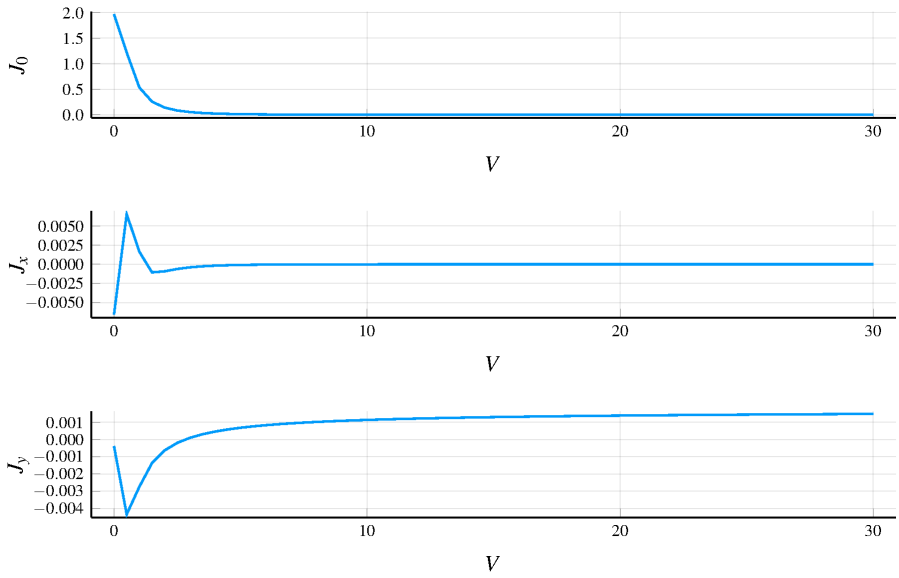

Figure 5.13: Current integrated over in-plane momentum, plotted as a function of the increasing insulating potential barrier height. Extended range shows the slow divergence if the out-of plane component, contrasted against the rapid vanishing of the other components.

Chapter 6

Multi-Terminal Devices

6.1 Introduction

The model considered in the previous chapters comprised a multilayer structure attached to two semi-infinite leads, or terminals. Many of the formulae and notational elements were developed bearing in mind the carriers incident from the "left" and the "right" side of the device. In this chapter we consider a much wider class of problems concerning structures with 3 or more terminals.

Part of the motivation to study multi-terminal structures comes from interpreting the measurements of conductance at mesoscopic scales. In an experimental setting, even if we are only interested in the conductance of a two-terminal device, it is still necessary to attach voltage probes to measure the potential drop across the structure. However, in the mesoscopic and nanoscale pictures the probes cannot be treated as small perturbations because they make non-negligible contribution to scattering and are rarely identical. Furthermore, due to the prominence of interference effects, positioning of the probes may affect the results of the measurement. Theoretical significance of the multi-terminal model was put forward by Engquist and Anderson [88] who pointed out that, given the current flow between two reservoirs, electrochemical potentials are not well defined, and at least one extra pair of probes is needed to define the reference potentials. This corresponds to a typical configuration known as the Hall

bridge (see Figure 2.10). Since the probes contribute to scattering processes, in the light of the Landauer theory they also affect conductance. Büttiker [46] proposed an approach where leads and probes are treated equally. This results in a symmetric formula (2.24) that allows one to apply, in the absence of external magnetic fields, Kirchhoff's rules to calculating charge currents in all leads.

Besides the measurement considerations, multi-terminal structures, specifically 3-terminal fabrications are important for practical realisations of non-volatile CMOS logic elements based on magnetic tunnelling junctions (MTJ), see for example, Ohno *et al.*[89]. Separating read and write paths improves the speed of bit operations. It also reduces device wear by making it unnecessary to apply large bias across the MTJ during reads. A non-volatile two-transistor memory cell design was proposed in [90] to implement this approach. Device structures have been considered [91] that combine the operation of a spin-valve (SV) and MTJ providing approaches to manufacturing performant spin-torque MRAM. Multi-terminal structures allow device engineers to take advantage of a variety of phenomena, such as spin diffusion, spin Hall effect, domain wall motion, and magnetoelectric effect for efficient spin current generation. Efficiency in this case implies achieving large magnitude of spin current with very little movement of charge through the conductor. This means less heat dissipation and further improvements for memory cell density and durability.

Generalisation of the formalism we have been applying to the two-terminal structure to the case of multiple terminals presents several difficulties. The notation was developed with a distinction of the "left" and "right" parts of the system. This does not make sense in a 3-way junction where all electrodes are treated equally. Furthermore, the transfer matrix, by construction, relates amplitudes between exactly two neighbouring layers which does not make it immediately applicable to the more general case where, for example three layers meet at a central junction.

Multi-terminal spin-dependent transport has been studied using a number of approaches. Constructions have been proposed [7], [8] to calculate scattering amplitudes using the **S**-matrix extended to three and four terminals, in the presence of Rashba spin-orbit coupling. However,

in those examples the authors strongly rely on a particular geometry of the junction. We aim to relax that last restriction and consider coherent transport of carriers across the system, while taking account the successive reflections between the interfaces, similarly to the procedure employed for the two-terminal CPP geometry in the previous chapters.

Other models cover diffusive and tunnelling regimes, as well as the ballistic one [6], [92]. In the latter examples, although multi-moded transport is assumed, multiple reflections are again not taken into account. The central normal metal node serving as the junction is considered large and disordered, and its distribution function is taken to be isotropic. This reduces accounting for contributions, in each lead, just to the two neighbouring nodes and applying Kirchhoff's rules to ensure the total current balance. As far as the ballistic regime is concerned, the authors of [6] only consider a drastically simplified approach where transmission coefficients are assumed to be either 0 or 1.

Our objective in this chapter would be to extend the transfer matrix formalism we have been using for 2-terminal structures to ballistic multi-terminal devices, while including the effect of multiple reflections between the interfaces. Only in this approach can one correctly account for effects such as exchange coupling between magnetic elements of these devices.

6.2 Scattering Across a 3-Way Junction

6.2.1 Preliminary Considerations

As the simplest possible extension of a two-terminal geometry, we consider the schematic depicted in Figure 6.1 consisting of 3 wires, or *branches*, labelled α, β, γ, meeting at the central junction. Since the new system does not have any preferred spatial ordering, and all branches are treated equally, we will find it convenient to adopt a slightly different convention for the transmission and reflection coefficients. In particular, we are going to reverse the meaning of the subscript indices. Precisely, the first index will mean the branch the electron ends up in after scattering, whereas the second index will signify the branch it came out of. This mnemonic

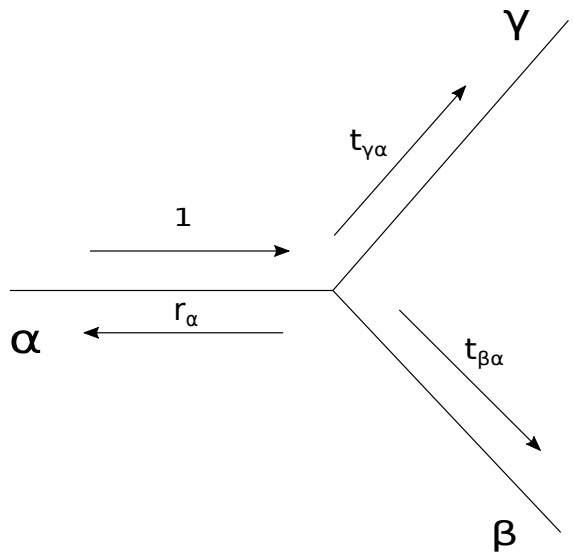

Figure 6.1: Transmission and reflection amplitudes of waves scattering across a 3-way junction.

could be illustrated by writing, for example, $\mathbf{t}_{\beta\leftarrow\alpha}$ for the amplitude of the wave transmitted from α to β. For brevity we will drop $\leftarrow$ in subscripts. The matrices describing reflection from the central junction require a new convention too. In the introductory example depicted in Figure 6.1, where all branches are homogeneous we will denote the amplitude of a wave reflected from the junction back into the branch it arrived from, say α, simply by $\mathbf{r}_\alpha$. In the next section, however, where we consider the case of multilayer branches, we will have to specify indices of the layers in all branches the effect of which on scattering we take into account. In the example shown in Figure 6.2 the unit wave incident in branch α can first transmit into either of the branches β or γ, get reflected from the interfaces $\beta_1|\beta_2$ or $\gamma_1|\gamma_2$, respectively, and ultimately reflect back into α. In this case we denote the resulting reflection amplitude by $\mathbf{r}_{\alpha_1\,\beta_2\atop\gamma_2}$. Finally, we will drop the primes in this convention because there is no universally defined notion of the "left" and "right" side of an interface here.

Now each branch may constitute a multilayer CPP structure of the type studied in the previous chapters. Therefore, for any branch taken in isolation we may apply the usual transfer matrix formalism and the corresponding boundary conditions to calculate transmission in any given layer. However, the same method does not work for transmission across the central junction. This is because the transfer matrix is derived based on the boundary conditions at the interface of precisely two neighbouring layers. We have to make use of the so-called **S**-matrix instead,

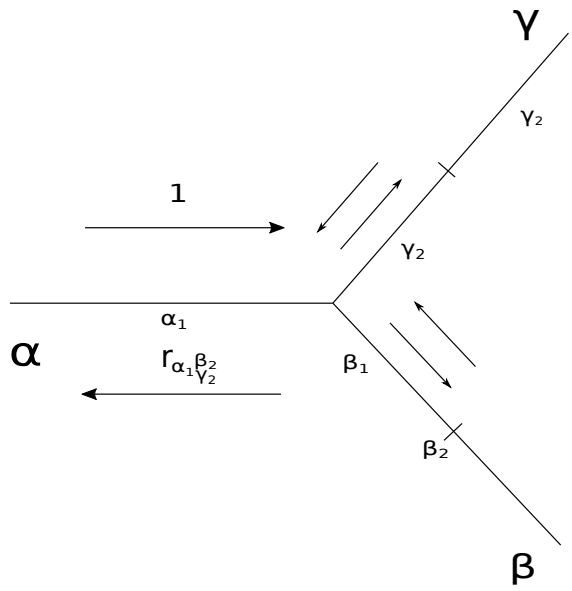

Figure 6.2: Reflection from a 3-way junction taking into account scattering processes in the branches.

also known as the *scattering matrix*. Unlike the **T**-matrix that relates the amplitudes on the left to the ones on the right, the **S**-matrix relates the incoming waves to the outgoing ones. In the case of a single interface, similarly to Figure 2.11, we depict the incoming and outgoing waves, as shown in Figure 6.3. Now by definition the **S**-matrix relates the amplitudes as follows

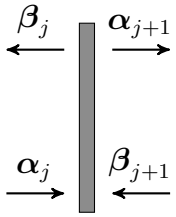

Figure 6.3: Incoming and outgoing waves near a scattering interface.

$$\begin{bmatrix} \boldsymbol{\beta}_j \\ \boldsymbol{\alpha}_{j+1} \end{bmatrix} = \mathbf{S} \begin{bmatrix} \boldsymbol{\alpha}_j \\ \boldsymbol{\beta}_{j+1} \end{bmatrix}. \tag{6.1}$$

Again, denoting the 2×2 blocks of $\mathbf{S}$ by $\mathbf{h}_{ij}$, and considering unit waves incident from the left

and the right we obtain, respectively

$$\begin{aligned}\begin{bmatrix}\mathbf{r}\\ \mathbf{t}'\end{bmatrix} &= \begin{bmatrix}\mathbf{h}_{11} & \mathbf{h}_{12}\\ \mathbf{h}_{21} & \mathbf{h}_{22}\end{bmatrix}\begin{bmatrix}\mathbf{1}\\ \mathbf{0}\end{bmatrix},\\ \begin{bmatrix}\mathbf{t}\\ \mathbf{r}'\end{bmatrix} &= \begin{bmatrix}\mathbf{h}_{11} & \mathbf{h}_{12}\\ \mathbf{h}_{21} & \mathbf{h}_{22}\end{bmatrix}\begin{bmatrix}\mathbf{0}\\ \mathbf{1}\end{bmatrix}.\end{aligned} \tag{6.2}$$

Solving (6.2) for $\mathbf{h}_{ij}$ we get the general form of $\mathbf{S}$

$$\mathbf{S} = \begin{bmatrix}\mathbf{r} & \mathbf{t}\\ \mathbf{t}' & \mathbf{r}'\end{bmatrix}. \tag{6.3}$$

One often quoted property of $\mathbf{S}$ is the unitarity $\mathbf{S}^\dagger\mathbf{S} = \mathbf{1}$, following from the charge current conservation. However, there is an important distinction to be made, depending on whether we work in the amplitude or the current picture (recall (3.26)). If we are to keep the meanings of the transmission and reflection matrices consistent with the two-terminal discussion, we must use a rescaled scattering matrix. If m and n are the layer indices, and $\mathbf{r}_{mn}$, $\mathbf{t}_{mn}$, $\mathbf{r}'_{mn}$, $\mathbf{t}'_{mn}$ are taken in the amplitude picture then $\mathbf{S}_{mn}$ has the form

$$\mathbf{S}_{mn} = \begin{bmatrix}\boldsymbol{\xi}_m & \mathbf{0}\\ \mathbf{0} & \boldsymbol{\xi}_n\end{bmatrix}^{-1}\begin{bmatrix}\mathbf{r}_{mn} & \mathbf{t}_{mn}\\ \mathbf{t}'_{mn} & \mathbf{r}'_{mn}\end{bmatrix}\begin{bmatrix}\boldsymbol{\xi}_m & \mathbf{0}\\ \mathbf{0} & \boldsymbol{\xi}_n\end{bmatrix}, \tag{6.4}$$

where

$$\boldsymbol{\xi}_i = \operatorname{diag}\left[\sqrt{k_i^\uparrow}, \sqrt{k_i^\downarrow}\right]. \tag{6.5}$$

The conservation equations (3.25) are then recovered from the unitarity requirement of $\mathbf{S}_{mn}$, as defined by (6.4). Now $\mathbf{S}$ readily generalises to an arbitrary number of terminals. With these consideration in mind, and remembering the convention about the subscripts, we consider the

following 6×6 matrix to describe transmission across the junction in Figure 6.1

$$\check{\mathbf{S}} = \begin{bmatrix} \boldsymbol{\xi}_\alpha & \mathbf{0} & \mathbf{0} \\ \mathbf{0} & \boldsymbol{\xi}_\beta & \mathbf{0} \\ \mathbf{0} & \mathbf{0} & \boldsymbol{\xi}_\gamma \end{bmatrix}^{-1} \begin{bmatrix} \mathbf{r}_\alpha & \mathbf{t}_{\alpha\beta} & \mathbf{t}_{\alpha\gamma} \\ \mathbf{t}_{\beta\alpha} & \mathbf{r}_\beta & \mathbf{t}_{\beta\gamma} \\ \mathbf{t}_{\gamma\alpha} & \mathbf{t}_{\gamma\beta} & \mathbf{r}_\gamma \end{bmatrix} \begin{bmatrix} \boldsymbol{\xi}_\alpha & \mathbf{0} & \mathbf{0} \\ \mathbf{0} & \boldsymbol{\xi}_\beta & \mathbf{0} \\ \mathbf{0} & \mathbf{0} & \boldsymbol{\xi}_\gamma \end{bmatrix}, \tag{6.6}$$

where $\boldsymbol{\xi}_i$ is defined as in (6.5). Here we use the check $\check{}$ sign to distinguish 6×6 from 4×4 matrices.

We will not be making any assumptions regarding the geometry or internal state of the junction, except that scattering is coherent, and that when one of the leads is removed the rest of the system reduces to the ordinary two-terminal device. Since the components of $\check{\mathbf{S}}$ can no longer be determined from wave-function matching we are going to assume they are given, either from the microscopic calculation or fitted from experimental data, for a particular device geometry. For the purposes of accounting for spin we, effectively, introduce a local coordinate system in each branch similarly to the two terminal case, that is, with y-axis directed perpendicularly to the interfaces, and z being the spin quantisation axis.

In order to study any interesting effects in 3-terminal structures the schematic shown in Figure 6.1 will certainly not be enough. We will have to introduce scattering layers (magnetic and non-magnetic) with different electrostatic potentials, at least in some of the branches. Calculating transmission into a given branch will therefore involve combining the scattering matrices describing interfaces of the layers, and the matrix of the central junction. As we are working in the ballistic transport picture we would like to find a way to account for all the successive reflections. This requires extending the procedure described in Subsection 2.5.2. However, in this case we find that the final answer will not be given automatically by matrix multiplication.

6.2.2 Spinless Case

Before considering the spin-resolved calculation with magnetic scatterers we will work through the steps of a simpler single-band calculation. This leads up to a result stated in [10] and based

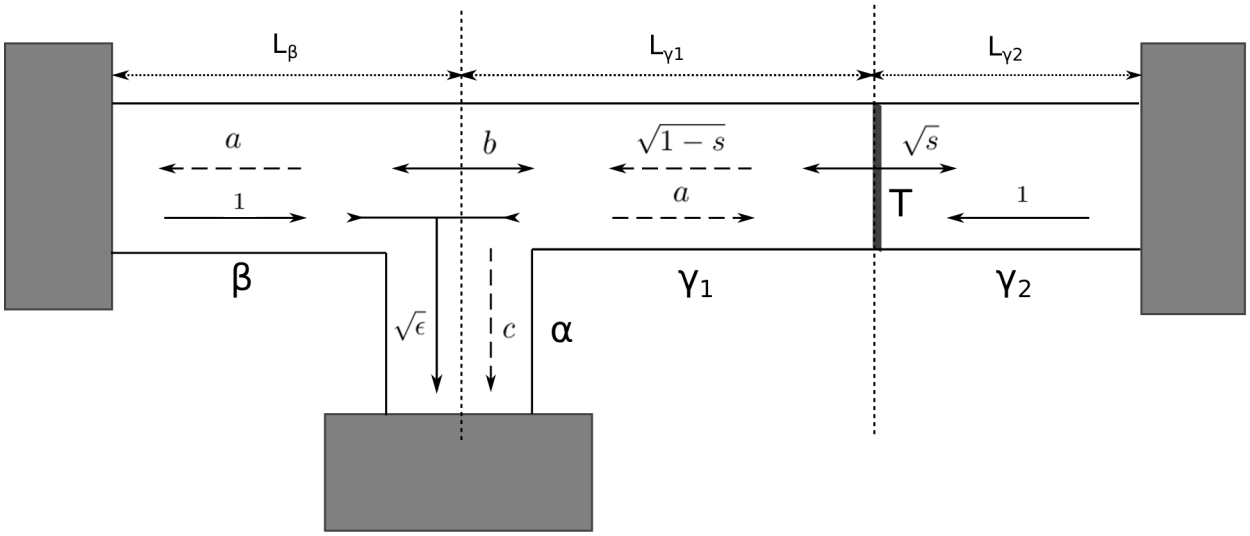

Figure 6.4: Calculating transmission into the probe with a scatterer in the conductor. Solid lines depict the transmitted amplitudes, whereas dashed lines show the reflections.

on the work of Büttiker in [9]. Following Büttiker, we consider a probe weakly coupled to a conductor at a certain position along its length, as depicted in Figure 6.4. The conductor is not uniform, but includes a scatterer labelled T. In this example we disregard the thickness of the scatterer and any reflections that occur inside it. Coupling of the probe to the conductor is described phenomenologically by the parameter $|t_{\alpha\beta}| = |t_{\alpha\gamma_1}| = \sqrt{\epsilon}$. Transmission between β and γ occurs with amplitude $|t_{\beta\gamma_1}| = |t_{\gamma_1\beta}| = b$, and reflection amplitude is $|r_\beta| = |r_{\gamma_1}| = a$. Finally, electrons emerging from α are reflected back with amplitude $|r_\alpha| = c$. This leads to the following form of the scattering matrix

$$\mathbf{S} = \begin{bmatrix} a & b & \sqrt{\epsilon} \\ b & a & \sqrt{\epsilon} \\ \sqrt{\epsilon} & \sqrt{\epsilon} & c \end{bmatrix}. \tag{6.7}$$

The unitarity requirement for $\mathbf{S}$ leads to the following relations

$$c = \pm\sqrt{1-2\epsilon}, \qquad a = (1-c)/2, \qquad b = \mp(1+c)/2. \tag{6.8}$$

Note that in [9] ϵ is treated as a small parameter to reflect the role of α as a probe weakly coupled to the conductor. For the purposes of this discussion, however, we do not require ϵ to

be small, and will consider it over the entire range of permissible values. Note that (6.7) does not include phase information, which we will be taking into account when summing reflections. The scatterer T can be described by the matrix

$$\mathbf{S}' = \begin{bmatrix} \mathrm{i}\sqrt{1-s} & \sqrt{s} \\ \sqrt{s} & \mathrm{i}\sqrt{1-s} \end{bmatrix},$$

where $\sqrt{s}$ is the transmission amplitude, and the factor of i is added to satisfy the unitarity requirement. Transmission from the conductor into the probe can be then be calculated by counting reflections in the segments between the junction and the scatterer. Total transmission is found as the sum of the contributions from electrons emerging from α and β, denoted $t_{\alpha\beta}$ and $t_{\alpha\gamma}$, respectively. From β electrons can transmit directly into the probe α with amplitude $\sqrt{\epsilon}$ and phase shift $e^{\mathrm{i}kL_\beta}$. Another possible path consists of transmission into γ with amplitude b and reflection from the scatterer with amplitude $\mathrm{i}\sqrt{1-s}$, acquiring a total phase shift of $e^{\mathrm{i}k(L_\beta+2L_{\gamma_1})}$. Finally, after reflection from the scatterer there can occur multiple successive reflections from the central junction to the scatterer and back again. These are summed as in Figure 2.10 and add multiples of $\mathrm{i}a\sqrt{1-s}e^{\mathrm{i}2kL_{\gamma_1}}$ on each round-trip. Adding it all together, we obtain

$$\begin{aligned} t_{\alpha\beta} &= \sqrt{\epsilon}e^{\mathrm{i}kL_\beta} + \sqrt{\epsilon}\left(\sum_{k=0}^{\infty}\left(\mathrm{i}a\sqrt{1-s}e^{\mathrm{i}2kL_{\gamma_1}}\right)^k\right)\cdot(\mathrm{i}\sqrt{1-s}e^{\mathrm{i}kL_{\gamma_1}})\cdot(be^{\mathrm{i}kL_{\gamma_1}})\cdot(e^{\mathrm{i}kL_\beta}) \\ &= \sqrt{\epsilon}e^{\mathrm{i}kL_\beta}\left(1+\frac{\mathrm{i}b\sqrt{1-s}e^{\mathrm{i}2kL_{\gamma_1}}}{1-\mathrm{i}a\sqrt{1-s}e^{\mathrm{i}2kL_{\gamma_1}}}\right). \end{aligned} \tag{6.9}$$

Following a similar process for electrons incident from γ we find

$$\begin{aligned} t_{\alpha\gamma} &= (\sqrt{\epsilon}e^{\mathrm{i}kL_{\gamma_1}})\cdot\left(\sum_{k=0}^{\infty}\left(\mathrm{i}a\sqrt{1-s}e^{\mathrm{i}2kL_{\gamma_1}}\right)^k\right)\cdot(\sqrt{s}e^{\mathrm{i}kL_{\gamma_3}}) \\ &= \frac{\sqrt{\epsilon}\sqrt{s}e^{\mathrm{i}k(L_{\gamma_2}+L_{\gamma_3})}}{1-\mathrm{i}a\sqrt{1-s}e^{\mathrm{i}2kL_{\gamma_1}}} \end{aligned} \tag{6.10}$$

.

The total transmission is then found as the sum of (6.9) and (6.10)

$$t_\alpha = t_{\alpha\beta} + t_{\alpha\gamma}.$$

We can explore the model by plotting $|t_\alpha|^2$ as a function of the model parameters, in particular, the scattering parameter s in Figure 6.5, the coupling parameter ϵ in Figure 6.6 and, finally, the thickness of the segment of the conductor between the central junction and the scatterer L_{γ_1} in Figure 6.7. The latter is chosen because that is where the successive reflections happen. We set $L_\beta = 1.0$, $L_{\gamma_1} = \pi$ and $L_{\gamma_2} = 0.5$, except where L_{γ_1} is varied. In Figure 6.7 $k = 1.0$. We note in particular that the scattering parameter s is sensitive to the phase shift, as demonstrated by varying k. Where the shift is close to causing destructive interference in the conductor there is a pronounced minimum observed. This is explained by the fact that more amplitude escapes via the scatterer into γ, until the effect is compensated by more amplitude arriving from γ. In case of constructive interference and low coupling the dependence is almost linear. Dependence on the coupling parameter is not so sensitive to the phase shift. When varying spacer thickness we observe the expected anharmonic quasi-periodicity in the amplitude.

6.2.3 Spin-Resolved Case

We now proceed to calculate transmission in the spin-resolved case, in the presence of non-collinear magnetisation. We consider the structure shown in Figure 6.8, where in the segment between β and γ we introduce magnetic layers (α_2, β_2 and γ_2) and set the polarisation direction of γ_2 rotated at an arbitrary angle in-plane. We are particularly interested in the spin current incident on the magnet in α. Here we no longer ignore the thickness of the scatterers (magnets) and account for all the successive reflections occurring inside them. Let us now calculate the incoming transmission into α_1. Following the approach taken in the previous section, we obtain contributions from electrons incident in β and γ, as follows. Transmission from β_3 (lead) to β_1 is described by $\mathbf{t}_{\beta_1\beta_3}$. This is followed by repeated reflections between the central junction and the interface $\beta_2|\beta_3$, while also taking into account reflections within β_2, given by the factor $\left(\mathbf{1} - \mathbf{r}_{\beta_1\beta_3}\mathbf{r}_{\beta_1\,\alpha_3^{\gamma_3}}\right)^{-1}$. Putting it all together, and repeating the argument for branch γ as the

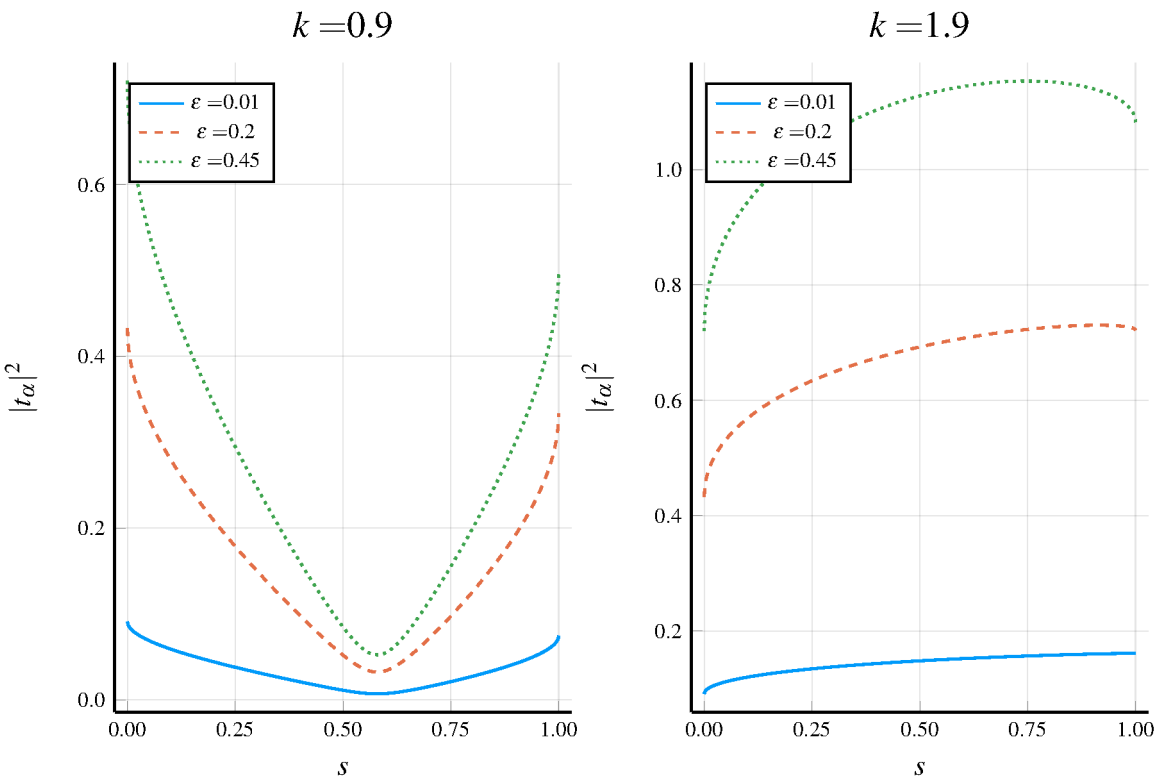

Figure 6.5: Transmission into the probe as a function of the scattering parameter.

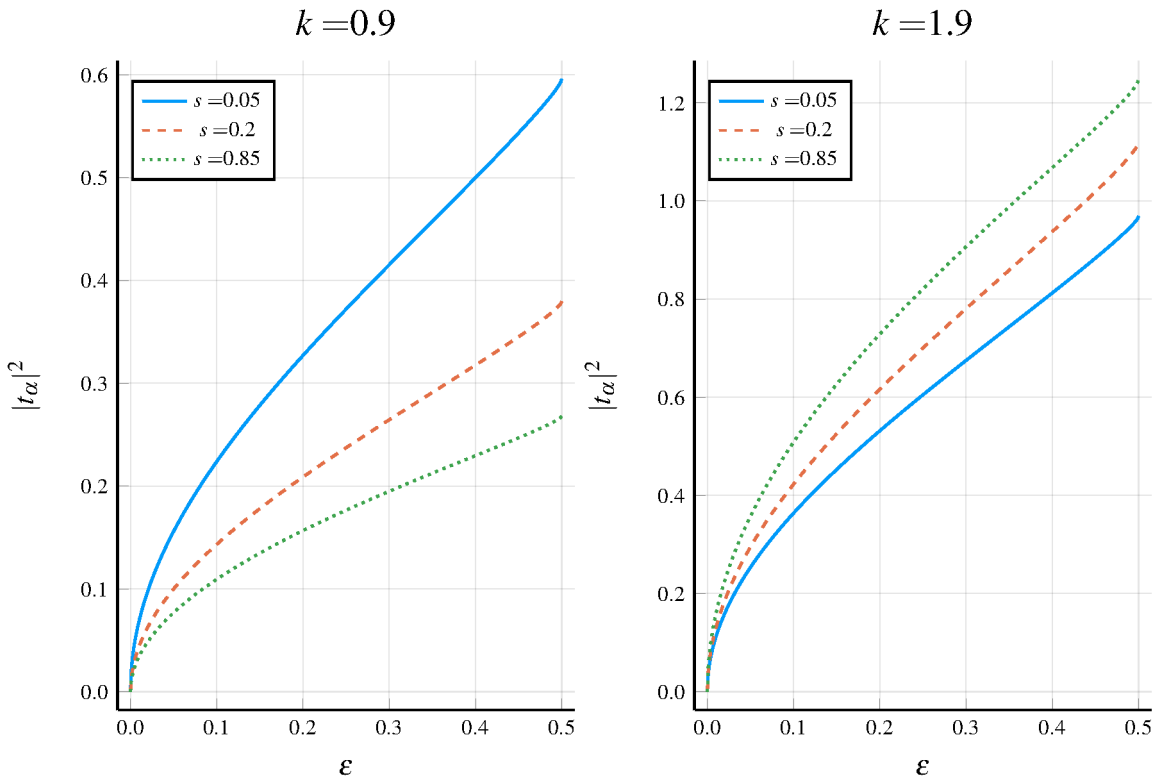

Figure 6.6: Transmission into the probe as a function of the coupling parameter.

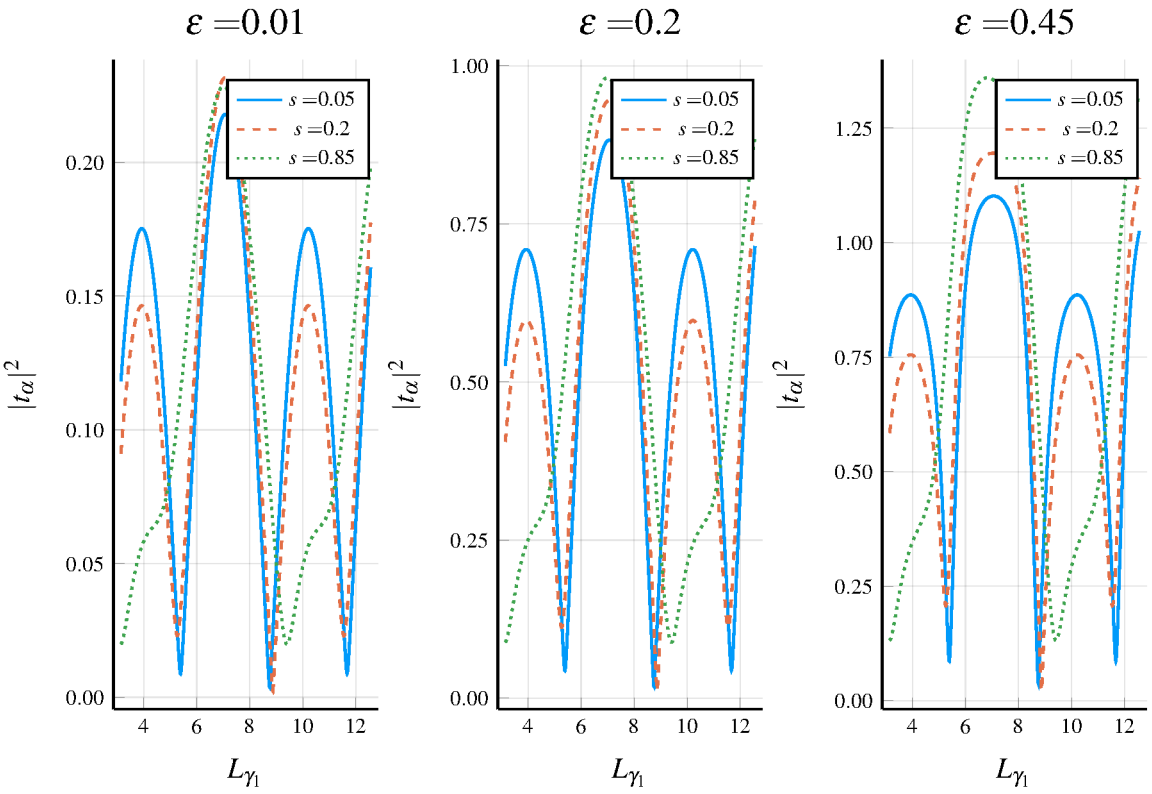

Figure 6.7: Transmission into the probe as a function of the spacer thickness L_{γ_1}.

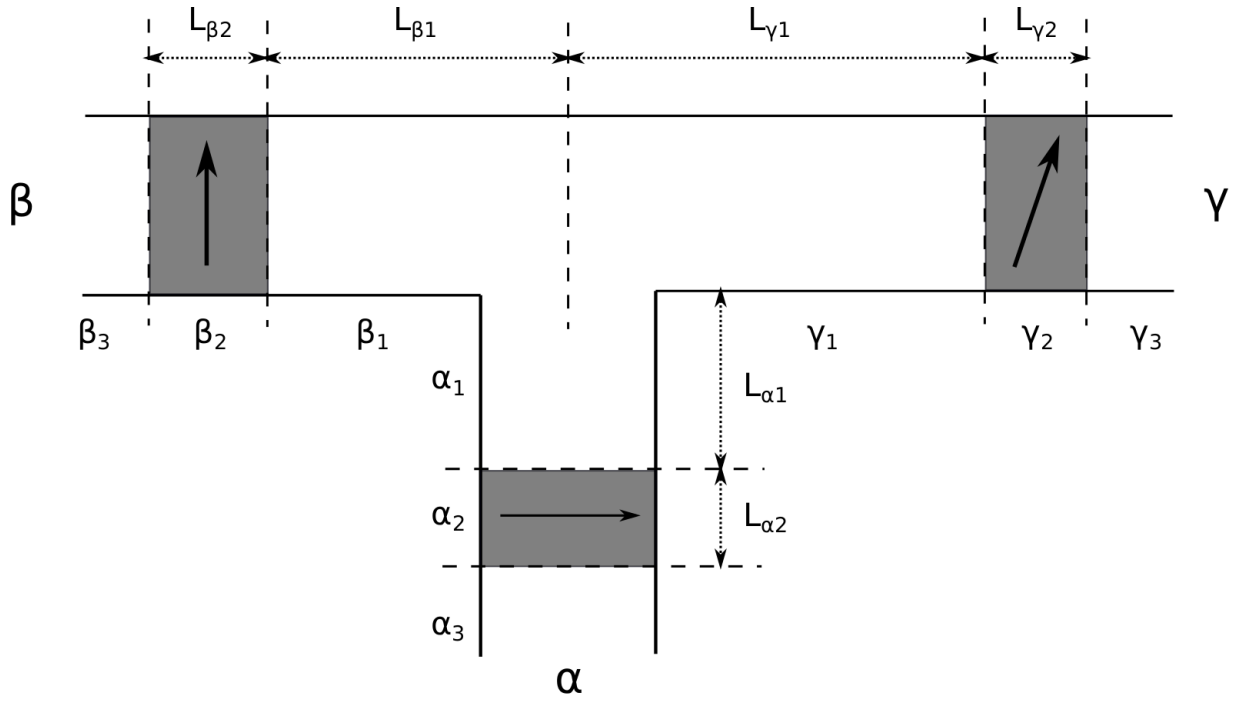

Figure 6.8: 3-terminal device with ferromagnetic layers and in-plane polarization.

source, we obtain

$$\mathbf{t}_{\alpha_1\beta_3} = \mathbf{t}_{\alpha_1\beta_1}\Big(\mathbf{1} - \mathbf{r}_{\beta_1\beta_3}\mathbf{r}_{\beta_1\,\gamma_3}^{\,\alpha_3}\Big)^{-1}\mathbf{t}_{\beta_1\beta_3}, \tag{6.11a}$$

$$\mathbf{t}_{\alpha_1\gamma_3} = \mathbf{t}_{\alpha_1\gamma_1}\Big(\mathbf{1} - \mathbf{r}_{\gamma_1\gamma_3}\mathbf{r}_{\gamma_1\,\beta_3}^{\,\alpha_3}\Big)^{-1}\mathbf{t}_{\gamma_1\gamma_3}. \tag{6.11b}$$

We now need to determine the structure of $\mathbf{r}_{\beta_1\,\gamma_3}^{\,\alpha_3}$ and $\mathbf{r}_{\gamma_1\,\beta_3}^{\,\alpha_3}$. We shall do so by expressing them in terms of the two-terminal matrices and $\mathbf{r}_{\beta_1\,\gamma_1}^{\,\alpha_1}$ and $\mathbf{r}_{\gamma_1\,\beta_1}^{\,\alpha_1}$ that are not reducible any further within our formalism. We assume that those are given by the microscopic theory and depend on a particular geometry of the junction. Separating in $\mathbf{r}_{\beta_1\,\gamma_3}^{\,\alpha_3}$ and $\mathbf{r}_{\gamma_1\,\beta_3}^{\,\alpha_3}$ from (6.11a) the scattering within γ by using expansion of the form (2.31d) we obtain

$$\mathbf{r}_{\beta_1\,\gamma_3}^{\,\alpha_3} = \mathbf{r}_{\beta_1\,\gamma_1}^{\,\alpha_3} + \mathbf{t}_{\beta_1\gamma_1}\Big(\mathbf{1} - \mathbf{r}_{\gamma_1\gamma_3}\mathbf{r}_{\gamma_1\,\beta_1}^{\,\alpha_3}\Big)^{-1}\mathbf{r}_{\gamma_1\gamma_3}\mathbf{t}_{\gamma_1\beta_1} \tag{6.12}$$

$$\mathbf{r}_{\gamma_1\,\beta_3}^{\,\alpha_3} = \mathbf{r}_{\gamma_1\,\beta_1}^{\,\alpha_3} + \mathbf{t}_{\gamma_1\beta_1}\Big(\mathbf{1} - \mathbf{r}_{\beta_1\beta_3}\mathbf{r}_{\beta_1\,\gamma_1}^{\,\alpha_3}\Big)^{-1}\mathbf{r}_{\beta_1\beta_3}\mathbf{t}_{\beta_1\gamma_1}. \tag{6.13}$$

Then we expand $\mathbf{r}_{\beta_1\,\gamma_1}^{\,\alpha_3}$ and $\mathbf{r}_{\gamma_1\,\beta_1}^{\,\alpha_3}$ until only the lowest-order reflection amplitudes (from the junction) remain

$$\mathbf{r}_{\beta_1\,\gamma_1}^{\,\alpha_3} = \mathbf{r}_{\beta_1\,\gamma_1}^{\,\alpha_1} + \mathbf{t}_{\beta_1\alpha_1}\Big(\mathbf{1} - \mathbf{r}_{\alpha_1\alpha_3}\mathbf{r}_{\alpha_1\,\gamma_1}^{\,\beta_1}\Big)^{-1}\mathbf{r}_{\alpha_1\alpha_3}\mathbf{t}_{\alpha_1\beta_1}, \tag{6.14}$$

$$\mathbf{r}_{\gamma_1\,\beta_1}^{\,\alpha_3} = \mathbf{r}_{\gamma_1\,\beta_1}^{\,\alpha_1} + \mathbf{t}_{\gamma_1\alpha_1}\Big(\mathbf{1} - \mathbf{r}_{\alpha_1\alpha_3}\mathbf{r}_{\alpha_1\,\gamma_1}^{\,\beta_1}\Big)^{-1}\mathbf{r}_{\alpha_1\alpha_3}\mathbf{t}_{\alpha_1\gamma_1}. \tag{6.15}$$

We can now obtain the total amplitudes of electrons going into the junction, and emerging from the junction generalising those defined in (2.39) and (2.37) to the multi-terminal case. In order to distinguish the direction of the flow we will write $\mathbf{a}^{\odot}$, $\mathbf{b}^{\odot}$ and $\mathbf{a}^{\otimes}$, $\mathbf{b}^{\otimes}$ for the amplitudes going into and out of the junction, respectively. In this notation we obtain for electrons incident from the lead (going into the junction)

$$\mathbf{a}_{\alpha}^{\odot} = \Big(\mathbf{1} - \mathbf{r}_{\alpha_1\alpha_3}\mathbf{r}_{\alpha_1\,\gamma_3}^{\,\beta_3}\Big)^{-1}\mathbf{t}_{\alpha_1\alpha_3}, \tag{6.16a}$$

$$\mathbf{b}_{\alpha}^{\odot} = \mathbf{r}_{\alpha_1\,\gamma_3}^{\,\beta_3}\,\mathbf{a}_{\alpha}^{\odot}. \tag{6.16b}$$

Here $\mathbf{r}_{\substack{\alpha_1 \beta_3 \\ \gamma_3}}$ is expanded similarly to (6.12) and (6.13)

$$\mathbf{r}_{\substack{\gamma_1 \alpha_3 \\ \beta_3}} = \mathbf{r}_{\substack{\gamma_1 \alpha_3 \\ \beta_1}} + \mathbf{t}_{\gamma_1\beta_1}\Big(\mathbf{1} - \mathbf{r}_{\beta_1\beta_3}\mathbf{r}_{\substack{\beta_1 \alpha_3 \\ \gamma_1}}\Big)^{-1}\mathbf{r}_{\beta_1\beta_3}\mathbf{t}_{\beta_1\gamma_1}.$$

For electrons emerging from the junction, using (6.11), we can write

$$\mathbf{b}_\alpha^\otimes = \Big(\mathbf{1} - \mathbf{r}_{\substack{\alpha_1 \beta_3 \\ \gamma_3}}\mathbf{r}_{\alpha_1\alpha_3}\Big)^{-1}\Big(\mathbf{t}_{\alpha_1\beta_3} + \mathbf{t}_{\alpha_1\gamma_3}\Big), \tag{6.17a}$$

$$\mathbf{a}_\alpha^\otimes = \mathbf{r}_{\alpha_1\alpha_3}\mathbf{b}_\alpha^\otimes. \tag{6.17b}$$

Equations (6.16), (6.17) enable us to calculate spin current in α_1. It is easy to see that through permuting the labels similar formulae can be derived for transmission into branches β and γ. Equations (6.11), together with (6.16), (6.17) comprise the extension of the Landauer formalism to 3-terminal devices. It is conceivable that the same approach could be carried over to structures with more terminals.

For illustration purposes we provide the plots of the spin current density components in α_1 (travelling into the junction), as functions of the coupling parameter ϵ (Figure 6.9) and the in-plane polarisation angle in the magnet γ_2 (Figure 6.10), respectively. We consider a symmetric system with $L_{\alpha_1} = L_{\beta_1} = L_{\gamma_1} = 1.0$, $L_{\alpha_2} = L_{\beta_2} = L_{\gamma_2} = 3.0$, Fermi level $E_\mathrm{F} = 0.4$, potentials in the magnets α_2, β_2 and γ_2 set at $V = 0.5$, exchange splitting $\Delta = 0.03$, and all other potentials set to 0. The central junction is described by matrix $\check{\mathbf{S}}$ obtained from $\mathbf{S}$ given by (6.7) where each component s_{ij} is replaced by matrix diag $[s_{ij}, s_{ij}]$. As expected, all spin and charge components vanish at $\epsilon = 0$, that is, when α gets disconnected from the system. When, on the other hand, $\epsilon = 0.5$ there is perfect transmission across the central junction. Furthermore, j_x and j_y vanish at $\theta = 0$ and $\theta = \pi$.

6.2.4 Coupling Parameter

Expressions (6.7) and (6.8) describing scattering from the junction in terms of the coupling parameter ϵ were originally proposed to model a probe (potentiometer) attached to a conduc-

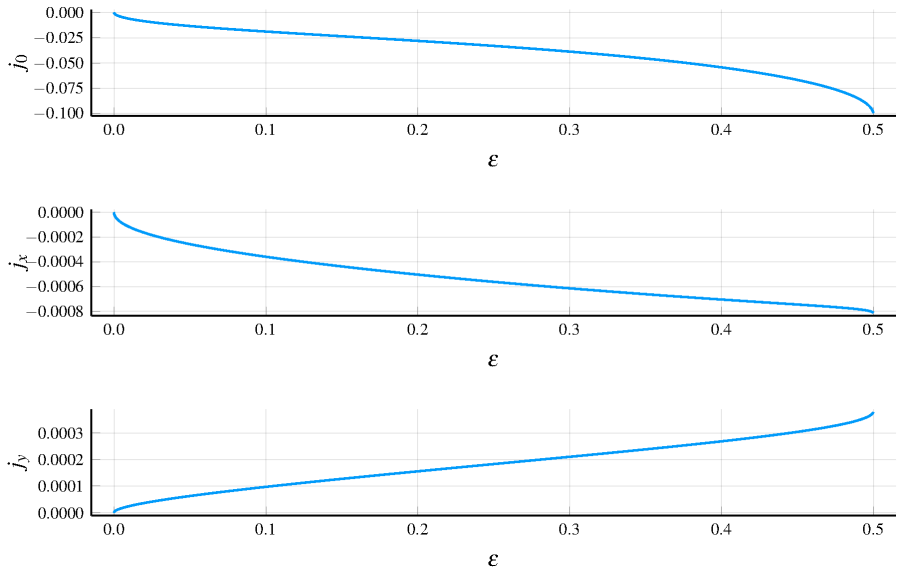

Figure 6.9: Current density components in layer α_1 plotted as functions of the coupling strength.

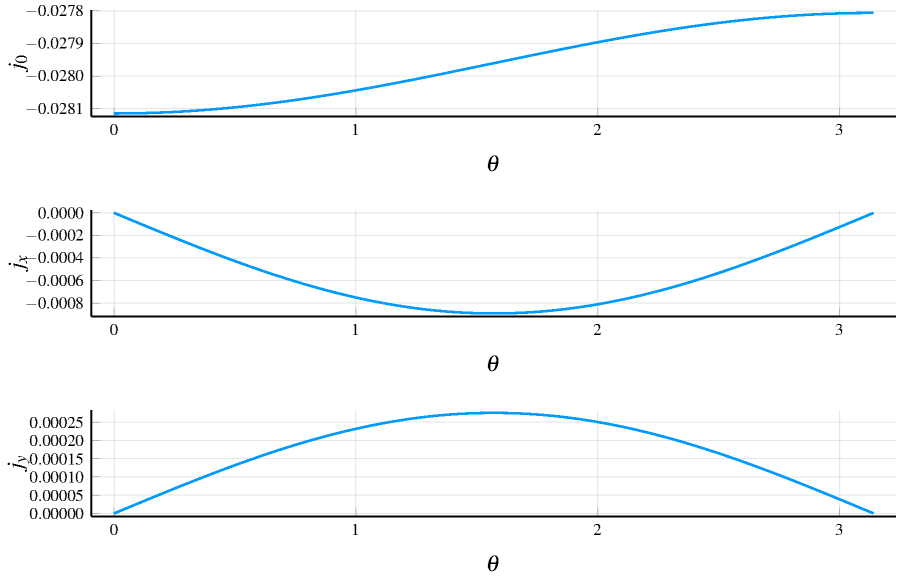

Figure 6.10: Current density components in layer α_1 plotted as functions of the polarisation angle in layer γ_2.

tor. This formulation has the disadvantage that it gives one of the branches of a multi-terminal structure a special role. In our model we would like to treat all branches equally. We will still not be able to calculate reflection from the junction in terms of the transmission formalism. However, we can consider an alternative parametrisation scheme that separates a phenomenological design parameter from the properties of the material in the layers meeting at the junction. We will need to ensure that the resulting expressions satisfy the unitarity requirement, and behave correctly in a number of limiting cases. For brevity we will write

$$\tilde{\tilde{\mathbf{a}}} \equiv \mathbf{a}^\dagger \mathbf{a}$$

for all matrices involved. Assuming that the junction is non-magnetic we can write the current conservation condition for electrons incident in lead α (see Figure 6.1)

$$k_\alpha \left(\mathbf{1} - \tilde{\tilde{\mathbf{r}}}_\alpha\right) = k_\beta \tilde{\tilde{\mathbf{t}}}_{\beta\alpha} + k_\gamma \tilde{\tilde{\mathbf{t}}}_{\gamma\alpha}. \tag{6.18}$$

We would like to approximate $\mathbf{r}_\alpha$ in terms of the respective 2-terminal reflection coefficients that it would reduce to when either of the branches β or γ is detached. To this end, we replace the transmission coefficients in (6.18) with their two-terminal versions given by the expressions (3.14a)-(3.14d), which we denote $\mathbf{t}^{(2)}_{\beta\alpha}$, $\mathbf{t}^{(2)}_{\gamma\alpha}$, $\mathbf{r}^{(2)}_{\alpha\beta}$, $\mathbf{r}^{(2)}_{\alpha\gamma}$. However, in order to satisfy all the limiting cases, we cannot assume transmission to be fully independent and have to postulate an interaction term characterised by a phenomenological parameter δ to (6.18) as follows

$$k_\alpha \left(\mathbf{1} - \tilde{\tilde{\mathbf{r}}}_\alpha\right) = k_\beta \tilde{\tilde{\mathbf{t}}}^{(2)}_{\beta\alpha} + k_\gamma \tilde{\tilde{\mathbf{t}}}^{(2)}_{\gamma\alpha} + k_\alpha(1+\delta)(\mathbf{1} - \tilde{\tilde{\mathbf{r}}}^{(2)}_{\alpha\beta})(\mathbf{1} - \tilde{\tilde{\mathbf{r}}}^{(2)}_{\alpha\gamma}), \tag{6.19}$$

where $\delta > 0$. Now from (3.25a) we obtain

$$k_\beta \tilde{\tilde{\mathbf{t}}}^{(2)}_{\beta\alpha} = k_\alpha \left(\mathbf{1} - \tilde{\tilde{\mathbf{r}}}^{(2)}_{\alpha\beta}\right), \tag{6.20a}$$

$$k_\gamma \tilde{\tilde{\mathbf{t}}}^{(2)}_{\gamma\alpha} = k_\alpha \left(\mathbf{1} - \tilde{\tilde{\mathbf{r}}}^{(2)}_{\alpha\gamma}\right). \tag{6.20b}$$

Substituting (6.20) into (6.19) we find

$$\tilde{\tilde{\mathbf{r}}}_\alpha = \tilde{\tilde{\mathbf{r}}}^{(2)}_{\alpha\beta} + \tilde{\tilde{\mathbf{r}}}^{(2)}_{\alpha\gamma} - (1+\delta)(\mathbf{1} - \tilde{\tilde{\mathbf{r}}}^{(2)}_{\alpha\beta})(\mathbf{1} - \tilde{\tilde{\mathbf{r}}}^{(2)}_{\alpha\gamma}) - \mathbf{1}. \tag{6.21}$$

Analysing expression (6.21) we see that when either of $\tilde{\tilde{\mathbf{r}}}^{(2)}_{\alpha\beta}$ or $\tilde{\tilde{\mathbf{r}}}^{(2)}_{\alpha\gamma}$ tends to $\mathbf{1}$ $\tilde{\tilde{\mathbf{r}}}_\alpha$ reduces to the value of the other coefficient, hence the system correctly degenerates to a 2-terminal one. When, say, $\tilde{\tilde{\mathbf{r}}}^{(2)}_{\alpha\beta} \to 0$ we get that $\tilde{\tilde{\mathbf{r}}}_\alpha \to \delta\left(\mathbf{1} - \tilde{\tilde{\mathbf{r}}}^{(2)}_{\alpha\gamma}\right)$. Physically, this means that when there is unimpeded transmission from α to β, a fraction of the electrons will still transmit into γ, and this fraction will be characterised by the parameter δ. In other words, we can interpret $\epsilon = 1-\delta$ as a measure of the coupling strength, similarly to the Büttiker calculation in the spinless case. In order to ensure the conservation law (6.18) is satisfied we must add the corresponding terms to the transmission amplitudes if we are to use the same parametrisation scheme. Denoting

$$\boldsymbol{\rho}(\delta) = (1+\delta)(1 - \tilde{\tilde{\mathbf{r}}}^{(2)}_{\alpha\beta})(1 - \tilde{\tilde{\mathbf{r}}}^{(2)}_{\alpha\gamma}) + \mathbf{1}$$

we obtain

$$\tilde{\tilde{\mathbf{r}}}_\alpha = \tilde{\tilde{\mathbf{r}}}^{(2)}_{\alpha\beta} + \tilde{\tilde{\mathbf{r}}}^{(2)}_{\alpha\gamma} - \boldsymbol{\rho}(\delta), \tag{6.22a}$$

$$\tilde{\tilde{\mathbf{t}}}_{\alpha\beta} = \tilde{\tilde{\mathbf{t}}}^{(2)}_{\alpha\beta} + \frac{k_\alpha}{k_\beta + k_\gamma}\boldsymbol{\rho}(\delta), \tag{6.22b}$$

$$\tilde{\tilde{\mathbf{t}}}_{\alpha\gamma} = \tilde{\tilde{\mathbf{t}}}^{(2)}_{\alpha\gamma} + \frac{k_\alpha}{k_\beta + k_\gamma}\boldsymbol{\rho}(\delta), \tag{6.22c}$$

The parametrisation described by (6.22) generalises (6.7) to the spin-resolved case with multiple scatterers. It can be used to model spin transport across the junction into other parts of the device with a single fitting parameter δ. With this we conclude the discussion of the Landauer method for multi-terminal structures within the scope of this thesis. A more detailed analysis and classification of the various regimes of the devices will be performed in the future studies.

Chapter 7

Conclusion

7.1 Summary of Thesis Achievements

In this thesis we have studied several related problems in ballistic spin-resolved transport across a metallic magnetic multilayer of the CPP structure.

We have used the Landauer formalism as the computational framework. It has proven convenient for reasoning about summing reflections, extracting approximations and deriving symmetries. We have employed several important extensions to the original Landauer formula. The first one is the generalisation to the spin resolved transmission, which is actually a particular case of the multi-moded transport. The other one is the non-collinear in-plane magnetisation that adds rotation matrix factors. Finally, we use the recursive relations expressing transmission and reflection matrices across multiple layers in terms of transmission between adjacent layers.

We have shown in detail how the in-plane and the out-of-plane components of spin current arise in the central non-magnetic region of the multilayer. We demonstrated the importance of taking into account the successive reflections and formulated the origins of spin current in terms of wave function matching at the interfaces and precession in the layers. We investigated several symmetry properties satisfied by the current and certain commonly made assumptions

about the model that lead to exact vanishing of the out-of-plane current. Building on earlier results obtained for charge current we demonstrated the effectiveness of the transfer matrix approach for the asymptotic analysis of spin current.

We explored the connections between the transfer matrix formalism and the methods in the study of the polarisation of light. At this stage we have drawn only some of the basic parallels and proposed the idea of spin Müller-Jones calculus. Some of the deeper results from the classic Müller-Jones calculus do not appear to feature in the spintronics-related literature and may be the subjects of further investigation. Other well established methods, such as the (generalised) Iwasawa decomposition do not seem to have been actively explored either. In any case, the amount of research in the field of optics using those methods gives reasons to believe that a number of techniques and results can be reinterpreted or generalised sufficiently to address certain problems in spin transport.

We have examined the fundamental assumption of the Landauer model, namely, that the carriers arrive into the mesoscopic junction from large phase-randomising reservoirs, at all possible energies, momenta and spin orientations. We took that assumption to a limiting case where the system was gradually isolated from the reservoirs (closed), until the external supply of electrons was cut off. Formally applying the Landauer method to such process we calculated the energy of interlayer exchange coupling between the two magnets. In the earlier sections we showed that only the out-of-plane component of the current would contribute to exchange coupling. In the context of a closed system we further obtained a physically and mathematically appealing conclusion that spin current density in the momentum space reduces to a distinct number of sharp peaks or resonances. Calculating total current and, consequently, the exchange energy then corresponds to summing over residues evaluated precisely at the points where the peaks occur. This is equivalent to the conventional sum over discrete eigenvalues.

We then took the transfer matrix approach in a yet another direction by applying it to spin-resolved transport in multi-terminal structures. Generalising upon the canonical examples by Büttiker derived for charge current, we constructed a model of a ballistic multi-terminal device with multiple scatterers and calculated transmission between its terminals using the

transmission and reflection matrices. Unlike some of the earlier work, our model both includes all the reflections (and is therefore adequate for studying exchange coupling), and does not make any assumptions about the properties of the central junction. The latter comes at a cost of having to introduce a phenomenological coupling parameter.

7.2 Future Work

Throughout this work we have discarded the effects of spin-orbit interaction in the spacer and magnets. However, this phenomenon is so important, both from the point of view of the applications, and theoretically, that it must be taken into account in any further development of this research. In the general case, including SOI makes the problem no longer exactly solvable, which does not permit introducing the transfer matrix method the way we have done here. Nevertheless, several researchers have studied ballistic transport in the presence of the Rashba-type SOI under certain conditions where the Hamiltonian could still be diagonalised, and the transmission formalism could be employed [8], [93], [94]. It has also been pointed out that, in the presence of non-collinear polarisation, care must be taken when specifying boundary conditions [95], which should be expressed in terms of the velocity operator. It would be an interesting extension to combine these results with the potential profile chosen in our model, and the in-plane (and even out-of-plane) polarisation direction in the magnets.

For the multi-terminal structures, the generalisation of the reflection-counting procedure we obtained in Chapter 6 potentially allows us to study a whole new class of problems, motivated by the results obtained earlier for the two-terminal case. For example, properly defining the transport and exchange parts of the current and investigating which, if any, of the symmetry properties studied in Chapter 5 hold. Once again, the model could be further enriched by including the effect of SOI in the central junction.

Connections to the optical methods highlighted in Chapter 4 provide a link to a large body of research applying geometric and group theoretic methods to the study of electromagnetic wave propagation in multilayers, for example [58], [70], [71], [72], [73], [76] and [3]. In this context,

a classification of magnetic multilayers and the way they give rise to spin current components could be a valuable extension of the similar work done for optical multilayers.

Lastly, we remark that the models we have considered are *discrete* in their essence, that is the devices are composed of a finite number of homogeneous layers. The study of *continuous* systems, however, is an important subject too (magnetic textures, domain wall movement). An interesting question to pose is to what extent the transfer matrix method can be applied to the continuous case. Several variants of the method and their accuracy have been studied, in the spinless case [96], [97]. Mathematically, the limiting process of calculating the transfer matrix over a large number of thin layers could potentially be represented by the Volterra's multiplicative integral [98]. All these possibilities would be interesting ones to investigate in the context of magnetic multilayers.

Appendix A

Symmetry Properties of the Transfer Matrix

In this section we derive some of the symmetry properties satisfied by the transfer matrix and the transmission and reflection submatrices under transposition and complex conjugation.

A.1 Symmetry of Reflection and Transmission Matrices Under Transposition

First consider transmission matrix $\mathbf{t}_{n,n+1}$ at $\theta_n = \theta_{n+1} = 0$. From (3.14a) and (3.14b), we get

$$\mathbf{t}_{n,n+1}\big|_{\substack{\theta_n=0\\ \theta_{n+1}=0}} = \mathbf{k}_{n+1}\mathbf{k}_n^{-1}\,\mathbf{t'}_{n,n+1}\Big|_{\substack{\theta_n=0\\ \theta_{n+1}=0}},$$

where $\mathbf{k}_n = \mathrm{diag}[k_n^{\uparrow}, k_n^{\downarrow}]$. Now considering transmission between layers 1 and 3, and temporarily setting $\theta_2 = 0$ we obtain

$$\mathbf{t}_{13} = \mathbf{t}_{12}(\mathbf{1} - \mathbf{r}_{23}\mathbf{r'}_{12})^{-1}\mathbf{t}_{23},$$

$$\mathbf{t'}_{13} = \mathbf{t'}_{23}(\mathbf{1} - \mathbf{r'}_{12}\mathbf{r}_{23})^{-1}\mathbf{t'}_{12},$$

hence on taking the transpose we get

$$\mathbf{t'}_{13}(0)^T = k_1 k_3^{-1} \mathbf{t}_{13}(0)$$

because all the factors involved are diagonal. However, by (3.17) we can reintroduce the angular dependence as follows

$$\mathbf{t}'_{13}(\theta_2) = \mathbf{s}(-\theta_2)\mathbf{t'}_{13}(0)\mathbf{s}(\theta_2),$$

whereby taking the transpose we deduce that

$$\mathbf{t'}_{13}(\theta_2)^T = k_1 k_3^{-1} \mathbf{t}_{13}(\theta_2).$$

More generally, considering a system where magnetic and non-magnetic are interleaved (Figure 2.14), we get

$$\mathbf{t'}_{n,n+2}(\theta_{n+1})^T = k_n k_{n+2}^{-1} \mathbf{t}_{n,n+2}(\theta_{n+1}), \tag{A.1}$$

where a non-magnetic layer $n+1$ is sandwiched between magnetic layers n and $n+2$. By (3.17), we also note that $\mathbf{t'}_{n,n+2}$, $\mathbf{t}_{n,n+2}$, $\mathbf{r'}_{n,n+2}$, and $\mathbf{r}_{n,n+2}$, are all symmetric. Now consider reflection and transition matrices between layers 1 and 5, for arbitrary values of θ_2 and θ_4. We have

$$\mathbf{r}_{15} = \mathbf{r}_{13} + \mathbf{t}_{13}\mathbf{r}_{35}(\mathbf{1} - \mathbf{r'}_{13}\mathbf{r}_{35})^{-1}\mathbf{t'}_{13},$$

hence

$$\mathbf{r}_{15}^T = \mathbf{r}_{13} + \mathbf{t'}_{13}(\mathbf{1} - \mathbf{r}_{35}\mathbf{r'}_{13})^{-1}\mathbf{r}_{35}\mathbf{t}_{13} = \mathbf{r}_{15},$$

where we made use of (A.1). Returning to the general case, we deduce that

$$\mathbf{r}_{n,n+4}^T = \mathbf{r}_{n,n+4}, \qquad \mathbf{r'}_{n,n+4}^T = \mathbf{r'}_{n,n+4},$$

where layers n and $n+4$ are non-magnetic. For the transmission matrices we have

$$\mathbf{t'}_{15} = \mathbf{t'}_{35}(\mathbf{1} - \mathbf{r'}_{13}\mathbf{r}_{35})^{-1}\mathbf{t'}_{13},$$
$$\mathbf{t}_{15} = \mathbf{t}_{13}(\mathbf{1} - \mathbf{r}_{35}\mathbf{r'}_{13})^{-1}\mathbf{t}_{35},$$

so that

$$\mathbf{t'}^{T}_{15} = \mathbf{t'}^{T}_{13}(\mathbf{1} - \mathbf{r}_{35}\mathbf{r'}_{13})^{-1}\mathbf{t'}^{T}_{35} = k_1 k_5^{-1}\mathbf{t}_{15}.$$

More generally, we obtain

$$\mathbf{t'}^{T}_{n,n+4} = k_n k_{n+4}^{-1}\mathbf{t}_{n,n+4},$$

where layers n and $n+4$ are non-magnetic. Proceeding this way we can deduce that

$$\mathbf{r'}^{T}_{nm} = \mathbf{r'}_{nm}, \quad \mathbf{r}^{T}_{nm} = \mathbf{r}_{nm}, \tag{A.2}$$
$$\mathbf{t'}^{T}_{nm} = k_n k_m^{-1}\mathbf{t}_{nm}. \tag{A.3}$$

when n and m are arbitrary layers.

A.2 Symmetry of the Transfer Matrix Under Complex Conjugation

If a given layer is a metallic ferromagnet, hence $k^{\uparrow}$ and $k^{\downarrow}$ are both real, then from (3.7) we have

$$\mathbf{X}(k^{\uparrow,\downarrow})^* = \mathbf{X}(k^{\uparrow,\downarrow})\mathbf{I} \quad \text{where} \quad \mathbf{I} = \begin{bmatrix} \mathbf{0} & \mathbf{1} \\ \mathbf{1} & \mathbf{0} \end{bmatrix}.$$

If, on the other hand, we have a magnetic insulator where $k^{\uparrow}$ and $k^{\downarrow}$ are both pure imaginary, then $\mathbf{X}$ is real, and hence $\mathbf{X}(k^{\uparrow,\downarrow})^* = \mathbf{X}(k^{\uparrow,\downarrow})$. If one of $k^{\uparrow}$, $k^{\downarrow}$ is real and one is pure imaginary, then since both $\mathbf{e}$ and $\mathbf{k}$ are diagonal we get a mixture of the above two cases, giving

$$\mathbf{X}(k^{\uparrow,\downarrow})^* = \mathbf{X}(k^{\uparrow,\downarrow})\mathbf{J}(k^{\uparrow,\downarrow}) \quad \text{where} \quad \mathbf{J}^2 = \mathbf{1},$$

and $\mathbf{J}$ is explicitly given by

$$\mathbf{J}(k^{\uparrow,\downarrow}) = \begin{bmatrix} \mathbf{1}-\mathbf{j} & \mathbf{j} \\ \mathbf{j} & \mathbf{1}-\mathbf{j} \end{bmatrix},$$

where $\mathbf{j} = \mathrm{diag}[f(k^{\uparrow}), f(k^{\downarrow})]$, and $f(k) = \Re(k)/k = 1$ or 0 if k is pure real or imaginary, respectively. Hence the transfer matrix between adjacent layers satisfies

$$\mathbf{T}^{*}_{n,n+1} = \mathbf{J}(k_n^{\uparrow,\downarrow})\mathbf{T}_{n,n+1}\mathbf{J}(k_{n+1}^{\uparrow,\downarrow}),$$

from which we deduce that the following holds for the transfer matrix between two general layers

$$\mathbf{T}^{*}_{n,m} = \mathbf{J}(k_n^{\uparrow,\downarrow})\mathbf{T}_{n,m}\mathbf{J}(k_m^{\uparrow,\downarrow}).$$

In particular, if layers n and m are conducting, then

$$\mathbf{T}^{*}_{n,m} = \mathbf{I}\,\mathbf{T}_{n,m}\,\mathbf{I}, \tag{A.4}$$

so that $\mathbf{T}$ must have the block-diagonal form

$$\mathbf{T}_{n,m} = \begin{bmatrix} \boldsymbol{\tau}_{11} & \boldsymbol{\tau}_{12} \\ \boldsymbol{\tau}^{*}_{12} & \boldsymbol{\tau}^{*}_{11} \end{bmatrix}, \tag{A.5}$$

where $\boldsymbol{\tau}_{ij}$ are complex 2×2 matrices.

Appendix B

Green's Function and the Density of States in the Spacer

We provide a proof of the explicit formula for the spectral density $\rho(E, L)$ given in (5.19) as part of the energy-based calculation of exchange coupling. In the process we derive an expression of the Green's function in the spacer in terms of the reflection coefficients from the transfer matrix method. The formula for $\rho(E, L)$ is stated in [4] where it differs slightly from the result we are going to obtain. The difference, apparently, has to do with the fact that the said paper is concerned with the asymptotic behaviour of spectral density where the additional term we find becomes negligible. As for the formula for the Green's function for piecewise-constant potentials, this problem is certainly not new and has been discussed, for example in, [84] and [83]. However, the cited papers focus on the results for step-potentials and potential barriers/wells, essentially relying on wave-function matching to obtain the reflection and transmission amplitudes. We show that by applying the transfer matrix formalism to this problem it is possible to generalise the results to arbitrary multilayers in a straightforward way. For the sake of clarity we confine the argument to a single spin band, so all the quantities involved are scalars.

We start with the defining equation of the Green's function

$$(\hat{\mathcal{H}} - E)G(y, y'; E) = \delta(y - y'),$$

where

$$\hat{\mathcal{H}} = -\frac{\hbar^2}{2m}\frac{\mathrm{d}^2}{\mathrm{d}x^2} + V(y),$$

$$V(y) = \begin{cases} V_0, & y < 0, y > L \\ 0, & 0 \leq y \leq L \end{cases}. \tag{B.1}$$

Consider the case where $y' < y < L$. The solution consists of a right-moving wave and a reflection off the right lead with coefficient r_{23}. Since the equation is now homogeneous, multiplying by a constant gives a family of solutions

$$G(y, y'; E) = A\left(e^{\mathrm{i}k_2 y} + r_{23}e^{-\mathrm{i}k_2 y}\right), \tag{B.2}$$

where $k_2 = \frac{\sqrt{2mE}}{\hbar}$. Now we turn to the case where $0 < y < y'$. The solution consists of a left-moving wave and a reflection from the left lead with coefficient r'_{12}. Again, multiplying by a constant we get another family of solutions

$$G(y, y'; E) = B\left(e^{-\mathrm{i}k_2 y} + r'_{12}e^{\mathrm{i}k_2 y}\right). \tag{B.3}$$

Constants A and B are eliminated from the defining matching equations of the Green's function

$$\begin{gathered} G(y, y'; E)\big|_{y=y'+0} - G(y, y'; E)\big|_{y=y'-0} = 0, \\ \frac{\mathrm{d}}{\mathrm{d}y}G(y, y'; E)\bigg|_{y=y'+0} - \frac{\mathrm{d}}{\mathrm{d}y}G(y, y'; E)\bigg|_{y=y'-0} = \frac{2m}{\hbar^2}. \end{gathered} \tag{B.4}$$

Using the results from (B.2) and (B.3) we obtain

$$G(y, y'; E) = \begin{cases} \dfrac{m}{\mathrm{i}\hbar^2 k_2}\dfrac{\left(e^{-\mathrm{i}k_2 y'} + r'_{12}e^{\mathrm{i}k_2 y'}\right)\left(e^{\mathrm{i}k_2 y} + r_{23}e^{-\mathrm{i}k_2 y}\right)}{1 - r_{23}r'_{12}}, & y' < y < L \\ \dfrac{m}{\mathrm{i}\hbar^2 k_2}\dfrac{\left(e^{\mathrm{i}k_2 y'} + r_{23}e^{-\mathrm{i}k_2 y'}\right)\left(e^{-\mathrm{i}k_2 y} + r'_{12}e^{\mathrm{i}k_2 y}\right)}{1 - r'_{12}r_{23}}, & 0 < y < y' \end{cases}. \tag{B.5}$$

Now instead of the original potential profile we consider an arbitrary N-layer ($N \geq 3$) and the problem of calculating the Green's function in a given layer ($1 < n < N$) with wave-vector k_n. It is clear that all we need to do is replace r'_{12} and r_{23} with r'_{1n} and r_{nN}, respectively. All the complexity introduced by the intermediate reflections in the neighbouring layers will be encapsulated in the reflection coefficients by virtue of the recursive nature of the transfer matrix formalism. The general result is therefore stated as follows

$$G_n(y,y';E) = \begin{cases} \dfrac{m}{\mathrm{i}\hbar^2 k_n} \dfrac{\left(e^{-\mathrm{i}k_n y'} + r'_{1n}e^{\mathrm{i}k_n y'}\right)\left(e^{\mathrm{i}k_n y} + r_{nN}e^{-\mathrm{i}k_n y}\right)}{1 - r_{nN}r'_{1n}}, & y' < y < y_{n+1} \\ \dfrac{m}{\mathrm{i}\hbar^2 k_n} \dfrac{\left(e^{\mathrm{i}k_n y'} + r_{nN}e^{-\mathrm{i}k_n y'}\right)\left(e^{-\mathrm{i}k_n y} + r'_{1n}e^{\mathrm{i}k_n y}\right)}{1 - r'_{1n}r_{nN}}, & y_n < y < y' \end{cases}. \tag{B.6}$$

We proceed to evaluate $\rho(E,L)$ from (5.19). First we calculate r'_{12}, r_{23}

$$r'_{12} = \frac{k_2 - k_1}{k_2 + k_1}, \quad r_{23} = \frac{k_2 - k_1}{k_2 + k_1}e^{2\mathrm{i}k_2 L}.$$

since $k_1 = k_3 = \frac{\sqrt{2m(E-V_0)}}{\hbar}$, $k_2 = \frac{\sqrt{2mE}}{\hbar}$, $y_{12} = 0$, $y_{23} = L$. The diagonal part of the Green's function is then found using (B.5)

$$\begin{aligned} G(y,y;E) &= \frac{m}{\mathrm{i}\hbar^2 k_2} \frac{1 + r'_{12}r_{23} + r'_{12}e^{2\mathrm{i}k_2 y} + r_{23}e^{-2\mathrm{i}k_2 y}}{1 - r'_{12}r_{23}} \\ &= \frac{m}{\mathrm{i}\hbar^2 k_2} \frac{(k_2+k_1)^2 + (k_2-k_1)^2 e^{2\mathrm{i}k_2 L} + (k_2^2 - k_1^2)\left(e^{2\mathrm{i}k_2 y} + e^{2\mathrm{i}k_2(L-y)}\right)}{(k_2+k_1)^2 - (k_2-k_1)^2 e^{2\mathrm{i}k_2 L}}. \end{aligned}$$

Here, following [4], we introduce the dimensionless energy parameter $\varepsilon = \frac{E}{V_0}$. Then, observing that $k_2^2 - k_1^2 = \frac{2mV_0}{\hbar^2}$, and dividing through by $\frac{2mV_0}{\hbar^2}$ we find

$$G(y,y;E) = \frac{m}{\mathrm{i}\hbar^2 k_2} \frac{(\sqrt{\varepsilon} + \sqrt{\varepsilon - 1})^2 + (\sqrt{\varepsilon} - \sqrt{\varepsilon - 1})^2 e^{2\mathrm{i}k_2 L} + \left(e^{2\mathrm{i}k_2 y} + e^{2\mathrm{i}k_2(L-y)}\right)}{(\sqrt{\varepsilon} + \sqrt{\varepsilon - 1})^2 - (\sqrt{\varepsilon} + \sqrt{\varepsilon - 1})^2 e^{2\mathrm{i}k_2 L}}.$$

Integrating over y we obtain

$$\int_0^L G(y,y;E)\mathrm{d}y = \frac{mL}{\mathrm{i}\hbar^2 k_2} \frac{2(2\varepsilon - 1 + \frac{\sin 2k_2 L}{2k_2 L})\sqrt{\varepsilon(\varepsilon-1)} + i\left(\sin k_2 L \cos k_2 L - \frac{(2\varepsilon-1)}{k_2 L}\sin^2 k_2 L\right)}{4\varepsilon(\varepsilon-1) + \sin^2 k_2 L}. \tag{B.7}$$

Taking the imaginary part we find

$$\Im \int_0^L G(y,y;E)dy = -\frac{2mL}{\hbar^2 k_2} \frac{\left(2\varepsilon - 1 + \frac{\sin 2k_2 L}{2k_2 L}\right)\sqrt{\varepsilon(\varepsilon-1)}}{4\varepsilon(\varepsilon-1) + \sin^2 k_2 L}. \tag{B.8}$$

Now introducing the dimensionless spacer length parameter $d = \frac{\sqrt{2mV_0}}{\hbar}L$ and rewriting k_2 in terms of ε

$$k_2 = \frac{\sqrt{2mE}}{\hbar} = \frac{\sqrt{2mV_0\varepsilon}}{\hbar},$$

we can express the factor $\frac{2mL}{\hbar^2 k_2}$ in B.8 as follows

$$\frac{2m}{\hbar^2}\frac{L}{k_2} = \frac{2m}{\hbar^2}\frac{\hbar^2 d}{2mV\sqrt{\varepsilon}} = \frac{d}{V_0}\frac{1}{\sqrt{\varepsilon}}.$$

We also find that $k_2 L = d\sqrt{\varepsilon}$. Hence

$$\Im \int_0^l G(y,y;E)\mathrm{d}y = -\frac{1}{V_0} \frac{d\left(2\varepsilon - 1 + \frac{\sin\left(2d\sqrt{\varepsilon}\right)}{2d\sqrt{\varepsilon}}\right)\sqrt{\varepsilon-1}}{4\varepsilon(\varepsilon-1) + \sin^2\left(d\sqrt{\varepsilon}\right)}.$$

Finally ρ is given by the following equation

$$\rho(\varepsilon,d) = \frac{1}{\pi V_0} \frac{d\left(2\varepsilon - 1 + \frac{\sin\left(2d\sqrt{\varepsilon}\right)}{2d\sqrt{\varepsilon}}\right)\sqrt{\varepsilon-1}}{4\varepsilon(\varepsilon-1) + \sin^2\left(d\sqrt{\varepsilon}\right)}. \tag{B.9}$$

Formula (B.9) differs from the corresponding result in [4] only in the term $\frac{\sin\left(2d\sqrt{\varepsilon}\right)}{2d\sqrt{\varepsilon}}$ which obviously does not affect the result for sufficiently large values of $d\sqrt{\epsilon}$.

Appendix C

Relation Between Green's Function and Transmission

In this section we give a variant of the proof of the relation between the transmission and reflection coefficients, and the T-operator that features in the perturbation theory, particularly in the statement of the Lippmann-Schwinger equation [53]. We make use of these relations in (5.23) when calculating IEC via the energy method. The most general version of the proof in the multi-band case is given in [5]. Reproducing that would take us too far beyond the scope of the present discussion, therefore we confine ourselves to a single-band case, similarly to the derivation in Appendix B. Consider the case where the one-particle Hamiltonian $\hat{\mathcal{H}}$ can be separated into an unperturbed part $\hat{\mathcal{H}}_0$ and a perturbation V

$$\hat{\mathcal{H}} = \hat{\mathcal{H}}_0 + V$$

The T-matrix is then defined by the operator equation

$$TG_0 = VG,$$

where G and G_0 are the Green's functions of $\hat{\mathcal{H}}$ and $\hat{\mathcal{H}}_0$, respectively. Using the definition of the Green's function T can be given by the following formula

$$T = V(E - V - \hat{\mathcal{H}}_0)^{-1}(E - \hat{\mathcal{H}}_0) = V\,(1 - G_0 V)^{-1}$$

With the help of T Dyson's equation

$$G = G_0 + G_0 V G$$

can be written as follows

$$G = G_0 + G_0 T G_0 \tag{C.1}$$

Now consider the case of two scattering potentials V_{L} and V_{R}

$$G = \left(E - \hat{\mathcal{H}} - V_{\mathrm{L}} - V_{\mathrm{R}}\right)^{-1},$$

where the Hamiltonian $\hat{\mathcal{H}}$ can be taken to be the same as in (B.1). Using the reflection counting argument it can be shown that

$$G = G_0 + G_0 T_{\mathrm{L}} G_0 + G_0 T_{\mathrm{R}} G_0 + R_{\mathrm{L}} + R_{\mathrm{R}},$$

where $T_{\mathrm{R|L}} = V_{\mathrm{R|L}}\left(I - G_0 V_{\mathrm{R|L}}\right)^{-1}$ and

$$R_{\mathrm{L}} = G_0 T_{\mathrm{L}} G_0 T_{\mathrm{R}} G_0 + G_0 T_{\mathrm{L}} G_0 T_{\mathrm{R}} G_0 T_{\mathrm{L}} G_0 + \ldots$$
$$R_{\mathrm{R}} = G_0 T_{\mathrm{R}} G_0 T_{\mathrm{L}} G_0 + G_0 T_{\mathrm{R}} G_0 T_{\mathrm{L}} G_0 T_{\mathrm{R}} G_0 + \ldots$$

Separating the terms with odd and even number of factors in R_{L} and R_{R} we find

$$R_{\mathrm{L}} = G_0 T_{\mathrm{L}}\left(I - G_0 T_{\mathrm{R}} G_0 T_{\mathrm{L}}\right)^{-1} G_0 T_{\mathrm{R}}\left(I + G_0 T_{\mathrm{L}}\right) G_0,$$
$$R_{\mathrm{R}} = G_0 T_{\mathrm{R}}\left(I - G_0 T_{\mathrm{L}} G_0 T_{\mathrm{R}}\right)^{-1} G_0 T_{\mathrm{L}}\left(I + G_0 T_{\mathrm{R}}\right) G_0.$$

Now taking the trace and using the cyclical property we obtain

$$\operatorname{tr} R_{\mathrm{L}} = \operatorname{tr}\left(\left(I - G_0 T_{\mathrm{L}} G_0 T_{\mathrm{R}}\right)^{-1} \left(I + G_0 T_{\mathrm{L}}\right) G_0^2 T_{\mathrm{L}} G_0 T_{\mathrm{R}}\right),$$
$$\operatorname{tr} R_{\mathrm{R}} = \operatorname{tr}\left(\left(I - G_0 T_{\mathrm{R}} G_0 T_{\mathrm{L}}\right)^{-1} \left(I + G_0 T_{\mathrm{R}}\right) G_0^2 T_{\mathrm{R}} G_0 T_{\mathrm{L}}\right).$$

Using the identity

$$\frac{\mathrm{d}}{\mathrm{d}E} G = -G^2 \tag{C.2}$$

we can rewrite the following factors

$$G_0^2 T_{\mathrm{L}} G_0 T_{\mathrm{R}} = -\left(\frac{\mathrm{d}}{\mathrm{d}E} G_0\right) T_{\mathrm{L}} G_0 T_{\mathrm{R}},$$
$$G_0 T_{\mathrm{L}} G_0^2 T_{\mathrm{R}} = -G_0 T_{\mathrm{L}} \left(\frac{\mathrm{d}}{\mathrm{d}E} G_0\right) T_{\mathrm{R}}.$$

We now need to calculate $\frac{\mathrm{d}}{\mathrm{d}E} T$. To this end, we substitute (C.1) in (C.2). Upon cancellation we obtain

$$G_0 \left(\frac{\mathrm{d}}{\mathrm{d}E} T + T G_0^2 T\right) G_0 = 0,$$

from which it follows that

$$\frac{\mathrm{d}}{\mathrm{d}E} T = -T G_0^2 T.$$

Therefore

$$G_0 T_{\mathrm{L}} G_0^2 T_{\mathrm{L}} G_0 T_{\mathrm{R}} = -G_0 \left(\frac{\mathrm{d}}{\mathrm{d}E} T_{\mathrm{L}}\right) G_0 T_{\mathrm{R}},$$
$$G_0 T_{\mathrm{L}} G_0 T_{\mathrm{R}} G_0^2 T_{\mathrm{R}} = -G_0 T_{\mathrm{L}} G_0 \left(\frac{\mathrm{d}}{\mathrm{d}E} T_{\mathrm{R}}\right).$$

Finally, we obtain

$$\begin{aligned}\operatorname{tr}\left(R_{\mathrm{L}} + R_{\mathrm{R}}\right) &= \operatorname{tr}\left(\left(I - G_0 T_{\mathrm{L}} G_0 T_{\mathrm{R}}\right)^{-1} \frac{\mathrm{d}}{\mathrm{d}E} \left(G_0 T_{\mathrm{L}} G_0 T_{\mathrm{R}}\right)\right) \\ &= \frac{\mathrm{d}}{\mathrm{d}E} \operatorname{tr} \ln\left(I - G_0 T_{\mathrm{L}} G_0 T_{\mathrm{R}}\right).\end{aligned}$$

Now reflection coefficients are related to the T-matrix [53] as follows

$$r = \langle y \,|\, G_0 \,|\, y \rangle \, \langle -k \,|\, T \,|\, k \rangle \,,$$

where

$$\langle -k \,|\, T \,|\, k \rangle = \int e^{ik(x'+x'')} \, \langle x' \,|\, T \,|\, x'' \rangle \, \mathrm{d}x' \mathrm{d}x''$$

Starting from the free-particle wave-function

$$G_0(y, y') = \tfrac{m}{i\hbar^2 k} e^{ik|y-y'|}$$

and projecting (C.1) onto the real space we obtain

$$\begin{aligned}
G_L(y, y') &= G_0(y, y') + \int G_0(y, u) T(u, v) G_0(v, y') \mathrm{d}u \mathrm{d}v \\
&= \frac{m}{i\hbar^2 k} e^{ik|y-y'|} + \Big(\frac{m}{i\hbar^2 k}\Big)^2 \int e^{ik|y-u|} T(u, v) e^{ik|v-y'|} \mathrm{d}u \mathrm{d}v \\
&= \frac{m}{i\hbar^2 k} e^{ik|y-y'|} + \frac{m}{i\hbar^2 k} e^{ik(y+y')} \frac{m}{i\hbar^2 k} \int e^{ik(u+v)} T(u, v) \mathrm{d}u \mathrm{d}v \\
&= \frac{m}{i\hbar^2 k} e^{ik|y-y'|} + \frac{m}{i\hbar^2 k} e^{ik(y+y')} \, \langle y \,|\, G_0 \,|\, y \rangle \, \langle -k \,|\, T \,|\, k \rangle \\
&= \frac{m}{i\hbar^2 k} \Big(e^{ik|y-y'|} + r e^{-ik(y+y')} \Big) \,.
\end{aligned}$$

Hence, the diagonal Green's function to the left of the scatterer is $G_L = \frac{m}{i\hbar^2 k} \big(1 + r e^{-i2ky}\big)$. Similarly, to the right of the scatterer we find $G_R = \frac{m}{i\hbar^2 k} \big(1 + r' e^{i2ky}\big)$. Therefore, the Green's function in the spacer is

$$G_S = G_0 + G_0 T_L G_0 + G_0 T_R G_0 + \Delta G_{LR},$$

where ΔG_{LR} is the interaction term which gives rise to exchange coupling. Bearing in mind that $G_0 T_{L(R)} G_0 = G_{L(R)} - G_0$ we obtain

$$\begin{aligned}\Delta G_{LR} &= G_S - G_L - G_R - G_0 \\ &= \frac{m}{i\hbar^2 k}\left(\frac{1 + r'r + r'e^{-i2ky} + r^{-i2ky}}{1 - r'r} - 1 - re^{-i2ky} - 1 - r'^{i2ky} + 1\right) \\ &= \frac{r'r\left(2 + r'e^{i2ky} + re^{-i2ky}\right)}{1 - r'r},\end{aligned}$$

which is the one-dimensional version of the general result proved in [5]

Bibliography

[1] V. Fadeev and A. Umerski. Application of the Landauer formalism to the calculation of spin current, 2019.

[2] J. Mathon, M. Villeret, and H. Itoh. Selection rules for oscillations of the giant magnetoresistance with nonmagnetic spacer layer thickness. *Phys. Rev. B*, 52:R6983–R6986, 9 1995.

[3] Luis L. Sánchez-Soto, Juan J. Monzón, Alberto G. Barriuso, and José F. Cariñena. The transfer matrix: A geometrical perspective. *Physics Reports*, 513(4):191–227, 2012.

[4] D.M. Edwards and A. Umerski. *Exchange coupling in magnetic multilayers*. Wiley, 2007.

[5] P. Bruno. Theory of interlayer magnetic coupling. *Phys. Rev. B*, 52:411–439, 7 1995.

[6] A. Brataas, Y.V. Nazarov, and G.E.W. Bauer. Spin-transport in multi-terminal normal metal-ferromagnet systems with non-collinear magnetizations. *The European Physical Journal B - Condensed Matter and Complex Systems*, 22(1):99–110, 7 2001.

[7] P. Brusheim, D. Csontos, U. Zülicke, and H. Q. Xu. Multiterminal multimode spin-dependent scattering matrix formalism: Electron and hole quantum spin transport in multiterminal junctions. *Phys. Rev. B*, 78:085301, 8 2008.

[8] Lebo Zhang, P. Brusheim, and H. Q. Xu. Multimode electron transport through quantum waveguides with spin-orbit interaction modulation: Applications of the scattering matrix formalism. *Phys. Rev. B*, 72:045347, Jul 2005.

[9] M. Büttiker. Chemical potential oscillations near a barrier in the presence of transport. *Phys. Rev. B*, 40:3409–3412, Aug 1989.

[10] S. Datta. *Electronic Transport in Mesoscopic Systems*. Cambridge Studies in Semiconductor Physics. Cambridge University Press, 1997.

[11] L. Esaki, P.J. Stiles, and S. von Molnar. Magnetointernal Field Emission in Junctions of Magnetic Insulators. *Phys. Rev. Lett.*, 19:852–854, 10 1967.

[12] S. Bandyopadhyay and M. Cahay. *Introduction to Spintronics*. CRC Press, 2008.

[13] Supriyo Datta and Biswajit Das. Electronic analog of the electro-optic modulator. *Applied Physics Letters*, 56(7):665–667, 1990.

[14] S. Parkin, Xin Jiang, C. Kaiser, A. Panchula, K. Roche, and M. Samant. Magnetically engineered spintronic sensors and memory. *Proceedings of the IEEE*, 91(5):661–680, 5 2003.

[15] J. Daughton, J. Brown, E. Chen, R. Beech, A. Pohm, and W. Kude. Magnetic field sensors using GMR multilayer. *IEEE Transactions on Magnetics*, 30(6):4608–4610, Nov 1994.

[16] Gary A. Prinz. Magnetoelectronics. *Science*, 282(5394):1660–1663, 1998.

[17] S. Maekawa and U. Gafvert. Electron tunneling between ferromagnetic films. *IEEE Transactions on Magnetics*, 18(2):707–708, 3 1982.

[18] J. Mathon and A. Umerski. Tight-binding theory of tunneling giant magnetoresistance. *Phys. Rev. B*, 56:11810, 11 1997.

[19] H. Ohno, M. D. Stiles, and B. Dieny. Advancements in spintronics. *Proceedings of the IEEE*, 104(10):1782–1786, Oct 2016.

[20] Daniel T. Pierce and Felix Meier. Photoemission of spin-polarized electrons from GaAs. *Phys. Rev. B*, 13:5484–5500, Jun 1976.

[21] Yaroslav Tserkovnyak, Arne Brataas, and Gerrit E. W. Bauer. Enhanced Gilbert Damping in Thin Ferromagnetic Films. *Phys. Rev. Lett.*, 88:117601, Feb 2002.

[22] Yaroslav Tserkovnyak, Arne Brataas, Gerrit E. W. Bauer, and Bertrand I. Halperin. Nonlocal magnetization dynamics in ferromagnetic heterostructures. *Rev. Mod. Phys.*, 77:1375–1421, Dec 2005.

[23] Moosa Hatami, Gerrit E. W. Bauer, Qinfang Zhang, and Paul J. Kelly. Thermal Spin-Transfer Torque in Magnetoelectronic Devices. *Phys. Rev. Lett.*, 99:066603, Aug 2007.

[24] J.-E. Wegrowe. Spin transfer from the point of view of the ferromagnetic degrees of freedom. *Solid State Communications*, 150(11):519 – 523, 2010. Spin Caloritronics.

[25] Duan Feng and Guojun Jin. *Introduction to Condensed Matter Physics.* Number Volume 1 in Introduction to Condensed Matter Physics. World Scientific Publishing Company, 2005.

[26] J. E. Moore and L. Balents. Topological invariants of time-reversal-invariant band structures. *Phys. Rev. B*, 75:121306, Mar 2007.

[27] M. Z. Hasan and C. L. Kane. Colloquium: Topological insulators. *Rev. Mod. Phys.*, 82:3045–3067, Nov 2010.

[28] Xiao-Liang Qi and Shou-Cheng Zhang. Topological insulators and superconductors. *Rev. Mod. Phys.*, 83:1057–1110, Oct 2011.

[29] Jing Shi, Kevin Pettit, E. Kita, S. S. P. Parkin, R. Nakatani, and M. B. Salamon. Field-dependent thermoelectric power and thermal conductivity in multilayered and granular giant magnetoresistive systems. *Phys. Rev. B*, 54:15273–15283, Dec 1996.

[30] Laurent Gravier, Santiago Serrano-Guisan, Fran çois Reuse, and Jean-Philippe Ansermet. Thermodynamic description of heat and spin transport in magnetic nanostructures. *Phys. Rev. B*, 73:024419, Jan 2006.

[31] Laurent Gravier, Santiago Serrano-Guisan, Fran çois Reuse, and J.-Ph. Ansermet. Spin-dependent Peltier effect of perpendicular currents in multilayered nanowires. *Phys. Rev. B*, 73:052410, Feb 2006.

[32] S. Maekawa, S.O. Valenzuela, T. Kimura, and E. Saitoh. *Spin Current.* Oxford science publications. Oxford University Press, 2017.

[33] S. E. Barnes, J. Ieda, and S. Maekawa. Magnetic memory and current amplification devices using moving domain walls. *Applied Physics Letters*, 89(12):122507, 2006.

[34] Wayne M. Saslow. Spin pumping of current in non-uniform conducting magnets. *Phys. Rev. B*, 76:184434, Nov 2007.

[35] S. D. Bader. Colloquium: Opportunities in nanomagnetism. *Rev. Mod. Phys.*, 78:1–15, Jan 2006.

[36] G. Srajer, L.H. Lewis, S.D. Bader, A.J. Epstein, C.S. Fadley, E.E. Fullerton, A. Hoffmann, J.B. Kortright, Kannan M. Krishnan, S.A. Majetich, T.S. Rahman, C.A. Ross, M.B. Salamon, I.K. Schuller, T.C. Schulthess, and J.Z. Sun. Advances in nanomagnetism via X-ray techniques. *Journal of Magnetism and Magnetic Materials*, 307(1):1 – 31, 2006.

[37] Walther Gerlach and Otto Stern. Der experimentelle Nachweis der Richtungsquantelung im Magnetfeld. *Zeitschrift für Physik*, 9(1):349–352, Dec 1922.

[38] N. F. Mott. The electrical conductivity of transition metals. *Proceedings of the Royal Society of London A: Mathematical, Physical and Engineering Sciences*, 153(880):699–717, 1936.

[39] S. Douglas Stone and Aaron Szafer. What is Measured when You Measure a Resistance? - The Landauer Formula Revisited. *IBM J. Res. Dev.*, 32(3):384–413, 5 1988.

[40] D A Wharam, T J Thornton, R Newbury, M Pepper, H Ahmed, J E F Frost, D G Hasko, D C Peacock, D A Ritchie, and G A C Jones. One-dimensional transport and the quantisation of the ballistic resistance. *Journal of Physics C: Solid State Physics*, 21(8):L209–L214, mar 1988.

[41] B. J. van Wees, H. van Houten, C. W. J. Beenakker, J. G. Williamson, L. P. Kouwenhoven, D. van der Marel, and C. T. Foxon. Quantized conductance of point contacts in a two-dimensional electron gas. *Phys. Rev. Lett.*, 60:848–850, 2 1988.

[42] R. Landauer. Spatial Variation of Currents and Fields Due to Localized Scatterers in Metallic Conduction. *IBM Journal of Research and Development*, 1(3):223–231, 7 1957.

[43] S. Datta and Cambridge University Press. *Quantum Transport: Atom to Transistor*. Cambridge University Press, 2005.

[44] C. Kittel. *Introduction to Solid State Physics*. Wiley, 2004.

[45] Daniel S. Fisher and Patrick A. Lee. Relation between conductivity and transmission matrix. *Phys. Rev. B*, 23:6851–6854, Jun 1981.

[46] M. Büttiker. Four-Terminal Phase-Coherent Conductance. *Phys. Rev. Lett.*, 57:1761–1764, Oct 1986.

[47] I.J. Maddox. *Elements of Functional Analysis*. Cambridge University Press, 1988.

[48] E. Cartan and A. Mercier. *The Theory of Spinors*. Dover Books on Mathematics. Dover Publications, 1981.

[49] J.C. Slonczewski. Current-driven excitation of magnetic multilayers. *Journal of Magnetism and Magnetic Materials*, 159(1):L1 – L7, 1996.

[50] L. Berger. Emission of spin waves by a magnetic multilayer traversed by a current. *Phys. Rev. B*, 54:9353–9358, 10 1996.

[51] M. Tsoi, A. G. M. Jansen, J. Bass, W.-C. Chiang, M. Seck, V. Tsoi, and P. Wyder. Erratum: Excitation of a Magnetic Multilayer by an Electric Current. *Phys. Rev. Lett.*, 81:493–493, Jul 1998.

[52] E. B. Myers, D. C. Ralph, J. A. Katine, R. N. Louie, and R. A. Buhrman. Current-Induced Switching of Domains in Magnetic Multilayer Devices. *Science*, 285(5429):867–870, 1999.

[53] E.N. Economou. *Green's Functions in Quantum Physics*. Springer Series in Solid-State Sciences. Springer Berlin Heidelberg, 2006.

[54] J. d'Albuquerque e Castro, J. Mathon, Murielle Villeret, and A. Umerski. Confinement mechanism for strong temperature dependence of the interlayer exchange coupling in Co/Cu(001). *Phys. Rev. B*, 53:R13306–R13309, 5 1996.

[55] D.M. Edwards, F. Federici, J. Mathon, and A. Umerski. Self-consistent theory of current-induced switching of magnetization. *Physical Review B*, 71(5), 2 2005.

[56] Y.-H. Tang, Nicholas Kioussis, Alan Kalitsov, W. H. Butler, and Roberto Car. Influence of asymmetry on bias behavior of spin torque. *Phys. Rev. B*, 81:054437, Feb 2010.

[57] Ioannis Theodonis, Nicholas Kioussis, Alan Kalitsov, Mairbek Chshiev, and W. H. Butler. Anomalous Bias Dependence of Spin Torque in Magnetic Tunnel Junctions. *Phys. Rev. Lett.*, 97:237205, 12 2006.

[58] T. Yonte, J.J. Monzón, L.L. Sánchez-Soto, José F. Cari nena, and Carlos López-Lacasta. Understanding multilayers from a geometrical viewpoint. *J. Opt. Soc. Am. A*, 19(3):603–609, 3 2002.

[59] J. J. Monzón and L. L. Sánchez-Soto. Origin of the Thomas rotation that arises in lossless multilayers. *J. Opt. Soc. Am. A*, 16(11):2786–2792, 1 1999.

[60] A. Umerski. Closed-form solutions to surface Green's functions. *Phys. Rev. B*, 55:5266–5275, Feb 1997.

[61] Kenkichi Iwasawa. On Some Types of Topological Groups. *Annals of Mathematics*, 50(3):507–558, 1949.

[62] S. Helgason. *Differential Geometry, Lie Groups, and Symmetric Spaces*. Crm Proceedings & Lecture Notes. American Mathematical Society, 2001.

[63] J. J. Monzón, T. Yonte, and L. L. Sánchez-Soto. Basic factorization for multilayers. *Opt. Lett.*, 26(6):370–372, 3 2001.

[64] Tin-Yau Tam. Computing the Iwasawa decomposition of a symplectic matrix by Cholesky factorization. *Applied Mathematics Letters*, 19(12):1421–1424, 2006.

[65] Michele Benzi and Nader Razouk. On the Iwasawa decomposition of a symplectic matrix. *Applied Mathematics Letters*, 20(3):260–265, 2007.

[66] J. Lekner. *Theory of Reflection: Reflection and Transmission of Electromagnetic, Particle and Acoustic Waves*. Springer Series on Atomic, Optical, and Plasma Physics. Springer International Publishing, 2016.

[67] Xavier Waintal, Edward B. Myers, Piet W. Brouwer, and D. C. Ralph. Role of spin-dependent interface scattering in generating current-induced torques in magnetic multilayers. *Phys. Rev. B*, 62:12317–12327, 11 2000.

[68] V. P. Amin and M. D. Stiles. Spin transport at interfaces with spin-orbit coupling: Formalism. *Phys. Rev. B*, 94:104419, Sep 2016.

[69] R.C. Jones. A New Calculus for the Treatment of Optical Systems. I. Description and Discussion of the Calculus. *J. Opt. Soc. Am.*, 31(7):488–493, 7 1941.

[70] S.R. Cloude. Lie Groups in Electromagnetic Wave Propagation and Scattering. *Journal of Electromagnetic Waves and Applications*, 6(7):947–974, 1992.

[71] Gil, J. J. Polarimetric characterization of light and media - Physical quantities involved in polarimetric phenomena. *Eur. Phys. J. Appl. Phys.*, 40(1):1–47, 2007.

[72] E. Kuntman, M.A. Kuntman, A. Canillas, and O. Arteaga. Quaternion algebra for Stokes-Mueller formalism. *J. Opt. Soc. Am. A*, 36(4):492–497, 4 2019.

[73] E. Kuntman, M.A. Kuntman, and O. Arteaga. Vector and matrix states for Mueller matrices of nondepolarizing optical media. *J. Opt. Soc. Am. A*, 34(1):80–86, 1 2017.

[74] L.D. Landau and E.M. Lifshitz. *The Classical Theory of Fields*. Course of Theoretical Physics. Elsevier Science, 1975.

[75] R. W. Schmieder. Stokes-Algebra Formalism. *J. Opt. Soc. Am.*, 59(3):297–302, 3 1969.

[76] Donald G. M. Anderson and Richard Barakat. Necessary and sufficient conditions for a Mueller matrix to be derivable from a Jones matrix. *J. Opt. Soc. Am. A*, 11(8):2305–2319, 8 1994.

[77] A. Aiello and J. P. Woerdman. Linear Algebra for Mueller Calculus. *arXiv e-prints*, pages math–ph/0412061, 12 2004.

[78] L.D. Landau and E.M. Lifshitz. *Quantum Mechanics: Non-Relativistic Theory*. Course of Theoretical Physics. Elsevier Science, 1981.

[79] J.C. Slonczewski. Conductance and exchange coupling of two ferromagnets separated by a tunneling barrier. *Physical review. B*, 39:6995–7002, 5 1989.

[80] R.P. Erickson, Kristl B. Hathaway, and James R. Cullen. Mechanism for non-heisenberg-exchange coupling between ferromagnetic layers. *Physical Review B*, 47(5):2626, 1993.

[81] Yang Liu, Bing Zhou, and Jian-Gang Zhu. Field-free Magnetization Switching by Utilizing the Spin Hall Effect and Interlayer Exchange Coupling of Iridium. *Scientific Reports*, 9:325, 12 2019.

[82] D.M. Edwards. *Exotic States in Quantum Nanostructures*, chapter Giant Magnetoresistance and Layered Magnetic Structures, pages 213–262. Springer Netherlands, Dordrecht, 2002.

[83] F. M. Andrade. Exact Green's function for rectangular potentials and its application to quasi-bound states. *Physics Letters A*, 378(21):1461–1468, 2014.

[84] M. de Aguiar. Exact Green's function for the step and square-barrier potentials. *Physical review. A*, 48:2567–2573, 11 1993.

[85] J. Kudrnovský, V. Drchal, I. Turek, P. Bruno, P. Dederichs, and P. Weinberger. Ab Initio Theory of the Interlayer Exchange Coupling. In Hugues Dreyssé, editor, *Electronic Structure and Physical Properies of Solids*, pages 313–346, Berlin, Heidelberg, 2000. Springer Berlin Heidelberg.

[86] L.V. Ahlfors. *Complex Analysis: An Introduction to the Theory of Analytic Functions of One Complex Variable*. International Series in pure and applied mathematics. McGraw-Hill Interamericana, 1953.

[87] Petarpa Boonserm and Matt Visser. Analytic bounds on transmission probabilities. *Annals of Physics*, 325(7):1328 – 1339, 2010. July 2010 Special Issue.

[88] H.-L. Engquist and P. W. Anderson. Definition and measurement of the electrical and thermal resistances. *Phys. Rev. B*, 24:1151–1154, 7 1981.

[89] H. Ohno, T. Endoh, T. Hanyu, N. Kasai, and S. Ikeda. Magnetic tunnel junction for nonvolatile CMOS logic. In *2010 International Electron Devices Meeting*, pages 9.4.1–9.4.4, 12 2010.

[90] C. Pan and A. Naeemi. A Nonvolatile Fast-Read Two-Transistor SRAM Based on Spintronic Devices. *IEEE Journal on Exploratory Solid-State Computational Devices and Circuits*, 3:93–100, Dec 2017.

[91] P. M. Braganca, J. A. Katine, N. C. Emley, D. Mauri, J. R. Childress, P. M. Rice, E. Delenia, D. C. Ralph, and R. A. Buhrman. A Three-Terminal Approach to Developing Spin-Torque Written Magnetic Random Access Memory Cells. *IEEE Transactions on Nanotechnology*, 8(2):190–195, March 2009.

[92] A. Brataas, Yu. V. Nazarov, and G.E.W. Bauer. Finite-Element Theory of Transport in Ferromagnet-Normal Metal Systems. *Phys. Rev. Lett.*, 84:2481–2484, 3 2000.

[93] X. F. Wang, P. Vasilopoulos, and F. M. Peeters. Ballistic spin transport through electronic stub tuners: Spin precession, selection, and square-wave transmission. *Applied Physics Letters*, 80(8):1400–1402, 2002.

[94] Duan-Yang Liu and Jian-Bai Xia. Conductance of two-dimensional waveguide in presence of the Rashba spin-orbit interaction. *Physica E: Low-dimensional Systems and Nanostructures*, 98:6 – 9, 2018.

[95] Laurens W. Molenkamp, G. Schmidt, and G. E. W. Bauer. Rashba Hamiltonian and electron transport. *Phys. Rev. B*, 64:121202, Sep 2001.

[96] C. Jirauschek. Accuracy of Transfer Matrix Approaches for Solving the Effective Mass Schrödinger Equation. *IEEE Journal of Quantum Electronics*, 45(9):1059–1067, 9 2009.

[97] Debabrata Biswas and Vishal Kumar. Improved transfer matrix methods for calculating quantum transmission coefficient. *Phys. Rev. E*, 90:013301, Jul 2014.

[98] F.R. Gantmakher, K.A. Hirsch, and American Mathematical Society. *The Theory of Matrices*. Number v. 1 in AMS Chelsea Publishing Series. Chelsea Publishing Company, 1959.